QUANTUM IMPURITIES IN INTERACTING ENVIRONMENTS

By

COLIN RYLANDS

A dissertation submitted to the

School of Graduate Studies

Rutgers, The State University of New Jersey

in partial fulfillment of the requirements

for the degree of

Doctor of Philosophy

Graduate Program in Physics and Astronomy

written under the direction of

Prof. Natan Andrei

and approved by

_____

_____

_____

_____

New Brunswick, New Jersey

October, 2018

ABSTRACT OF THE DISSERTATION

Quantum Impurities in Interacting Environments

By COLIN RYLANDS

Dissertation Director:

Prof. Natan Andrei

The quantum physics of one dimensional systems exhibits many remarkable and exotic physical phenomena. These are the result of the strong correlations which exist in such systems due to the reduced dimensionality and in many cases can be described by Luttinger Liquid theory. Likewise quantum impurity systems, where a bath of particles couples to the same impurity, exhibit well known non perturbative phenomena like the Kondo effect. In this thesis we study the physics of quantum impurities in interacting environments - the intersection of these two areas. Such Luttinger-impurity systems can be realized experimentally in a range of different settings from quantum wires and carbon nano tubes to edges of fractional quantum hall systems and cold atom gases. We show that many of the models used to describe these experiments are integrable and can be studied by means of the Bethe Ansatz. This powerful and exact method provides us with the exact eigenstates and energy levels of the model Hamiltonian. The models considered include two which describe a Luttinger liquid coupled to a back scattering impurity, the Kane-Fisher and weak tunnelling model as well as Luttinger liquids coupled a quantum dot in various geometries: at the boundary, sidecoupled and embedded. To incorporate both the backscattering nature of

the impurities and the interacting bulk particles a new formulation of the Bethe Ansatz is developed and implemented. The eigenstates and spectra of the models are found and used to investigate their ground state and thermodynamic properties.

Acknowledgments

This thesis would have in no way been possible without a the support, guidance and friendship of large number of people. First among these I want to thank Natan Andrei with whom this work has been carried out. I am indebted to him for introducing me to condensed matter physics and in particular the fascinating and beautiful field of one dimensional physics. He has been an excellent teacher, mentor and I am especially grateful for him being so supportive regarding my extended periods away from Rutgers. I am also thankful to all the members of his research group, past and present who provided countless valuable comments and suggestions on the work presented in this thesis.

I have had the pleasure of getting to know many wonderful people throughout my time at Rutgers which I am proud to call friends. I would especially like to mention Raghav Kunnawalkam-Elayavalli, Dan Brennan, John Wu, Kartheik Iyer, John Bonini, Jesse Rivera, Jesus Rives, Willow Kion-Crosby, Ian Laflotte, Caitlin Carpenter and Ethan Cline. Thank you all for your friendship and for always giving me rides everywhere. I would also like to thank my fellow occupants of Serin room 287 -the institute of one dimensional motion- for sometimes inane, often distracting but predominantly fun conversations for the last few years.

It is hard to know if something is special if that is what you have always known, but over the last few years I have come to realize just how lucky I am to have the family I do. The kindness and support shown in the tough moments is only matched by *craic* had in the joyous times. Thank you to my amazing grandparents, Marie and Joe, my brothers Eoin, Shane and Mark and my loving parents Mary and Gerard without whom I could never have hoped to be where I am. Above all I want to thank my wife Katie for her love support and

understanding.

Dedication

To my dearest Katie

Table of Contents

List of Figures

1

Introduction and Motivation

Amongst all branches of the physical sciences, physics is most often associated with discovering the fundamental laws of nature. Indeed, one could be forgiven for thinking that this is the ultimate goal of the field. In particle physics, researchers seek a "theory of everything" which unites the standard model of particle physics with Einstein's theory of gravity into a single fundamental framework[1, 2]. Likewise in cosmology. Roughly 95% of the universe consists of, for want of a better word "stuff" [3] about which we know practically nothing and discovering the laws by which it is governed is a necessity to understand cosmic history, present and future[4].

In contrast the fundamental theory of everything for condensed matter physics is known, and has been known since the early part of the 20^{th} century [5]. The entirety of the field can be reduced down to understanding the behaviour of a gas of electrons interacting via the Coulomb force in a potential created by some ions [6, 7]. Armed with this knowledge the condensed matter physicist can confidently answer any question that could be posed with the statement: "That is a result of the interaction between the electrons or the interaction between the electrons and the ions or a combination of both". The follow up question is most decidedly a harder one to answer: "How?"

The basic premise of condensed matter physics, or many-body physics to give it a more all encompassing title, is to understand how, the same basic building blocks can result in vastly different phenomena. Metals and insulators, superconductors and topological matter all emerge from the same fundamental theory and it is the goal of a condensed matter physicist to discern how this occurs and moreover predict and measure new and interesting

behavior.

At the outset it seems a daunting task to solve the Schrödinger equations of $N \sim 10^{23}$ electrons and ions and indeed such a task is entirely intractable. A more refined approach is therefore necessary. Typically one is interested in the effects a system exhibits within a certain energy range and inside this region only certain degrees of freedom may be relevant to our understanding. For instance, probing a metal on the Planck scale gives one no more understanding of it's electrical conductivity then probing it with a hammer would. This is when the concepts of renormalization and universality, the foundations of modern condensed matter physics come to the fore [8]. Starting from the fundamental theory, the unimportant degrees of freedom maybe integrated out resulting in simplified description. Ideally this simplified model then captures not only the physics of the particular system under scrutiny but also a whole class of systems with related properties.

In practice, it is not often, if ever that one carries out this renormalization procedure from beginning to end but instead relies upon experience and physical arguments to discern an appropriate effective description. Both discovering and understanding these effective theories is central to help our understanding of the physical systems we hope to measure or create.

One of the most renowned effective theories is Fermi Liquid theory which succcessfully captures the low energy behavior of many metals. The idea is based upon the existence of long lived quasiparticles which interact with each other only weakly and are adiabatically connected to non interacting fermions [6]. As a result the behavior of Fermi liquids is qualitatively that of a non interacting Fermi gas and although it is remarkable that so many materials behave in this way it is rather uninteresting.

To witness more exotic and striking effects one must turn to systems which exhibit strong correlations between the relevant degrees of freedom. In such systems perturbative methods can no longer applied and more powerful non-perturbative or exact methods are required to understand them [7]. Two paradigms of strongly correlated systems are quantum

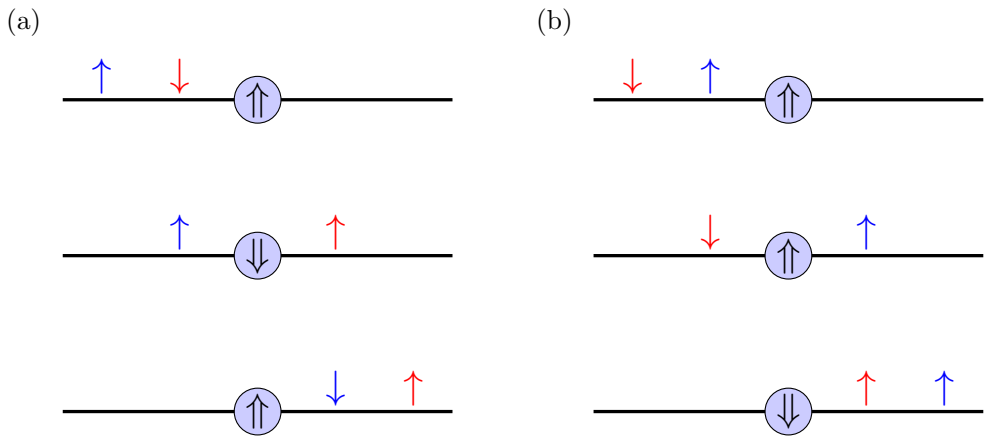

Figure 1.1: Here we depict two sequences of scattering events which show how the impurity correlates the bulk. Consider a localized spin interacting with bulk fermions via spin exchange. (a) If the red particle moves past the impurity first followed by the blue then the final state of the system is depicted at the bottom. (b) If instead we move the blue particle past the red first and the two are not coupled to each other we get the final state on the right. Swapping the order of the red and blue particles again we see that the two end states are different and so there must be some effect of swapping their order i.e the bulk particles must be correlated by the impurity.

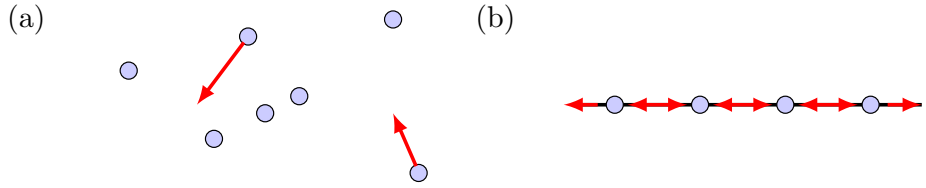

Figure 1.2: For a system of particles in 2 or higher dimensions shown in (a), particles may easily avoid each other however when they are restricted to move on a line as in (b) interactions become unavoidable. In the former case one can envisage starting with a non interacting system and adiabatically turning on the interactions, a quasi particle picture is therefore appropriate. In the later case as soon as a non vanishing interaction is included a drastic change in the system occurs, excitations necessarily involve all the particles meaning that there are only collective excitations.

impurity models (QIM) and interacting one dimensional (1D) models. In the first example a bath of particles which may be 1D or higher dimensional, interacts with a single localized impurity. The correlations induced amongst the bath particles by interacting with the same impurity, see FIG. 1.1 can then result in non perturbative phenomena like the Kondo effect where a magnetic impurity is screened at low temperature[9]. In the second example, the reduced dimensionalty of the 1D system means that no matter how weak the interactions any excitation of the system is a collective one [10], see FIG. 1.2. This signals a breakdown in a perturbative quasiparticle picture and leads to numerous unique phenomena which exist only in 1D systems. The low energy physics of many one dimensional systems is successfully captured by Luttinger liquid theory, the 1D counterpart to Fermi liquid theory [11].

In this thesis we will study the overlap between these two areas, wherein quantum impurities are coupled to Luttinger liquids. This is by no means the first study of such systems and there exists a wealth of literature on the topic dating back to the groundbreaking work of Kane and Fisher [12, 13]. The majority of the (analytical) work utilizes the method of bosonization [14], an extremely useful method for dealing with one dimensional systems in general not just impurity models. The power of this method lies in the ability to map an interacting theory (see for example (2.5)) to a quadratic bosonic theory after which the impurity can be treated perturbatively. Another popular though less widely used method is the Coulomb gas formalism wherein the partition function of the model is mapped to that of classical gas with logarithmic interactions [15]. Both methods have been highly successful and predicted many exotic phenomena which where later observed experimentally however they still rely on a perturbative treatment of the impurity. To complement the results of these approaches and expand upon their findings, in this thesis we will employ a more powerful, exact method known as the Bethe Ansatz.

Originally developed by Bethe to study the XXX spin chain[16], Bethe Ansatz provides one with all the eigenstates and eigenvalues of a Hamiltonian which can then lead to a complete analytic description of the physics of the model. The list of models solvable

by Bethe Ansatz is now quite extensive. Some notable inclusions are the extensions to anisotropic chains like the XXZ[17], XYZ [18] and related vertex models[19, 20] as well as higher spin chains [21] and different symmetry groups like the $SU(N)$ chain[22]. Among some of the early works were solutions to continuum models like Lieb Liniger model[23, 24] and its extension to arbitrary symmetry, the Gaudin Yang model[25]. Later lattice models like the famous Hubbard [26] and $t-J$ [27, 28, 29] models were also solved. Following these quantum field theories were also shown to be amenable to the Bethe Ansatz treatment with solutions of the massive Thirring [30], Gross-Neveu [31] and Bukvostov-Lipatov models[32] appearing in quick succession. Later impurity models were also added to the list with some prominent successes being the solutions of the the Kondo [33, 34] and Anderson impurity models [35].

The list above includes both interacting models and quantum impurity models however up till this point the method has not been applied to genuine models of a quantum impurity coupled to an interacting environment, a Luttinger-impurity model. While there have been several Bethe Ansatz studies of impurity models with interacting bulks [36, 37, 38] they have either required additional unphysical bulk interaction terms, bizarre impurity couplings or do not allow for particle to change chirality. The impediment thus far has been an appropriate formulation of the Bethe ansatz which allows for bulk particles to interact with each other in a sensible way as well as with an impurity which may cause them to change chirality. In this thesis we introduce such a formulation and use it find exact solutions to a number of widely used Luttinger-impurity models. The exact solution provided by the method then allows us to study ground state and thermodynamic properties of the system.

The work presented herein has previously been reported in a number of papers written in collaboration with Prof. Natan Andrei:

- "*Quantum impurity in a Luttinger liquid: Exact solution of the Kane-Fisher model*", C. Rylands and N. Andrei, Phys. Rev. B94, 115142 (2016)

- "*Quantum dot at a Luttinger liquid edge*", C. Rylands and N. Andrei, Phys. Rev. B96, 115424 (2017)

- "*Quantum dot in interacting environments*", C. Rylands and N. Andrei, Phys. Rev. B97, 155426 (2018)

as well as the preprint "*Simplified thermodynamics for Quantum impurity models*", C. Rylands and N. Andrei, arXiv:1804.00726. These form the basis of Chapters 3-5.

The outline of this thesis is as follows: In chapter 2 we provide a brief introduction to some aspects of low dimensional physics and particularly Luttinger liquid theory. Following this we examine a number of quantum impurity models using the Bethe Ansatz method and introduce the concepts and basic calculations underpinning the method as well as set up our conventions and notations. We do this by examining the relatively simplistic resonant level model and then the more complex anisotropic Kondo model. In both cases we show how the eigenstates are constructed and determine the single particle energy levels. Using this information the ground state properties of the models as well as the basic excitations above this are studied. The Yang Yang approach to thermodynamics is also discussed and the free energy of both models is calculated. In the end we make some comments regarding calculations in quantum impurity models and also give a very short discussion of the interacting resonant level model which is closely related to the other two. The bulk of this chapter is review of known work and results.

In chapter 3 we implement the methods introduced in chapter 2 in a model of a quantum dot or resonant level coupled to the boundary of a Luttinger liquid. All eigenstates and eigenvalues of the model are found which allows us to calculate the ground state dot occupation and free energy. We find that the strongly correlated bulk causes a Kondo like effect to occur with the dot being fully hybridized with the bulk at low energy and decoupled at high energy. This occurs in the absence of any Kondo type interaction between the dot and bulk however by including such a term we see that the system remains strongly coupled at

low energy even in the ferromagnetic Kondo regime[39].

In chapter 4 a different type of impurity model is discussed. Here the impurity is placed in the bulk of the Luttinger liquid system and causes backscattering to occur. We exactly solve two models with impurities of this type, the Kane-Fisher model and the weak tunnelling model. To do this a new formulation of the Bethe Ansatz which can be applied to models of this type is introduced. Subsequently the eigenstates and eigenvalues of these models are found. Using these it is shown that the spectrum of the two models are related by changing the sign of the interaction. We then calculate the free energy and see that the repulsive Kane-Fisher model generates a strong coupling scale below which the system is split into two by the impurity. We calculate the impurity entropy along the RG flow and determine the dimensions of the leading relevant and irrelevant operators about the fixed points [40].

In the penultimate chapter we study two models which incorporate effects from the previous two chapters. They consist of Luttinger liquids coupled to quantum dots which cause backscattering and are arranged in a sidecoupled or embedded geometry. The two models are solved exactly using the methods developed in the previous chapter and it is seen that they similarly related to each other by changing the sign of the bulk interaction. We derive exact expressions for the dot occupation in the sidecoupled model at $T = 0$ and derive the free energy of the system also. We find that the dot becomes fully hybridized with the bulk at low energy for all values of the interaction considered and decoupled at high energy (a Kondo like effect). The hybridized dot acts like a backscattering impurity at low temperature which either enhances or suppresses the dot occupation depending on the sign of the bulk interaction (a Kane-Fisher effect) [41]. In the final chapter we summarize and discuss outstanding questions and future directions the work can take.

2

Low Dimensions, Quantum Impurity Models and Bethe Ansatz

2.1 Low dimensional physics

When a system is restricted to reside in only one spatial dimension a host of surprising and exotic physical phenomena can occur which have no analogue in higher dimensional systems. The list of such uniquely one dimensional phenomena is extensive and throughout the course of this thesis some of them, in particular those pertaining to quantum impurities, will be encountered.

The fact that there should be a plethora of physical phenomena unique to one dimensional quantum physics can be traced back to a very simple observation observation. If a collection of particles can only move in one spatial dimension then they either go left or right so they have no choice but to interact with each other. In comparison, when systems have a higher number of spatial dimensions in which to travel the likelihood of two particles crossing paths decreases see FIG. 1.2. In this higher dimensional scenario it is possible to adopt a Fermi liquid picture of quasiparticles. Starting from a free system the interactions can be turned on adiabatically and the excitations of the interacting system viewed as being perturbatively connected to the non interacting particles. In one dimension this is viewpoint is not possible. No matter how weak the interaction that is introduced the chiral nature of particle motion means that any excitation necessarily involves all particles. Each particle becomes strongly correlated with every other particle and the only excitations possible are collective ones. These collective excitations can be viewed as sound waves propagating in

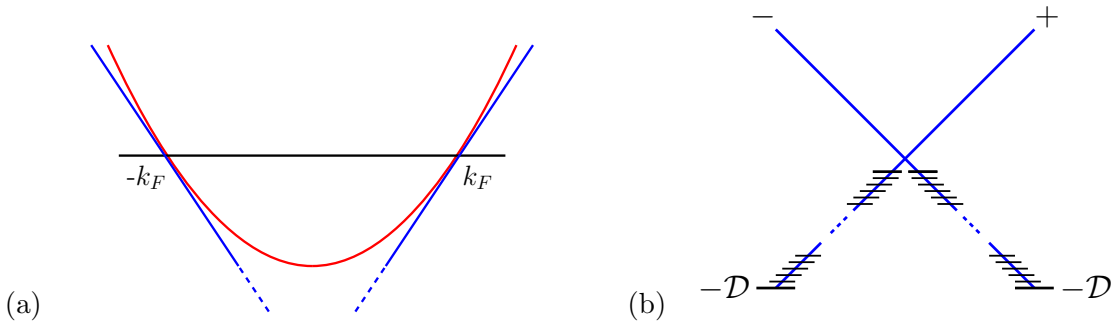

Figure 2.1: (a)A one dimensional system generically has two Fermi points around which the spectrum can be approximated as linear. (b) The low energy theory of such a system is a spinless Luttinger liquid which consists of two branches, one left moving (-) and one right moving (+). The figure depicts the energy levels of the ground state with energy being the vertical axis and k the horizontal. To render the theory finite a cutoff has been imposed.

a 1D quantum fluid. The consequences of this are the many fascinating observable effects unique to one dimensional systems.

To formalize these statements a little consider a system of noninteracting fermions in one dimension. The particles have a general dispersion relation $\epsilon(k)$ and are described by the Hamiltonian

$$H = \sum_k \epsilon(k) c_k^\dagger c_k \tag{2.1}$$

with $c_k^\dagger$ and c_k are fermion creation and annihilation operators with commutation relations $\{c_k^\dagger, c_q\} = \delta_{k,q}$. Typical dispersion relations are $\epsilon(k) = (v_F k)^2/2m$ for a continuum model of mass m particles or $\epsilon(k) = t\cos(v_F k)$ for a lattice system with hopping t and where v_F is the Fermi velocity. In a generic case the system has finite number of discrete Fermi *points* instead of an extended Fermi *surface* as would be expected in higher dimensional systems. For instance in the examples just cited there are only two Fermi points, located at $\pm k_F$ and in the region of these the dispersion is approximately linear, $\epsilon(k \pm k_F) \approx \pm v_F k$ see FIG. 3(a). At low energy one can expand around these points and neglect higher order terms so

that the system can be described by the Hamiltonian

$$H \approx \sum v_F k \left[\psi_+^\dagger(k)\psi_+(k) + \psi_-^\dagger(k)\psi_-(k)\right] \tag{2.2}$$

$$= -i\int \mathrm{d}x \left[\psi_+^\dagger(x)\partial_x\psi_+(x) - \psi_-^\dagger(x)\partial_x\psi_-(x)\right] \tag{2.3}$$

where $\psi_\pm^\dagger$ are fermionic operators which create particles around the right and left Fermi points which obey $\{\psi^\dagger(x), \psi(y)\} = \delta(x-y)$. These particles have a fixed chirality and are right moving, ψ_+ or left moving ψ_-, see FIG. 2.1 (b). An expansion around the Fermi points like this is not unique to 1D systems but in this case the reduction leaves a very simple Hamiltonian consisting of two distinct particle types. In addition to the kinetic part of the Hamiltonian, density-density interaction terms like

$$H_{\text{int}} = \sum_{k,q} V_{k,q} c_k^\dagger c_k c_q^\dagger c_q \tag{2.4}$$

can be treated in a similar fashion. Expanding the operators around the Fermi points, limiting ourselves to only short range interactions and ignoring Umklapp processes gives us the Luttinger liquid Hamiltonian[10]

$$H_{\text{LL}} = -i\int \mathrm{d}x \left[\psi_+^\dagger(x)\partial_x\psi_+(x) - \psi_-^\dagger(x)\partial_x\psi_-(x)\right] + 4g\int \mathrm{d}x\, \psi_+^\dagger(x)\psi_-^\dagger(x)\psi_-(x)\psi_+(x). \tag{2.5}$$

Where the only survivor of the interaction term is a point like interaction of strength $4g$ between particles of different chiralities. A remarkable feature of this low energy Hamiltonian is that it is Lorentz invariant which not only has implications for the dynamics of the system but also provides a pleasing symmetry between the long and short wavelength descriptions of 1D systems[1]. This spinless Hamiltonian will form the bulk of the models which

[1] By measuring the system with high enough energy or at short enough length scales directions transverse to the 1D system will be exposed. Electrons in this 3D system are ultimately governed by the Dirac equation which is also Lorentz invariant.

we will study in future chapters and as alluded to already has some surprising features when compared to its higher dimensional counterpart, the Fermi Liquid. The strong correlations amongst the particles dissolve the individual fermions, $\psi_\pm$ and the excitations of the system are instead bosonic density perturbations or sound waves. Although it is possible to exactly resum perturbation theory[42] for this model and see these effects they can be understood more clearly by utilizing the bosonized description of the Luttinger liquid [43, 11].

Bosonization maps the fermions appearing in the above Hamiltonian to bosonic operators described by the equivalent Hamiltonian [10]

$$H_{LL} = \frac{u_F}{2\pi} \int \mathrm{d}x\, K \left[\nabla\varphi(x)\right]^2 + \frac{1}{K} \left[\Pi(x)\right]^2 \tag{2.6}$$

where $\nabla\varphi(x)$ and $\Pi(x)$ are conjugate boson fields related to the density and current of the fermions

$$\nabla\varphi(x) = -\frac{1}{\pi}\left[\psi_+^\dagger(x)\psi_+(x) + \psi_-^\dagger(x)\psi_-(x)\right] \tag{2.7}$$

$$\Pi(x) = \psi_+^\dagger(x)\psi_+(x) - \psi_-^\dagger(x)\psi_-(x). \tag{2.8}$$

Here u_F is the renormalized Fermi velocity and K is the Luttinger parameter which is related to the interaction strength $K \approx 1 - 2g/\pi$. In this notation $K = 1$ are non interacting fermions, $K < 1$ indicates repulsive interactions and $K > 1$ attractive interactions. Note that in bosonic form the Hamiltonian is quadratic and its thermodynamics and correlation functions can be calculated exactly. Using this one can then check that provided $K \neq 1$ the quasiparticle weight of the fermions vanishes meaning that such a description is no longer valid. More explicitly it can be shown that the zero temperature occupation of the ψ_+ fermions is[10]

$$n(k) \sim |k - k_F|^{\frac{K}{2} + \frac{2}{K} - 1} \tag{2.9}$$

which exhibits a power law singularity at $k = k_F$ indicating an absence of fermionic quasi-particles from the spectrum.

Spin may also be included in the analysis which allows for more general interactions. Possible additions to the Hamiltonian are

$$H_{\parallel} = 4g_{\parallel} \sum_{\sigma=\uparrow,\downarrow} \int \mathrm{d}x\, \psi^{\dagger}_{\sigma,+}(x)\psi^{\dagger}_{\sigma,-}(x)\psi^{\dagger}(x)_{\sigma,-}\psi^{\dagger}_{\sigma,+}(x) \tag{2.10}$$

$$H_{\perp} = 4g_{\perp} \sum_{\sigma\neq\bar{\sigma}} \int \mathrm{d}x\, \psi^{\dagger}_{\sigma,+}(x)\psi^{\dagger}_{\bar{\sigma},-}(x)\psi^{\dagger}(x)_{\bar{\sigma},-}\psi^{\dagger}_{\sigma,+}(x) \tag{2.11}$$

where the first term is the interaction between parallel spins and the second is between anti parallel spins. The spinful Hamiltonian may be bosonized using an identical procedure. Upon doing this one obtains two copies of the bosonic theory, one describing the spin degrees of freedom through $\varphi_s = (\varphi_\uparrow - \varphi_\downarrow)/\sqrt{2}$ and characterized by K_s and the other describing the charge through $\varphi_c = (\varphi_\uparrow + \varphi_\downarrow)/\sqrt{2}$ and characterized by K_c. This decoupling of the spin and charge degrees of freedom is known as spin-charge separation and is one of the more notable predictions of the theory. Not only have the fermions been dissolved to form a bosonic fluid but their charge and spin properties have been disassociated from each other and moreover the excitations of spin and charge fluids are characterized by different Luttinger parameters and velocities. In the remainder of the thesis we will not discuss models with spin and deal predominantly with the fermionic description however any discussion of 1D systems would be deficient without mentioning spin-charge separation and bosonization.

Luttinger liquids provide the low energy effective description of many one dimensional systems quantum systems. At one point this may have been seen as a purely academic statement however since the early 90's 1D systems have been realized in a number of experimental settings including quantum wires, edge states of fractional quantum hall materials and more recently cold atomic gases to name a few.

There are many different types and construction methods for quantum wires however a typical method is to layer GaAs and AlGaAs sheets so as to form a 2 dimensional electron

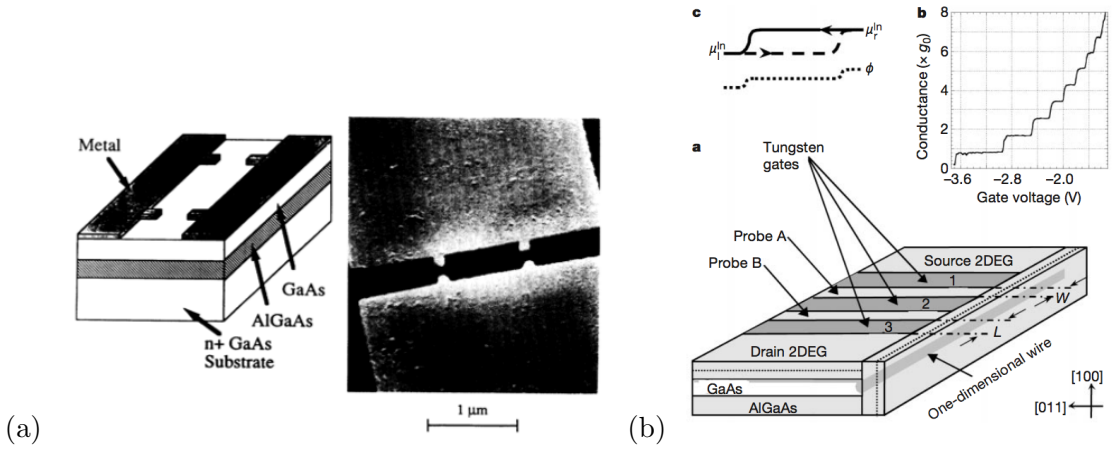

Figure 2.2: Two types of quantum wire constructed using Layered GaAs and AlGaAs. (a) An early example of this method uses electrodes to form a 1D wire in the centre of the sample. To the right is a scanning electron microscope image of the device. Image taken from [44]. (b) On the right a more recent construction method known as cleaved edge overgrowth is depicted. In this setup the electrodes create the wire at the edge of the sample The multiple probes allow for different conductance measurements to be made. Image taken from [45].

gas[44, 46, 45]. Then using either lithography or attaching electrodes and applying a potential the 2D gas can be restricted to a narrow region, see FIG. 2.2. If the energy gap of the transverse modes is larger than the temperature and an external gate is used to tune the chemical potential so that only the lowest band is occupied then the result is a 1D system whose transport properties conform to Luttinger liquid theory.

Another type of quantum wire and classic realization of Luttinger liquid behavior is through single walled, carbon nanotubes (CNT). These are sheets of graphene that have

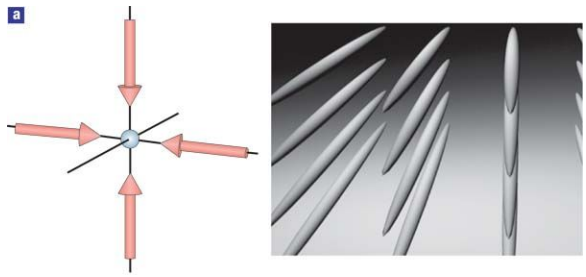

Figure 2.3: In cold atom gas experiments neutral atoms are cooled to nK temperatures and confined using counter propagating lasers. By using lasers in two directions the particles can propagate in one direction only. Image taken from [47]

been rolled into tubes[48]. Depending on the orientation of the sheet way on which the sheet the nanotubes ranging from metallic to insulator however for short CNTs at low temperatures Luttinger liquid physics is found. By attaching the CNT to leads via bad contacts one can measure the transport properties of the nanotubes [49]. The results of these experiments are in agreement with a liquid charachterized by $K \approx 0.22$. CNTs are particularly nice examples of a Luttinger liquid as one study the effects of an impurity which can be realized by kink in the tube. We shall discuss this further in later chapters.

The edges of fractional quantum Hall systems are known to support chiral edge modes [50][51][52]. These are distinct from the interacting left and right movers of (2.5) since the left and right movers lie on opposite edges of a sample and so cannot interact locally. Nevertheless they admit a hydrodynamic description, (3.7) with $K = 1/m$, m being the filling factor of the material. Again impurities can be engineered into such systems. For example using lithography to oppositely moving edges can be brought close enough to each to cause backscattering. We discuss this further in chapter 4.

A more recent experimental realization of 1D systems is through cold atomic gas experiments [53][54][55][47]. Using a combination of cooling techniques, neutral atoms can be cooled to nK temperatures. These can then be constrained using optical lattices and magnetic traps to an array of different geometries including one dimensional tubes, see FIG. 2.3. The rapid advancement in the experimental techniques has lead to extraordinary control, precision and tunability of cold atom experiments. The number and type of particle can all be varied and moreover the interaction strength between them can be tuned by Feschbach resonance. A wide variety of different 1D systems with tunable parameters can be created using these methods with Luttinger liquid theory providing a description of the low energy behavior.

Other less prominent realizations of Luttinger liquids include, some SrCuO compounds in which spin-charge separation has been observed[56], ^{4}He flowing through nano pores [57][58], Fermi liquid leads with dissipative contacts [59, 60] or through a quantum simulator

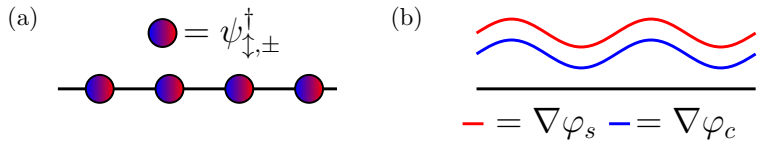

Figure 2.4: Spin charge separation. Non interaction fermions in one dimension or interacting fermions in higher dimensions may have spin and charge as intrinsic properties. If interactions are introduced between the fermions in one dimension however the the fermions are dissolved and the system is described by two decoupled Luttinger liquids formed of the spin and charge degrees of freedom.

consisting of a chain large numbers of Josephson junctions[61, 62]. The last two of these is again of particular interest as one is not only able to engineer different values of the Luttinger parameter but also couple it to impurities. The realization using impurities will be discussed later.

2.2 Quantum impurities and Bethe Ansatz

Quantum impurity models are ubiquitous throughout physics describing many experimental systems, from quantum dots coupled to electronic leads [63, 64, 65] and kinks in carbon nanotubes [66] to isolated atoms in wave guides to name but a few [67]. Impurity systems consist of a bath of particles, free or interacting, coupled to a small localized system of few degrees of freedom, the impurity. Their apparent simplicity often belies the intricate strong correlation physics that is at play. Examples include the Kondo model [68, 69] where the bath is a non interacting Fermi liquid and the impurity is a single isolated spin or the Kane-Fisher model [12] where the bath consists of a 1D gas of interacting fermions and the impurity is a featureless localized potential which causes backscattering. Such systems can also provide insight to the more complicated problems such as heavy fermion systems [9] or other correlated systems through the use of dynamical mean field theory [70].

Many QIMs, in particular the examples cited above, are in fact exactly solvable through Bethe Ansatz [68, 69, 40]. Here we will review the main concepts of the Bethe Ansatz

method as it applies to QIMs. We study two models here, the resonant level model and the anisotropic Kondo model and apart from providing an introduction to the formalism and allow us to introduce our conventions, the results we derive will serve as good benchmarks with which to examine the results of the forthcoming chapters.

2.2.1 The Resonant level model

Perhaps the simplest quantum impurity model is the resonant level (RL) model. The Hamiltonian is given by

$$H = \int -i\psi^\dagger(x)\partial_x\psi(x) + t\left[\psi^\dagger(0)d + d^\dagger\psi(0)\right] + \epsilon_0 d^\dagger d\,. \tag{2.12}$$

It describes a system of right moving fermions coupled to a localized level on which either zero or one fermion may reside. The operators $\psi^\dagger(x)$ and $\psi(x)$ are the creation and annihilation operators of a right moving fermion at position x while $d^\dagger$ and d create and destroy fermions on the level. The right movers are said to be part of the bulk system however throughout this thesis they may be referred to as being lead or bath fermions also. The resonant level is the impurity part of the system but will also be referred to as the dot part as it provides a simplified description of a quantum dot. The two systems, bulk and dot are coupled via a tunnelling term which allows bulk fermions to hop onto the dot and vice versa. This simple model may describe the interaction of a quantum dot with a one dimensional wire provided there are no bulk fermion-fermion interactions or a dot coupled to higher dimensional Fermi liquid leads, in which case the right movers represent the incoming and outgoing spin polarized, s-wave electrons and the electron-electron interactions can be ignored.

The RL model is integrable and its eigenstates, spectrum and thermodynamic properties are well known. Although there are a number of methods that can be used on this simple model, herein these properties will be derived using Bethe Ansatz. This non perturbative

and exact method is a powerful tool in studying one-dimensional or quasi one-dimensional models. The method is very systematic and follows several main steps which we will go through now. Firstly, one writes down the most general single particle eigenstate allowable by the symmetries of the model. Typically this takes the form of a plane wave expansion whose coefficients depend upon the region of configuration space. In the RL model the most general state is given by

$$|k\rangle = \int e^{ikx} f(x,k)\psi^\dagger(x)\,|0\rangle + Bd^\dagger\,|0\rangle \tag{2.13}$$

where $f(x,k)$ and B are the bulk and impurity parts of the wavefunction and $|0\rangle$ is the vacuum state containing no particles, $\psi(x)\,|0\rangle = 0$. For this to be an eigenstate of (2.12), f and B must satisfy the associated Schrödinger equations. Applying the Hamiltonian to $|k\rangle$ and integrating by parts we find it is an eigenstate of energy k provided

$$-i\partial_x f(x,k) + t\delta(x)B = 0 \tag{2.14}$$

$$tf(0) + \epsilon_0 B = kB \tag{2.15}$$

The solution of these equations is found without too much difficulty by writing the bulk part as a sum of Heaviside functions, $f(x) = A^{[10]}\theta(-x) + A^{[01]}\theta(x)$ and determining the amplitudes. The result is that the single particle eigenstate of the RL model is

$$|k\rangle = \int e^{ikx}\left[\theta(-x) + \frac{k-\epsilon_0-i\Gamma}{k-\epsilon_0+i\Gamma}\theta(x)\right]\psi^\dagger(x)\,|0\rangle + \frac{t/2}{k-\epsilon_0+i\Gamma}d^\dagger\,|0\rangle \tag{2.16}$$

where $\Gamma = t^2/2$ is called the hybridization or the level width. In deriving this we have used the fact that $\partial_x\theta(x) = \delta(x)$ and $\theta(x)\delta(x) = \frac{1}{2}\delta(x)$ which will be used throughout this thesis. The above state is not normalized but this may be done easily enough and d following this it can be checked that states of this form a complete basis of single particle states. The next step in the Bethe ansatz method is to write down the most general two particle state,

apply the Hamiltonian to that and solve the resulting Schrödinger equations. If the model is intergable then knowing the two particle eigenstate is in general sufficient to construct the N-particle state. We will comment more on this in the next section however in the present circumstances this is unnecessary as the model is actually non interacting and multiparticle eigenstates are merely products of single particle states. It can be checked by applying the Hamiltonian that

$$\begin{aligned}\left|\vec{k}\right\rangle &= \int \prod_{j=1}^{N} \mathrm{d}x_j \, e^{ik_j x_j} f(x_j, k_j) \psi^\dagger(x_j) \left|0\right\rangle \\ &\quad + \sum_{l=1}^{N} (-1)^l \left[\int \prod_{j\neq l}^{N} \mathrm{d}x_j \, e^{ik_j x_j} f(x_j, k_j) \psi^\dagger(x_j) \right] \frac{t/2}{k_l - \epsilon_0 + i\Gamma} d^\dagger \left|0\right\rangle \end{aligned} \tag{2.17}$$

is an eigenstate with energy $E = \sum_j^N k_j$. In verifying this one needs to remember that $\psi^\dagger$ are fermions and that the N-particle wavefunction is anti-symmetrized. Indeed we note that the Hamiltonian, (2.12) with ψ being bosonic is the Dicke model which is fully interacting, quantum impurity model whose multiparticle states are not products as they are here [71]. This completes the construction of the eigenstates of the RL model on the infinite line.

The next step is to determine the spectrum which we do in the standard manner of quantum theory by restricting the system to be of size L and imposing some kind of boundary conditions. Here periodic boundary conditions will be used as they are most convenient but we will encounter other types in future chapters. In terms of the bulk operators this condition is $\psi^\dagger(x + L) = \psi^\dagger(x)$. The single particle energies are then quantized according to

$$e^{-ik_j L/2} = \frac{k_j - \epsilon_0 - i\Gamma}{k_j - \epsilon_0 + i\Gamma} e^{ik_j L/2} \tag{2.18}$$

or rather

$$e^{-ik_j L} = \frac{k_j - \epsilon_0 - i\Gamma}{k_j - \epsilon_0 + i\Gamma} \tag{2.19}$$

The interpretation of this is that a single particle travelling around the system acquires a phase shift, the $\frac{k_j-\epsilon_0-i\Gamma}{k_j-\epsilon_0+i\Gamma}$ term due to moving past the impurity. At the point $x = L/2$ it also has a phase due to the plane wave part of $e^{ik_jL/2}$. The wavefunction must then be equal to that at $x = -L/2$ which has not scattered past the impurity but has a total phase of $e^{-ik_jL/2}$. The resulting equations, (2.19) are known as the Bethe Ansatz equations (BAE) or simply Bethe equations. We will encounter BAE again and again throughout this thesis and see that (2.19) are a particularly simple example. Since the model is non interacting, the single particle energies are not coupled. In forthcoming interacting models this will not be the case.

Taking the log of the Bethe equations and rearranging a bit the single particle energy is seen to satisfy

$$k_j = \frac{2\pi}{L} n_j + \frac{2}{L} \arctan\left[\frac{\Gamma}{k_j - \epsilon_0}\right] \tag{2.20}$$

where n_j are integers which are the quantum numbers of the state and must all be distinct to have a non vanishing wavefunction. The form of this equation and the interpretation is fairly transparent, the single particle energy is given by a bulk term, $2\pi/L$ times an integer which is then shifted by the phase shift the particle acquires when going past the impurity. The same basic form will also hold in more complicated impurity models wherein the excitations and impurity phase shift become dressed. This will allow us to determine the physical impurity phase shift in those models.

At this point we must discuss some issues when dealing with models which have a linear dispersion. As Dirac pointed out in the early days of quantum theory Hamiltonians with linear dispersion relations like the RL model and others which will be considered in future chapters are unbounded from below. In order to construct physical states one must first fill the empty vacuum $|0\rangle$ with negative energy particles from some cutoff, which we denote -$\mathcal{K}$ up to the Fermi level. This will give the ground state, on top of which holes or particles

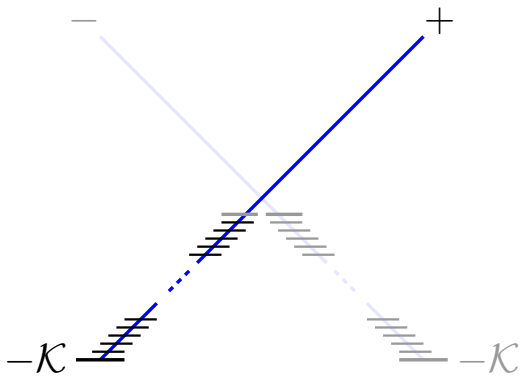

Figure 2.5: The linear spectrum of the RL model requires that we impose a cutoff on the single particle energy of $-\mathcal{K} = -2\pi N/L$. The ground state is the constructed by filling the vacuum with negative energy particles from the cutoff up to the Fermi level. In the RL model there is only a single branch of right movers as opposed to the two branches of the Luttinger liquid.

can be added to get the rest of the Hilbert space. Any calculation can be performed in the presence of this cutoff however if we wish to get expressions independent of the cutoff scheme we have used it should be removed, i.e $\mathcal{K} \to \infty$. To implement this in the RL model the number of particles is taken to be N and the cutoff to be $\mathcal{K} = 2\pi N/L$. Filling up the negative energy particles by taking n_j to be negative integers such that $n_j = -N, \ldots, -1$ gives the ground state, see FIG. 2.5. In the thermodynamic limit it is better to work with k_j rather than the discrete quantum numbers n_j. To this end note that the distance between adjacent single particle energies in the ground state is

$$k_{j+1} - k_j = \frac{2\pi}{L} + \frac{2}{L}\left(\arctan\left[\frac{\Gamma}{k_{j+1} - \epsilon_0}\right] - \arctan\left[\frac{\Gamma}{k_j - \epsilon_0}\right]\right) \tag{2.21}$$

In the limit of large system size $k_{j+1} - k_j$ vanishes as $1/L$ and we can derive a continuous distribution for them, i.e the single particle density of states. Defining this by

$$\rho = \lim_{L\to\infty} \frac{1}{L}\frac{n_{j+1} - n_j}{k_{j+1} - k_j}, \tag{2.22}$$

the resonant level model density of states is

$$\rho(k) = \frac{1}{2\pi} + \frac{1}{\pi L}\frac{\Gamma}{(k-\epsilon_0)^2+\Gamma^2} \tag{2.23}$$

for $-\mathcal{K} < k < 0$ while when $k > 0$, $\rho(k) = 0$. The form of this expression, a sum of two distinct terms is a common feature of QIMs. The first term is the standard one dimensional density of states and is the contribution coming form the bulk fermions. The second term is the modification due to the presence of the impurity, it depends explicitly on the dot parameters and is of the order $1/L$ smaller than the bulk. In more complicated models the impurity term will be identified by depending on some impurity parameter and it being an order $1/L$ or $1/N$ term. This procedure to derive the density and in particular the definition (2.22) will feature prominently in other analyses. In the interacting models which will be studied however the coupling between different single particle energies will result in an integral equation to determine the density.

Using this the ground state energy density of the system is given by

$$E_{\rm gs}/L = \frac{1}{L}\sum_j^N k_j \tag{2.24}$$

$$= \int_{-\mathcal{K}}^0 \mathrm{d}k\, \rho(k)k \tag{2.25}$$

It is typical to consider separately the bulk and impurity/dot parts of the density by writing $\rho(k) = \rho_{\rm b}(k) + \rho_{\rm d}(k)/L$ with the dot part naturally being the second term in (2.23). The dot contribution to the energy is then obtained by integrating over the dot density of states only $E_{\rm d} = \int \rho_{\rm d}(k)k$ which predominantly receives contributions from energies resonant with the dot energy $k \sim \epsilon_0$.

A quantity of interest when studying models of this kind is the occupation or charge of the dot in the ground state, $n_d = \langle d^\dagger d\rangle$ which can be measured in an experimental system by means of a quantum point contact [72]. There are a number of ways one may obtain this

which are equivalent. The first is by integrating over the dot density of states $n_d = \int \rho_{\rm d}(k)$ while the second is via the Hellmann-Feynmann theorem which tell us that

$$n_d = \frac{\partial E_{\rm gs}}{\partial \epsilon_0} = \int_{-\mathcal{K}}^{0} {\rm d}k\, k \frac{\partial \rho_{\rm d}(k)}{\partial \epsilon_0}. \tag{2.26}$$

Using the fact that $\frac{\partial \rho_{\rm d}(k)}{\partial \epsilon_0} = -\frac{\partial \rho_{\rm d}(k)}{\partial k}$ and integrating by parts one can see that these two ways are indeed equivalent. An additional method to calculate this quantity which works in the thermodynamic limit is to return to the Behte equation, (2.20) and sum over all particles,

$$E = \sum_j^N k_j = \frac{2\pi}{L}\sum_j^N n_j + \frac{2}{L}\sum_j^N \arctan\left[\frac{\Gamma}{k_j - \epsilon_0}\right] \tag{2.27}$$

The second sum is the dot contribution to the energy which in thermodynamic limit can be turned into an integral. When doing this, only the bulk part of the density of states is required as only this will contribute for $L \to \infty$. The dot occupation is therefore given by

$$n_{\rm d} = \frac{\partial}{\partial \epsilon_0}\int_{-\mathcal{K}}^{0} \frac{{\rm d}k}{2\pi} \arctan\left[\frac{\Gamma}{k - \epsilon_0}\right] \tag{2.28}$$

which also gives the same answer. Nevertheless, in more complicated scenarios it may be more convenient to use one method over another. We close this discussion of the ground state by noting that one may safely remove the cutoff in any expression concerning the dot without suffering any divergences as the dot density of states is sharply peaked about $k \sim \epsilon_0$ and goes to zero at $k \to \pm\infty$. For the ground state dot occupation we get

$$n_d = \int_{-\infty}^{0} \frac{{\rm d}k}{\pi} \frac{\Gamma}{(k-\epsilon_0)^2 + \Gamma^2} \tag{2.29}$$

$$= \frac{1}{2} - \frac{1}{\pi}\arctan\left(\frac{\epsilon_0}{\Gamma}\right) \tag{2.30}$$

Any bulk quantity will still depend upon the cutoff however this is not always the case in

QIMs. We will comment more on this expression below but for the moment we note that the it is a function of ϵ_0/Γ and that in addition to being the coupling constant of the theory it also sets a scale with respect to which all energies are measured.

The excitations above the ground state can be obtained by adding further electrons above the Fermi surface, $k = 0$ which add $2\pi n/L$ to the energy of the system. Alternatively one can introduce a hole to the ground state distribution so that $n_{j+1} - n_j > 1$ for some j. In the presence of this excitation the density of states is similar to (2.23) but with the hole subtracted,

$$\rho(k) = \frac{1}{2\pi} - \delta(k - k_{\rm h}) + \frac{1}{\pi L}\frac{\Gamma}{(k-\epsilon_0)^2 + \Gamma^2} \tag{2.31}$$

where $k_{\rm h} < 0$. Integrating this with k the total energy is now $E = E_{gs} + |k_{\rm h}|$. Extra holes contribute additively to the energy in the same way. If there are a macroscopic number of holes the density of states of the particles and holes can be described by continuous distributions, $\rho(k)$, $\rho^{\rm h}(k)$ which satisfies

$$\rho(k) + \rho^{\rm h}(k) = \frac{1}{2\pi} + \frac{1}{\pi L}\frac{\Gamma}{(k-\epsilon_0)^2 + \Gamma^2}. \tag{2.32}$$

Note that a single hole corresponds to $\rho^{\rm h}(k) = \delta(k - k_{\rm h})$, in agreement with our previous statement. The energy associated to this is then given by integrating over the particle density, $\int k\rho(k) = E_{\rm gs} - \int k\rho^{\rm h}(k)$.

We turn now to study the thermodynamic properties of the system and in particular the finite temperature dot occupation. To begin we write down the partition function of the theory

$$Z \;=\; {\rm Tr} e^{-\beta H} = \sum_{\{n_j\}} e^{-\beta E(\{n_j\})} \tag{2.33}$$

where the sum is over all different energy eigenstates which are labelled by the set of

quantum numbers $n_j, j = 1 \ldots N$. In the thermodynamic limit the description of the states in terms of n_j can be exchanged for one in terms of $\rho(k)$ and $\rho^{\mathrm{h}}(k)$. The partition function is then written as a functional integral over these densities

$$Z = \int \mathcal{D}[\rho]\mathcal{D}[\rho^{\mathrm{h}}] e^{-\beta(E-TS)} \tag{2.34}$$

with E being the energy of a particular particle hole configuration, T the temperature and S the entropy associated to this configuration. This entropy is known as the Yang-Yang entropy, it counts the number of microstates, labelled by a particular configuration of integers n_j, that are associated to a single macrostate given by the densities $\rho(k),\ \rho^{\mathrm{h}}(k)$[73]. To calculate it consider a small segment of the k line of size $\mathrm{d}k$ over which ρ and ρ^{h} are approximately constant. Within this region the number of available integers is given by $\big(\rho(k) + \rho^{\mathrm{h}}(k)\big)\,\mathrm{d}k$, of those $\rho^{\mathrm{h}}(k)\mathrm{d}k$ are filled while $\rho^{\mathrm{h}}(k)\mathrm{d}k$ are empty. The total number of configurations is

$$\frac{\big[L\,\big(\rho(k) + \rho^{\mathrm{h}}(k)\big)\,\mathrm{d}k\big]!}{[L\rho(k)\mathrm{d}k]!\,[L\rho^{\mathrm{h}}(k)\mathrm{d}k]!}. \tag{2.35}$$

This means that the entropy within this region, $\mathrm{d}S$ is given by

$$\begin{aligned} \mathrm{d}S &= \log \frac{\big[\big(\rho(k) + \rho^{\mathrm{h}}(k)\big)\,\mathrm{d}k\big]!}{[\rho(k)\mathrm{d}k]!\,[\rho^{\mathrm{h}}(k)\mathrm{d}k]!} && (2.36)\\ &\approx L\mathrm{d}k\big\{\rho(k)\log\left[1+\eta(k)\right] + \rho^{\mathrm{h}}(k)\log\left[1+\eta^{-1}(k)\right]\big\}. && (2.37) \end{aligned}$$

In going to the second line we have employed Stirling's approximation. The total entropy density is therefore obtained by integrating this over all k,

$$S/L = \int \mathrm{d}k\rho(k)\log\left[1+\eta(k)\right] + \rho^{\mathrm{h}}(k)\log\left[1+\eta^{-1}(k)\right] \tag{2.38}$$

where $\eta = \rho(k)/\rho^{\mathrm{h}}(k)$. Once this is inserted into the partition function the functional

integrals can be evaluated by the stationary phase approximation. The result is that, Z is determined by the extremum of the functional $F = E - TS$

$$F/L = \int \mathrm{d}k\, k\, \rho(k) - T\Big\{\rho(k)\log\left[1+\eta(k)\right] + \rho^{\mathrm{h}}(k)\log\left[1+\eta^{-1}(k)\right]\Big\}. \tag{2.39}$$

Varying F with respect to the densities gives

$$\delta F/L = \int \mathrm{d}k\, k\, \delta\rho - T\Big\{\delta\rho\log\left[1+\eta(k)\right] + \delta\rho^{\mathrm{h}}(k)\log\left[1+\eta^{-1}(k)\right]\Big\}. \tag{2.40}$$

However since removing a particle is the same as adding a hole, the particle and hole distributions are not independent. By using (2.32) and varying with respect to the densities the dependence is found to be $\delta\rho = -\delta\rho^{\mathrm{h}}$. Plugging this into the above expression and setting $\delta F = 0$ then gives the the minimization condition

$$\eta(k) = e^{\frac{k}{T}}. \tag{2.41}$$

This equation is known as the Thermodynamic Bethe Ansatz (TBA) equation. It is particularly simple in this model but we will see later it becomes much more complicated in interacting models although the procedure to derive it is exactly the same as here. The interpretation of the TBA will be the same in interacting models also, for example the combination $T\log(\eta)$ gives the excitation energy of the system which can be readily seen in this case. Evaluating the functional F at its minimum gives the free energy of the model. After some algebra using (2.32) we find that the free energy density of the RL model is

$$F/L = -T\int \frac{\mathrm{d}k}{2\pi}\log\left[1+e^{-\frac{k}{T}}\right] - \frac{T}{L}\int\frac{\mathrm{d}k}{\pi}\frac{\Gamma}{(k-\epsilon_0)^2+\Gamma^2}\log\left[1+e^{-\frac{k}{T}}\right]. \tag{2.42}$$

What is seen here is a common feature of Bethe ansatz impurity models. The free energy, just like the ground state energy has split into two parts. The first is the bulk contribution and is exactly the free energy of a one dimensional, chiral Fermion gas. The second is

the free energy contribution due to the dot. Like before we identify it as it is order $1/L$ smaller than the bulk contribution and explicitly depends upon the impurity parameters. It takes a natural form, the quantity $\log\left[1+e^{-\frac{k}{T}}\right]$ is integrated with the dot density of states. It will be seen that this form is maintained even in interacting case although the TBA equations are more complicated meaning that the $e^{-\frac{k}{T}}$ term is replaced by a more complicated expression that is not always analytically known in closed form. We note here that the bulk term still requires a cutoff to be imposed by limiting the integration to be in the region, $-\mathcal{K} < k$ but due to the properties of the dot density of states it can be removed in the dot part. The dot contribution to the free energy density is therefore

$$f_{\mathrm{d}} = -T\int_{-\infty}^{\infty}\frac{\mathrm{d}k}{\pi}\frac{\Gamma}{(k-\epsilon_0)^2+\Gamma^2}\log\left[1+e^{-\frac{k}{T}}\right] \tag{2.43}$$

The Hellmann-Feynmann can then be used again so that differentiating this with respect to the dot energy gives the finite temperature dot occupation. After using $\partial_k = -\partial_{\epsilon_0}$ and integrating by parts we see it is merely given by the density of states of the dot integrated with the Fermi function

$$n_{\mathrm{d}} = \int_{-\infty}^{\infty}\frac{\mathrm{d}k}{\pi}\frac{\Gamma}{(k-\epsilon_0)^2+\Gamma^2}\frac{1}{1+e^{\frac{k}{T}}} \tag{2.44}$$

Again a similar expression will be found in interacting case also but with the Fermi function replaced by a more complicated distribution. In the zero temperature limit the Fermi function becomes a Heaviside function and we reproduce our ground state calculation.

Let us now examine our expression for the dot occupation and use it to determine the overall behaviour of the system. At high temperature, $T \gg \Gamma$ the free energy of the dot is found to be $f_{\mathrm{d}} = -T\log(2)$ which is the free energy of a two level system. This indicates that at high temperature the system is weakly coupled. It can be considered a decoupled two level system and a chiral Fermi gas. At low temperature the free energy vanishes indicating that the dot is delocalized or in other words is fully hybridized with the dot. We can check

this against the dot occupation which at high temperature is either $n_d = 0, 1$ depending on the value of ϵ_0 while at low temperature it is fixed to be $n_d = 1/2$ (for $\epsilon_0 = 0$). The same picture holds also if the relevant energy is ϵ_0 rather than temperature. Returning to the ground state expression we see that at low energy $\epsilon_0 \ll \Gamma$ the occupation is $1/2$ while at $\pm\epsilon_0 \gg \Gamma$ is is either 0 or 1. Note that here the quantity Γ has two meanings it is both the coupling constant of the theory and the scale with respect to which one measures the energy. In this light it is perhaps tautological to state that in the high temperature regime system is weakly coupled since $\Gamma \ll T$ defines this regime and similarly in the low temperature, strong coupling regime. As we move on to more complicated models however, similar statements will become less obvious and we can refer back to the intuition developed here.

2.2.2 Anisotropic Kondo Model

In this section we move on to a much more complicated and important model, the anisotropic Kondo model (AKM). The AKM is the archetypal quantum impurity model exhibiting many features common to QIMs such as asymptotic freedom, running coupling constants and spin-charge separation. The basic format of the last section will be followed here also, the eigenstates will be constructed, the ground state and its properties determined after which the finite temperture behavior is studied.

The Hamiltonian is

$$\begin{aligned} H = -i \sum_{a=\uparrow\downarrow} \int \psi_a^\dagger(x)\partial_x\psi_a(x) + J_\parallel \psi_a^\dagger(0)\psi_a^\dagger(0)\sigma_{aa}^z\sigma_0^z \\ + J_\perp \left(\psi_\uparrow^\dagger(0)\psi_\downarrow^\dagger(0)\sigma_0^+ + \psi_\downarrow^\dagger(0)\psi_\uparrow^\dagger(0)\sigma_0^-\right). \end{aligned} \tag{2.45}$$

where $\psi_a^\dagger(x)$ are right moving fermions with spin $a = \uparrow, \downarrow$ coupled via exchange interaction to a localized magnetic impurity at the origin described by the Pauli matrices $\vec{\sigma}_0$. It describes a free, chiral Fermi gas interacting with a magnetic impurity at the origin. Unlike the RL

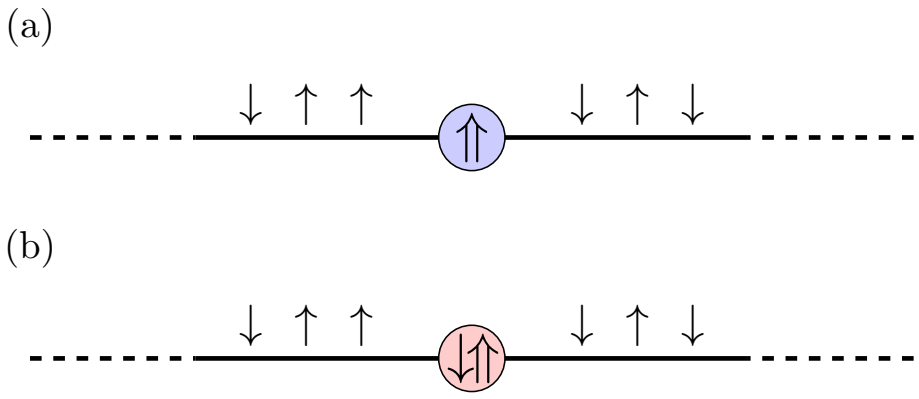

Figure 2.6: The anisotropic Kondo model describes a single impurity spin at the origin interacting via spin exchange with a bath of fermions. In (a) we depict the bath as a non interacting one dimensional wire. Alternatively the bath can be a higher dimensional Fermi liquid with $\psi^\dagger_{\uparrow,\downarrow}$ describing the radial part of s-wave electrons. In this perspective fermions to the left of the impurity are incoming and those to the right being outgoing. (b) At low temperature the impurity spin is screened by the bulk becoming a singlet. This is often depicted as being formed from a single bulk particle and the impurity spin as we do here but is actually a highly non trivial many body effect.

model the system is not spin polarized and the bulk fermions may exchange their spin with the impurity. In this form and in slightly modified versions it is perhaps the most studied and cited model in condensed matter physics. The physics of the Kondo model is encountered in almost every area of the field from heavy fermions [9] and topological materials[74] to quantum dots[64, 63] and AMO systems [75, 76]. It has been studied using using a plethora of different techniques both numerical and analytic and has been the proving ground for some fundamental approaches like Anderson's scaling theory[77], Wilson's renormalization group [78] and the Bethe Ansatz[68, 69].

The Hamiltonian presented here can be used as an effective description of dilute magnetic impurities inside a metal, in which case chiral fermions represent incoming and outgoing s-waves scattering off the impurity. Alternatively it could be realized as a quantum dot coupled to a 2-dimensional Fermi liquid leads, where the quantum dot has been tuned so

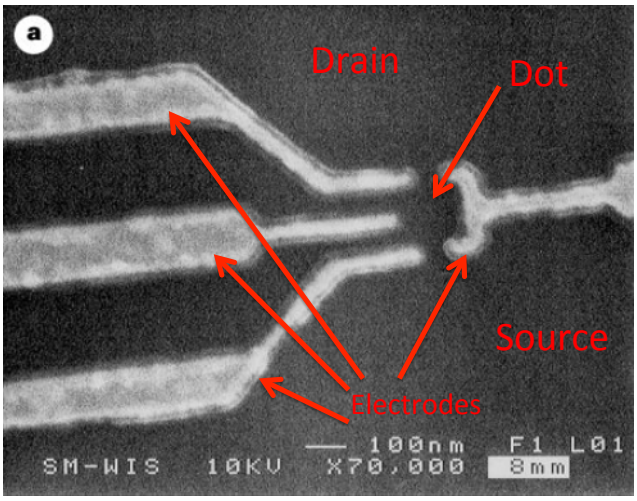

Figure 2.7: A scanning electron microscope image of a quantum dot system described by the Kondo model. A two dimensional electron gas is formed using layered GaAs and AlAs onto which elctorde are deposited. The electrodes deplete the gas below them forming two regions, the source and drain, separated by a small island. This island forms a quantum dot with discrete energy levels. Tunnelling to and from the dot is controlled by the middle electrodes on the left. Transport measurements through the system exhibit Kondo physics. Image adapted from [64]

that the electron number on the dot does not change, see FIG. 2.7.

The solution of the isotropic model, $J_\perp = J_\parallel$ was obtained by Andrei [33] and Wiegmann[79] while the anisotropic version in region $0 \leq J_\perp \leq J_\parallel$ was solved by Wiegmann[35]. Since then many extensions of the Kondo model have been solved, including higher spin[80, 81], multichannel[82, 83, 84] and multiflavor systems as well as generalizations to other symmetry groups[85]. Our review here mostly follows the comprehensive review paper of Tsvelik and Wiegmann [69] but includes some comments on alternative approaches to their methods later in the chapter .

We begin with the single particle solution, which is written generally as

$$|k\rangle = \sum_{a_j=\uparrow,\downarrow} \int f_{a_1,a_0}(x) e^{ikx} \psi^\dagger_{a_1}(x) \, |0\rangle \otimes |a_0\rangle \tag{2.46}$$

where $|a_0\rangle = |\uparrow\rangle$ or $|\downarrow\rangle$ is the state of the impurity spin. Following the logic of the last chapter, the wavefunction is expanded as a sum of Heaviside functions,

$$f_{a_1,a_0}(x) = A^{[10]}_{a_1,a_0}\theta(-x) + A^{[01]}_{a_1,a_0}\theta(x).$$

Applying the Hamiltonian to this state and requiring it to be an eigenstate with energy k fixes the relationship between the amplitudes on either side of the impurity. Upon doing this, the relation is found to be

$$A^{[01]}_{a_1 a_0} = \left[S^{10}A^{[01]}\right]_{a_1,a_0}. \tag{2.47}$$

Here S^{10} is a 4×4 matrix, called the single particle or impurity S-matrix which is given by

$$S^{10} = e^{i\zeta}\begin{pmatrix} 1 & 0 & 0 & 0 \\ 0 & \frac{\sinh(c)}{\sinh(c+i\gamma)} & \frac{\sinh(i\gamma)}{\sinh(c+i\gamma)} & 0 \\ 0 & \frac{\sinh(i\gamma)}{\sinh(c+i\gamma)} & \frac{\sinh(c)}{\sinh(c+i\gamma)} & 0 \\ 0 & 0 & 0 & 1 \end{pmatrix}, \tag{2.48}$$

$$\cos(\gamma) = \frac{\cos(J_\parallel)}{\cos(J_\perp)}, \qquad \coth^2(1/c) = \frac{\sin^2(J_\parallel)}{\sin\left(J_\parallel - J_\perp\right)\sin\left(J_\perp + J_\parallel\right)}, \tag{2.49}$$

$$\zeta = J_\parallel - J_\perp/2\,. \tag{2.50}$$

We have chosen here to replace the Hamiltonian parameters $J_{\perp,\parallel}$ with c and γ in order to bring S^{10} to the form above which will become important when determining the spectrum. Often c will be referred to as the impurity parameter and γ as the anisotropy. The mapping between $J_{\perp,\parallel}$ and c,γ was derived in [35] and is in fact not universal as the former are bare parameters which will become renormalized by the interactions and depend upon the renormalization scheme used and how one regularizes the delta function interaction. At weak coupling the different renormalization and regularization schemes agree so we may

write

$$\gamma \sim \sqrt{J_{\parallel}^2 - J_{\perp}^2}, \quad c/\gamma \sim 1/J_{\parallel}. \tag{2.51}$$

In the end these are replaced with a universal quantity, T_K known as the Kondo scale or Kondo temperature. Results written only in terms of this allow one to compare between the different schemes.

To understand this better, consider for the moment the equation

$$-i\partial_x f(x) + 2g\delta(x)f(x) = 0 \tag{2.52}$$

which can be solved using the Ansatz $f(x) = A\theta(-x) + B\theta(x)$. Inserting this into the above equation the coefficients are determine to be related by $B = e^{2i\arctan(g)}A$. This is the approach used in many works most notably [33]. Alternatively one can rewrite the equation as $\partial_x \log[f(x)] = 2g\delta(x)$. Integrating this equation gives the solution instead to be $f(x) = e^{2ig\mathrm{Sgn}(x)}$ which corresponds to $B = e^{2ig}A$. This second approach is favored by other authors including in [69]. The discrepancy between the two results comes from the pathological nature of the delta function interaction and the different ways it can be regularized. Equations of this type appear again and again in Bethe Ansatz solutions of QIMs and one therefore needs to be careful when dealing with them. The approach we take here is to work with the generic phase shift $B = e^{i\phi(g)}A$ with the understanding the relationship between g and ϕ depends on the manner in which we derived the eigenstates (although both schemes agree for at small g). The phase shift can thereafter be related to a physical parameter like the Fermi edge exponent, Luttinger parameter K or replaced entirely by the a scale like the Kondo scale in order to obtain universal results[86].

Obtaining the two particle eigenstate is the next step in the Bethe Ansatz procedure.

We write the 2 particle state as

$$\sum_{a_1,a_2,a_0} \int F_{a_1,a_2,a_0}(x_1,x_2) \prod_{j=1}^{2} e^{ik_j x_j} \psi^\dagger_{a_j}(x_j) \left|0\right\rangle \otimes \left|a_0\right\rangle \tag{2.53}$$

and again expand the wavefunction in Heavisides. This time we include extra regions corresponding to the ordering in configuration space of the bulk fermions,

$$\begin{aligned} F_{a_1,a_2,a_0}(x_1,x_2) &= \sum_Q A^{[Q]}_{a_1,a_2,a_0} \theta(x_Q) && (2.54) \\ &= A^{[120]}_{a_1,a_2,a_0} \theta(x_2-x_1)\theta(-x_1)\theta(-x_2) + A^{[210]}_{a_1,a_2,a_0} \theta(x_1-x_2)\theta(-x_1)\theta(-x_2) \\ &\quad + A^{[102]}_{a_1,a_2,a_0} \theta(-x_1)\theta(x_2) + A^{[201]}_{a_1,a_2,a_0} \theta(x_1)\theta(-x_2) \\ &\quad + A^{[012]}_{a_1,a_2,a_0} \theta(x_2-x_1)\theta(x_1)\theta(x_2) + A^{[021]}_{a_1,a_2,a_0} \theta(x_1-x_2)\theta(x_1)\theta(x_2) && (2.55) \end{aligned}$$

Where Q refers to all different ordering of the 2 particles and the impurity and $\theta(x_Q)$ is a Heaviside which is non zero only inside that region. In the RL model our two particle state only consisted of 4 bulk terms labelled by the position of the fermion in relation to the impurity here we also include different amplitudes for different orderings of the bulk fermions in relation to each other.

Applying the Hamiltonian to our 2-particle state and suppressing spin indices we find that

$$A^{[102]} = S^{20} A^{[120]}, \quad A^{[012]} = S^{10} A^{[102]} \tag{2.56}$$

$$A^{[201]} = S^{10} A^{[210]}, \quad A^{[021]} = S^{20} A^{[201]} \tag{2.57}$$

where S^{10} acts as in (2.48) in the a_1, a_0 spaces and as the identity on the a_2 space and S^{20} similarly acts as the matrix in (2.48) but in the a_2, a_0 spaces and the identity in the a_1 space. The relationship between the two sets of orderings of particles $x_1 < x_2$ and $x_2 < x_1$ is however *not* fixed by the Hamiltonian. The reason for this is because the kinetic part of

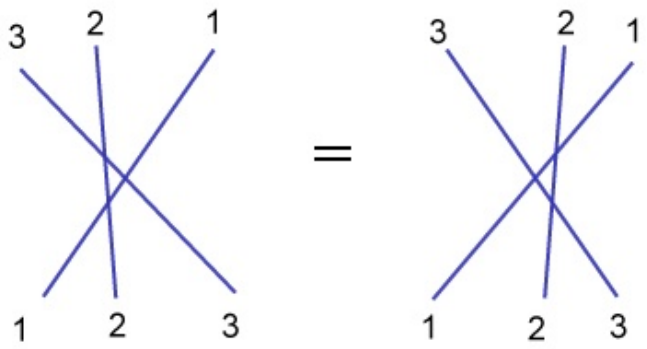

Figure 2.8: The Yang Baxter equation is a statement that in an integrable model the order of scattering events does not matter. In this figure we depict the a three particle scattering event. On the left particles 1 and 2 scatter first followed by 1 and 3 and then 2 and 3. On the right hand side 2 and 3 scatter first then 1 and 3 followed by 1 and 2. Assigning an S-matrix to each intersection of lines we arrive at the Yang Baxter equation. In more than one dimension the Coleman-Mandula theorem states that a symmetry such as this cannot occur unless all the S-matrices are trivial[87]. In one dimensional system the theorem does not apply and integrable models exhibit non trivial conservation laws which allow one to independently move each of the lines. Holding the 1 and 3 lines fixed one can shift the 2 line to the right, such a shift is associated to a constant of motion and therefore the amplitude for this event is unchanged resulting in the Yang Baxter equation.

the Hamiltonian gives zero when acting on the Heavisides,

$$[\partial_{x_1} + \partial_{x_2}]\,\theta(x_2 - x_1) = 0 \tag{2.58}$$

Thus according to the Hamiltonian $A^{[120]} = S^{12}A^{[210]}$ with S^{12}, the two particle S-matrix being completely arbitrary. This ultimately results from the enormous degeneracy present in a massless system with linear dispersion, as is the case for the bulk of the AKM. This degeneracy can be seen in the two particle case by noting that the state with single particle energies $k_1,\ k_2$ is degenerate with a $k_1 - q,\ k_2 + q$ state. Practically this means that there are an infinite number of different bases in which the bulk can be diagonalized, the addition of the impurity breaks translational invariance and lifts the degeneracy [88]. The form of the impurity dictates that a particular basis or rather a particular S^{12} is picked out.

The "choice" of basis is fixed by the consistency of the construction which is enforced by the Yang Baxter equation. This equation is central to the Bethe Ansatz construction

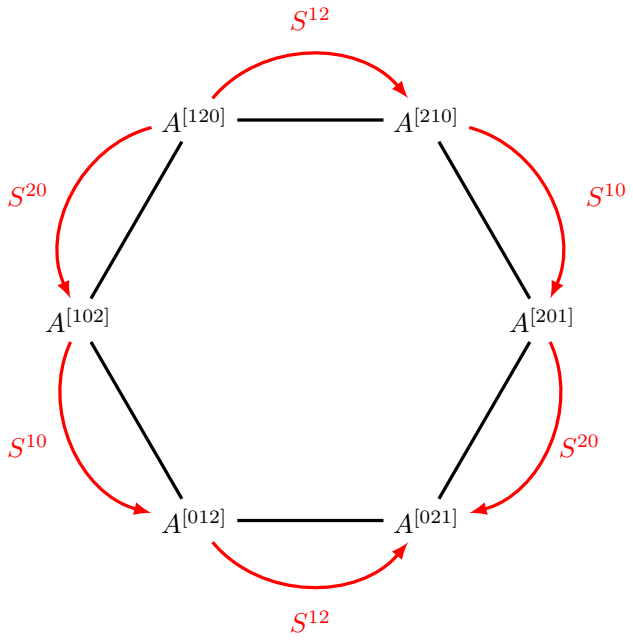

Figure 2.9: The amplitudes in the two particle wavefunction are related to each other by application of the single and two particle S-matrices. Starting from one set of amplitudes $A^{[120]}$ (suppressing the spin indices) we can proceed either clockwise or counter clockwise direction. The result should be the same in either direction if the construction is consistent. Equating the two final expressions gives the Yang Baxter equation (2.59)

and appears as a crucial element in all studies of integrable models. In general it is written as

$$S^{ij}S^{ik}S^{jk} = S^{jk}S^{ik}S^{ij} \tag{2.59}$$

while in the 2 particle case under consideration now takes $i = 1, j = 2, k = 0$. It states that the ordering of a scattering event in an integrable model should not matter, see FIG. 2.8. In addition if the S-matrices satisfy this equation then starting from one set of amplitudes, for example $A^{[120]}_{a_1,a_2,a_0}$ one can consistently construct the rest of the wavefunction, see FIG. 2.9. In a non interacting model, like the RL one may take $S^{12} = 1$ as the single particle S-matrices are c-numbers however in the AKM they are non commuting matrices, $S^{20}S^{10} \neq S^{10}S^{20}$. In addition to this the S-matrix should satisfy a unitarity condition, $S^{12}S^{21} = 1$ which states that if we swap the order of particles 1 and 2 and then swap them back there should be no effect. Given these conditions we take $S^{12} = S^{21} = P^{12}$ where P^{12} is the permutation operator on the spaces labelled by a_1, a_2. It acts as $\left[P^{12}\right]^{a'_1 a'_2}_{a_1,a_2} A_{a'_1,a'_2} = A_{a_2,a_1}$ and therefore satisfies the unitarity condition but also using $P^{12}S^{10}P^{12} = S^{20}$ satisfies the Yang -Baxter equation. Alternatively one can directly substitute the matrix form

$$P^{12} = \begin{pmatrix} 1 & 0 & 0 & 0 \\ 0 & 0 & 1 & 0 \\ 0 & 1 & 0 & 0 \\ 0 & 0 & 0 & 1 \end{pmatrix}. \tag{2.60}$$

into (2.59) and confirm that it is a solution of the Yang Baxter equation. Using this in (2.55) we get the consistent 2 particle eigenstate of the AKM. Therefore despite the fact that there are no fermion-fermion interactions present in the Hamiltonian the impurity dictates that we should include S^{12} in the wavefunction. This is the first indication that the impurity causes strong correlations to occur between bulk fermions. The choice of P^{12} is not unique,

an overall phase can be included and still the Yang Baxter equation is satisfied. This will not effect the final results however and so we do not include it.

We may now go on to construct the N particle wavefunctions. The state with energy $E = \sum_j^N k_j$ is a standard generalization of the 2 particle case,

$$\left|\vec{k}\right\rangle = \sum_Q \int \mathrm{d}\vec{x}\, A^Q_{\vec{a}} \theta(x_Q) \prod_{j=1}^{N} e^{ik_j x_j} \psi^\dagger_{a_j}(x_j) \left|0\right\rangle \otimes \left|a_0\right\rangle . \tag{2.61}$$

Where $\vec{a} = \{a_1, \ldots a_N, a_0\}$ with $a_j = \uparrow, \downarrow$ the spin of the j^{th} particle, 0 indicating the impurity, Q are orderings of the N particles and the impurity in configuration space and $\theta(x_Q)$ is a Heaviside function which is non zero only for a certain ordering. There are $(N+1)!$ regions in the N particle state. The amplitudes are related to each other via products of S-matrices, for example $A^{[\ldots jk\ldots]} = S^{jk} A^{[\ldots kj\ldots]}$ where $S^{ij} = P^{ij}$ for $j, k \neq 0$ or if $k = 0$ S^{j0} is given by the operator acting as the matrix in (2.64) in the j^{th} particle and impurity spaces and the identity elsewhere. The consistency of the construction is guaranteed by the fact that all the S-matrices satisfy the Yang-Baxter equation (2.59) and also $S^{ij} S^{ji} = 1$ which is the unitarity condition. That this is a sufficient condition to give a consistent wavefunction can be see explicitly in the three particle case as shown by FIG. 2.10 or more generally by noting that the S-matrices form a representation of the symmetric group of N objects who's group law is equivalent to the Yang Baxter equation [89].

We have successfully diagonalized the AKM on the infinite line which in itself is a worthy accomplishment given the highly nontrivial nature of the model however it is rather difficult to discern the physics of the model directly through its Bethe Ansatz eigenstates. To study the equilibrium properties of the AKM however we instead go beyond this and determine its spectrum. This is done, as before by imposing periodic boundary conditions on the system

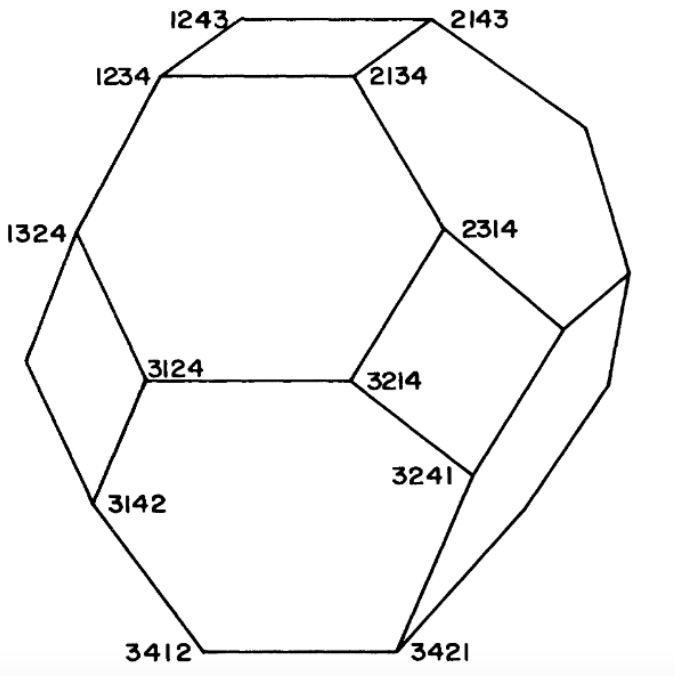

Figure 2.10: For the three particle state the Yang Baxter diagrom of FIG. 2.9 is generalized to the above figure with the numbers at the vertices indicating the ordering of particles. In this diagram 4 indicates the impurity. Each face of the three dimensional shape gives a new consistency condition which needs to be satisfied. There are only two types however which occur, the Yang Baxter equation and the unitarity condition $S^{ij}S^{ji} = 1$ which are satisfied by the choice $S^{ij} = P^{ij}$. Figure taken from [68]

of size L. The resulting equation (c.f (2.19)) is

$$e^{-ik_jL}A^{[12\ldots N0]}_{\sigma_1\ldots\sigma_N} = (Z_j)^{\sigma'_1\ldots\sigma'_N}_{\sigma_1\ldots\sigma_N} A^{[12\ldots N0]}_{\sigma'_1\ldots\sigma'_N} \tag{2.62}$$

$$Z_j = S^{jj-1}\ldots S^{j1}S^{j0}S^{jN}\ldots S^{jj+1} \tag{2.63}$$

where Z_j is an operator which acts in the spin space of the particles that takes the j^{th} particle around the system scattering past all others and the impurity on the way. Using the Yang Baxter equation it is straightforward to not only show $[Z_j, Z_k] = 0$ but furthermore that $Z_j = Z_1,\ \forall j$. The fact that all Z_j are equal comes from the lack of a dimensionful parameter in the Hamiltonian, in cases where the coupling constants are dimensionful (see chapter 6) we will see that they Z_j are not equal but nevertheless commute with each other. The task is now to diagonalize Z_1 operator whose eigenvalues will give us the single particle energy levels according to (2.62).

2.2.3 Quantum Inverse Scattering Method

This new diagonalization problem can be solved by a second Bethe ansatz method known as the quantum inverse scattering method (QISM). We will not go into all the details here, mostly providing results and refer the reader to several excellent reviews in [88, 69, 90]. The first step in this procedure is to introduce the R-matrix

$$R(u) \quad = \quad \begin{pmatrix} 1 & 0 & 0 & 0 \\ 0 & \frac{\sinh(u)}{\sinh(u+i\gamma)} & \frac{\sinh(i\gamma)}{\sinh(u+i\gamma)} & 0 \\ 0 & \frac{\sinh(i\gamma)}{\sinh(u+i\gamma)} & \frac{\sinh(u)}{\sinh(u+i\gamma)} & 0 \\ 0 & 0 & 0 & 1 \end{pmatrix} \tag{2.64}$$

which is a function if u, the spectral parameter and satisfies a continuous version of the Yang Baxter equation,

$$R^{ij}(u-v)R^{ik}(u)R^{jk}(v) = R^{jk}(v)R^{ik}(u)R^{ij}(u-v) \tag{2.65}$$

with i, j, k labelling 2 dimensional vectors spaces on which the R-matrices act e.g. R^{ij} acts on the i and j spaces. This particular choice of R-matrix is associated to numerous integrable models including the XXZ spin chain, [91], the 6-vertix model[19] and the massive Thirring model [92] and shall feature later on in this thesis also. In the context of the AKM it allows us to package both the impurity and two particle S-matrices together as $S^{i0} = e^{i\zeta}R^{i0}(c)$ and $S^{ij} = R^{ij}(0)$. The next step is to construct the monodromy matrix, $\Xi(u)$ which is a product of R-matrices

$$\Xi^A(u) = R^{1A}(u-\theta_1)\dots R^{NA}(u-\theta_N)R^{0A}(u-\theta_0) \tag{2.66}$$

where the index A refers to an auxiliary particle space, $0, \dots, N$ refer to the impurity and particle spaces and we introduced shifts in the spectral parameters, θ_j known as inhomogeneities. The monodromy matrix also satisfies a version of the Yang Baxter equation

$$R^{AB}(u-v)\Xi^A(u)\Xi^B(v) = \Xi^B(v)\Xi^A(u)R^{AB}(u-v). \tag{2.67}$$

The trace of the monodromy matrix over the auxiliary space is an important object known as the transfer matrix,

$$t(u) = \mathrm{Tr}_A\{\Xi^A(u)\}. \tag{2.68}$$

By taking the trace of (2.67) over the spaces A and B we find that the transfer matrix commutes with itself for any spectral parameter

$$[t(u), t(v)] = 0.$$

The obvious consequence of this is that one can simultaneously diagonalize transfer matrices evaluated at different spectral parameters. In addition by writing $t(v)$ as a series expansion, $t(v) = \sum_0^\infty v^n I_n$ with I_n being some operators we get that

$$[t(u), I_n] = 0 \tag{2.69}$$

which means that $t(u)$ has an extensive number of commuting partners. Consequently the transfer matrix is integrable. By Using QISM one can prove that a certain problem is integrable before actually constructing any eigenstates. In contrast when using the Bethe Ansatz method one cannot know if it will be possible before actually attempting to solve the problem.

While this is an interesting construction and ties in somewhat with our theme of integrability one may ask what it has to do with the problem of diagonalizing Z_j. The answer is that by choosing the inhomogeneities $\theta_0 = -c$ and $\theta_j = 0,\ j > 0$ and taking $u = 0$ we get

$$e^{i\zeta} t(0)|_{\theta_j=0,\theta_0=-c} = Z_j \tag{2.70}$$

Therefore our diagonalization problem stemming from the application of periodic boundary conditions is also integrable. This mapping of the periodic boundary condition problem onto another integrable system is the crucial ingredient to solving a QIM through Bethe Ansatz and accordingly is the most difficult part. There are many QIMs for which one can construct the appropriate eigenstates on the infinite line as we did in the last section but which lack a R-matrix description, as in (2.64), and therefore a mapping such as this when

periodic boundary conditions are introduced.

Aside from proving that one can solve the eigenvalue problem we are interested in, the quantum inverse scattering method provides a way to construct the eigenstates of the transfer matrix. In the auxiliary space, A the monodromy matrix can be written as a 2×2 matrix

$$\Xi^A(u) = \begin{pmatrix} A(u) & B(u) \\ C(u) & D(u) \end{pmatrix} \tag{2.71}$$

where A, B, C, D are rather complicated operators acting on the $0, \ldots, N$ spaces. In this notation the transfer matrix is given by $t(u) = A(u) + D(u)$. The commutation relations between these operators at different spectral parameters can be derived by writing out the Yang Baxter equation (2.67) in this notation and upon doing this one finds that the operators commute with themselves, $[A(u), A(v)] = [B(u), B(v)] = [C(u), C(v)] = [D(u), D(v)] = 0$ but also

$$A(u)B(v) = \frac{\sinh(u - v + i\gamma)}{\sinh(u - v)} B(v)A(u) - \frac{\sinh(i\gamma)}{\sinh(u - v)} B(u)A(v) \tag{2.72}$$

$$D(u)B(v) = \frac{\sinh(v - u + i\gamma)}{\sinh(v - u)} B(v)D(u) - \frac{\sinh(i\gamma)}{\sinh(v - u)} B(u)D(v). \tag{2.73}$$

The C and B operators are then used as creation and annihilation operators to construct the eigenstates of the transfer matrix. Consider the state constructed from C operators at different spectral parameters,

$$\prod_{j=1}^{M} C(\lambda_j) \left|\Downarrow\right\rangle \tag{2.74}$$

where $M \leq (N + 1)/2$ and $\left|\Downarrow\right\rangle = \otimes^N \left|\downarrow\right\rangle$ is called the reference state which acts as the vacuum for the construction. The action of the transfer matrix on the reference state can be computed easily using (2.64) (2.66) and (2.71). Acting upon the state (2.74) with the

transfer matrix and employing the commutations relations above one finds that it is indeed an eigenstate provided certain conditions on the λ_j are met. For our particular choices of inhomgeneities the eigenvalues of $t(0)$ associated with the state (2.74) are

$$\prod_j^M \frac{\sinh(\lambda_j - i\gamma/2)}{\sinh(\lambda_j + i\gamma/2)} \tag{2.75}$$

with the λ_j satisfying a set of Bethe Ansatz equations

$$\left[\frac{\sinh(\lambda_j - i\gamma/2)}{\sinh(\lambda_j + i\gamma/2)}\right]^N = \frac{\sinh(\lambda_j + c + i\gamma/2)}{\sinh(\lambda_j + c - i\gamma/2)} \prod_{j\neq k}^M \frac{\sinh(\lambda_j - \lambda_k - i\gamma)}{\sinh(\lambda_j - \lambda_k + i\gamma)}. \tag{2.76}$$

The λ_j are known as Bethe parameters or Bethe roots and they encode all the information about the spin degrees of freedom in the AKM. In addition to the Bethe equations the Bethe parameters must also satisfy a type of Pauli exclusion principle $\lambda_j \neq \lambda_k$. If this is not satisfied it is possible to check that the state (2.74) vanishes[93]. It is another peculiarity of 1D physics that Bethe Ansatz models always exhibit a Pauli principle of this sort regardless of the statistics of the system.

We can interpret these set of equations in a similar way we did before as a particle moving around the system. In this instance however the "particle" here is a flipped spin and the system around which this up spin travels is the spin space of the N particles and impurity of which M are flipped. The left hand side of the equations is the plane wave phase that the spin acquires as it moves around the system. The product on the right hand side is the phase shift acquired each time the spin moves past other flipped spins of bulk particles while the remaining term, which depends on c is the phase shift of the spin moving past the impurity. We see here again the impact that the impurity has on the bulk system. Despite them having no interactions amongst themselves the particles or rather their spin parts acquire complicated phase shifts and become strongly correlated with each other. Interestingly only a single term in these equations actually depends on the impurity parameter, c.

Collecting the results of this and the previous section we have that an N-particle eigenstate of the AKM has energy $E = \sum_{l=1}^{N} k_l$ where the single particle energies are determined by

$$e^{-ik_l L} = e^{i\zeta} \prod_{j=1}^{M} \frac{\sinh(\lambda_j - i\gamma/2)}{\sinh(\lambda_j + i\gamma/2)} \tag{2.77}$$

$$\left[\frac{\sinh(\lambda_j - i\gamma/2)}{\sinh(\lambda_j + i\gamma/2)}\right]^N = \frac{\sinh(\lambda_j + c + i\gamma/2)}{\sinh(\lambda_j + c - i\gamma/2)} \prod_{j\neq k}^{M} \frac{\sinh(\lambda_j - \lambda_k - i\gamma)}{\sinh(\lambda_j - \lambda_k + i\gamma)} \tag{2.78}$$

and the total z component of spin, which is conserved, for this eigenstate is $S^z = (N + 1 - M)/2$. Before proceeding with the analysis of these equations, two important limits should be noted. The first is $\gamma \to 0$ which is the isotropic limit. To take this one rescales the Bethe parameters $\lambda \to \gamma\lambda$ and then takes the limit. This reproduces the isotropic Kondo Bethe equations [33, 34]. The other limit is taking $\gamma = \pi/2$ in which case all two particle phase shifts disappear and it can be checked that one obtains the RL model of the previous section. This is often called the Toulouse limit. In the next section the Bethe equations are studied with γ arbitrary and any results are valid also when either of these limits is taken.

2.2.4 Groundstate and excitations

The exact diagonalization of the AKM has been achieved with the spectrum completely described at finite N and L by (2.77) and (2.78). We are now in a position to examine the ground state and excitations of the system. Before proceeding however we make some definitions which will be useful throughout the thesis

$$p(x,n,1) = i\log\left[\frac{\sinh\left(x+in\gamma/2\right)}{\sinh\left(x-in\gamma/2\right)}\right] \tag{2.79}$$

$$p(x,n,-1) = i\log\left[\frac{\cosh\left(x+in\gamma/2\right)}{\cosh\left(x-in\gamma/2\right)}\right] \tag{2.80}$$

$$a_n(x) = \frac{1}{2\pi}\frac{\mathrm{d}}{\mathrm{d}x}p(x,n,1) \tag{2.81}$$

$$b_n(x) = \frac{1}{2\pi}\frac{\mathrm{d}}{\mathrm{d}x}p(x,n,-1) \tag{2.82}$$

the Fourier transform of a_n and b_n are also used extensively and are given by

$$\tilde{a}_n(\omega) = \frac{\sinh\left([\pi-n\gamma]\omega/2\right)}{\sinh\left(\pi\omega/2\right)}, \quad \tilde{b}_n(\omega) = -\frac{\sinh\left(n\gamma\omega/2\right)}{\sinh\left(\pi\omega/2\right)} \tag{2.83}$$

With these in place the ground state of the model can be constructed. To do this the appropriate quantum numbers of the system must be identified. Taking the log of (2.77) and (2.78) gives

$$k_l = \frac{2\pi}{L}n_l + \frac{1}{L}\zeta + \frac{1}{L}\sum_{j=1}^{M}p(\lambda_j,1,1) \tag{2.84}$$

$$Np(\lambda_j,1,1) + p(\lambda_j+c,1,1) = 2\pi I_j + \sum_{j\neq k}p(\lambda_j-\lambda_k,2,1) \tag{2.85}$$

with n_l and I_j being integers or half integers depending on the value of M. These serve as the quantum numbers of the system and can be associated with the charge and spin degrees of freedom respectively. Inserting (2.85) into (2.84) and summing over all particles gives the total energy of the system to be

$$E = \sum_{l}^{N}\frac{2\pi}{L}n_l + \sum_{j}^{M}\frac{2\pi}{L}I_j + \frac{N}{L}\sum_{j}^{M}p(\lambda_j,1,1) + \frac{N}{L}\zeta. \tag{2.86}$$

The first two terms here are the bulk energy while the second two, which are order $1/N$ smaller, correspond to the impurity energy. The last term is a constant phase shift which is routinely ignored in analyses of QIMs as it has no effect on the overall physics of the

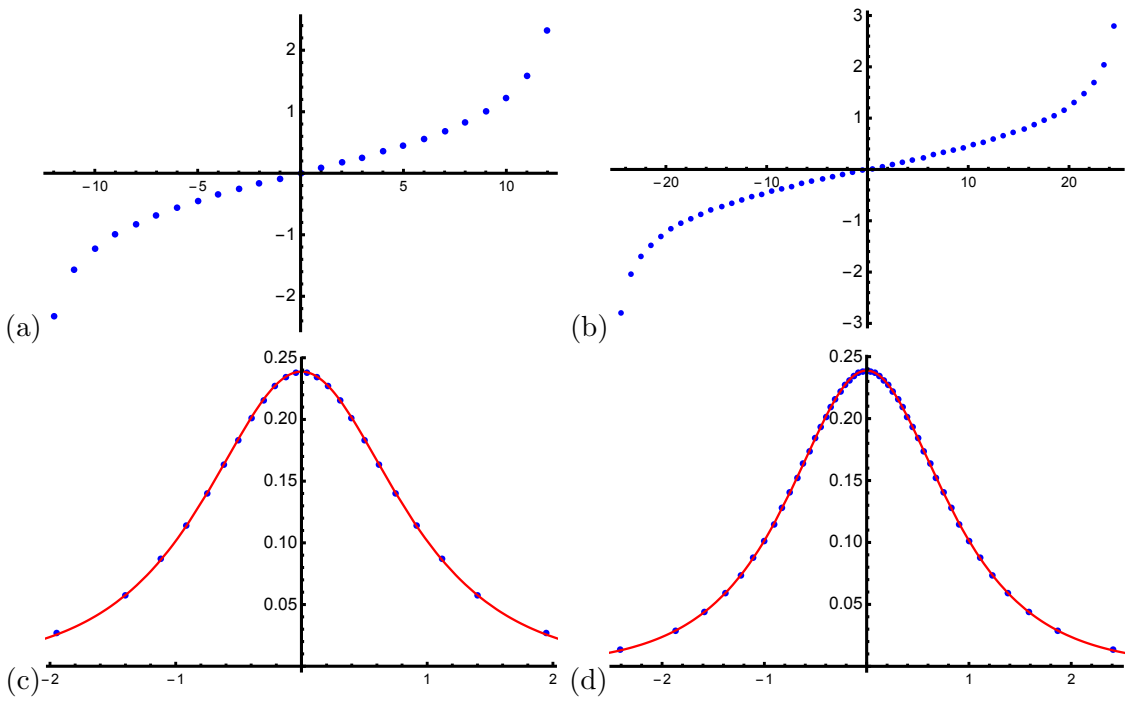

Figure 2.11: Here we plot the Bethe parameters vs their quantum numbers I_j for the ground state configuration of the AKM with $\gamma = \pi/3$ and (a) $N = 50$ (b) $N = 100$. Below this we plot continuous ground state distribution, $\rho_{\rm gs}(\lambda)$ (Red solid line) from (2.87) again for $\gamma = \pi/3$. The points are the discrete version evaluated using (2.21) and the Bethe roots with (c) $N = 50$ and (d)$N = 100$. Even for 50 particles the continuous distribution provides a good fit to the roots with the gaps between the points closing as we increase N.

system[69, 68]. It can be removed entirely by adding a forward scattering delta function impurity at the origin with an appropriate strength[88] and in what follows it shall be dropped from our analysis.

Considering just the bulk energy for the moment we see it is described by two sets of quantum numbers associated to spin and charge which are decoupled from each other. One may independently change one set of quantum numbers with out affecting the other. This is a manifestation of the famous spin-charge separation which was encountered already through bosonization [10, 14]. The ground state of the model is constructed by filling the charge quantum numbers up from the cutoff. As in the RL model we take $\mathcal{K} = 2\pi D$ with $D = N/L$ and $n_l = -l$. For the spin part we must take $M = (N+1)/2$ and fill the spin quantum numbers up from $-(N+1)/4$ to $(N+1)/4$ (we consider odd N for convenience). The spin quantum numbers are in one to one correspondence with the Bethe parameters

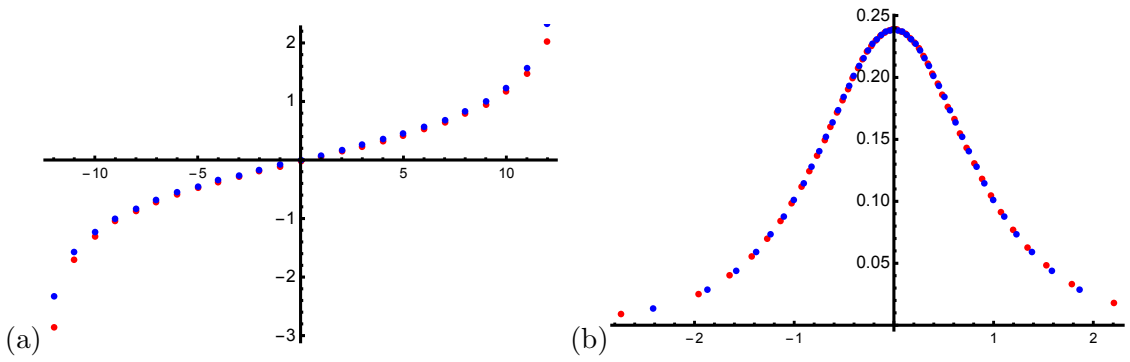

Figure 2.12: (a) We plot the Bethe roots at $\gamma = \pi/3,\ c = 10$ both with (Red dots) and without (Blue dots) the impurity contribution for $N = 50$. (b) The discrete distribution of the roots for $N = 100$ with and without the impurity contribution. We see that the impurity contributes to a small shift in the distribution of the roots which reduces with increasing N.

λ_j and so the spin part of the system may be descirbed in terms of these instead. The advantage of doing this is that we may proceed just as in (2.21) and derive an equation for the density of the λ_j

$$\rho_{\rm gs}(\lambda) = N a_1(\lambda) + a_1(\lambda + c) - \int \mathrm{d}\mu\, a_2(\lambda - \mu)\rho_{\rm gs}(\mu) \tag{2.87}$$

Note that now the density appears on both sides of the equation due to the correlations between the spins of the particles giving us a linear integral which must be solved. The solution is found straightforwardly via Fourier transform with the result

$$\rho_{\rm gs}(\lambda) = \frac{N}{2\gamma \cosh\left(\frac{\pi}{\gamma}\lambda\right)} + \frac{1}{2\gamma \cosh\left(\frac{\pi}{\gamma}(\lambda + c)\right)}. \tag{2.88}$$

In FIG. 2.11 we plot the Bethe roots for the ground state distribution for $N = 50, 100$ and compare the them with the distribution derived above. One can see that already for these small numbers the continuous distribution provides a good fit to the roots and that as N is increased they become more and more dense along the curve.

This density of states enjoys the same separable structure we saw before. We can identify the first term with the bulk spin degrees of freedom and the second as the impurity

part which provides an order $1/N$ contribution compared to the bulk part. In FIG. 2.12 we compare the positions and distribution of the Bethe roots when the impurity term is present and absent.

The total S^z of the groundstate can be calculated by integrating over the density of states and in particular the impurity spin has

$$s_0^z = \frac{1}{2} - \int \frac{1}{2\gamma \cosh\left(\frac{\pi}{\gamma}(\lambda + c)\right)} \tag{2.89}$$

$$= 0 \tag{2.90}$$

which shows the the impurity spin is screened in the ground state, see FIG. 2.6. The spin contribution to the energy is similarly calculated to be

$$E_{\text{imp}} = \frac{N}{L} \int \mathrm{d}\lambda \frac{p(\lambda, 1, 1)}{2\gamma \cosh\left(\frac{\pi}{\gamma}(\lambda + c)\right)} \tag{2.91}$$

The excitations above the ground state can be either in the charge or spin sector. The former, called *holons* are the same as in the RL model and arise from removing one of the charge quantum numbers. The spin excitations, termed *spinons* similarly come from a hole in the spin quantum numbers. Unlike holons, however the strongly correlated nature of the spin degrees of freedom means that by introducing a spinon the entire Fermi sea is modified by its presence. To see this back reaction and calculate the spinon energy we consider two holes introduced to the ground state at $\lambda = \lambda_1, \lambda_2$. The density of states of is then a solution of

$$\rho(\lambda) = N a_1(\lambda) + a_1(\lambda + c) - \delta(\lambda - \lambda_1) - \delta(\lambda - \lambda_2) \tag{2.92}$$

$$- \int \mathrm{d}\mu \, a_2(\lambda - \mu)\rho(\mu) \tag{2.93}$$

The linear nature of this integral equation allows one to separate out the undisturbed ground state contribution from the modification due to the excitation, $\rho(\lambda) = \rho_{\text{gs}}(\lambda) + \rho^{\text{h}}(\lambda)$, where

the latter solves

$$\rho^{\rm h}(\lambda) = -\delta(\lambda-\lambda_1) - \delta(\lambda-\lambda_2) - \int {\rm d}\mu\, a_2(\lambda-\mu)\rho^{\rm h}(\mu) \tag{2.94}$$

and the former is given by (2.88). This new integral equation can also be solved via Fourier transform and upon doing so can be used to find that the excitation energy of the two holes is

$$\begin{aligned} E_{\rm h} &= \frac{N}{L}\int {\rm d}\lambda\, p(\lambda,1,1)\rho^{\rm h}(\lambda) && (2.95)\\ &= 2D\arctan e^{\frac{\pi}{\gamma}\lambda_1} + 2D\arctan e^{\frac{\pi}{\gamma}\lambda_2} && (2.96)\end{aligned}$$

The total spin of this excitation can be determined by $S^z_{\rm h} = -\int \rho^{\rm h} = \frac{\pi}{\pi-\gamma}$ which is unexpectedly not an integer or half integer but in the isotropic limit $\gamma \to 0$ gives $S^z = 1$ [2]. So in the isotropic limit this gives a spin-1 or triplet excitation and it is natural then to assume that in this limit each spinon carries spin 1/2. To confirm that this is the case one should be able to construct a singlet excitation also using two holes. To do so one must consider a complex conjugate pair of Bethe roots, $\lambda_{\rm s} \pm i\gamma/2$ called a 2-string in addition to the two holes at $\lambda_1,\ \lambda_2$ with $\lambda_{\rm s} = (\lambda_1+\lambda_2)/2$. This modifies the density to $\rho = \rho_{\rm gs}(\lambda)+\rho^{\rm h}(\lambda)+\rho_{\rm s}(\lambda)$ where the $\rho_{\rm s}(\lambda)$ is the modification to the density of states caused by the presence of the 2-string. It is determined by the equation

$$\rho_{\rm s}(\lambda) = -a_3(\lambda-\lambda_{\rm s}) - a_1(\lambda-\lambda_{\rm s}) - \int {\rm d}\mu\, a_2(\lambda-\mu)\rho_{\rm s}(\mu). \tag{2.97}$$

Proceeding as before the excitation energy is $E = E_{\rm h} + E_{\rm s}$ with the part due to the string

[2] In [69], this non integer value is attributed to a renormalisation of the compressibility and g-factors due to the the two particle S-matrix, S^{12}. In the AKM this is seen as a spurious effect and subsequent calculations redefine both quantities with this fact accounted for. As we shall see later on the same S-matrix appears in studies of the Luttinger impurity systems. In that case however the effect is not disregarded in this way and must occur in order to obtain the correct current and compressibility.

being

$$E_{\rm s} = p(\lambda_s,3,1)+p(\lambda_s,1,1)+\int {\rm d}\lambda\, p(\lambda,1,1)\rho_{\rm s}(\lambda) \tag{2.98}$$

$$= 0. \tag{2.99}$$

The proof of this is most easily seen by Fourier transforming the expression on the right hand side, recalling that the transform of a convolution is just the product of the transforms. The addition of the string therefore causes no change in the energy, the singlet excitation energy being given by (2.96). It does however change the total z spin, which is now given by $\int \rho^{\rm h}+\rho_{\rm s}=\frac{2\gamma}{\pi-2\gamma}$. In the isotropic limit this becomes 0, justifying the name of singlet excitation. More excitations can be created by adding more holes or holes and 2-strings to the ground state.

What we have seen here is that introducing an excitation to the system causes the ground state density of states to be disturbed due to the strong correlations amongst the particles. This in turn dresses the excitations and results in a relativistic dispersion, $2D\arctan e^{\frac{\pi}{\gamma}\lambda}$. Note that these spinon excitations are eigenstates of the Hamiltonian meaning the system can be viewed as a gas of spinons which have infinite lifetime and are unaffected by the impurity other than to pick up a phase shift as they move past it. This phase shift is the physical impurity phase shift and comes from the dressing of the bare phase shift which appears in the Bethe equations, the $p(\lambda+c,1,1)$ term. It is possible to calculate this object using boundary conformal field theory [13] and the bootstrap method[94] and so it is an important cross check to be able to obtain it using Bethe Ansatz. The method of doing this was developed in the context of the chiral Gross-Neveu model[95] and relies on being able to take the universal limit $D\to\infty$ while still having L finite.

To calculate it we define the counting function,

$$Z(\lambda) = Np(\lambda,1,1)+p(\lambda+c,1,1)-\sum_{j\neq k}p(\lambda-\lambda_k,2,1) \tag{2.100}$$

which has the property $Z(\lambda_j) = 2\pi I_j/L$ provided λ_j is a solution of the Bethe equations (2.85) and furthermore is related to the density by $\partial_\lambda Z(\lambda) = \rho(\lambda)$. If the solution of the Bethe equations contains a hole at say $\lambda^{\rm h}$ corresponding to $I^{\rm h}$ being missing from the sequence $\{I_j\}$ then we have $Z(\lambda^{\rm h}) = 2\pi I^{\rm h}/L$. In the thermodynamic limit we can replace the sum in (2.101) by an integral over the density of states so for the state with two holes at $\lambda^{\rm h}_{1,2}$ corresponding to the missing quantum numbers $I^{\rm h}_{1,2}$ we get

$$Z(\lambda) = Np(\lambda,1,1) + p(\lambda+c,1,1) - \int {\rm d}\mu\, p(\lambda-\mu,2,1)\left[\rho_{\rm gs}(\mu) + \rho^{\rm h}(\mu)\right]. \qquad (2.101)$$

Evaluating this at one of the hole positions $\lambda = \lambda^{\rm h}_1$ and using (2.92) we find after some algebra that

$$\begin{aligned} 2D\arctan e^{\frac{\pi}{\gamma}\lambda^{\rm h}_1} &= \frac{2\pi}{L}I^{\rm h}_1 + \frac{1}{L}\int_{-\infty}^{\infty}\frac{{\rm d}\omega}{4\pi i\omega}\frac{e^{i\omega(\lambda^{\rm h}_1+c)}}{\cosh(\gamma\omega/2)} \\ &\quad + \frac{1}{L}\int_{-\infty}^{\infty}\frac{{\rm d}\omega}{4\pi i\omega}e^{i\omega(\lambda^{\rm h}_1-\lambda^{\rm h}_2)}\frac{\sinh[(\pi-2\gamma)\omega/2]}{\sinh[(\pi-\gamma)\omega/2]\cosh(\gamma\omega/2)} \end{aligned} \qquad (2.102)$$

Comparing this with our equation for the single particle energy in the RL model (2.20) we can identify the second term on the right with the physical impurity phase shift and the third term with the phase shift of the $\lambda^{\rm h}_1$ hole scattering past the $\lambda^{\rm h}_2$ hole. It is interesting to note that the after a redefinition of the rapidity $\lambda \to \gamma\lambda$ the impurity phase shift is independent of the anisotropy and coincides with the isotropic case [88] and is given by

$$\delta(\lambda) = \pi - 2\arctan(e^{\pi(\lambda+c/\gamma)}). \qquad (2.103)$$

2.2.5 Thermodynamics of the AKM

We now examine the thermodynamic properties of the AKM, following the the same logic as the RL model. Rather than the very simple expressions encountered in that instance however, the correlations amongst the spin degrees of freedom will result in a huge increase in complexity. To get started we must discuss the types of solutions to the Bethe equations

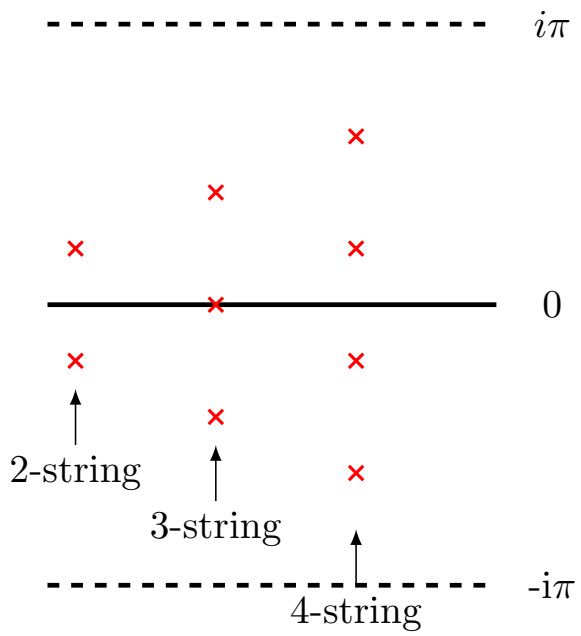

Figure 2.13: We depict here some of the types of strings allowed by the choice of $\gamma = \pi/\nu$ in the complex λ plane as given by (2.104). The distance between adjacent red crosses in the imaginary direction is $\gamma/2$.

that are possible. As was seen in the last section, the Bethe parameters, may be real as in the ground state or come in complex conjugate pairs called a 2-string as in a singlet excitation. These do not exhaust the possibilities however and other configurations of complex Bethe parameters are also allowed. The simplest types, called j-strings occur when $\gamma = \pi/\nu$ with $\nu > 2$ a positive integer. Other values of γ allow for different string configurations but in this section we shall only discuss this simplest case, for a full account see [96]. A j-string is a collection of Bethe parameters, arranged in a string like pattern around the real axis taking the form

$$\lambda^{(j,m)} = \lambda^j + i(2j+1-m)\gamma/2, \tag{2.104}$$

for $m = 1\ldots, j$, see FIG. 2.13. Given our choice for the anisotropy only strings of length $j \leq \nu - 1$ are allowed. These types of strings are said to have parity $v_j = 1$ and within this nomenclature real Bethe parameters are called 1-strings. In addition to these we may also have strings of negative parity which we refer to as ν-strings. These, $v_\nu = -1$ strings are centred on the $i\pi/2$ axis, taking the form $\lambda_\nu + i\pi/2$. Solutions containing Bethe parameters which do not fall into the string classification are also known to exist however in the thermodynamic limit and when considering the finite temperature properties of the system it is known that only the string solutions contribute[97, 98, 99, 100, 101, 102]. For an arbitrary configuration of j-strings, $\lambda_{\alpha_j}^{(j,m)} = \lambda_{\alpha_j}^{(j)} + i(2j+1-m)\gamma/2$ with $\alpha_j = 1, \ldots, M_j$. The Bethe equations become

$$Np(\lambda_{\alpha_j}^{(j)}, n_j, v_j) + p(\lambda_{\alpha_j}^{(j)} + c, n_j, v_j) = 2\pi I_{\alpha_j}^{(j)} + \sum_k^\nu \sum_{\alpha_k}^{M_k} \Theta_{jk}(\lambda_{\alpha_j}^{(j)} - \lambda_{\alpha_k}^{(k)}) \tag{2.105}$$

where Θ is the phase shift of a j-string and a k-string,

$$\begin{aligned} \Theta_{jk}(\lambda) &= p(\lambda, |n_j - n_k|, v_j v_k) + p(\lambda, n_j + n_k, v_j v_k) \\ &\quad +2 \sum_q^{n_j+n_k-2} p(\lambda, |n_j - n_k| + 2q, v_j v_k) \end{aligned} \tag{2.106}$$

with $n_j = j$, for $v_j = 1$ $j = 1 \ldots, \nu - 1$, $n_\nu = 1$ for $v_\nu = -1$. In the thermodynamic limit the real part of these strings can be described by their own continuous distributions denoted $\rho_n(\lambda)$ and $\rho_n^{\rm h}(\lambda)$ where the later is the distribution of n-string holes which satisfy the set of coupled integral equations

$$N a_j(\lambda) + a_j(\lambda + c) = \rho_j(\lambda) + \rho_j^{\rm h}(\lambda) + \sum_k^\nu A_{jk} * \rho_k(\lambda) \tag{2.107}$$

$$N a_\nu(\lambda) + a_\nu(\lambda + c) = -\rho_\nu(\lambda) - \rho_\nu^{\rm h}(\lambda) + \sum_k^\nu A_{\nu k} * \rho_k(\lambda) \tag{2.108}$$

for $1 \leq j \leq \nu$ where we have introduced $A_{jk}(\lambda) = \frac{1}{2\pi}\frac{\rm d}{{\rm d}\lambda}\Theta_{jk}(\lambda)$ and also defined $a_\nu(\lambda) = b_1(\lambda)$ and $*$ denotes a convolution $f * g(x) = \int {\rm d}y\, f(x-y)g(y)$. These are known as the Gaudin-Takahashi equations and are equivalent to (2.32) in the RL model. There are some obvious differences however, firstly there are ν of them (for ν irrational there will infact be an infinite number of them) and secondly they are all coupled. The (spin) energy of the state described by these is

$$E = \sum_{j=1}^\nu \int {\rm d}\lambda\, p(\lambda, n_j, v_j)\rho_j(\lambda) \tag{2.109}$$

and the Yang Yang entropy associated to it is a straightforward generalization of what we had before

$$S = \sum_{j=1}^\nu \int {\rm d}\lambda \rho_j(\lambda) \log\left[1 + \eta_j(\lambda)\right] + \rho_j^{\rm h}(\lambda) \log\left[1 + \eta_j^{-1}(\lambda)\right]. \tag{2.110}$$

where $\eta_j = \rho_j / \rho_j^{\rm h}$. Using this we can construct the spin part of the free energy by minimizing the functional $F = E - TS$ with respect to ρ_j and $\rho_j^{\rm h}$. As we said before this works the same in interacting and noninteracting models alike. The TBA equations determining the

saddle point of the free energy are

$$\eta_j(\lambda) = \frac{D}{T}p(\lambda, n_j, 1) + \sum_k^{\nu}(-1)^{\delta_{j,\nu}} A_{jk} * \log\left[1+\eta_j(\lambda)\right] \tag{2.111}$$

for $j < \nu$ and $\log \eta_\nu = -\log \eta_{\nu-1}$. And the free energy is given by

$$F = N\sum_j^{\nu}(-1)^{\delta_{j,\nu}} \int a_j(\lambda)\log\left[1+\eta_j(\lambda)\right] + \sum_j^{\nu}(-1)^{\delta_{j,\nu}} \int a_j(\lambda+c)\log\left[1+\eta_j(\lambda)\right] \tag{2.112}$$

Note that the TBA do not depend upon the impurity parameter, c. This is because the saddle point of the free energy in the thermodynamic limit should only depend upon bulk quantities, a term of order $1/L$ cannot shift the position of the saddle point. As should be expected however the free energy does receive an impurity contribution. These equations can be simplified considerably by inverting the matrix A_{jk} in the TBA. We carry out a similar calculation in the next chapter so we merely state that the resummed TBA are

$$\log \eta_j(\lambda) = s * \log\left(1+\eta_{j+1}(\lambda)\right)\left(1+\eta_{j-1}(\lambda)\right) + \delta_{j,\nu-2} s * \log\left(1+\eta_\nu^{-1}(\lambda)\right) - \delta_{j,1}\frac{2D}{\gamma T}\arctan e^{\frac{\pi}{\gamma}\lambda} \tag{2.113}$$

$$\log \eta_{\nu-1}(\lambda) = s * \log\left(1+\eta_{\nu-2}(\lambda)\right) = -\log \eta_\nu(\lambda) \tag{2.114}$$

where $s(\lambda) = \frac{1}{2\gamma}\mathrm{sech}(\pi\lambda/\gamma)$. The driving term in these set of integral equations can be identified as being proportional to the excitation energy of a single spinon, which is a common occurrence in TBA of this kind. One can also resum the free energy, using the $j = 1$ TBA equation (2.111) inserted into (2.112) one finds it is

$$F = E_{\mathrm{gs}} - TN\int \mathrm{d}\lambda s(\lambda)\log\left[1+\eta_1^{-1}(\lambda)\right] - T\int \mathrm{d}\lambda s(\lambda+c)\log\left[1+\eta_1^{-1}(\lambda)\right] \tag{2.115}$$

We see here a recognizable form consisting of a sum of bulk and impurity terms. The second term is the bulk part of the free energy, it can be checked that this is the as in

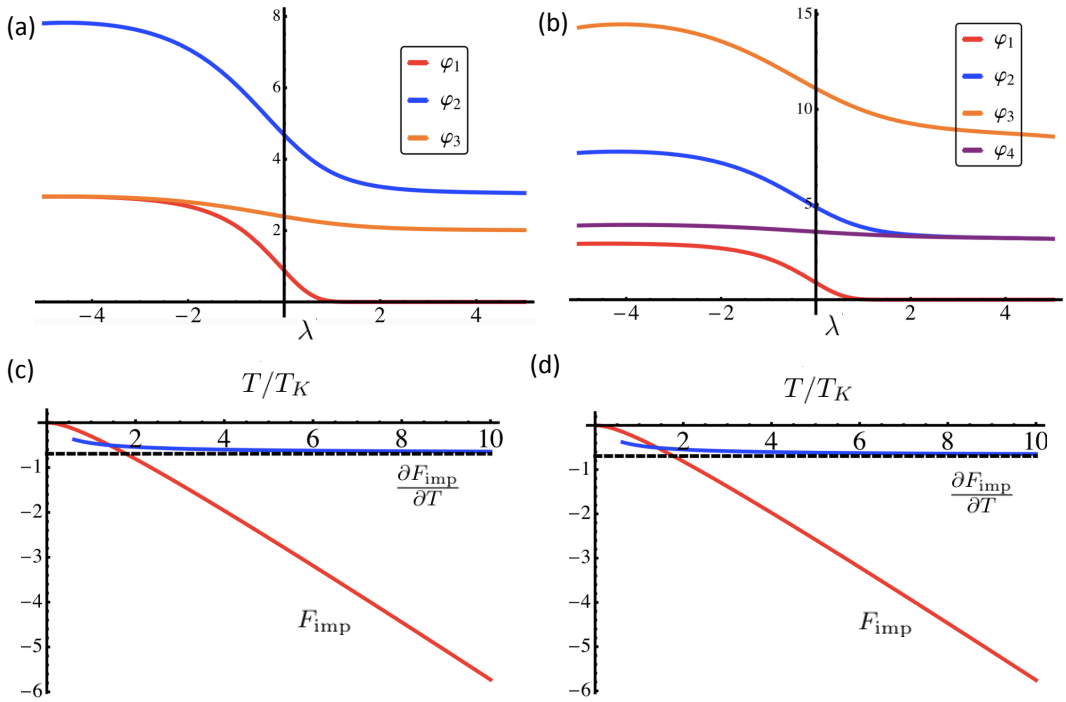

Figure 2.14: The universal TBA equations (2.118) can be numerically integrated using an iterative procedure. Here we plot the thermodynamic function e^{φ_j}, $j < \nu$ for (a) $\gamma = \pi/4$ and (b) $\gamma = \pi/5$. Below this we plot the impurity free energy (red solid) given by (2.120) as function of T/T_K for (c) $\gamma = \pi/4$ and (d) $\gamma = \pi/5$. We also plot $\frac{\partial F_{\rm imp}}{\partial T}$ (blue solid) and see it approaches $-\log(2)$ (dashed black). Thus the free energy vanishes at low temperature while the high temperature value approaches $-T\log(2)$ in agreement with our RG analysis.

the RL model[69] (recall that we consider here only the spin part so it should be the same half of a two component free, chiral Fermi gas, i,e a one component chiral, free Fermi gas). The last term is the impurity contribution, it takes a similar form to the RL model in that it is an integral over the impurity ground state density of states times the many body generalization of $\log\left(1 + e^{-k/T}\right)$.

We are now almost ready to analyze the thermodynamics of the AKM, the only step remaining being to take the universal limit. Recall in the RL model we could safely remove the cutoff on the impurity terms and obtain results which only depended on ϵ_0/Γ. The same is true here also. We must take $D \to \infty$ in both the free energy and the TBA to do

this we define the universal thermodynamic functions

$$\varphi_j(\lambda) \;=\; \frac{1}{T}\log\left(\eta_j(\lambda+\frac{\gamma}{\pi}\log\gamma\frac{T}{D})\right). \tag{2.116}$$

Inserting these into (2.114) and approximating the driving term,

$$-\frac{2D}{T}\arctan\,\exp\left(\pi(\lambda+\frac{\gamma}{\pi}\log\gamma\frac{T}{D})/\gamma\right)\simeq -2e^{\frac{\pi}{\gamma}\lambda}, \tag{2.117}$$

an approximation valid since only this range of values contributes to $\eta_1(\lambda)$, we obtain the universal (or scaling) form of the TBA equations,

$$\varphi_j(\lambda) \;=\; s*\log\left(1+e^{\varphi_{j-1}(\lambda)}\right)(1+e^{\varphi_{j+1}(\lambda)})^{1+\delta_{j,\nu-2}}-\delta_{j,1}2e^{\frac{\pi}{\gamma}\lambda},\quad j<\nu-1 \tag{2.118}$$

$$\varphi_{\nu-1}(\lambda) \;=\; s*\log\left(1+e^{\varphi_{\nu-2}(\lambda)}\right)=-\varphi_\nu(\lambda) \tag{2.119}$$

which are independent of the cutoff. In terms of these the impurity part of the free energy is given by

$$F_{\rm imp}=-T\int \mathrm{d}\lambda\, s\left(\lambda+\frac{\gamma}{\pi}\log\frac{T}{T_K}\right)\log\left[1+e^{-\varphi_1(\lambda)}\right] \tag{2.120}$$

wherein we have introduced the Kondo temperature, T_K. This scale has been dynamically generated by the model and expressed in terms of the bare parameters is

$$T_K=De^{-\frac{\pi}{\gamma}c}. \tag{2.121}$$

We can now take the universal limit by removing the cutoff $D\to\infty$ while holding T_K fixed. For weak bare coupling and anisotropy we can write this in terms of the original Hamiltonian coupling constant using (2.51)

$$T_K\sim De^{-\pi/J_\parallel} \tag{2.122}$$

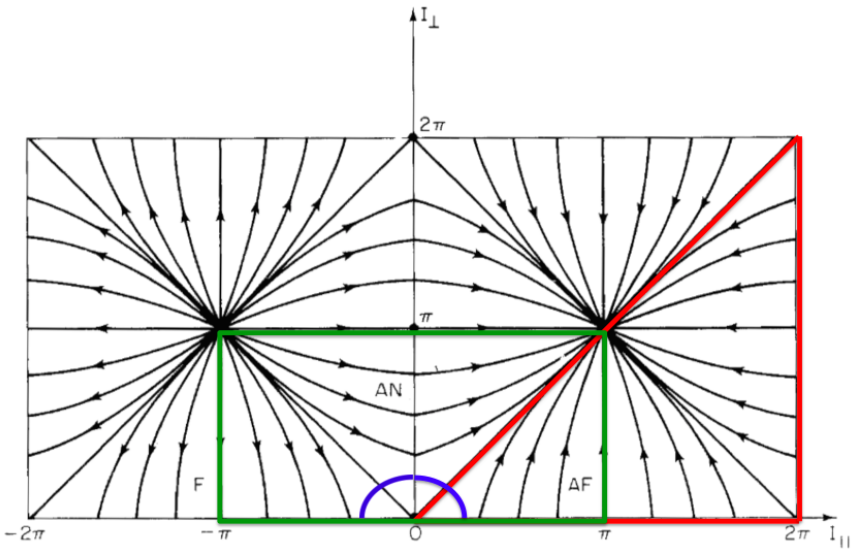

Figure 2.15: The RG flow diagram of the AKM reproduced and adapted from [69]. The vertical and horizontal axes are $J_\perp$ and $J_\parallel$ respectively and the trajectories are lines of constant γ. The red triangle represents the region for which there is a Bethe Ansatz solution, the green square is the physical parameter regime and the blue dome the weak coupling region where poor mans scaling can be applied. The remainder of the diagram is produced by invoking symmetry arguments. Image adapted from [69].

in agreement with perturbation theory. Beyond weak coupling expansion the dependence of the Kondo scale on the bare parameters does not agree with perturbation theory due to the different renormalisation schemes used. Importantly though all quantities calculated in either perturbation theory, numerically or in this way via Bethe Ansatz agree once expressed in terms of T/T_K.

The form of the Kondo scale allows us to gain a picture of the RG flow of the AKM. Inverting the relationship we see that that the coupling constant runs meaning that its strength depends upon the relevant energy scale,

$$J_\parallel(\Lambda) \sim \frac{\pi}{\log\left(\frac{T_K}{\Lambda}\right)} \tag{2.123}$$

for some energy scale, Λ which could be temperature or an external magnetic field. In particular as $\Lambda \to \infty$ the coupling constant c vanishes. This is the phenomena of asymptotic freedom, the coupling constant flows from weak coupling at high energy to strong coupling at

low energy with the consequence that the impurity becomes screened at low temperatures and is decoupled at high temperature. Away from the isotopic line the picture is more complicated and $J_\perp$ runs also with the quantity γ being a constant along the flow.

In FIG. 2.15 we depict the RG flow of the model. The vertical and horizontal axes are $J_\perp$ and $J_\parallel$ respectively, the curves are lines of constant γ which does not run under the RG flow and the arrows indicate the direction of the flow from high energy to low. The physical region which corresponds to the Kondo effect is contained within $J_\perp, |J_\parallel| \leq \pi$, the green rectangle and the region for which the Bethe ansatz solution was obtained in [35] is $0 < J_\parallel < J_\perp$, the red triangle. The region in which we have analyzed the thermodynamics the overlap of the two regions, the physical Bethe Ansatz region. Note that there exists a region which is unphysical yet still solvable by Bethe Ansatz. The blue dome indicates the perturbative region where the poor man scaling analysis of Anderson can be applied and agrees with the diagram as a whole[77]. We see that within the physical region all lines flow to (π, π) which is the strong coupling point where the impurity is screened. The vertical line at the edge of the region has the value $\gamma = \pi/2$ and is the Toulouse line, the physics of which is described by the RL model we discussed in the previous section, and the diagonal red line has $\gamma = 0$ and describes the isoptropic model. Note that the anisotropy is irrelevant and both the AKM and iostropic models flow to the same point.

This overall picture can then be confirmed by explicitly calculating the high and low temperature impurity entropy as we did for the RL model which can be done analytically or by numerically integrating the TBA equations. In FIG. 2.14 carry out a numerical integration of the TBA and free energy, we plot the thermodynamic functions e^{φ_j} for $\gamma = \pi/4$ and $\pi/5$. One sees that the free energy vanishes at low energy and approaches $-T \log 2$ as the temperature increases.

2.2.6 Alternative approach to impurity thermodynamics

An important observation to make regarding calculation of impurity quantities using Bethe Ansatz is that any impurity terms may effectively be ignored when calculating say the saddle point of the free energy or determining the ground state. The reason being that once we have identified the appropriate basis in which to diagonalize the system, i.e the correct S^{12}, the impurity only modifies the bulk behavior by terms of order $1/N$. Such a term could therefore not change the overall ground state or finite temperature properties of the bulk. Adopting such a viewpoint when studying QIMs can sometimes be advantageous due the simplifications that can occur when the impurity terms are dropped. To see this in action we can take an alternative approach to calculating the impurity free energy along the lines of the final method used to calculate the dot occupation of the RL model (2.28). Inserting (2.105) into (2.109) we find that the impurity contribution to the energy is

$$E_{\text{imp}} = -\frac{1}{L}\sum_{j=1}^{\nu}\int \mathrm{d}\lambda\, p(\lambda+c, n_j, v_j)\rho_j(\lambda). \tag{2.124}$$

where we have already taken N and L large so the system is described by the densities ρ_j. At finite temperature the particular densities appearing here are those which correspond to the solutions of the TBA, η_j. The relationship between these can be found by inverting the matrix $\mathbb{1}+A$ in (2.107) which gives

$$\rho_j(\lambda)+\rho_j^{\text{h}}(\lambda) = s * \left[\rho_{j-1}^{\text{h}}(\lambda)+\rho_{j+1}^{\text{h}}(\lambda)\right] + \left[Ns(\lambda)+s(\lambda+c)\right]\delta_{j,1} \tag{2.125}$$

along with $\rho_{\nu-1}+\rho_{\nu-1}^{\text{h}} = s * \rho_{\nu-2}^{\text{h}}$ and $\rho_{\nu-1}+\rho_{\nu-1}^{\text{h}} = \rho_\nu + \rho_\nu^{\text{h}}$. Since the densities will be used in the dot energy the $s(\lambda+c)$ term from the $j=1$ equation can be dropped as it will not contribute in the thermodynamic limit giving,

$$\rho_j(\lambda)+\rho_j^{\text{h}}(\lambda) = s * \left[\rho_{j-1}^{\text{h}}(\lambda)+\rho_{j+1}^{\text{h}}(\lambda)\right] + Ns(\lambda)\delta_{j,1}. \tag{2.126}$$

Comparing these with the TBA (2.111) one can identify

$$\rho_j(\lambda) = (-1)^{1+\delta_{j,\nu}}\gamma\frac{TL}{2\pi}\frac{\mathrm{d}}{\mathrm{d}\lambda}\log\left[1+\eta_j^{-1}(\lambda)\right]. \tag{2.127}$$

This relation is exact when the impurity term is neglected and otherwise receives an additional correction of the order $1/N$. To find the exact correction caused by the impurity requires a more careful treatment than allowed by the Yang Yang method as presented here. Using the methods developed in [103] it would be possible to find it, however when working in the $N \to \infty$ limit it is not necessary.

Inserting this into the expression for the dot energy we find that the contribution to the free energy is given by

$$F_{\mathrm{imp}} = \sum_{j=1}^{\nu}(-1)^{1+\delta_{j,\nu}}\int\frac{\mathrm{d}\lambda}{2\pi}\,p(\lambda+c,n_j,v_j)\frac{\mathrm{d}}{\mathrm{d}\lambda}\log\left[1+\eta_j(\lambda)\right] \tag{2.128}$$

$$= \sum_{j}^{\nu}(-1)^{\delta_{j,\nu}}\int a_j(\lambda+c)\log\left[1+\eta_j(\lambda)\right] \tag{2.129}$$

in agreement with our previous calculation. Therefore both approaches, this one and the exact method of the previous section yield identical results in the thermodynamic limit. The advantage of the former is that we have gained the expression (2.127) which can be very useful when calculating properties of the impurity.

2.2.7 The Interacting Resonant Level model

Before concluding our review of Bethe Ansatz and QIMs we briefly discuss another model closely related to the AKM and RL model, the interacting resonant level (IRL). The Hamiltonian was first introduced as a means of studying the AKM[104] and then subsequently solved via Bethe ansatz [105]. Following the discovery of the exact solution of the Kondo model the model fell out of favor somewhat but has since enjoyed a resurgence as an effective description of a quantum dot coupled to Fermi liquid leads.

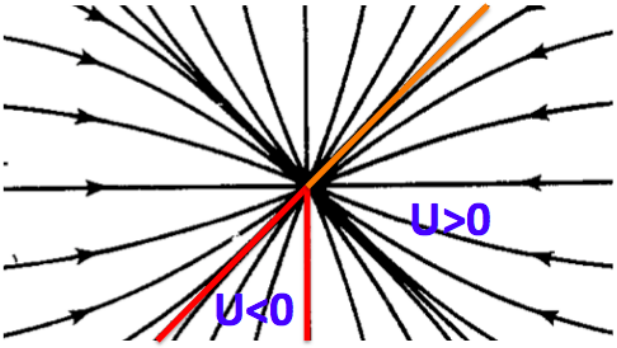

Figure 2.16: The IRL model is strongly coupled at low energy and describes the physics in the region of the Kondo strong coupling fixed point. The RG flow in the neighborhood of the fixed point is depicted above. The $U < 0$ region coincides with the physical AKM model, (bounded by the red lines) whereas the unphysical region corresponds to $U > 0$. Image adapted form [69].

The system in its simplest form consists of right moving fermions coupled to a resonant level at the origin like the RL model but with an additional Coulomb interaction between the occupied level and the bulk. The Hamiltonian is

$$H = \int -i\psi^\dagger(x)\partial_x\psi(x) + t\left[\psi^\dagger(0)d + d^\dagger\psi(0)\right] + \epsilon_0 d^\dagger d \\ + U d^\dagger d\psi^\dagger(0)\psi(0) \tag{2.130}$$

where we have taken the Coulomb interaction to be strength U. As mentioned before, this Hamiltonian is integrable and one can construct the eigenstates in the same manner as the previous models. The single particle eigenstates are the same as the RL model and given by (2.16) while the general two particle state can be written

$$|k_1, k_2\rangle = \int \sum_Q A^Q \theta(\vec{x}_Q) e^{ik_1x_1 + ik_2x_2} \psi^\dagger(x_1)\psi^\dagger(x_2)\,|0\rangle \\ + \int \sum_P \left[B_1^P e^{ik_1x} + B_2^P e^{ik_2x}\right] \theta(x_P)\psi^\dagger(x)d^\dagger\,|0\rangle\,. \tag{2.131}$$

Here, in the first line we have expanded the two fermion part of the wavefunction into 6 regions which contain every ordering of the particles with respect to the origin [3]

$$\begin{aligned}\sum_Q A^Q\theta(\vec{x}_Q) &= A^{[120]}\theta(x_2-x_1)\theta(-x_2)\theta(-x_1)+A^{[210]}\theta(x_1-x_2)\theta(-x_2)\theta(-x_1)\\ &\quad +A^{[201]}\theta(-x_2)\theta(x_1)+A^{[102]}\theta(-x_2)\theta(x_1)\\ &\quad +A^{[021]}\theta(x_1-x_2)\theta(x_2)\theta(x_1)+A^{[012]}\theta(x_2-x_1)\theta(x_2)\theta(x_1) \qquad (2.132)\end{aligned}$$

In the second line of (2.131), the wavefunction in the dot part is expanded in regions P which correspond to the fermion being either to the left or to the right of the origin e.g. $B_2^{[10]}$ is the amplitude for the particle with k_2 to the left of the dot while the other particle is on it.

Acting on this state with the Hamiltonian we find it is an eigenstate provided,

$$\frac{A^{[201]}}{A^{[210]}} = \frac{A^{[012]}}{A^{[102]}} = \frac{k_1-\epsilon_0-i\Gamma}{k_1-\epsilon_0+i\Gamma}, \qquad (2.133)$$

$$\frac{A^{[102]}}{A^{[120]}} = \frac{A^{[021]}}{A^{[201]}} = \frac{k_2-\epsilon_0-i\Gamma}{k_2-\epsilon_0+i\Gamma} \qquad (2.134)$$

where these are recognizable as being the phase acquired by a particle with energy k_j scattering past the dot. Furthermore the two particle interaction U imposes the condition

$$\frac{A^{[210]}}{A^{[120]}} = \frac{A^{[021]}}{A^{[012]}} = S^{12} \qquad (2.135)$$

$$S^{12} = \frac{k_1+k_2-2\bar{\epsilon}_0-i\frac{U}{2}(k_1-k_2)}{k_1+k_2-2\bar{\epsilon}_0+i\frac{U}{2}(k_1-k_2)}. \qquad (2.136)$$

S^{12} being the S-matrix when a particle of energy k_1 scatters past one of energy k_2, and we defined $\bar{\epsilon}_0=\epsilon_0-\Gamma U/2$. Proceeding in the same way all the eigenstates of the IRL can be constructed and the spectrum determined by applying periodic boundary conditions.

[3] The original solution of the model in [105] had a different expansion of the general 2 particle wavefunction corresponding to a different regularization of the delta functions and Heavisides. The resulting wavefunction is similar however there are some slight but important differences.

In contrast to the AKM this does not lead to another eigenvalue problem which needs to be solved via QISM. Since the two particle S-matrix, S^{12} is actually just a phase, the Bethe equations are obtained directly by writing down the periodic boundary conditions equation. In this sense the IRL is a much easier model to solve but one which contains no less interesting physics. The resulting set of Bethe equations are

$$e^{-ik_jL} = \frac{k_j - \epsilon_0 - i\Gamma}{k_j - \epsilon_0 + i\Gamma}\prod_l^N \frac{k_j + k_l - 2\bar{\epsilon}_0 - i\frac{U}{2}(k_j - k_l)}{k_j + k_l - 2\bar{\epsilon}_0 + i\frac{U}{2}(k_j - k_l)}. \tag{2.137}$$

As was the case with the AKM there is some ambiguity in how the parameter U appears in the above two particles phase shift. It must be related to some measurable quantity. To do this we recall that using the Coulomb gas representation of Anderson and Yuval[15, 106, 107] one can view the partition function of this model as being due to a series of Fermi edge singularities [108]. By comparing results in both the Bethe formulation and the Coulomb gas we can replace any instance of U with the Fermi edge exponent

$$\alpha_{\mathrm{FES}}(U) \leftrightarrow 1 - \frac{2}{\pi}\arctan(U/2). \tag{2.138}$$

Note that usually Fermi edge exponent consists of two terms the Mahan term and the Anderson term. It would seem that the above relation is missing the latter and would only agree for $U \ll 1$ however this the same discrepancy we encountered when studying the AKM. Once the above replacement is made the results in both methods agree.

In opening this section we mentioned that there exists a close relationship between the IRL and the AKM, in fact it is often stated that the two models are the same. To expand more on this we rewrite the IRL Bethe equations in terms of the particle rapidity $k_j = \mathcal{D}e^{x_j} - \bar{\epsilon}_0$ [109],

$$e^{-i\mathcal{D}e^{x_j}L} = e^{i\bar{\epsilon}_0 L}\frac{\cosh\frac{1}{2}(x_j - c + i\gamma)}{\cosh\frac{1}{2}(x_j - c - i\gamma)}\prod_l^N \frac{\sinh\frac{1}{2}(x_j - x_l - 2i\gamma)}{\sinh\frac{1}{2}(x_j - x_l + 2i\gamma)}$$

where we have taken $\gamma = \frac{\pi}{2} + \arctan\left(\frac{U}{2}\right)$ and $e^c \propto \frac{\Gamma}{\mathcal{D}}$. Which are very close to those describing the AKM. We shall encounter very similar equations in the next section and so leave a full analysis to then however it should be noted that the left hand side of the two sets of Bethe equations are different. This difference prevents one from equating the two models outside of the low energy regime where one can show they agree [69]. Thus the low energy physics of the IRL is the same as the AKM and its RG diagram is the same as the AKM in the region of the strong coupling fixed point see FIG. 2.16. Comparing the definition of the anisotropy parameter in both models at weak bare coupling gives $\sqrt{J_\parallel^2 - J_\perp^2} \approx \pi/2 + U/2$ meaning that the physical region of the AKM corresponds to an attractive Coulomb interaction $U < 0$.

2.3 Conclusion

In this chapter we have studied the physics of a number of quantum impurity models, the resonant level model, the anisotropic Kondo model and then very briefly the interacting resonant level model. To do this we have used the Bethe Ansatz method which allowed us to calculate the exact eigenstates and spectra of each model. We saw that the same basic principles applied in both the relatively simple RL model and more complicated the AKM. The exact solution allowed us to determine the ground state, excitations and free energy although we only carried this out in the first two. We also discussed some subtleties regarding coupling constants in Bethe Ansatz solutions and emphasized the importance of relating constants to physical quantities.

In this very brief overview of QIMs and Bethe Ansatz we have neglected to mention some important topics. For example the AKM remains integrable in the presence of an applied magnetic field, in fact since the total z-component of spin is conserved the eigenstates are the same as we derived above but the energy level naturally get shifted. It is possible then to derive the ground state and finite temperature properties of the impurity in the presence of this field, we shall complete such calculations in subsequent chapters and so for brevity have

omitted them in this chapter. Another omission is the quantum transfer matrix method approach to integrable thermodynamics. This elegant approach does not require the string hypothesis but gives entirely equivalent results. Throughout the thesis we shall rely upon the Yang Yang method and the string hypothesis however we present a brief overview of this method as it applies to QIMs in the appendix.

Throughout the rest of the thesis we will re use the same concepts and techniques sometimes in a modified form. We will endeavor to provide a very brief review of these concepts when they are employed in future chapters and ask the reader to refer back here for a more complete account.

3

Quantum Dot at a Luttinger Liquid edge

3.1 Quantum dot at a Luttinger liquid edge

In this chapter we begin to present the original work of this thesis. We study a system consisting of a Luttinger liquid coupled to a quantum dot on the boundary. The Luttinger liquid is expressed in fermionic form and the dot is modeled as an interacting resonant level on to which the bulk fermions can tunnel. We use the fermionic form of the Hamiltonian so as to make use of the Bethe Ansatz method which is the main theoretical tool of this thesis. The model can be considered a warm up problem to those presented in the next chapters. It is simpler as the bulk system has no internal degrees of freedom and the impurity only allows forward scattering.

We will solve the Hamiltonian exactly and construct all eigenstates using a nonstandard coordinate Bethe Ansatz. This nonstandard appraoch will be extended in the next chapters to more complex models.

3.2 Introduction

As we discussed in the introductory chapter Luttinger liquid theory posesses some remarkable features. Notably, the presence of interaction causes the Fermi surface to be destroyed so that the excitations are collective bosonic density perturbations. The effects of the electrons being dissolved are most dramatic when the system is coupled to an impurity and in particular to a quantum dot [12]. Quantum dots are created by confining a two dimensional electron gas to small enough size that its energy levels become discrete and the relevant

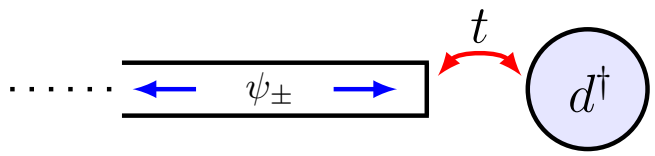

Figure 3.1: Our system consists of a semi infinite Luttinger liquid coupled to a quantum dot modeled as a resonant level. The Luttinger liquid consists of left and right moving interacting fermions which can tunnel to and from the level and experience a Coulomb force from an occupied dot.

degrees of freedom on the dot are fermionic. Therefore when coupled to a Luttinger liquid there exists an interplay between the tunneling which is mediated by fermions and the large number of bosons excited as a fermion is added to the bulk.

The system we study in this chapter is depicted in FIG. 3.1: a spinless Luttinger liquid is coupled to a quantum dot at the boundary. The model can describe a quantum dot placed at the end of a spin-polarized nano wire[110] or placed in the middle of a fractional quantum Hall edge [50]. We construct the exact eigenstates of the system through the Bethe Ansatz method and go on to study both the zero and finite temperature properties of the system. In particular we compute the exact dot occupation as a function of the dot energy in all parameter regimes. Through the exact solution we show system flows from weak to strong coupling for all values of the bulk interaction, with the flow characterized by a non-perturbative Kondo scale, T_K. The weak coupling regime corresponding to a decoupled (or localized) dot and Luttinger liquid while the strong coupling regime constitutes a dot that is fully hybridized with the bulk. We identify the critical exponents at the weak and strong coupling regimes.

Having analyzed the system thoroughly using Bethe Ansatz we compare with work done on this model using the method of Bosonization. We show that although a naive analysis of the system using this method will produce similar conclusions one must make an incorrect identification of the bulk system in order to do so.

3.3 The Hamiltonian

As depicted in FIG 3.1 we consider a Luttinger liquid on a half line. The Hamiltonian is given by

$$\begin{aligned} H_{\mathrm{LL}} &= -i\int_{-L/2}^{0} dx(\psi_+^\dagger\partial_x\psi_+ - \psi_-^\dagger\partial_x\psi_-) \\ &\quad +4g\int_{-L/2}^{0} dx\,\psi_+^\dagger(x)\psi_-^\dagger(x)\psi_-(x)\psi_+(x) \end{aligned} \tag{3.1}$$

where $\psi_\pm^\dagger$ are right and left moving fermions restricted to the space $x \in [-L/2, 0]$ [10] and we have set $v_f = 1$ and $\epsilon_f = 0$. There are normally two $U(1)$ conserved charges present in H_{LL} namely the number of left and right movers, $\hat{N}_\pm = \int_{-L/2}^{0}\psi_\pm^\dagger(x)\psi_\pm(x)$. These are combined to a single conservation law by the boundary condition $\psi_-(0) = -\psi_+(0)$ mixing the two chirality particles.

By itself this Hamiltonian is easy to diagonalize and it is most conveniently done by unfolding the system to the full line using $\psi_-(x) = -\psi(-x)$ and $\psi_+(x) = \psi(x)$ for $x \leq 0$. The result of this is

$$H'_{\mathrm{LL}} = -i\int_{-L/2}^{L/2} dx\psi^\dagger\partial_x\psi + \int_{-L/2}^{L/2} 4g\psi^\dagger(x)\psi^\dagger(-x)\psi(-x)\psi(x)$$

so that only right movers are present but the interaction is now non local and the system extends from $-L/2$ to $L/2$. In the unfolded model the interaction occurs between two particles only when $x_1 + x_2 = 0$ and we can expand the wavefunction in plane waves and as a sum of Heaviside functions $\theta(\pm(x_1 + x_2))$. The general two particle eigenstate with energy $E = k_1 + k_2$ can therefore be written as,

$$|k_1, k_2\rangle = \int \mathrm{d}\vec{x} F(x_1 + x_2)\prod_{j=1}^{2} e^{ik_j x_j}\psi^\dagger(x_j)\,|0\rangle$$

where similar to previous models we take $F(z) = A\theta(-z) + B\theta(z)$. Acting on this state

with H'_{LL} we find it to be an eigenstate provided

$$\left[-i\partial_{x_1} - i\partial_{x_2} + 4g\delta(x_1 + x_2)\right] F(x_1 + x_2) = 0. \tag{3.2}$$

The solution of this is easily found to be

$$F(x_1 + x_2) = \theta(x_1 + x_2) + e^{i\phi}\theta(-x_1 - x_2) \tag{3.3}$$

where $\phi = -2\arctan(g)$ is the two particle phase shift. The relation between ϕ and g is dependent on how one regularizes the delta function interaction however the different schemes one can use agree at weak coupling so that one can write $\phi \sim -2g$, (c.f. (2.51)).

The generalization to higher particle numbers is straightforward. The N particle eigenstate with energy $E = \sum_j k_j$ is

$$\left|\vec{k}\right\rangle = \int \mathrm{d}\vec{x} \prod_{i<j} F(x_i + x_j) \prod_{j=1}^{N} e^{ik_j x_j} \psi^\dagger(x_j) \left|0\right\rangle \tag{3.4}$$

which can be confirmed explicitly by acting upon this state with H'_{LL}.

Having identified the eigenstates of the Luttinger liquid on a half line we can now determine the spectrum. As is standard in quantum mechanics we do this by imposing a boundary condition which will give us a quantization condition for the single particle energy levels. Imposing periodic boundary conditions $\psi(L/2) = \psi(-L/2)$ in the unfolded language of H' corresponds to an open boundary condition, $\psi_+(-L/2) = -\psi_-(-L/2)$ in the original folded system of H_{LL}. This constrains the single particle energies k_j, $j = 1, \ldots N$ according to

$$e^{-ik_j L} = e^{i(N-1)\phi} \tag{3.5}$$

with the total energy being the sum of these $E = \sum_j^N k_j$. Thus the energy levels of a

Luttinger liquid in a box are shifted by a constant compared to those of a free model,

$$E = \sum_{j}^{N} \frac{2\pi n_j}{L} - N(N-1)\frac{\phi}{L} \tag{3.6}$$

with n_j being integers which serve as the quantum numbers of the state.

As we discussed in the previous chapter the system can likewise be described using bosonization so that the Hamiltonian takes the form

$$H_{LL} = \frac{u_F}{2\pi} \int_{-L/2}^{0} \mathrm{d}x\, K \left[\nabla\varphi(x)\right]^2 + \frac{1}{K}\left[\Pi(x)\right]^2 \tag{3.7}$$

where $\varphi(x)$ and $\Pi(x)$ are canonically conjugate bosonic fields and $K \approx 1 - 2g/\pi$. We will naturally want to compare the bosonic and fermionic approaches which requires us to determine this relation between K and ϕ. To do so we compute the compressibility in the fermionic language and match it to the known result from bosonization. With this in mind we recall that the linear spectrum of the fermionic model (3.1) means we need to impose a momentum cutoff of $-\mathcal{D}$ and construct the ground state by populating states from this level up. Therefore in the thermodynamic limit the ground state energy for the system with density $D = N/L$ and chemical potential μ is,

$$\frac{E}{L} = \int_{-\mathcal{D}}^{2\pi D - \mathcal{D}} \left[k - \left(\phi \int_{-\mathcal{D}}^{2\pi D - \mathcal{D}} \frac{\mathrm{d}q}{2\pi}\right) - \mu\right] \frac{\mathrm{d}k}{2\pi}. \tag{3.8}$$

Varying the density with both the cutoff and μ held fixed we can find how the Density depends upon μ which is used to find the compressibility of the bulk. Sending $D \to D + \delta D$ and minimizing E with respect to δD we get $2\pi(1 - \frac{\phi}{\pi})D = \mathcal{D} + \mu$ and so the compressibility is related to ϕ by $\phi/\pi = 1 - \varkappa/\varkappa_0$ where we denote the free compressibility by $\varkappa_0 = 1/2\pi$ and that of the Luttinger liquid $\varkappa$. An analogous calculation performed in the bosonic language gives the compressibility in terms of K[10, 14]. The relation between the our

bosonic and fermionic parameters is

$$\frac{\phi}{\pi} = 1 - \frac{1}{K}. \tag{3.9}$$

We replace the renormalization scheme dependent coupling g with the scattering phase ϕ which can be directly related to measurable quantities via (3.9). Note that being a phase ϕ is restricted to lie in the interval $[-\pi, \pi]$ and therefore the fermionic Hamiltonian (3.1) can only realize $K \in [1/2, \infty]$. It should be kept in mind however that the Luttinger Hamiltonian serves only as the low energy description of many one dimensional systems provided g and K are not too large. The allowed range of values of K depending upon specifics of the original model.

The Luttinger wire is attached to a quantum dot modeled by a resonant level with energy ϵ_0 via a tunneling term t [111]. They are further coupled via a Coulomb interaction U,

$$H_t = \frac{t}{2}(\psi_+^\dagger(0) - \psi_-^\dagger(0))d + \text{h.c}, \tag{3.10}$$

$$H_d = \epsilon_0 d^\dagger d + \frac{U}{2} d^\dagger d \sum_{\sigma=\pm} \psi_\sigma^\dagger(0)\psi_\sigma(0). \tag{3.11}$$

When coupled to the dot the conservation law takes the form $\hat{N} = \hat{N}_+ + \hat{N}_- + \hat{n}_d$, the total particle number (here $\hat{n}_d = d^\dagger d$). In writing the Coulomb term in this may we can view $U > 0$ as being a repulsion between an occupied dot and a fermion at the edge of the wire or alternately as an attractive interaction between a hole on the dot and a fermion on the edge. The later viewpoint will prove useful when analyzing the renormalization group behaviour of the model.

3.4 The Eigenstates

We will proceed with the diagonalization of $H = H_{LL} + H_t + H_d$ in the usual Bethe Ansatz manner by first finding the single particle eigenstates, then the two particle states from which we deduce the N particle solution. Following this the spectrum is determined in terms of the Bethe Ansatz equations by imposing boundary conditions on the system.

Turning now to the full model we again unfold the system as before but this time must consider first the single particle state. The most general single particle state of energy k can be written as

$$|k\rangle = \int e^{ikx} \left[A^{[10]}\theta(-x) + A^{[01]}\theta(x) \right] \psi^\dagger(x) |0\rangle + Bd^\dagger |0\rangle \tag{3.12}$$

Upon acting on this state with the Hamiltonian we find it is an eigenstate provided,

$$S^{10} = \frac{A^{[01]}}{A^{[10]}} = \frac{k - \epsilon_0 - i\Gamma}{k - \epsilon_0 + i\Gamma}, \tag{3.13}$$

$$B = \frac{t}{k - \epsilon_0} \left(A^{[10]} + A^{[01]} \right). \tag{3.14}$$

The quantity $\Gamma = t^2/2$ is the hybridization width while S^{10} is the single particle S-matrix for fermion scattering past the dot. Since the bulk interaction is not active in the single particle sector this eigenstate coincides with the resonant level model of the previous chapter.

Moving to the two particle case the interaction parameters U and g enter into play. We can write the state with energy $E = k_1 + k_2$ as

$$\begin{aligned} |k_1, k_2\rangle = & \int \sum_Q A^Q \theta(\vec{x}_Q) e^{ik_1x_1 + ik_2x_2} \psi^\dagger(x_1)\psi^\dagger(x_2) |0\rangle \\ & + \int \sum_P \left[B_1^P e^{ik_1x} + B_2^P e^{ik_2x} \right] \theta(x_P)\psi^\dagger(x) d^\dagger |0\rangle . \end{aligned} \tag{3.15}$$

Here, in the first line we have expanded the two fermion part of the wavefunction into 8 regions which contain every ordering of the particles in addition to distinguishing whichever is

closest to the origin, labelled by $Q \in \{[120],[210],[012],[021],[102A],[102B],[201A],[201B]\}$. For example the amplitude $A^{[102B]}$ corresponds to the region with $x_1 < 0 < x_2$ and $|x_1| > |x_2|$ whereas $A^{[102A]}$ has $|x_2| > |x_1|$. The $\theta(\vec{x}_Q)$ are Heaviside functions which are non zero only in the region Q. Explicitly we have

$$\begin{aligned}\sum_Q A^Q\theta(\vec{x}_Q) &= A^{[120]}\theta(x_2-x_1)\theta(-x_2)\theta(-x_1) + A^{[210]}\theta(x_1-x_2)\theta(-x_2)\theta(-x_1) \\ &+A^{[102A]}\theta(-x_2-x_1)\theta(x_2)\theta(-x_1) + A^{[102B]}\theta(x_2+x_1)\theta(x_2)\theta(-x_1) \\ &+A^{[201A]}\theta(x_2+x_1)\theta(-x_2)\theta(x_1) + A^{[201B]}\theta(-x_2-x_1)\theta(x_2)\theta(-x_1) \\ &+A^{[021]}\theta(x_1-x_2)\theta(x_2)\theta(x_1) + A^{[012]}\theta(x_2-x_1)\theta(x_2)\theta(x_1) \qquad (3.16)\end{aligned}$$

These extra regions compared to standard Bethe wavefunctions are required by the non local interaction and we will see throughout this thesis that this is necessary when searching for Bethe Ansatz solutions of Luttinger impurity sytems. In the second line of (3.15), the wavefunction in the dot part is expanded in regions P which correspond to the fermion being either to the left or to the right of the origin e.g. $B_2^{[10]}$ is the amplitude for the particle with k_2 to the left of the dot while the other particle is on it represented by $d^\dagger$.

Acting on this state with the Hamiltonian we find it is an eigenstate provided,

$$\frac{A^{[201A]}}{A^{[210]}} = \frac{A^{[012]}}{A^{[102A]}} = \frac{k_1-\epsilon_0-i\Gamma}{k_1-\epsilon_0+i\Gamma}, \qquad (3.17)$$

$$\frac{A^{[102B]}}{A^{[120]}} = \frac{A^{[021]}}{A^{[201B]}} = \frac{k_2-\epsilon_0-i\Gamma}{k_2-\epsilon_0+i\Gamma}, \qquad (3.18)$$

$$\frac{A^{[102A]}}{A^{[102B]}} = \frac{A^{[201B]}}{A^{[201A]}} = e^{i\phi} \qquad (3.19)$$

$$\frac{A^{[210]}}{A^{[120]}} = \frac{A^{[021]}}{A^{[012]}} = S^{12} \qquad (3.20)$$

with

$$S^{12} = \frac{k_1+k_2-2\bar{\epsilon}_0-i\frac{U'}{2}(k_1-k_2)}{k_1+k_2-2\bar{\epsilon}_0+i\frac{U'}{2}(k_1-k_2)} \qquad (3.21)$$

being the S-matrix when a particle of energy k_1 scatters past one of energy k_2, and we defined,

$$\begin{aligned} \arctan\left(U'/2\right) &= \arctan\left(U/2\right) - \arctan\left(g\right) \\ \bar{\epsilon}_0 &= \epsilon_0 - \Gamma U'/2. \end{aligned}$$

The parameters U' and $\bar{\epsilon}_0$ are bare quantities and as such depend upon the regularization scheme employed. These parameters must be related to universal quantities to acquire meaning as is always the case for renormalizable field theories. Below we relate U' to K and $\bar{\epsilon}_0$ to the renormalized dot energy.

Generalizing to N particles, the state consists of parts with the dot occupied or unoccupied. The latter is written as

$$\left|\vec{k}\right\rangle = \sum_Q \int A^Q \theta(\vec{x}_Q) e^{\sum_j^N k_j x_j} \prod_{j=1}^N \psi^\dagger(x_j) \left|0\right\rangle . \tag{3.22}$$

The sum is now over $2^N N!$ regions Q and the amplitudes are related to each by generalisations of the the various phase shifts given in (3.13), (3.21) and (3.19),

$$S^{j0} = \frac{k_j - \epsilon_0 - i\Gamma}{k_j - \epsilon_0 + i\Gamma} \tag{3.23}$$

$$S^{ij} = \frac{k_i + k_j - 2\bar{\epsilon}_0 - i\frac{U'}{2}\left(k_i - k_j\right)}{k_i + k_j - 2\bar{\epsilon}_0 + i\frac{U'}{2}\left(k_i - k_j\right)}. \tag{3.24}$$

The occupied dot part can also be written in such a fashion, we omit it here as we will only require (3.22) to proceed. The consistency of the solution is guaranteed as the S-matrices satisfy the reflection equation [112],

$$S^{k0} e^{i\phi} S^{j0} S^{jk} = S^{jk} S^{j0} e^{i\phi} S^{k0} \tag{3.25}$$

along with the Yang Baxter equation $S^{ki}S^{ji}S^{jk} = S^{jk}S^{ji}S^{ki}$. In contrast to the AKM they satisfy these consistency conditions trivially as all the S-matrices are phases and furthermore note that S^{ij} was determined by the Hamiltonian rather than being a solution of the Yang Baxter equation.

The k dependent two body S-matrix (3.21) is the same form as the IRL model which describes a dot coupled to Fermi liquid leads [105]. The effect of the bulk interaction on this is to shift $U \to U'$. This makes explicit the relationship between the IRL and the Luttinger resonant level model seen in [113], that is, when only the thermodynamics of the dot are concerned one can deal with the level-lead interaction instead of a bulk interaction. Bulk properties, however, differ in both models as does the structure of the wave functions which will show up as different correlation functions. We comment further on this below when comparing the Bethe Ansatz results to those obtained using bosonization.

To determine the spectrum we impose periodic boundary conditions in the unfolded system which as stated before corresponds to an open boundary condition at $x = -L/2$ in the folded language. Upon doing so we find the Bethe equations which determine the k_j,

$$e^{-ik_jL} = e^{i(N-1)\phi}\frac{k_j - \epsilon_0 - i\Gamma}{k_j - \epsilon_0 + i\Gamma}\prod_l^N \frac{k_j + k_l - 2\bar{\epsilon}_0 - i\frac{U'}{2}(k_j - k_l)}{k_j + k_l - 2\bar{\epsilon}_0 + i\frac{U'}{2}(k_j - k_l)}. \tag{3.26}$$

The interpretation of these in the folded system is an incoming right mover incident from the left, moving toward the dot and scattering past the other particles in the system. When the other particle is an outgoing left mover a constant phase $e^{i\phi}$ is acquired whereas if it goes past another incoming particle it gains the k dependent two particle phase shift (3.21). After scattering off the dot and picking a factor as in (3.13), the particle moves back across the system as a left mover this time picking up $e^{i\phi}$ from the remaining incoming particles and (3.21) from the other outgoing left movers.

We conclude this section by remarking that the coupling of the dot to the bulk system has caused two differences in the Bethe equations as compared to the $e^{-ik_jL} = e^{i(N-1)\phi}$ we

found above for a Luttinger liquid in a box. These are the inclusion of the dot phase shift and the k dependent two particle phase shift. The complicated nature of the two particle phase shift that has been induced by the presence of the impurity is a reflection of the fact that quantum impurities can cause strong correlations of bulk materials. The physics of the impurity is the result of highly nontrivial many body effects. In the absence of the Luttinger liquid interaction we recover the Bethe equations of the IRL model discussed in the previous chapter.

Moreover we would like to comment that the relation between K and ϕ obtained before is still valid despite the inclusion of this new two particle phase shift. To see this we drop the dot term in the Bethe equations and take their log to recover the Luttinger liquid energy,

$$E = \frac{2\pi}{L}\sum_{j}^{N} n_j - N(N-1)\frac{\phi}{L} \tag{3.27}$$

with n_j being integers. The log of the two particle phase shift is odd and therefore cancels out when summed over all particles. This is the discrete form of (3.8) and we could proceed as we did before to obtain the same relation.

3.5 Zero Temperature properties

Having obtained the Bethe equations, (3.26), we seek to identify the ground state of the system. This is most easily accomplished by describing the particles in terms of their rapidity x_j defined by $k_j = \mathcal{D}e^{x_j} + \bar{\epsilon}_0$, where $-\mathcal{D}$ is the lower momentum cutoff. The energy is now: $E = \sum_j^N \mathcal{D}e^{x_j} + N\bar{\epsilon}_0$ and (3.26) becomes,

$$\begin{aligned} e^{-i\mathcal{D}e^{x_j}L} &= e^{i(N-1)\phi + i\bar{\epsilon}_0 L}\frac{\cosh\frac{1}{2}(x_j - c + i\Delta)}{\cosh\frac{1}{2}(x_j - c - i\Delta)} \\ &\quad \times \prod_{l}^{N}\frac{\sinh\frac{1}{2}(x_j - x_l - 2i\Delta)}{\sinh\frac{1}{2}(x_j - x_l + 2i\Delta)} \end{aligned} \tag{3.28}$$

The parameters Δ, c and ϕ encode the interactions in the model and the effect of the dot, they are defined as

$$e^c = \gamma\frac{\Gamma}{\mathcal{D}} \tag{3.29}$$

$$\Delta = \frac{\pi}{2}\left(2-\frac{1}{K}\right)+\arctan\left(\frac{U}{2}\right). \tag{3.30}$$

with $\gamma = 1/\sqrt{1+(U'/2)^2}$. Here we see that the presence of the U contributes to a local modification of ϕ or K in the bosonized language. This could be understood physically by integrating out the dot degrees of freedom, whereupon the interaction term in the Hamiltonian is modified locally near the dot. Alternatively recall also that we can relate $\arctan(U/2)$ to $\alpha_{\rm FES}(U)$ and so we can see that the bulk interaction causes a shift in this quantity $\alpha_{\rm FES} \leftrightarrow \frac{1}{K}-\frac{2}{\pi}\arctan(U/2)$. Bulk properties are still dependent only on ϕ or K but dot quantities like the occupation calculated below depend on Δ. At $\Delta = \pi/2$ the two particle phase shift vanishes and the system simplifies considerably. Setting $U = 0$ this corresponds to the resonant level model of free fermions coupled to the dot. At nonzero U however it is possible to tune bulk and boundary interactions in a manner which results in a free model.

Identifying the ground state

To identify the ground state of the system we must list the possible types of solutions to the Bethe equations (3.28). In order to do so we note that apart from the dot term the Bethe equations are similar to those of the massive Thirring model which have been widely studied [114][115][116][117] and in fact can be thought of as a massless limit of these [118][119]. This massless limit is known not to change the possible types of solutions known as strings which depend upon Δ and we now list. First consider $\Delta > \pi/2$ and in particular take

$$\pi\frac{\nu-2}{\nu-1} < \Delta \leq \pi\frac{\nu-1}{\nu} \tag{3.31}$$

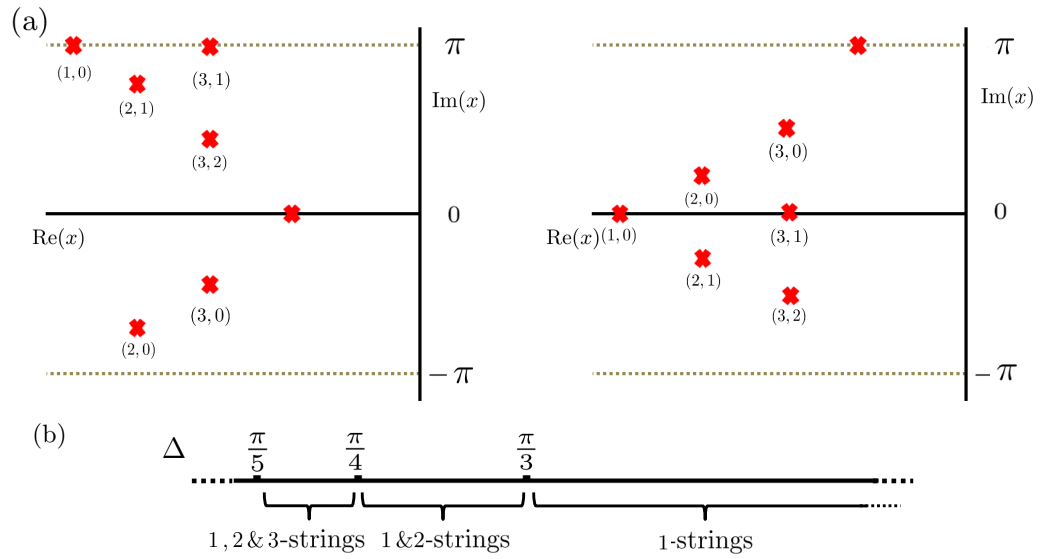

Figure 3.2: (a) The configurations of allowed strings for $\pi/4 \leq \Delta < \pi/3$ on the left and for $2\pi/3 < \Delta \leq 3\pi/4$ on the right. In both cases strings of length up $n \leq 3$ are allowed, as well as additional 1-strings corresponding to a positive/negative energy particle (analogous to the negative parity strings of the AKM). Red crosses mark the string elements and underneath each (n, l) denotes the string length and the element of the string (see text). On the left, the spacing between adjacent elements of a string, i.e between l and $l+1$ for fixed n, is $i\Delta$ and the elements are symmetrically placed (modulo 2π) with respect to $i\pi$ axis, in addition to real 1-strings. For the strings on the right, the spacing is $i(\pi - \Delta)$, the elements are symmetrically placed around the real axis and there are 1-strings occupying the $i\pi$ axis. 2 (b) The form of the ground state depends on the regime in which Δ lies. For $\Delta > \pi/3$ it consists of $1-$ strings only, below this it changes to consisting of $1-$ and $2-$ strings and then to include $3-$strings and so on.

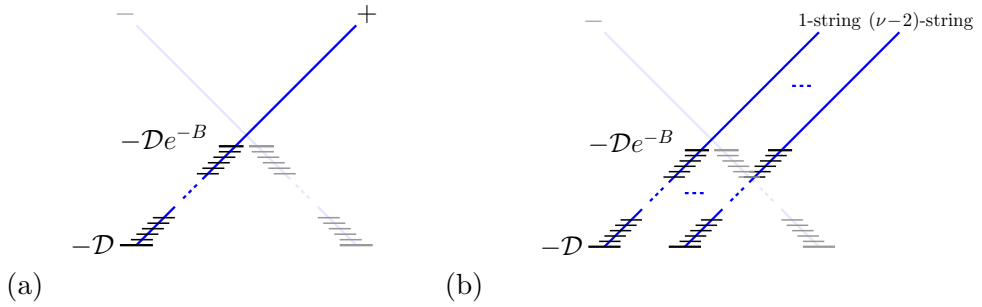

Figure 3.3: (a) In the regime $\Delta \geq \pi/3$ the ground state consists of a single type of right moving particle. The state is constructed by populating all negative energy particles of from the cutoff $-\mathcal{D}$ up to some level $-\mathcal{D}e^{-B}$ with B determine by the dot energy ϵ_0. (b) For $\Delta < \pi/3$ there are additional (right moving) negative energy particles in the spectrum corresponding to strings. The ground state is constructed by populating all off these negative energy particles from the cutoff up. We choose to impose the same cutoff on all these branches.

with $\nu \geq 3$ a positive integer. In this region the rapidities may form n-strings such that $x^l = x + i(\pi - \Delta)(n - 1 - 2l)$ with x real, $l = 0, \ldots, n-2$ and $0 \leq n \leq \nu - 1$. These n-strings can be thought of as bound states and have positive bare energy

$$E_n(x) = \frac{\sin(n(\pi - \Delta))}{\sin(\Delta)} \mathcal{D} e^x. \tag{3.32}$$

Additionally there are negative energy particles, the equivalent of the negative parity string in the AKM, that have $\mathrm{Im}(x) = \pi$ and bare energy $-\mathcal{D}e^x$. For $\Delta \leq \pi/2$ the range slips into regions,

$$\frac{\pi}{\nu} \leq \Delta < \frac{\pi}{\nu - 1} \tag{3.33}$$

in which the n-strings take the different form $x^l = x + i\pi + i\Delta(n - 1 - 2l)$, $l = 0, \ldots, \nu - 2$ and $n \leq \nu - 2$. The n-strings now have negative bare energy

$$E_n(x) = -\frac{\sin(n\Delta)}{\sin(\Delta)} \mathcal{D} e^x \tag{3.34}$$

and are in addition to particles with positive bare energy $E = \mathcal{D}e^x$ which have real rapidity. The arrangement of the allowed strings for two values of Δ are shown explicitly in FIG. 3.2 (a). As mentioned before, deviations to these string solutions as well solutions which fall outside this class are known to exist and are important when studying the completeness of the Bethe ansatz eigenstates as well as when correlation functions are considered [97, 98, 99, 100, 101, 102]. For our purposes however we shall simply use the strings as presented above.

Following [115], we now proceed to construct the ground state which consists of all possible negative energy particles filled from the cutoff, $-\mathcal{D}$, upwards. The same analysis also works in the case of the IRL model and was done for the first time in this work. We begin by considering the regime $\Delta \geq \pi/3$ where only one type of negative energy particle is available (below $\pi/2$ 2-strings are also allowed but these can be shown to increase the

energy). Therefore we set $\mathrm{Im}(x_j) = \pi$ in (3.28) and take the thermodynamic limit by sending $N, L \to \infty$ while the cutoff $\mathcal{D}$ is held fixed at a value larger than all quantities such as $\bar{\epsilon}_0, \Gamma$. The density, $D = N/L$ is then obtained by minimizing the energy for a given large $\mathcal{D}$, see FIG. 3.3. In this limit the particle rapidities x_j approach each other and can be described by the density of states, $\rho(x)$. Similarly holes added to this state can be described by the density $\rho^{\mathrm{h}}(x)$. The Bethe equations become an integral equation determining these distributions,

$$\frac{1}{2\pi}\mathcal{D}e^x + \frac{1}{L}a_1\left(\frac{x-c}{2}\right) = \rho(x) + \rho^{\mathrm{h}}(x) + \int_{-B}^{0} a_2\left(\frac{x-y}{2}\right)\rho^p(y) \tag{3.35}$$

where the lower integration limit B depends on $\bar{\epsilon}_0$ and is determined by minimizing the energy with the dot energy fixed and $a_j(x)$ was defined in (2.81). This then determines the hole distribution $\rho^{\mathrm{h}}(x)$.

If we set $\bar{\epsilon}_0 = 0$ then no holes appear in the ground state meaning $\rho^{\mathrm{h}}(x) = 0$ and $B = \infty$. Since we are interested in the physics at scales well below the cutoff $\mathcal{D}$ which we later send to ∞, we need only be concerned with rapidities $x \ll 0$. The ground state distribution, denoted $\rho^0(x)$ can therefore be found by Fourier transform giving

$$\rho^0(x) = \frac{\tan\left(\frac{\pi^2}{2\Delta}\right)}{\pi - 2\Delta}\frac{\mathcal{D}}{2\pi}e^{\frac{\pi}{2\Delta}x} + \frac{1}{L}s(x-c) \tag{3.36}$$

$$s(x) = \frac{1}{4\Delta\cosh(\pi x/2\Delta)} \tag{3.37}$$

The first term of $\rho^0(x)$ is the bulk contribution and the second is due to the dot.

To confirm that that this is indeed the ground state of the system for $\Delta \geq \pi/3$ we can construct excitations and check that they increase the energy. The simplest type of excitation consists of adding a hole to the ground state. Following the procedure of Chapter

2 we find that the energy $\varepsilon^h(x)$

$$\varepsilon^h(x) = \frac{\tan\left(\frac{\pi^2}{2\Delta}\right)}{\pi - 2\Delta}\mathcal{D}e^{\frac{\pi}{2\Delta}x} > 0. \tag{3.38}$$

Here the excitation is proportional to the bulk part of the ground state density of states, this a feature shared by many Bethe Ansatz solvable models although not by the AKM. Other excitations consist of adding n-strings or positive energy particles which can also be shown to increase the energy.

We now consider the parameter regime, $\Delta < \pi/3$. The availability of additional negative energy particles in this regime changes the nature of the ground state [116]. More specifically, for values of Δ specified by (3.33) the ground state consists of all n-strings for $n \leq \nu - 2$ filled from the cutoff upwards; e.g for $\pi/4 \leq \Delta < \pi/3$ the ground state consists of both 1- and 2-strings, while for $\pi/5 \leq \Delta < \pi/4$ the ground state consists of all possible 1-, 2- and 3-strings, see FIG. 4(b). Inserting these configurations into (3.28) and taking the thermodynamic limit the Bethe equations become $\nu - 2$ coupled integral equations for the n-string particle and hole distributions $\rho_j(x), \rho_j^h(x)$,

$$\begin{aligned}\frac{\sin(n\Delta)}{\sin(\Delta)}\frac{\mathcal{D}}{2\pi}e^x + \frac{1}{L}a_n\left(\frac{x-c}{2}\right) &= \rho_n(x) + \rho_n^{\mathrm{h}}(x) \\ &+ \sum_k^{\nu-2}\int_{-B}^{0} A_{nk}\left(\frac{x-y}{2}\right)\rho_k(y)\end{aligned} \tag{3.39}$$

Where as before

$$A_{nk} = a_{n+k}(x) + a_{k-n}(x) + 2\sum_{l=1}^{n-1} a_{k-n+2l}(x)$$

is the derivative of the phase shift between strings of length n and k with $n < k$ and has the property $A_{j,k} = A_{k,j}$. Also, as before B must be determined by minimizing the energy with $\bar{\epsilon}_0$ held fixed.

We first analyze the system with $\bar{\epsilon}_0 = 0$ where again there are no holes in the ground

state and $B = \infty$. The solution is obtained by inverting the matrix $\mathbb{1} + A$ [116],

$$(\mathbb{1} + A)^{-1}_{jk} = \delta_{jk}(\delta(x) - \delta_{k,\nu-1}b(x)) - (\delta_{j,k+1} + \delta_{j,k-1})\, s(x) \tag{3.40}$$

$$\tilde{b}(\omega) = \frac{\sinh\left[(\pi - (\nu-1)\Delta)\omega\right]}{2\cosh\left(\Delta\omega\right)\sinh\left[\pi - (\nu-2)\Delta)\omega\right]}. \tag{3.41}$$

Applying this to (3.39) we obtain the ground state distributions,

$$\rho^0_n(x) = d_n \frac{\mathcal{D}}{2\pi} e^{\frac{\pi}{2\Delta}x} + \delta_{j,1}\frac{1}{L}s(x-c) \tag{3.42}$$

where the coefficients d_n are

$$\begin{aligned} d_n &= \frac{1}{\pi - 2\Delta}\left(\frac{2\sin\left(n\Delta\right)}{\tan\left(\Delta\right)}\right) \quad \text{for } n < \nu - 2 \\ d_{\nu-2} &= \frac{1}{\pi - 2\Delta}\left(\frac{\sin\left((\nu-3)\Delta\right)}{\sin\left(\Delta\right)}\frac{\sin\left((\nu-2)\Delta\right)}{\sin\left(\Delta\right)}\tan\left(\pi - (\nu-1)\Delta\right)\frac{\pi}{2\Delta}\right) \end{aligned} \tag{3.43}$$

Note that the dot contribution appears only in the distribution of 1-stings $\rho^0_1(x)$ and is the same as for $\Delta \geq \pi/3$ (3.36). Again, to verify this is the ground state we show that any modification results in excitations that increase the energy. The simplest type of excitation is adding a hole to the n-string distribution. Just as before the energy of this is given by

$$\varepsilon^h_n(x) = d_n \mathcal{D} e^{\frac{\pi}{2\Delta}x} > 0. \tag{3.44}$$

Other excitations consist of adding ν-strings or positive energy particles which can be also checked to increase the energy.

The Dot Occupation

In this section we calculate the ground state occupation of the dot $n_d = \left\langle d^\dagger d \right\rangle$ as a function of the dot energy $\bar{\epsilon}_0$ and Δ. The non zero dot energy means that the ground state will contain holes as well as particles and furthermore that B is finite. To determine B we recall

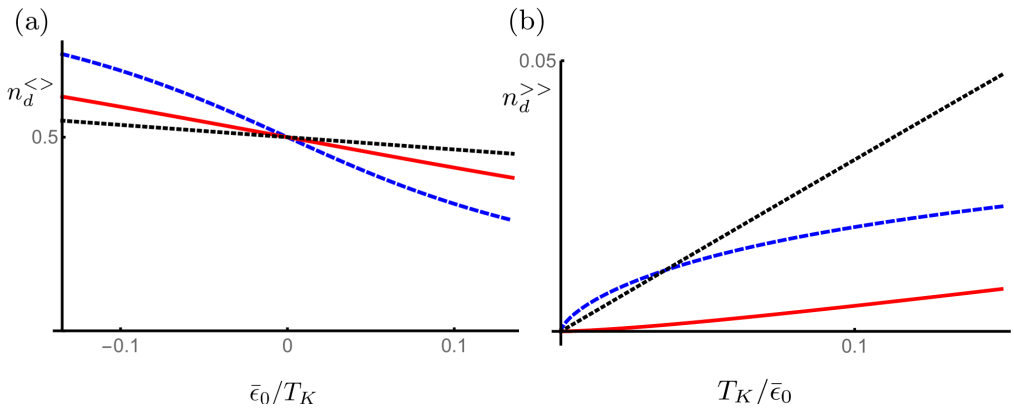

Figure 3.4: (a) The dot occupation, $n_d^{<>}$, as a function of $\bar{\epsilon}_0/T_K$ for $\Delta = \pi/3$ (dashed, blue), $\Delta = \pi/2$ (dotted black) and $\Delta = 3\pi/4$ (solid, red) from (3.53) (b) $n_d^{>>}$ from (3.54) as function of $T_K/\bar{\epsilon}_0$ for $\Delta = \pi/3$ (dashed, blue), $\Delta = \pi/2$ (dotted black) and $\Delta = 3\pi/4$ (solid, red) from (3.54). Recall that for $\Delta = \pi/2$ the system interactions simplify considerably, corresponding to $K = 1/2$ (maximally repulsive) for $U = 0$.

that the energy is given generically by $E = -\mathcal{D}\sum_j e^{x_j} + N\bar{\epsilon}_0$ and that the ground state is found by balancing the energy cost due to the second term with that of a hole. Therefore provided $\bar{\epsilon} > 0$ and given that $\varepsilon_n^h(x), \varepsilon^h(x) \propto \mathcal{D}e^{\frac{\pi}{2\Delta}x}$ we have

$$\bar{\epsilon}_0 = \alpha\mathcal{D}e^{-\frac{\pi}{2\Delta}B} \tag{3.45}$$

where α is a positive constant whose value depends on the regime in which Δ lies. We derive an explicit expression for α in each regime in appendix B. The case of negative dot energy can be treated using particle hole symmetry.

Since the ground state differs considerably above and below $\Delta = \pi/3$ we will employ the two different methods to find n_d that were discussed in the context of the RL model. We begin with the region $\Delta \geq \pi/3$ and obtain the desired quantity by integrating over the dot contribution to the density of states,

$$n_d = \int_{-B}^{0} \rho_d(x)\mathrm{d}x \tag{3.46}$$

$$a_1\left(\frac{x-c}{2}\right) = \rho_d(x) + \int_{-B}^{\infty} a_2\left(\frac{x-y}{2}\right)\rho_d(y)\mathrm{d}y \tag{3.47}$$

The second line is obtained by extracting the dot dependent quantities from (3.35) and extending the upper integral limit to ∞ which can be done as the driving term is localised about $x = c \ll 0$. The dot distribution can be found by means of the Wiener-Hopf method (See [69], [68] or [96] and references therein for a full account). We factorize the Fourier transform of the kernel into factors $G_{\pm}(\omega)$ that are analytic in the upper and lower half planes,

$$\frac{1}{1 + 2\tilde{a}_2(2\omega)} = G_+(\omega)G_-(\omega)$$

where $G_+(\omega) = G_-(-\omega)$,

$$G_+(\omega) = \frac{\Gamma(\frac{1}{2} - i\frac{\Delta}{\pi}\omega)\Gamma(1 - i\frac{\pi-\Delta}{\pi}\omega)}{\sqrt{2(\pi-\Delta)}\Gamma(1-i\omega)} e^{i\omega a}, \tag{3.48}$$

$$a = \left(\frac{\pi-\Delta}{\pi}\right)\log\left(\frac{\pi-\Delta}{\Delta}\right) - \log\left(\frac{\pi}{\Delta}\right). \tag{3.49}$$

and $\Gamma(x)$ is the Gamma function. Then, noting that $n_d = \tilde{\rho}_d^p(0)$ we find

$$n_d = \frac{-i}{2\pi} G_+(0) \int_{-\infty}^{\infty} \frac{G_-(\omega)\tilde{a}_1(\omega)}{\omega - i0} e^{i\omega(c+B)}. \tag{3.50}$$

which can be evaluated by closing the contour in the upper or lower half plane depending upon the sign of $c + B$. Having determined B through (3.45) we have that,

$$c + B = \frac{2\Delta}{\pi}\log\left(\frac{T_K}{\bar{\epsilon}_0}\right) \tag{3.51}$$

$$T_K \equiv \alpha\mathcal{D}\left(\gamma\frac{\Gamma}{\mathcal{D}}\right)^{\frac{\pi}{2\Delta}} \tag{3.52}$$

where we have defined the strong coupling scale T_K. All physical energies are measured with respect to this scale which has been dynamically generated by the model. We hold it fixed while taking $\mathcal{D} \to \infty$ thereby obtaining universal results. The form of T_K will be discussed further below.

We now proceed to obtain expressions for the dot occupation using (3.50). By closing

the contour in the upper half plane we determine the expansion for $\bar{\epsilon}_0 < T_K$ (and $\Delta \geq \pi/3$) which we denote $n_d^{<>}(\bar{\epsilon}_0, \Delta)$,

$$n_d^{<>}(\bar{\epsilon}_0, \Delta) = \frac{1}{2} - \frac{1}{\sqrt{\pi}} \sum_{n=0}^{\infty} \frac{(-1)^n}{n!} \frac{e^{\frac{\pi}{2\Delta}(2n+1)a}}{2n+1} \left(\frac{\bar{\epsilon}_0}{T_K}\right)^{2n+1} \times \frac{\Gamma(1+\frac{\pi}{2\Delta}(2n+1))}{\Gamma(1+\frac{\pi-\Delta}{2\Delta}(2n+1))}. \tag{3.53}$$

On the other hand, closing the contour in the lower half plane we get the occupation when the dot energy is larger than the strong coupling scale, $\bar{\epsilon}_0 \geq T_K$. Denoting this $n_d^{>>}(\bar{\epsilon}_0, \Delta)$, the expansion is now,

$$n_d^{>>}(\bar{\epsilon}_0, \Delta) = \frac{1}{2\sqrt{\pi}} \sum_{n=1}^{\infty} \frac{(-1)^{n+1}}{n!} e^{-na} \frac{\Gamma(\frac{1}{2}+\frac{\Delta}{\pi}n)}{\Gamma(1-\frac{\pi-\Delta}{\pi}n)} \left(\frac{T_K}{\bar{\epsilon}_0}\right)^{\frac{2\Delta}{\pi}n}. \tag{3.54}$$

The dot occupation is plotted for some values of Δ in FIG. 3.4 where we have used $n_d(-\bar{\epsilon}_0) = 1 - n_d(\bar{\epsilon}_0)$ [111] to obtain the expressions for negative dot energy.

To find the expressions analogous to (3.53) and (3.54) in the region $\Delta < \pi/3$ is more difficult. We employ a different method and will derive only the form of the dot expansion by examining the analytic structure of the resulting equations. Starting from (3.28) it can be shown that the dot contribution to ground state energy of the system is,

$$E_d = E_d^0 - \int_{-\infty}^{-B} S(x-c)\rho_1^{\mathrm{h}}(x)$$

where $S'(x) = s(x)$ and E_d^0 is the dot energy when $\bar{\epsilon}_0$. The dot occupation is therefore given by,

$$n_d = \frac{1}{2\pi} \frac{\partial}{\partial \bar{\epsilon}_0} \int_{-\infty}^{\infty} \frac{\tilde{s}(\omega)}{i\omega} \tilde{r}_1(\omega) e^{-i\omega(c+B)} \mathrm{d}\omega \tag{3.55}$$

where we have defined $r_n(x) = \rho_n^{\mathrm{h}}(x-B)$ with $B(\bar{\epsilon}_0)$ already determined. Now to evaluate this explicitly one needs to solve (3.39) for the hole distributions which cannot be achieved

analytically. We can however determine the positions of its zeros and poles. Given that $\rho_1^{\rm h}(x) = 0$ for $x > -B$ we know that $\tilde{r}_1(\omega)$ is analytic in the lower half plane and additionally $r_1(x) \propto \mathcal{D}e^{-\frac{\pi}{2\Delta}B}$. Furthermore the zeros and poles of $\tilde{r}_1^h(\omega)$ are fixed by the poles and zeros of the determinant of $\mathbb{1}+A$ respectively [116]. Thus it has zeros at $i\pi(n+1/2)/\Delta$ and poles at $i(n+1)$. Combining all this we find the dot occupation for $\Delta < \pi/3$. For small $\bar{\epsilon}_0 < T_K$ we denote it $n_d^{<<}$,

$$n_d^{<<}(\bar{\epsilon}_0, \Delta) = \frac{1}{2} + \sum_{n=0}^{\infty}(-1)^n c_n \left(\frac{\bar{\epsilon}_0}{T_K}\right)^{2n+1} \tag{3.56}$$

for some constants, c_n depending on $r_1(\omega)$.

3.6 Thermodynamic properties of the dot

In this section we will study the system at finite temperature and calculate the free energy of the dot. We shall find a RG flow from weak to strong coupling as the temperature is lowered (from a localized to a delocalized dot) in agreement to the previously section. To simplify matters we specify that either $\Delta = \pi/\nu$ with $\nu \geq 3$ being a positive integer or $\Delta = \pi - \pi/\nu$. The former covers the region $\Delta < \pi/2$ and the later $\Delta > \pi/2$. It is expected that the free energy of the system be a smooth function of Δ so our choice here will not affect the overall picture of the finite temperature properties it presents.

In contrast to the zero temperature properties the region $\Delta \leq \pi/3$ is easier to analyze and so we shall concentrate on $\Delta = \pi/\nu$ and also setting $\bar{\epsilon}_0 = 0$. For this choice of parameter there are strings of length up to $\nu - 1$ and so excitations are created by introducing holes in these string distributions and adding particles above the Fermi sea with real rapidity. Following [96] (see also chapter 2) we consider the free energy $F = E - TS$ where E is the energy of a state with an arbitrary configuration of strings, holes and particles,

$$E = -\mathcal{D}\sum_{j}^{\nu-1}\int_{-\infty}^{0}\frac{\sin(j\Delta)}{\sin(\Delta)}e^x\rho_j(x) + \mathcal{D}\int_{-\infty}^{0}e^x\rho_\nu(x) \tag{3.57}$$

and S is the Yang-Yang entropy $S = \sum_j \int \left[(\rho_j + \rho_j^{\rm h}) \log(\rho_j + \rho_j^{\rm h}) - \rho_j \log(\rho_j) - \rho_j^{\rm h} \log(\rho_j^{\rm h})\right]$ where the sum is over $j = 1, \ldots, \nu$ with ν denoting the distributions of the real rapidity particles. We minimize F with respect to ρ_j to obtain the thermodynamic Bethe Ansatz equations (TBA) for $\eta_j(x) \equiv \rho_j^{\rm h}(x)/\rho_j(x)$ which determine the saddle point,

$$\log(\eta_j(x)) = s* \left[\log(1+\eta_{j-1}(x))(1+\eta_{j+1}(x))^{1+\delta_{j,\nu-2}}\right] - d_j \frac{\mathcal{D}}{T} e^{\frac{\pi}{2\Delta}x}. \tag{3.58}$$

Here $*$ denotes the convolution $f * g = \int f(x-y)g(y)\mathrm{d}y$ and additionally $\log(\eta_{\nu-1}(x)) = -\log(\eta_+(x))$. The driving terms of these equations, are the energies of the fundamental excitations above the ground state, namely those obtained by adding holes to the j-string distributions. Comparing these to the TBA for the AKM we derived in Chapter 2 one can see that they are similar however driving terms appear in all of the equations rather than just $j = 1$.

We can then use (3.58) to simplify the free energy and after doing so the part which depends on the dot is given by

$$F_d = E_d - T \int s(x-c) \log(1+\eta_1(x)). \tag{3.59}$$

The first term is the ground state energy of the dot and the second term captures the finite temperature behaviour. Similar to the case of zero temperature discussed in previous sections the behaviour away from the fixed point it is determined by the 1-string distribution. At this stage the free energy and TBA still depend on the cutoff but we can remove this dependence and take the universal limit as we did before by introducing the functions $\varphi(x + \frac{2\Delta}{\pi} \log \alpha' T/\mathcal{D})$ with $1/\alpha' = \alpha\gamma^{\pi/2\Delta}$. Taking $\mathcal{D} \to \infty$ while holding T_K fixed then gives

$$\varphi_j(x) = s * \left[\log(1+e^{\varphi_{j-1}(x)})(1+e^{\varphi_{j+1}(x)})^{1+\delta_{j,\nu-2}}\right] - \alpha' d_j e^{\frac{\pi}{2\Delta}x} \tag{3.60}$$

along with $\varphi_{\nu-1}(x) = -\varphi_\nu(x)$. The temperature dependent part of the free energy is now dependent on T_K,

$$F_d = -T\int_{-\infty}^{\infty} s(x + \frac{2\Delta}{\pi}\log\left(\frac{T}{T_K}\right))\log\left(1 + e^{\varphi_1(x)}\right). \tag{3.61}$$

At high temperature $T \gg T_K$ the integral is dominated by $x \to -\infty$. In this limit the driving terms of (3.60) vanish and the solutions are given by constants $e^{\varphi_j} = (j+1)^2 - 1$, $e^{\varphi_{\nu-1}} = \nu - 1$. Using these in the free energy (dropping the non universal part, E_d) we find

$$F_d(T \gg T_K) = -T\log 2 \tag{3.62}$$

which is the free energy of a two level system without energy splitting. Thus at high energy the dot is decoupled as expected from our analysis at $T = 0$ of the large $\bar{\epsilon}_0$ regime. Similarly the low temperature, $T \ll T_K$, behavior of the dot is determined by the $x \to \infty$ part of the free energy. In this case the driving terms of (3.60) blow up giving $\varphi_j = -\alpha' d_j e^{\frac{\pi}{2\Delta}x}$ allowing us to obtain an expansion for the free energy at low temperature. We achieve this following the arguments of [69] by introducing $\tilde{c}(\omega) = \int \exp\left(-i\omega x\right)\log(1 + \exp\left(\varphi_1(x)\right))$, which is finite for $\mathrm{Im}(\omega) > 0$. Rewritten in terms of this new function the dot free energy is

$$\begin{aligned} F_d &= -T\frac{1}{2\pi}\int_{-\infty}^{\infty} \tilde{s}(\omega)\tilde{c}(\omega)e^{-\frac{2\Delta}{\pi}i\omega\frac{T}{T_K}} & (3.63)\\ &= -T\sum_{n=0}^{\infty}(-1)^n\tilde{c}(i\frac{\pi}{2\Delta}(2n+1))\left(\frac{T}{T_K}\right)^{2n+1} & (3.64)\end{aligned}$$

where to obtain the second line we have closed the contour in the upper half plane and picked up the poles from $\tilde{s}(\omega)$. The entropy of the dot $S_d = -F_d/T$ vanishes at $T = 0$ as expected for a dot that is fully hybridised with the bulk. The coefficients of the expansion

can be determined for large n

$$\tilde{c}(i\frac{\pi}{2\Delta}(2n+1)) = \int_{-\infty}^{\infty} e^{\frac{\pi}{2\Delta}(2n+1)} \log\left(1+e^{\varphi_1(x)}\right) \tag{3.65}$$

$$\rightarrow \int_{-\infty}^{\infty} e^{\frac{\pi}{2\Delta}(2n+1)} e^{-\alpha' d_1 e^{\frac{\pi}{2\Delta}x}} = \frac{1}{(\alpha' d_1)^{2n+1}}(2n)!\,. \tag{3.66}$$

We see that the free energy is of a form similar to the expansion of the dot occupation in powers of $\bar{\epsilon}_0/T_K$ obtained at zero temperature and again the leading irrelevant operator about the strong coupling fixed point is the stress energy tensor resulting in a power law dependence in the specific heat $C_v \sim T/T_K$.

The thermodynamics for $\Delta = \pi - \pi/\nu$ can be investigated by similar means. We omit the details here but it can be shown that at high temperature the dot is again decoupled while at low temperature it is fully hybridized with the free energy having an expansion in terms of odd powers of T/T_K as in (3.63).

3.7 The RG Flow

In the preceding sections we have derived the dot occupation in the ground state and dot free energy as a function of Δ and $\bar{\epsilon}_0/T_K$ or T/T_K, with T_K being a strong coupling scale generated by the model. The dynamic generation of a scale T_K, akin to the Kondo scale, can be understood in this spinless model by making the analogy between the charge fluctuations on the dot and the spin fluctuations in the Kondo model. By identifying the impurity spin and dot occupation via $s_0^z = n_d - 1/2$, a screened Kondo spin corresponds to a fully hybridized dot with fixed occupation, $n_d = 1/2$ while the unscreened spin corresponds to the dot being decoupled and therefore being either full or empty, $n_d = 0, 1$. The role of an external magnetic field in the Kondo model is fulfilled here by the dot energy $\bar{\epsilon}_0$. It is interesting to note that while the Kondo model is also integrable[68, 69] there is no known solution of the model in the presence of a local field acing on the impurity. In the present case however one is free to choose any dot energy and retain integrability. We will now

discuss appearance of these localized/unscreened and delocalized/screened regimes in our model.

In order to obtain universal results we have held T_K fixed while removing the cutoff $\mathcal{D} \to \infty$ having previously assumed all scales are much smaller than $\mathcal{D}$. In particular we must have $T_K \ll \mathcal{D}$ and so to fulfill this we need $\Delta > 0$. For $\Delta < 0$ on the other hand there is no universal regime as the would-be scale is above the cutoff and universal results cannot be obtained. If we set $U = 0$ then this transition between universal and non-universal regimes occurs at $K = 1/2$ and is shifted by a non zero U in agreement with perturbation theory [111]. One can understand this by calculating the density of states at the edge of the boundary. Following the procedure in [88] or alternatively using bosonization[10, 14] one see that the density of states enjoys an enhancement at the boundary for $K > 1/2$ while it is suppressed below this. This enhancement allows for the dot to become hybridized with the bulk even in the absence of U or more surprisingly even in the presence of strong repulsive interaction between an edge fermion and hole on the dot, U large and negative. Therefore by tuning the bulk interaction we can cause the onset of the strong coupling regime well beyond were the system would otherwise be weakly coupled. In the absence of bulk interaction, the approach to the critical point $\Delta \to 0$ can be considered the isotropic limit in the Kondo language with $\Delta < 0$ being the ferromagnetic regime and $\Delta > 0$ the anti-ferromagnetic.

We may also explore the low energy behavior of the system. Rewriting (3.52) as,

$$\frac{\Gamma}{\mathcal{D}} = \gamma^{-1} \left(\frac{T_K}{\alpha \mathcal{D}} \right)^{\frac{2\Delta}{\pi}} \tag{3.67}$$

we see that reducing the cut-off à la Wilson[78], $\Gamma/\mathcal{D}$ flows to strong coupling provided $0 < \Delta < \pi$. Note that despite the change in the ground state the renormalization group analysis is unaffected and so we have a unified picture for all $0 < \Delta < \pi$ of the system being weakly coupled at high energy and flowing to strong coupling at low energy. The strong

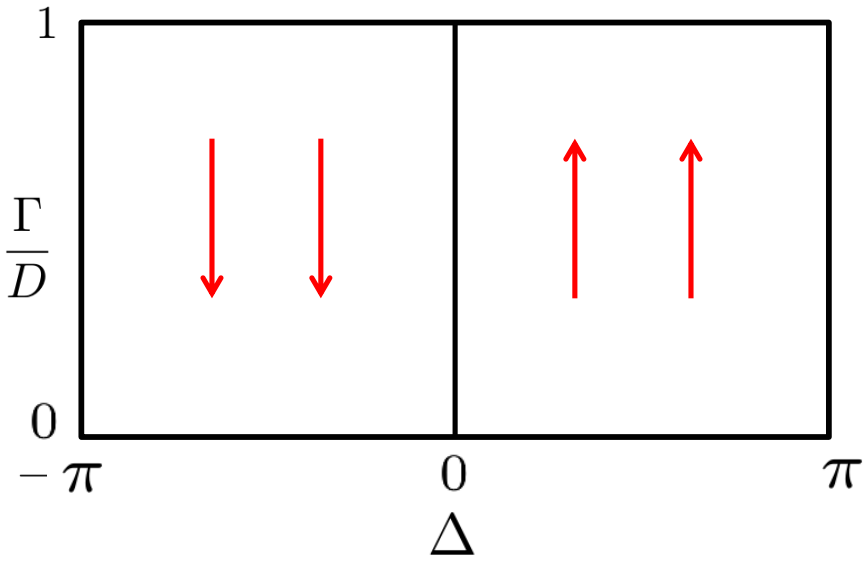

Figure 3.5: The RG flow of the system. For $\Delta > 0$ the system flows to strong coupling and generates a scale T_K allowing for universal results. In the region of the strong coupling fixed point the RG flow is the same as the IRL model which is depicted in FIG. 2.16 with $U \to U'$. For $\Delta < 0$ it flows to weak coupling and the system is non universal. The point $\Delta = 0$ is the isotropic point.

coupling fixed point controls the impurity behavior for low T and low $\bar{\epsilon}_0$, while the weak coupling regime is reached when either of these quantities is large.

We can obtain from our expressions for the dot occupation information about how the RG flow approaches the strong and weak coupling fixed points by identifying the respective leading irrelevant and relevant operators [94]. For $\bar{\epsilon}_0 < T_K$, i.e in the region of the strong coupling fixed point the expansions for all $\Delta > 0$ are given in terms of odd powers of $\bar{\epsilon}_0/T_K$ and so the leading irrelevant operator that governs the flow about the strong coupling fixed point has dimension 2 . It is natural to identify this operator with the stress energy tensor. We can also extract the dimension of the leading relevant operator around the weak coupling fixed point i.e at high energy from the exponents in the dot occupation for $\bar{\epsilon}_0 > T_K$. Again although the ground state changes form these exponents do not change and so we have the dimension of the operator is $1 - \Delta/\pi$ for all $\Delta > 0$. The weak coupling fixed point corresponds to the decoupled dot so the leading relevant operator is $d^\dagger\psi(0)$. By setting

$U = 0$ we see that its dimension is $1/2K$ in agreement with perturbation theory [10] but is shifted if $U \neq 0$.

We have the following picture of the system: For $\Delta > 0$ the system exhibits a renormalization group flow from weak coupling at high energy to strong coupling at low energy. The strong coupling fixed point is at $\bar{\epsilon}_0 = 0$ and describes the system where the dot and the bulk are fully hybridized. By introducing an energy scale i.e. allowing $\bar{\epsilon}_0 \neq 0$ we perturb away from this fixed point. The leading irrelevant operator describing this is the stress energy tensor. The weak coupling fixed point is reached at high energy and describes a decoupled dot and bulk. By reducing the energy scale we move away from the fixed point allowing for tunneling to occur which is governed by the operator $d^\dagger\psi(0)$. At $\Delta = 0$ the system undergoes a quantum phase transition such that the low energy fixed point is no longer strongly coupled and the dot is not fully hybridized. Any results in this regime depend upon the RG scheme used. We depict the RG flow in terms of $\Gamma/\mathcal{D}$ as a function of $\Delta \in [-\pi, \pi]$ in FIG. 3.5.

3.8 Comparison to Bosonisation

The model has been studied in the past in an interesting paper by Furusaki and Matveev [111] who study the system in the perturbative regime. It was stated that the anisotropic Kondo model (AKM) is equivalent to the Luttinger dot model we study here and that further the equivalence holds also in the absence of bulk interaction $K = 1$ and $U \neq 0$ [14]. This was shown through bosonizing the model and performing a number of unitary transformations. In this section we show that in fact there are some subtleties to this relationship which are routinely overlooked when employing these methods with the result that the two models should not be considered equivalent. We review the method below and highlight some inconsistencies inherent in the method.

We start by bosonizing the unfolded Luttinger-dot model and take

$$\psi(x) \sim e^{-2i\varphi(x)} \tag{3.68}$$

where φ is a boson with the following mode expansion[10]

$$\varphi(x) = -\frac{\pi}{L}Nx - i\frac{\pi}{L}\sum\left(\frac{L|p|}{2\pi}\right)^{\frac{1}{2}}\frac{1}{p}e^{-ipx}\left(b_p^\dagger + b_{-p}\right)e^{-|p|/2D} \tag{3.69}$$

The Hamiltonian in bosonic form is thus

$$H = \frac{1}{\pi}\int_{-L/2}^{L/2} K\left(\nabla\varphi\right)^2 + U'd^\dagger d\nabla\varphi(0) + t'd^\dagger e^{-2i\varphi(0)} + h.c \tag{3.70}$$

where we have absorbed any constants into new U' and t' and suppressed Klein factors. We can then absorb the Luttinger parameter into a redefinition of the field $\varphi(x) = \Phi(x)/\sqrt{K}$ to get

$$H = \frac{1}{\pi}\int_{-L/2}^{L/2} \left(\nabla\Phi\right)^2 + \frac{U'}{\sqrt{K}}d^\dagger d\nabla\Phi(0) + t'd^\dagger e^{-2i\Phi(0)/\sqrt{K}} + h.c \tag{3.71}$$

$$\Phi(x) = -\frac{\sqrt{K}\pi}{L}Nx - i\frac{\sqrt{K}\pi}{L}\sum\left(\frac{L|p|}{2\pi}\right)^{\frac{1}{2}}\frac{1}{p}e^{-ipx}\left(b_p^\dagger + b_{-p}\right)e^{-|p|/2D} \tag{3.72}$$

Note the appearance of the factor $1/\sqrt{K}$ in the exponent of tunnelling term renders the operator therein single valued under the periodic boundary condition $x \to x + L$ also note the change in the zero mode is reflective of the fact that the fermions are interacting.

We now perform the bosonization of the AKM. Recall that the AKM Hamiltonian is

$$\begin{aligned} H = -i\sum_{a=\uparrow\downarrow}\int \psi_a^\dagger(x)\partial_x\psi_a(x) + J_\parallel\psi_a^\dagger(0)\psi_a^\dagger(0)\sigma_{aa}^z\sigma_0^z \\ + J_\perp\left(\psi_\uparrow^\dagger(0)\psi_\downarrow^\dagger(0)\sigma_0^+ + \psi_\downarrow^\dagger(0)\psi_\uparrow^\dagger(0)\sigma_0^-\right). \end{aligned} \tag{3.73}$$

Where the system is placed on a ring of length L with periodic boundary conditions $\psi_a(x+$

$L) = \psi_a(x)$ and after bosonization it becomes

$$\frac{1}{\pi}\int_{-L/2}^{L/2} (\nabla\phi_\uparrow)^2 + (\nabla\phi_\downarrow)^2 + J_z' \left(\nabla\phi_\uparrow(0) - \nabla\phi_\downarrow(0)\right) + J_\perp' e^{-2i(\phi_\uparrow(0)-\phi_\downarrow(0))} S^+ + h.c \quad (3.74)$$

where again we have the mode expansion

$$\phi_{\uparrow,\downarrow}(x) = -\frac{\pi}{L} N_{\uparrow,\downarrow} x - i\frac{\pi}{L}\sum \left(\frac{L|p|}{2\pi}\right)^{\frac{1}{2}} \frac{1}{p} e^{-ipx} \left(b^\dagger_{p\uparrow,\downarrow} + b_{-p,\uparrow,\downarrow}\right) e^{-|p|/2D} \quad (3.75)$$

We introduce the charge field $\phi_c = (\phi_\uparrow + \phi_\downarrow)/\sqrt{2}$ and spin field $\phi_s = (\phi_\uparrow - \phi_\downarrow)/\sqrt{2}$. These two sectors decouple and we have the spin Hamiltonian

$$H_s = \frac{1}{\pi}\int_{-L/2}^{L/2} (\nabla\phi_s)^2 + \sqrt{2} J_z' \left(\nabla\phi_s(0)\right) + J_\perp' e^{-2\sqrt{2}i\phi_s(0)} S^+ + h.c \quad (3.76)$$

with

$$\phi_s(x) = -\frac{\pi}{\sqrt{2}L}(N_\uparrow - N_\downarrow)x - i\frac{\pi}{L}\sum \left(\frac{L|p|}{2\pi}\right)^{\frac{1}{2}} \frac{1}{p} e^{-ipx} \left(b^\dagger_{p,s} + b_{-p,s}\right) e^{-|p|/2D} \quad (3.77)$$

Note that the zero mode of the spinon field has changed by a factor of $1/\sqrt{2}$ and also the Hamiltonian contains $\exp\left(2\sqrt{2}i\phi_s(0)\right)$ where as before the $\sqrt{2}$ present there is necessary for this operator to be single valued and also that the boundary conditions are correctly reproduced $\exp\left(2\sqrt{2}i\phi_s(0)\right) = \exp\left(2\sqrt{2}i\phi_s(L)\right)$. These new factors reflect the fact that ϕ_s is a spinon field and so does not describe a free fermion.

Now the trick that is employed is to apply the following transformation

$$\mathcal{U} = \exp\left((\sqrt{2}-1)S^z\phi_s(0)\right)$$

to the Hamiltonian. The result of this is

$$\mathcal{U}^\dagger H_s \mathcal{U} = \frac{1}{\pi}\int_{-L/2}^{L/2} (\nabla\phi_s)^2 + \sqrt{2} J_z'' \left(\nabla\phi_s(0)\right) + J_\perp' e^{-2i\phi_s(0)} S^+ + h.c \quad (3.78)$$

The effect has been to change the coefficient in the exponent appearing in the $J'_\perp$ term back to the original one and also $J'_z \to J''_z$. Similarly one can apply the rotation $\mathcal{U}_K = \exp\left((1/\sqrt{K}-1)S^z\Phi(0)\right)$ to the Luttinger-dot model (3.71) which gives

$$\mathcal{U}_K^\dagger H \mathcal{U}_K = \frac{1}{\pi}\int_{-L/2}^{L/2}(\nabla\Phi)^2 + \frac{U''}{\sqrt{K}}d^\dagger d\nabla\Phi(0) + t' d^\dagger e^{-2i\Phi(0)} + h.c \tag{3.79}$$

where we find a new exponent in the tunnelling term and also shifted $U' \to U''$. At this point it is very tempting to equate (3.78) with (3.79) however while the impurity terms look the same it is important to note that for arbitrary K the bulks are different as can be seen from the mode expansions of Φ and ϕ_s. To make this more clear we can take $K = 1$ in which case the bulk term of (3.79) represents free fermions while that of the AKM represents spinons. Again this is reflected in the different zero modes of their mode expansions (3.77) and (3.72). Furthermore one can note that the $e^{-2i\phi_s(0)} \neq e^{-2i\phi_s(L)}$ so the transformed AKM Hamiltonian does not respect the boundary condition. We can also consider the correlation function $\left\langle e^{-2i\phi_s(x)}e^{2i\phi_s(0)}\right\rangle$which is no longer single valued as we can shift $x \to x + L$ in which case

$$\left\langle e^{-2i\phi_s(x)}e^{2i\phi_s(0)}\right\rangle \to e^{-i\sqrt{2}(N_\uparrow - N_\downarrow)}\left\langle e^{-2i\phi_s(x)}e^{2i\phi_s(0)}\right\rangle \tag{3.80}$$

meaning that this correlator is well defined only if $N_\uparrow - N_\downarrow = 0$. The two mode expansions do however agree for $K = 1/2$.

Therefore in bosonization one can see that the two models are not equivalent although the impurity parts appear the same, the bulks are different. In the Bethe language one can see the difference by comparing the TBA equations of both models (2.118) and (3.60). In the former the driving terms appear only in the $j = 1$ term whereas in the later they occur in every equation. Since the TBA are determined solely by the bulk system we see that they differ in this formulation also.

3.9 Conclusion

In this chapter we have solved via the Bethe Ansatz the model of a Luttinger liquid coupled to an interacting resonant level at its boundary using Bethe Ansatz. We constructed the ground state and excitations of the model. It was seen that if the Luttinger interaction is sufficiently strong and repulsive (or alternatively if U is strong and attractive) the ground state changes from consisting of a single type of particle to a multicomponent condensate of strings. We then calculated the occupation of the dot as a function of the dot energy at $T = 0$ obtaining exact expressions at $\Delta \geq \pi/3$ and the functional form below this. Following this we calculated the free energy of the system and studied it at low and high temperature. From these calculations we determined that for $\Delta > 0$ the system is strongly coupled at low energy and weakly coupled at high energy. The weak coupled fixed point describes a dot that is decoupled from the bulk and the leading relevant operator is the tunnelling term $\psi^\dagger(0)d$, and has dimension $1 - \Delta/\pi$. The strong coupling fixed point describes a fully hybridized dot and bulk with the leading irrelevant operator being the stress energy tensor.

The system changes from being strongly coupled to weakly coupled coupled at low energy when $\Delta = 0$. In the absence of bulk interactions this can be considered as akin to the isotropic point in the AKM. When bulk interactions are present however, the strong correlations present in the model due to the bulk interaction and dot cause an enhancement of the density of states at the boundary which allows for a strong coupling regime to occur even in what would otherwise be the ferromagnetic Kondo regime.

4

Local Scatterer in a Luttinger Liquid

In the previous chapter we studied the physics of a quantum impurity which has internal degrees of freedom coupled to the edge of an interacting environment. We saw interesting interplay between the bosonic bulk degrees of freedom and the fermionic dot degrees of freedom. In this chapter we study a different type of impurity, a localized potential which has no internal degrees of freedom but which is placed in the bulk of the system and will cause backscattering to occur, that is it may change left movers to right movers and vice versa. This effect necessitates a new Bethe Ansatz approach which encorporates such processes. We formulate this approach in this chapter and apply it to the aformentioned backscattering impurity model, which we refer to as the Kane-Fisher model as well as the closely related weak-tunneling model.

These were the first instances models with impurities which allow for both reflection and transmission to be solved exactly using Bethe Ansatz.

4.1 Introduction

Perhaps the most well known and striking effect occurring in Luttinger-impurity systems was elucidated by Kane and Fisher [12]. Using bosonization and perturbation theory it was shown that a local impurity can be a relevant or irrelevant perturbation to a Luttinger Liquid depending on the sign of the interaction in the liquid. For repulsive interactions amongst the fermions the strength of the impurity will grow at low energy and the one dimensional system will be split into two Luttinger liquids weakly coupled at their edges

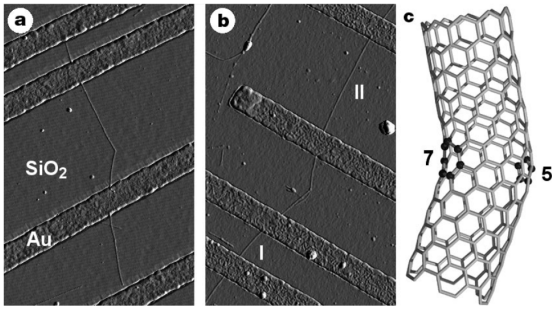

Figure 4.1: Atomic force microscope images of a kinked carbon nano tubes connected to three electrodes. The kink can occur as a result of two defects depicted on the left. Conductance measurements on these sample shows behavior indicative of a Luttinger liquid coupled to an impurity as we discuss here. Image taken from [49]

by a tunnelling term (weak-tunnelling Hamiltonian), while for attractive interactions the strength of the impurity will decrease and the system will heal itself. Hence one finds a vanishing conductance at the impurity site at low temperature in the first case and in a perfect conductance in the second.

Such a Luttinger impurity system can be realized in a number of experimental scenarios. The edge states of a fractional quantum hall material and utilizing either lithography or a top gate to create two edges that are pinched together. The close proximity of the two edges is enough to cause backscattering to occur which is described by the Kane-Fisher model [51, 52, 10]. Carbon nano tubes (CNT) are known to be excellent examples of systems described by Luttinger Liquid theory, with the value of K realized varying between individual CNTs. Defects in the hexagonal structure of the tube can result in kinks as shown in FIG. 4.1. Conductance measurements along straight and kinked sections of the CNT show that the kinks behave as impurities such as the ones we consider here[49].

Another scenario entails using a short CNT as a resonant level and coupling it to resistive 2-dimensional leads. By engineering the coupling between the CNT and leads as well as tuning the Fermi level in the tube one can realize the weak tunneling model[120, 60], see FIG. 4.2. We will discuss this realization more in the next chapter.

In this chapter we introduce a new type of coordinate Bethe Ansatz for use in quantum

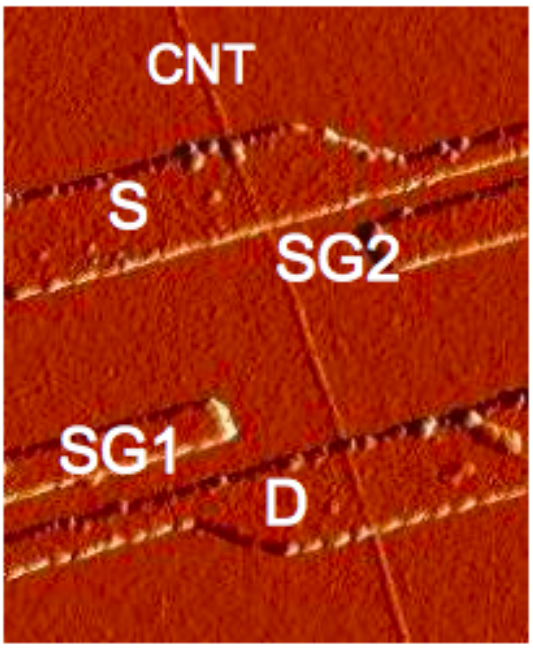

Figure 4.2: An atomic force microscope image of the experimental set up used by the Duke group[120]. A carbon nano tube (CNT) is coupled to resistive source (S) and drain (D) . The leads are 2 dimensional and non interacting but due to the dissipative tunnelling to the dot they can be described by Luttinger liquid theory [59]. By appropriately tuning the the various gate voltages (SG1) and (SG2) one can create tunnelling between the two leads which is described by the weak tunnelling model. The figure is taken from [120].

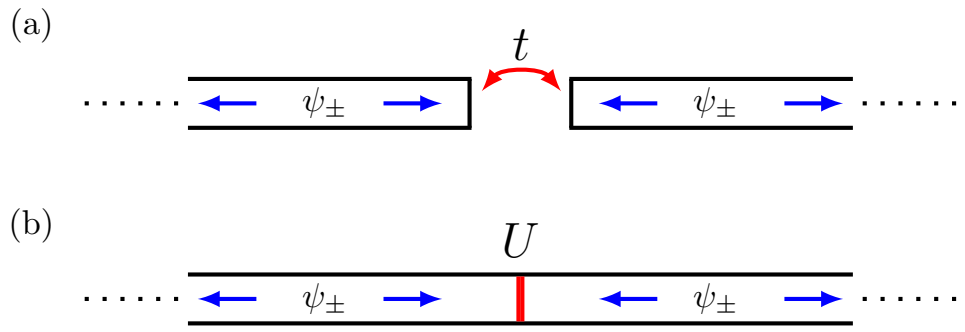

Figure 4.3: The two models studied in this chapter are depicted above: (a) The weak tunneling model consists of the two otherwise disjoint Luttinger Liquids which are connected by a tunneling term with strength t. (b) The Kane-Fisher model consists of a single Luttinger liquid with a local impurity in the centre of strength U which allows for both transmission and reflection of particles.

impurity models with bulk interaction. We present the method by solving exactly the Kane-Fisher model of an impurity in a Luttinger liquid with arbitrary boundary conditions, see FIG. 4.3 (b). The method uses a scattering Bethe basis which incorporates the impurity scattering processes that lead to a varying number of left and right movers. The boundary condition problem leads to a Quantum Inverse Scattering problem which is in turn solved using the Off Diagonal Bethe Ansatz (ODBA) [90] approach of deriving the Bethe Ansatz equations. Incorporating twisted boundary conditions being physically equivalent to driving a persistent current around the system allows for the possibility of studying transport across the impurity.

We also study the Weak-Tunnelling Hamiltonian describing two separate Luttinger liquids coupled via a tunnelling parameter, see FIG. see FIG. 4.3 (a). The model is of great interest by itself and is thought to describe the strong coupling fixed point of the Kane-Fisher model. We find that the Weak-Tunnelling Hamiltonian is solvable by the same procedure requiring only simple modifications and show it is dual to the impurity model. Having constructed the eigenstates of the two models and determined their spectra in terms

of the Bethe Ansatz equations we go on to study their thermodynamic behavior. The free energy is calculated and it is seen that both models dynamically generate a strong coupling scale T_{KF} or T_{WT}. We study the renormalization group flow of both models and determine their critical exponents. We compare the results with those of perturbation theory [12].

4.2 Bethe Basis of the impurity-Luttinger model

The Hamiltonian of the impurity model we seek to diagonalise is $H = H_{\rm LL} + H_I$ with the various terms given by,

$$\begin{aligned} H_{\rm LL} &= \sum_{\sigma=\pm} \int \sigma \psi^\dagger_\sigma \left(-i\partial_x - \mathcal{A}\right) \psi_\sigma(x) + 4g\psi^\dagger_+(x)\psi^\dagger_-(x)\psi_-(x)\psi_+(x), \qquad (4.1) \\ H_I &= U\left[\psi^\dagger_+(0)\psi_-(0) + \psi^\dagger_-(0)\psi_+(0)\right] + U'\left[\psi^\dagger_+(0)\psi_+(0) + \psi^\dagger_-(0)\psi_-(0)\right]. \end{aligned}$$

Here U' and U describe the forward and backward scattering off the impurity respectively with the later mediating a flip of chirality $\psi^\dagger_\pm \to \psi^\dagger_\mp$. As before we have set $v_f = 1$ and $\epsilon_f = 0$. In addition have included a gauge field $\mathcal{A}$ which, when the system is placed on a ring means it is threaded by a flux $\Phi = \int_x \mathcal{A}$. Equivalently we may solve for the wavefunction with twisted boundary conditions. This will induce a persistent current throughout the system and allow the effect of the impurity on the current to be studied.

To begin we discuss the construction of the eigenfunctions of H. In the presence of the impurity only the total number of fermions $N = N_+ + N_-$ is conserved, hence the wave functions must consist of components of left and right movers consistent with N. We start with the single particle eigenstates, the most general form for which can be written as

$$\begin{aligned} \int \mathrm{d}x \Big[&\left(e^{ikx} A^{[10]}_+ \psi^\dagger_+(x) + e^{-ikx} A^{[10]}_- \psi^\dagger_-(x)\right)\theta(-x) \\ &+ \left(e^{ikx} A^{[01]}_+ \psi^\dagger_+(x) + e^{-ikx} A^{[01]}_- \psi^\dagger_-(x)\right)\theta(x)\Big] |0\rangle . \qquad (4.2) \end{aligned}$$

Applying the Hamiltonian to the wave function fixes two of these amplitudes $A^{[\cdot\cdot]}_\pm$. Here we

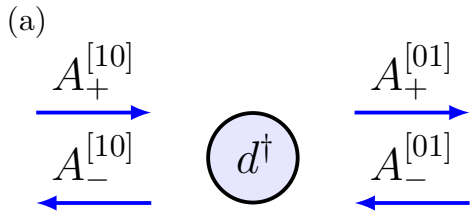

Figure 4.4: (a) The single particle wavefunction given by (4.3) is depicted. Particles are either incoming on the left or right with amplitudes $A_+^{[10]}, A_-^{[01]}$ or outgoing on the left or right with amplitudes $A_-^{[10]}, A_+^{[01]}$.

wish to take a physical picture and define a S^{10} which maps a particle past the impurity. This is in contrast to what is standard in Bethe ansatz where the S-matrix maps between regions of configuration space to the left and right of the impurity, see chapter 2. Therefore we consider $A_+^{[10]}$and $A_-^{[01]}$ as the incoming amplitudes and $A_-^{[10]}$and $A_+^{[01]}$ as the outgoing ones, see FIG. 4.4. The solution of the Schrödinger equation relates the two sets via

$$\begin{pmatrix} A_+^{[01]} \\ A_-^{[10]} \end{pmatrix} = S \begin{pmatrix} A_+^{[10]} \\ A_-^{[01]} \end{pmatrix}, \quad S = \begin{pmatrix} \alpha & \beta \\ \beta & \alpha \end{pmatrix}, \tag{4.3}$$

$$\alpha = \frac{1 - U^2/4 + U'^2/4}{1 + iU' + U^2/4 - U'^2/4}, \tag{4.4}$$

$$\beta = \frac{-iU}{1 + iU' + U^2/4 - U'^2/4}. \tag{4.5}$$

We recognize α and β as the transmission and reflection coefficients respectively and note the unimportant role of the forward scattering term. Its presence merely redefines these coefficients but does not change the left-right mixing imposed by the backward scattering term. In what follows we set $U' = 0$.

The form in which we have written the above equation allows us to easily apply periodic

or twisted boundary conditions,

$$e^{-ikL}\begin{pmatrix} A_+^{[10]} \\ A_-^{[01]} \end{pmatrix} = \begin{pmatrix} e^{i\Phi} & 0 \\ 0 & e^{-i\Phi} \end{pmatrix} S \begin{pmatrix} A_+^{[10]} \\ A_-^{[01]} \end{pmatrix}. \tag{4.6}$$

We now proceed to the two particle case. The bulk interaction term couples left- to right-movers only and preserves their number unchanged unlike the impurity term and unlike the previous chapter where the boundary condition caused mixing between the chiralities. Thus in the absence of the impurity a state consisting of one left mover and one right mover takes the form

$$\left|\vec{k}\right\rangle = \int \mathrm{d}x_1\, \mathrm{d}x_2\, F(x_1, x_2) e^{ik_1x_1 - ik_2x_2} \psi_+^\dagger(x_1)\psi_-^\dagger(x_2)|0\rangle$$

The wave function $F(x_1, x_2)$ must satisfy a Schrödinger equation,

$$[-i(\partial_{x_1} - \partial_{x_2}) + 4g\delta(x_1 - x_2)]F(x_1, x_2) = 0$$

The solution is easily found to be

$$F(x_1, x_2) = \theta(x_1 - x_2) + e^{i\phi}\theta(x_2 - x_1)$$

and the scattering phase shift given by $\phi = -2\arctan(g)$. For the scattering of two right movers or two left movers the phase shift is actually undetermined by the Schrodinger equation, we choose it to be: $e^{i\phi_{++}} = e^{i\phi_{--}} = 1$.

As seen for a single particle the impurity mixes both the left and right movers. A non-interacting model could therefore be handled via utilising an odd-even basis $\psi_{e/o}(x) = (\psi_+(x) \pm \psi_-(-x))/\sqrt{2}$. However doing so for the full model will only serve to complicate the interaction term. On the other hand in the absence of the impurity the left-right basis is appropriate. To diagonalise both we need to use a basis which naturally incorporates both aspects, we'll refer to it as an in-out scattering Bethe Basis.

To construct it we follow the logic of the previous chapter and divide configuration space into 8 regions, to be labelled Q , which are specified not only by the ordering of x_1, x_2 and the impurity but also according to which position is closer to the origin. For example if x_1 is to the left of the impurity, x_2 to its right with x_2 closer to the impurity then the amplitude in this region is denoted $A^{[102B]}_{\sigma_1\sigma_2}$, $\sigma_j = \pm$ being the chirality of the particle at x_j. The region in which x_1 is closer is denoted $A^{[102A]}_{\sigma_1\sigma_2}$. The consequence for the wavefunction is that we include Heaviside functions $\theta(x_Q)$ which have support only in a certain region, e.g $\theta(x_{[102B]}) = \theta(x_2)\theta(-x_1)\theta(-x_1 - x_2)$. A general two particle eigenstate for H can be written as,

$$|k_1, k_2\rangle = \sum_Q \sum_{\sigma_1\sigma_2} \int \theta(x_Q) A^Q_{\sigma_1\sigma_2} e^{\sigma_1 i k_1 x_1 + \sigma_2 i k_2 x_2} \psi^\dagger_{\sigma_1}(x_1)\psi^\dagger_{\sigma_1}(x_2)\,|0\rangle\,.$$

In contrast to the boundary dot case the amplitudes in each of the regions carries a chirality index σ_j for each particle. The form of this wavefunction requires some comment. The linear derivative acts as $\pm i(\partial_1 - \partial_2)$ when the particles are of opposite chirality and as $\pm i(\partial_1 + \partial_2)$ when they have the same chirality. This allows us to introduce an arbitrary function of $x_1 \pm x_2$ when the particles are of the same or opposite chirality. Accordingly, applying the Hamiltonian to this ansatz fixes some but not all the amplitudes. In particular when switching between the regions weighted by $\theta(\pm(x_1 - x_2))$ in the $\sigma_1 = \sigma_2$ sector and $\theta(\pm(x_1 + x_2))$ in the $\sigma_1 = -\sigma_2$ sector the linear derivative allows us to choose any S-matrix we like provided it does not mix the $\sigma_1 = \sigma_2$ with the $\sigma_1 = -\sigma_2$ amplitudes.

This is similar to the freedom we had when constructing eigenstates of the AKM. Just as in that case, the energy level $k_1 + k_2$ is degenerate with $(k_1 + q) + (k_2 - q)$ for any q. Thus, as degenerate perturbation theory requires, an appropriate basis in the degenerate subspace needs to be found in which the perturbation can be turned on. This corresponds to the consistent choice of the S-matrices, as described.

The specific form of this additional S-matrix is dictated by the requirement that the

wavefunction be consistent. Typically this would require the S-matrices be solutions of the Yang Baxter equation but here the different configuration space set up will modify this and will lead to a generalised Yang-Baxter relation. To make these statements more explicit let us form column vectors of the amplitudes,

$$\vec{A}_1 = \begin{pmatrix} A_{++}^{[120B]} \\ A_{+-}^{[102B]} \\ A_{-+}^{[201B]} \\ A_{--}^{[021B]} \end{pmatrix} \quad \vec{A}_2 = \begin{pmatrix} A_{++}^{[210A]} \\ A_{+-}^{[102A]} \\ A_{-+}^{[201A]} \\ A_{--}^{[012A]} \end{pmatrix} \quad \vec{A}_3 = \begin{pmatrix} A_{++}^{[201A]} \\ A_{+-}^{[012A]} \\ A_{-+}^{[210A]} \\ A_{--}^{[102A]} \end{pmatrix} \quad \vec{A}_4 = \begin{pmatrix} A_{++}^{[201B]} \\ A_{+-}^{[021B]} \\ A_{-+}^{[120B]} \\ A_{--}^{[102B]} \end{pmatrix} \tag{4.7}$$

$$\vec{A}_5 = \begin{pmatrix} A_{++}^{[021B]} \\ A_{+-}^{[201B]} \\ A_{-+}^{[102B]} \\ A_{--}^{[120B]} \end{pmatrix} \quad \vec{A}_6 = \begin{pmatrix} A_{++}^{[012A]} \\ A_{+-}^{[201A]} \\ A_{-+}^{[102A]} \\ A_{--}^{[210A]} \end{pmatrix} \quad \vec{A}_7 = \begin{pmatrix} A_{++}^{[102A]} \\ A_{+-}^{[210A]} \\ A_{-+}^{[012A]} \\ A_{--}^{[201A]} \end{pmatrix} \quad \vec{A}_8 = \begin{pmatrix} A_{++}^{[102B]} \\ A_{+-}^{[120B]} \\ A_{-+}^{[021B]} \\ A_{--}^{[201B]} \end{pmatrix}$$

We interpret $\vec{A}_1$ ($\vec{A}_2$) as the amplitudes where both particles are incident on the impurity but particle 2 (1) is closer, $\vec{A}_5$ ($\vec{A}_6$) are the amplitudes in which both particles are outgoing with particle 2 (1) closer to the impurity, $\vec{A}_8$ ($\vec{A}_3$) describes particle 2 (1) having scattered off the impurity and is still closer to the impurity than 1 (2) while $\vec{A}_7$ ($\vec{A}_4$) also describes particle 2 (1) having scattered but with 1 (2) is closer. We depict the first and last of these vectors in FIG.4.5 .

The Hamiltonian fixes the following relations between these amplitudes

$$\vec{A}_8 = S^{20}\vec{A}_1, \quad \vec{A}_3 = S^{10}\vec{A}_2, \tag{4.8}$$

$$\vec{A}_5 = S^{20}\vec{A}_4, \quad \vec{A}_6 = S^{10}\vec{A}_7, \tag{4.9}$$

$$\vec{A}_7 = S^{12}\vec{A}_8, \quad \vec{A}_4 = S^{12}\vec{A}_3, \tag{4.10}$$

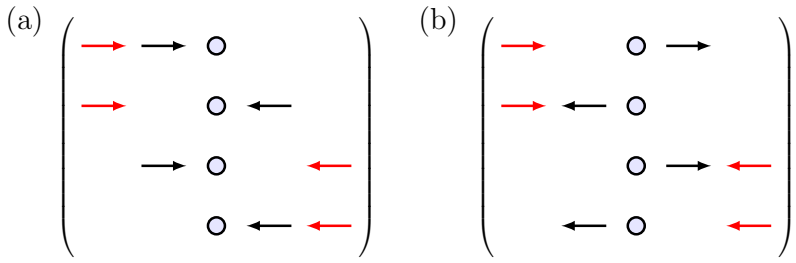

Figure 4.5: The amplitudes in the two particle wavefunction are arranged into 8 vectors given by (4.7) and according to whether the particles are incoming or outgoing as well as their ordering with respect to the impurity. (a) The amplitudes in $\vec{A}_1$ consist of both particles incoming but particle 2 (black) closer to the impurity than particle 1 (red). (b) The amplitudes in $\vec{A}_8$ consist of particle two outgoing. These vectors are related by S^{20}.

where

$$S^{20} = S \otimes \mathbb{1}, \quad S^{10} = \mathbb{1} \otimes S, \tag{4.11}$$

and the matrix S is given in (4.3). Additionally, as discussed above

$$S^{12} = \begin{pmatrix} 1 & 0 & 0 & 0 \\ 0 & e^{i\phi} & 0 & 0 \\ 0 & 0 & e^{i\phi} & 0 \\ 0 & 0 & 0 & 1 \end{pmatrix}. \tag{4.12}$$

The freedom mentioned previously enters upon considering $\vec{A}_1 \leftrightarrow \vec{A}_2$ and $\vec{A}_5 \leftrightarrow \vec{A}_6$. Again, these S-matrices are restricted only in that they cannot mix $\sigma_1 = \sigma_2$ amplitudes with

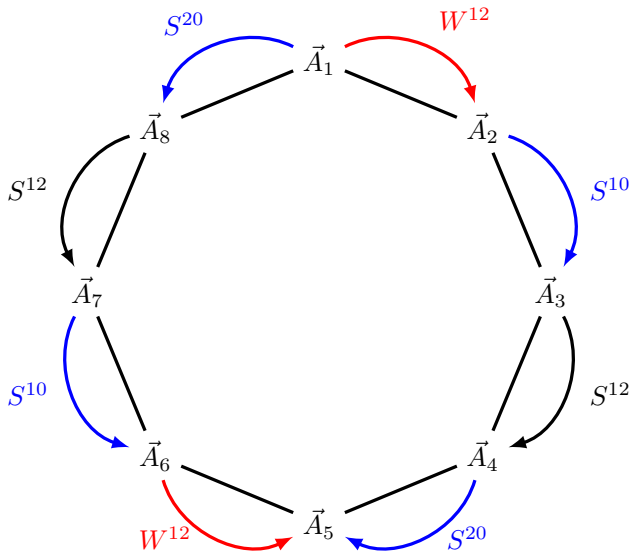

Figure 4.6: The amplitudes of the two particle wavefunction are related by applying the operators as depicted here. For consistency we require the amplitudes obtained by proceeding clockwise or counter-clockwise are the same resulting in (4.15).

$\sigma_1 = -\sigma_2$. We choose to take

$$\vec{A}_2 = W^{12}\vec{A}_1, \quad \vec{A}_6 = W^{12}\vec{A}_5, \tag{4.13}$$

$$W^{12} = \begin{pmatrix} 1 & 0 & 0 & 0 \\ 0 & 0 & 1 & 0 \\ 0 & 1 & 0 & 0 \\ 0 & 0 & 0 & 1 \end{pmatrix}. \tag{4.14}$$

This is dictated by the consistency of the wave function which requires the S-matrices to satisfy a reflection equation,

$$S^{20}S^{12}S^{10}W^{12} = W^{12}S^{10}S^{12}S^{20}. \tag{4.15}$$

Inserting (4.14)(4.11)(4.8) it is easy to see this indeed holds. By introducing the extra regions indexed by A, B we have changed the consistency condition from the Yang-Baxter equation to a generalised version that takes the form of a reflection equation. The same

generalised Yang-Baxter equation appears in studies of a two particle Bose-Hubbard model [121] and also appears in studying models with open boundary conditions [112]. In FIG. 4.6 we depict how one can construct the entire 2 particle wavefuction by application of the various S-matrices starting from $\vec{A}_1$. The consistency of the construction is guaranteed by satisfying (4.15). In addition, the two particle S-matirices must satisfy unitarity conditions, $S^{12}\left[S^{21}\right]^{-1} = \mathbb{1}$ and $W^{12}\left[W^{21}\right]^{-1} = \mathbb{1}$ which they do. These stem from the natural expectation that exchanging the order of two particles and then changing them back should have no effect overall.

We may interpret the W^{12} matrix as exchanging the positions the particles when they are both either incoming or outgoing. Similarly the S^{12} matrix describes the scattering of an incoming particle past an outgoing one and vice versa.

As explained, the partition to these extra regions is dictated by linear derivative and the degeneracies associated with it, which require us to choose the correct basis in the degenerate subspace. This basis, the Bethe basis, corresponds to the introduction of the S-Matrix W^{12} which satisfies the consistency conditions. Such a degeneracy is not present within a massive theory. The addition of a $m(\psi_+^\dagger\psi_- + \psi_-^\dagger\psi_+)$ changes the dispersion relation $k \to \pm\sqrt{k^2+m^2}$ thereby lifting the degeneracy. Consistency of a nontrivial bulk interaction in the presence of a transmitting and reflecting impurity within a massive theory requires a number of relations to be satisfied in addition to the Yang Baxter equation [122]. These relations are depicted in FIG. 4.7. We also show how by removing the mass they can be modified to reproduce the single consisitency condition of (4.15).

The generalization to N particles is immediate. The N particle eigenstate with energy $E = \sum_j^N k_j$ is,

$$\left|\vec{k}\right\rangle = \sum_Q \sum_{\vec{\sigma}} \int \theta(x_Q) A_{\vec{\sigma}}^Q e^{i\sum \sigma_j k_j x_j} \prod \psi_{\sigma_j}^\dagger(x_j)\left|0\right\rangle . \tag{4.16}$$

The sum is over the $2^N N!$ regions consisting of all orderings of x_j and the origin and indexed

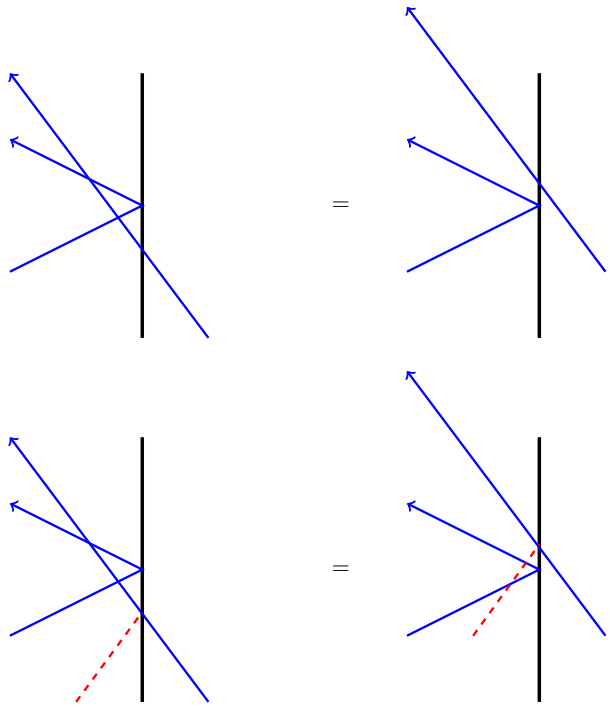

Figure 4.7: The top diagram is an example of a consistency relation for a massive field theory with a reflecting and transmitting impurity. If a particle approaching the impurity form the right is transmitted and one approaching form the left is reflected then the order in which this occurs should not matter if the theory is integrable. There are three other diagrams that must also be satisfied the mirror image along with both particles transmitted, both reflected etc. The bottom diagram depicts how this is modified in the massless case. In the massless theory, the linear derivative allows is to introduce the W^{12} represented here by dotted red line, all the other diagrams are modified in the same way and become identical. This leads to a single consistency relation (4.15).

by which particle is closest to the impurity. Just as in the two particle case the amplitudes $A^Q_{\vec{\sigma}}$ are related to each other by applying the S-matrices,

$$S^{j0} = S_j \otimes_{k\neq j} \mathbb{1}, \tag{4.17}$$

$$S^{ij} = \begin{pmatrix} 1 & 0 & 0 & 0 \\ 0 & e^{i\phi} & 0 & 0 \\ 0 & 0 & e^{i\phi} & 0 \\ 0 & 0 & 0 & 1 \end{pmatrix}_{ij} \otimes_{k\neq i,j} \mathbb{1}, \tag{4.18}$$

$$W^{ij} = \begin{pmatrix} 1 & 0 & 0 & 0 \\ 0 & 0 & 1 & 0 \\ 0 & 1 & 0 & 0 \\ 0 & 0 & 0 & 1 \end{pmatrix}_{ij} \otimes_{k\neq i,j} \mathbb{1}. \tag{4.19}$$

The subscripts denote which particle spaces the operators act upon. In order for this wavefunction to be consistent it must satisfy the following Yang-Baxter and reflection equations,

$$S^{k0}S^{jk}S^{j0}W^{jk} = W^{jk}S^{j0}S^{jk}S^{k0} \tag{4.20}$$

$$W^{jk}W^{jl}W^{kl} = W^{kl}W^{jl}W^{jk} \tag{4.21}$$

$$W^{jk}S^{jl}S^{kl} = S^{kl}S^{jl}W^{jk}. \tag{4.22}$$

The first equation is a simple N-particle generalizatioon of (4.15), the second is the consistency condition arising from swapping the order of three particles which are all incoming, see FIG. 4.8 while the last is when two particles are incoming and the other outgoing or two particles are outgoing and one incoming. Satisfying these is a sufficient condition for the consistency of the wave function because the S-matrices form a representation of the reflection group just as those in other integrable models form a representation of the permutation group [123, 89, 112]. This will be made evident in the next section when the continuous versions of the S-matrices and the Bethe equations are found.

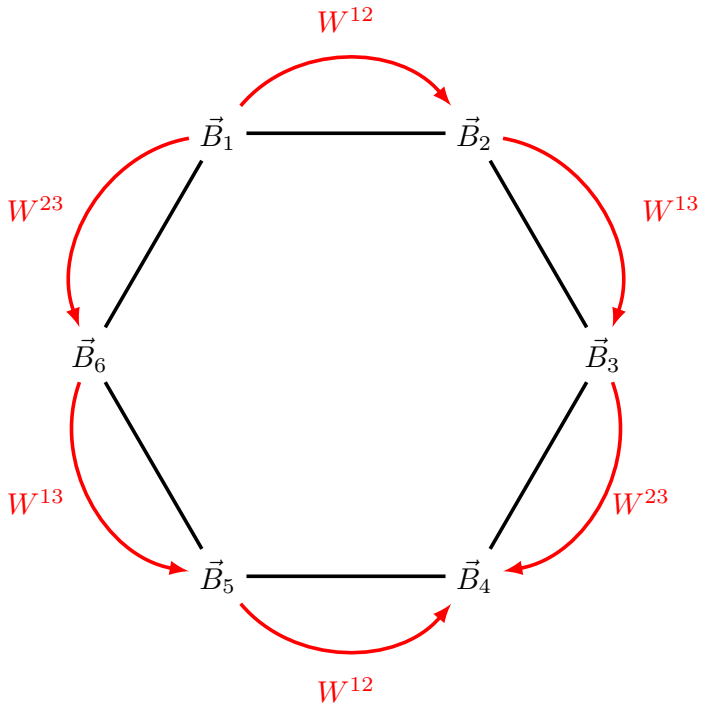

Figure 4.8: Consider an N-particle wavefunction of the form (4.16). The part of the wavfunction corresponding to particles 1,2 and 3 all being incident and in adjacent regions must satisfy the consistency condition (4.21). Any manner of swapping the order in which the particles will hit the impurity must be equivalent to any other. Denoting the amplitudes in this part of the wavefunction by $\vec{B}_j$ we see that consistency of the construction results in the figure above and (4.21).

To determine the spectrum of the model we place the system on a ring of size L. The flux, $\Phi = \mathcal{A}L$ through the loop then imposes twisted boundary conditions so that upon traversing the entire system a particle picks up an additional phase $e^{\sigma i\Phi}$, σ being the chirality of the particle. We obtain the following equations which determine k_j

$$e^{-ik_jL}A_{\sigma_1\ldots\sigma_N} = (Z_j)^{\sigma'_1\ldots\sigma'_N}_{\sigma_1\ldots\sigma_N} A_{\sigma'_1\ldots\sigma'_N} \tag{4.23}$$

$$Z_j = W^{j-1j}..W^{1j}B_jS^{1j}..S^{jN}S^{j0}W^{jN}..W^{jj+1} \tag{4.24}$$

where the matrix Z_j transfers the jth particle around the ring. Comparing with the same operator for the AKM we see that there are twice as many S-matrices as there are two types of bulk scattering processes, corresponding to the two types of S-matrices, S^{ij} (in-in or out-out) and W^{ij} (in-out or out-in). In the AKM only the first type occurs as once the particles are outgoing fr0m the impurity they non longer encounter incoming particles. Here the matrices B_j act in the jth particle chirality space and impose the twisted boundary conditions,

$$B_j = \begin{pmatrix} e^{i\Phi} & 0 \\ 0 & e^{-i\Phi} \end{pmatrix}. \tag{4.25}$$

We could also require hard wall boundary conditions at $x = \pm L/2$ by taking $B_j = -\sigma_x$. More complicated boundary conditions are easily included, indeed one can take B to be of the same form as the impurity S-matrix our system would then consist of a ring geometry with two diametrically opposed Kane-Fisher type impurities. In the thermodynamic limit the effects of the impurities decouple from each other and so one we will consider only a one impurity system.

As in the AKM there a no dimensionful parameters in the Hamiltonian and accordingly by using (4.15)(4.21)(4.22) it can be shown that all transfer matrices Z_j are equivalent. We

restrict our attention to solving,

$$\left(B_1 S^{12}\dots S^{1N} S^{10} W^{1N}\dots W^{12}\right)_{\sigma_1\dots\sigma_N}^{\sigma'_1\dots\sigma'_N} A_{\sigma'_1\dots\sigma'_N} = e^{-ikL} A_{\sigma_1\dots\sigma_N}. \tag{4.26}$$

and denote the operator on the left hand side Z. Its eigenvalues determine the allowed values of the momenta k_j and therefore the spectrum, $E = \sum_j k_j$. However, before proceeding to the diagonalization of the transfer matrix we turn to the solution of another closely related model, the Weak-Tunnelling model.

4.3 Bethe Ansatz eigenstates of the Weak -Tunnelling Hamiltonian

The embedding of an impurity in a Luttinger liquid could be viewed from the complementary scenario of two liquids which are coupled by a weak link or tunnel junction. Therefore in addition to the impurity model we will also consider the Weak-Tunnelling Hamiltonian, H_{WT} which is believed to govern the behaviour of the system in the vicinity of the strong coupling point but also can be realized experimentally in CNTs as discussed earlier. The model consists of two Luttinger liquids each described by $H_{\rm LL}$, occupying the regions from $-L/2$ to 0 and 0 to $L/2$ denoted by the subscripts l and r respectively (see (3.1)). These are coupled to each other via the tunnelling term,

$$H_t = t\left(\psi^\dagger_{+,r}(0) + \psi^\dagger_{-,r}(0)\right)\left(\psi_{+,l}(0) + \psi_{-,l}(0)\right) + \text{h.c} \tag{4.27}$$

which allows for tunnelling between the otherwise disjoint Luttinger liquids.

The single particle solution of the Weak-Tunnelling Hamiltonian is of a similar form to

(4.2),

$$\int_{-\frac{L}{2}}^{0}\left[e^{ikx}A_{+}^{[10]}\psi_{+,l}^{\dagger}(x)+e^{-ikx}A_{-}^{[10]}\psi_{-,l}^{\dagger}(x)\right]|0\rangle$$
$$+\int_{0}^{\frac{L}{2}}\left[e^{ikx}A_{+}^{[01]}\psi_{+,r}^{\dagger}(x)+e^{-ikx}A_{-}^{[01]}\psi_{-,r}^{\dagger}(x)\right]|0\rangle\,. \tag{4.28}$$

Here we have used the same notation as in the impurity case so that $A_{\sigma}^{[10]}$ is the amplitude of a particle of chirality σ in the left system and $A_{\sigma}^{[01]}$ in the right system. Acting on this with the Hamiltonian and using the boundary conditions $\psi_{+,l}^{\dagger}(0) = -\psi_{-,l}^{\dagger}(0)$ and $\psi_{+,r}^{\dagger}(0) = -\psi_{-,r}^{\dagger}(0)$ we find that

$$\begin{pmatrix}A_{+}^{[01]}\\A_{-}^{[10]}\end{pmatrix} = S_t\begin{pmatrix}A_{+}^{[10]}\\A_{-}^{[01]}\end{pmatrix} \quad , \quad S_t = \begin{pmatrix}\alpha_t & \beta_t\\ \beta_t & \alpha_t\end{pmatrix}, \tag{4.29}$$

$$\alpha_t = \frac{-4it}{1+4t^2}, \qquad \beta_t = \frac{1-4t^2}{1+4t^2}. \tag{4.30}$$

The imposition of hard wall boundary conditions at $x = \pm L/2$ gives this time

$$e^{-ikL}\begin{pmatrix}A_{+}^{[10]}\\A_{-}^{[01]}\end{pmatrix} = -\sigma_x S_t\begin{pmatrix}A_{+}^{[10]}\\A_{-}^{[01]}\end{pmatrix}. \tag{4.31}$$

The set up for higher particle number is the same as for the impurity model and the analysis of the preceding section transfers to the present case. This enables us to construct consistent N particle eigenstates. The two particle S-matrices are given by (4.18) and (4.19). The difference is the single particle S-matrix S^{j0} being replaced with $S_t^{j0} = S_{t\,j}\otimes_{k\neq j}^{N}\mathbb{1}$. These are readily seen to satisfy the consistency conditions (4.15)-(4.22).

As before we impose boundary conditions to determine the spectrum and obtain,

$$\left(B_1 S^{12}\dots S^{1N}S_t^{10}W^{1N}\dots W^{12}\right)_{\sigma_1\dots\sigma_N}^{\sigma_1'\dots\sigma_N'} A_{\sigma_1'\dots\sigma_N'} = e^{-ikL}A_{\sigma_1\dots\sigma_N}. \tag{4.32}$$

where for hard walls at $x = \pm L/2$, $B_1 = -\sigma_x$. We could also have applied periodic or twisted boundary conditions by including a more general B_1 instead of $-\sigma_x$. An interesting scenario would be when we include a tunnel junction and an impurity. The effects of both the impurity and junction would compete against each other and by including a twist also the persistent current through the system could be measured. We shall not consider this setup in this thesis but hope to return to the system in future work.

The system with periodic or twisted boundary conditions no longer describes two disjoint liquids filling the left and right half lines but rather a ring containing a weak link. We shall see below that this is the dual system to the impurity model on a ring and to distinguish it form the impurity model we denote the operator above by Z_t.

In what follows we will be concerned with properties of the impurity and weak link which in the thermodynamic limit will be independent of the type boundary condition imposed.

4.4 Off-Diagonal Bethe Ansatz

In the previous section we showed that in order to determine the spectrum of H or H_{WT} we must diagonalise Z or Z_t. To achieve this we will make use of the Off Diagonal Bethe Ansatz [90]. This method is related closely to the QISM we used when diagonalizing the Z operator of the AKM. Recall the procedure was to relate Z to the transfer matrix $t(u)$ which was constructed by taken the trace over a product of R-matrices. The eigenstates of $t(u)$ where obtained by using the operator C which was the lower left element of the monodromy matrix when written in the auxiliary basis. To construct them one merely had to take products of C operators evaulated a different spectral parameters acting on a reference state. The reference state we chose in the AKM was $|\Downarrow\rangle$ although $|\Uparrow\rangle$ in conjunction with B operators works also. In some models however an appropriate reference state is not available and so one knows that the system is integrable but the eighnestates cannot be constructed in the regular manner.

The ODBA is an alternative method which allows on to obtain the eigenvalues of $t(u)$

even in a system in which there is no reference state. It has already been successfully used to obtain the exact solutions for many integrable models with a broken $U(1)$ symmetry. The present problem will be shown to be mappable onto one arising when an XXZ Hamiltonian is diagonalised with open boundary conditions, which is amongst those already considered[124]. We will use its solution to obtain the eigenvalues of Z and Z_t. Although the following procedure can be used with any type of boundary conditions we will do so only for twisted boundary conditions.

We begin by following the initial steps of the QISM and construct the monodromy matrix. It is formed from an AKM - like R-matrix and of reflection matrices. The R-matrix is

$$\mathcal{R}(u) = \begin{pmatrix} 1 & 0 & 0 & 0 \\ 0 & \frac{\sinh u}{\sinh(u+\eta)} & \frac{\sinh \eta}{\sinh(u+\eta)} & 0 \\ 0 & \frac{\sinh \eta}{\sinh(u+\eta)} & \frac{\sinh u}{\sinh(u+\eta)} & 0 \\ 0 & 0 & 0 & 1 \end{pmatrix}. \tag{4.33}$$

where u is the spectral parameter and η the crossing parameter which encodes the interactions of the model. We shall identify it in our case as : $e^{-\eta} = e^{i\phi} = \frac{1-ig}{1+ig}$ with g the Luttinger liquid interaction coupling constant.

The reflection or boundary matrices, $K^{\pm}(u)$, we use take the form of integrable boundary conditions for the XXZ model [125]

$$K^{-}(u) = \begin{pmatrix} 2i\cosh(c+\theta/2)\cosh u & \sinh 2u \\ \sinh 2u & 2i\cosh(c+\theta/2)\cosh u \end{pmatrix} \tag{4.34}$$

$$K^{+}(u) = \begin{pmatrix} 2(\sinh(-\theta)\cosh(i\Phi)\cosh(u+\eta) & -\sinh(2u+2\eta) \\ -\cosh(\theta)\sinh(i\Phi)\sinh(u+\eta)) & \\ & 2(\sinh(-\theta)\cosh(i\Phi)\cosh(u+\eta) \\ -\sinh(2u+2\eta) & +\cosh(\theta)\sinh(i\Phi)\sinh(u+\eta)) \end{pmatrix}$$

Herein we have introduced the parameter $c = \log\left((1-U^2/4)/U\right)$ for the impurity

model, U being the strength of coupling of the impurity to the liquid, or $c = \log\left(4t/(1-4t^2)\right)$ for the Weak -Tunnelling model. Let us denote the latter by c_t when a distinction is required. The logarithmic dependence on the bare coupling constant will be important later when considering thermodynamic quantities, we will see that it leads to generation of a scale with power law dependence on the bare parameters in (4.1). In addition we have also introduced an inhomogeneity parameter θ which will enable us to relate the monodromy matrix to Z or Z_t. The R-matrices satisfy a continuous version of the Yang Baxter equation

$$\mathcal{R}^{12}(u-v)\mathcal{R}^{13}(u)\mathcal{R}^{23}(v) = \mathcal{R}^{23}(v)\mathcal{R}^{13}(u)\mathcal{R}^{12}(u-v) \tag{4.35}$$

and along with the K matrices satisfy a continuous reflection equation also

$$\mathcal{R}^{12}(u-v)K^1(u)\mathcal{R}^{12}(u+v)K^2(v) = K^2(v)\mathcal{R}^{12}K^1(u)\mathcal{R}^{12}(u-v). \tag{4.36}$$

Using the definitions above we construct the monodromy matrix,

$$\begin{aligned}\Xi^A(u) = \mathcal{C}K^+(u)\mathcal{R}^{A1}(u+\theta/2)\ldots\mathcal{R}^{AN}(u+\theta/2)\\ \times K^-(u)\mathcal{R}^{AN}(u-\theta/2)\ldots\mathcal{R}^{A1}(u-\theta/2)\end{aligned} \tag{4.37}$$

with $\mathcal{C} = \frac{-\beta e^{-\eta}}{\sinh\theta\sinh\frac{3\theta}{2}}$ and $\beta \to \beta_t$ for the Weak-Tunnelling model where β and β_t are given in (4.3) and (4.30) respectively. The form of (4.37) is similar to that of the XXZ model with two boundaries described by K^+ and K^-. The transfer matrix is given by the trace over this auxiliary space,

$$t(u) \quad = \quad \mathrm{Tr}_A\,\Xi^A(u). \tag{4.38}$$

The judicious choice of boundary matrices means that the transfer matrices commute for differing spectral parameter, $[t(u), t(v)] = 0$ [112] and by expanding in powers of u a set

of operators which commute with $t(v)$ is generated. This proves the integrability of the transfer matrix.

We now return to our original problem, the diagonalization of Z. The choice of (4.33) and (**??**)-(**??**) as well as the dependence of the monodromy matrix on θ means that we can relate this to the transfer matrix. In particular, setting $u = \theta/2$ we have,

$$Z = \lim_{\theta \to \infty} t(\theta/2). \tag{4.39}$$

and similarly Z_t with the appropriate replacements. What we have shown, therefore, is that determining the spectrum of Z or Z_t is related to that of the open XXZ chain with prescribed inhomogeneities, boundaries and twists. In addition we have established the integrability of both the Kane-Fisher impurity and Weak-Tunnelling models.

At this point the QISM ceases to be of use. The reason for this is the non diagonal nature of the boundary matrices means that there is no proper reference state upon which to build the eigenstates of $t(u)$ and determine the eigenvalues. And so we know that the boundary condition problem is integrable but according to the QISM we cannot construct the eigenstates.

This problem can be circumvented by means of the newly developed ODBA approach. We shall not go into the details here but the procedure is straightforward if a little tedious. The basic idea is to prove some relations which the transfer matrix satisfies and in particular how it behaves at the values $u = \theta_j$ with θ_j being the inhomogeneities. Combining this with the behaviour at $u \to \pm\infty$ provides enough information to fix the eigenvalues of $t(u)$[90].

The eigenvalue is parametrised by Bethe roots, μ_j which are fixed by the Bethe equations. The states can then also be recovered by means of separation of variables [126]. Presently we are only interested in eigenvalues of $t(u)$ and so postpone any discussion of the states to future work.

The transfer matrix $t(u)$ has previously been considered in [124] wherein the eigenvalues,

$\Lambda(u)$, and the Bethe equations were determined. Inserting (**??**)-(**??**) and (4.37) into their results we find for N even (see appendix C),

$$\Lambda(\theta/2) = -4i\beta e^{i\phi}\frac{\sinh(\theta - 2i\phi)\cosh(c)\cosh(\theta/2)}{\sinh(\theta - i\phi)\sinh\theta} \times \cosh(\theta/2 - i\Phi)\prod_{j}^{N}\frac{\sinh(\theta/2 - \mu_j + i\phi)}{\sinh(\theta/2 + \mu_j - i\phi)}. \tag{4.40}$$

We have restricted ourselves to $u = \theta/2$ since we are only interested in determining $e^{-ikL} = \lim_{\theta\to\infty}\Lambda(\theta/2)$. In addition we obtain the Bethe equations,

$$\left[\cosh\left(i(N+1)\phi + c + i\pi/2 + i\Phi - \theta/2 + 2\sum_{j=1}^{N}\mu_j\right) - 1\right] \times \frac{\sinh(2\mu_j - i\phi)\sinh(2\mu_j - 2i\phi)}{2i\cosh(\mu_j + c + \theta/2 - i\phi)\cosh(\mu_j - i\phi)\cosh(\mu_j - i\phi + i\Phi)\sinh(\mu_j - \theta - i\phi)} = \prod_{l=1}^{N}\frac{\sinh(\mu_j + \mu_l - i\phi)\sinh(\mu_j + \mu_l - 2i\phi)}{\sinh(\mu_j + \theta/2 - i\phi)\sinh(\mu_j - \theta/2 - i\phi)} \tag{4.41}$$

along with the selection rules $\mu_j \neq \mu_k$ and $\mu_j \neq \mu_k + i\phi$. These selection rules are analogous to the exclusion principle in other Bethe Ansatz problems and result in a vanishing wavefunction if not obeyed[93]. Upon taking the limit, $\theta \to \infty$ (4.40) and (4.41) completely determine the spectrum of Z. Prior to doing so we should consider the dependence of μ_j on θ. The dependence of the Bethe parameters on the inhomogeneity θ follows from the form of (4.40) and (4.41) with half the roots scaling as $-\theta/2$ while the other half go as $\theta/2$. This is also the case for N odd, as $N+1$ Bethe parameters are required by the ODBA solution[124]. We separate out the θ dependent part and introduce two sets of Bethe parameters $\{\lambda_j, \nu_j\}$,

$$\mu_j = \begin{cases} \lambda_j + i\phi/2 + \theta/2 & \text{if} j \leq \frac{N}{2} \\ -\nu_{j-N/2} + i\phi/2 - \theta/2 & \text{if} j > \frac{N}{2}. \end{cases} \tag{4.42}$$

The validity of this assumption will be checked by recovering the Luttinger liquid spectrum

when the impurity is removed. Inserting (5.48) into (4.40) the eigenvalues become

$$e^{-ikL} = \frac{-e^{-i\Phi}}{\alpha} \prod_j^{N/2} \frac{\sinh(\lambda_j - i\phi/2)}{\sinh(\nu_j + i\phi/2)} e^{-\lambda_j + \nu_j + i\phi}. \tag{4.43}$$

Two sets of Bethe equations for λ_j and ν_j are obtained from (4.41) and (5.48),

$$\begin{aligned}\sinh^N(\lambda_j - i\phi/2) &= -e^{-2\lambda_j - i\phi + 2c + 2i\Phi} e^{2\sum_k (2\lambda_k - \nu_k)} \\ &\times \prod_k^{N/2} \sinh(\lambda_j - \nu_k) \sinh(\lambda_j - \nu_k - i\phi) \qquad (4.44) \\ \sinh^N(\nu_j + i\phi/2) &= \frac{2i\cosh(c - \nu_j - i\phi/2)}{e^{\nu_j - c + i\phi/2}} e^{2\sum_k \lambda_k} \\ &\times \prod_k^{N/2} \sinh(\nu_j - \lambda_k) \sinh(\nu_j - \lambda_k + i\phi) \qquad (4.45)\end{aligned}$$

with the selection rules now reading $\lambda_j \neq \nu_k,\ \lambda_j \neq \lambda_k,\ \nu_j \neq \nu_k$.

4.5 Luttinger Liquid limit

The complexity of both the eigenvalues and Bethe equations is a common feature of models solved by ODBA and accordingly makes them more difficult to treat. However we can gain some insight as to the structure of the solutions by considering the case of weak or vanishing impurity strength $U \to 0$. This will also serve as a check on (5.48) by correctly reproducing the spectrum of the Luttinger Liquid. In this limit the impurity parameter, $c \to \infty$, blows up. Inserting this in (4.44), (4.45) we see that the solutions are either $\lambda_j = \nu_j$ or $\lambda_j = \nu_j + i\phi$. In terms of the original parameters these are $\mu_{j+N/2} = -\mu_j + i\phi$ or $\mu_{j+N/2} = -\mu_j + 2i\phi$. This leaves half the parameters, $\mu_j,\ j \leq N/2$ undetermined. To fix these remaining μ_j, we return to the expression for $\Lambda(u)$ as given by [124] and assume there are M pairs such that $\mu_{j+N/2} = -\mu_j + i\phi$ while the other $N/2 - M$ are of the form $\mu_{j+N/2} = -\mu_j + 2i\phi$. Upon taking $c \to \infty$ we find that the $N/2 - M$ latter pairs decouple and we are left with a T-Q

relation in terms of M parameters μ_j (see appendix D). From this we derive the eigenvalues

$$e^{-ikL} = e^{Mi\phi - i\Phi} \prod_{j=1}^{M} \frac{\sinh(\lambda_j - i\phi/2)}{\sinh(\lambda_j + i\phi/2)}. \tag{4.46}$$

The Bethe equations are similar to those of the XXZ and AKM models,

$$\frac{\sinh^N(\lambda_j - i\phi/2)}{\sinh^N(\lambda_j + i\phi/2)} = e^{i(N-2M)\phi + 2i\Phi} \prod_{k\neq j}^{M} \frac{\sinh(\lambda_j - \lambda_k - i\phi)}{\sinh(\lambda_j - \lambda_k + i\phi)} \tag{4.47}$$

and additionally the right hand side is similar to those found in the previous chapter. The extra phase factor in the Bethe equations will not change the structure of the solutions which are either real or form strings in the Thermodynamic limit [96] for $-\pi \leq \phi \leq \pi$, see previous chapters for further details. It is however, crucial in obtaining the correct energy of the Luttinger liquid. Combining (4.46) and (4.52) we obtain,

$$E = \frac{2\pi}{L}\sum_{k}^{N} n_k - \frac{2\pi}{L}\sum_{j}^{M} I_j - \frac{2M(N-M)}{L}\phi + \frac{\Phi}{L}(N-2M). \tag{4.48}$$

The last term is recognisable as $-\mathcal{A}(N_+ - N_-)$ and so we have reproduced the Luttinger liquid spectrum. This validates our choice of (5.48). As we saw with the AKM there are two sets of quantum numbers, n_k which are the charge degrees of freedom and I_j which now represent the chiral degrees of freedom. The independence of these sets is a chiral-charge separation akin to the spin-charge separation in other models. The ground state is associated to filing the charge quantum numbers p form the cutoff $n_j = -N, \ldots, -1$ while for the chiral quantum numbers we take $M = N/2$ and $-N/4 + 1/2 \leq I_j \leq N/4 - 1/2$. Excitations above this are found by placing holes in these sets of quantum numbers produces the simplest types of excitations. A hole in the charge numbers is still called a holon and we

introduce the term *chiron*[1] to describe a hole in the chiral quantum numbers. Despite the similarity to the AKM a chiron is very different from a spinon as can be seen by examining the wavefunctions of these excitations using (4.16) and (2.61).

Before proceeding to a study of the impurity thermodynamics we should recall that string solutions to the BAE represent gapless excitations of the Luttinger liquid and their structure depends heavily on the strength of the interaction. While we have successfully diagonalised the model for all ϕ and $U \geq 0$, for clarity we hereafter restrict ourselves to the simplest structure and take $|\phi| = \pi/\nu$ with $\nu > 2$ an integer. This then fixes the allowed string lengths and parities. Common to other integrable models we can have j-strings

$$\lambda^{(j,l)} = \lambda^j + i(2j + 1 - l)\phi/2, \tag{4.49}$$

for $j = 1 \ldots, \nu - 1$. These are said to have parity $v_j = 1$. In addition to these we may also have strings of negative parity, $v_\nu = -1$ which are centred on the $i\pi/2$ axis. As a consequence of our choice of ϕ, however only 1-strings of negative parity are allowed,

$$\lambda_\alpha^\nu + i\pi/2. \tag{4.50}$$

These string configurations are depicted in FIG. 2.13. Once again these represent bulk excitations and so will not be affected by the introduction of a local impurity. Our choice of scattering Bethe basis has dictated these as the appropriate excitations of the bulk which diagonalise the impurity.

The formal similarity between the Bethe Ansatz equations of the XXZ system with boundaries and the impurity Luttinger system arises from the analogy of spin degrees of freedom in the first and the chiral degrees of freedom in the second system, though their dynamics is of course very different. We note that for the XXZ with generic boundary fields

[1] Chiron was a centaur from greek mythology who was described as the "wisest and justest of all the centaurs" [127]

the residual $U(1)$ spin symmetry is broken by the off diagonal elements of the boundary matrices and it is this that necessitates the use of the ODBA. For the Luttinger liquid we also have a $U(1)$ symmetry (with charge $N_+ - N_-$) which is why we are led to taking the XXZ R-matrix while the inclusion of the impurity breaks this and forces us to adopt the ODBA. The remaining $U(1)$ symmetry in impurity model is associated with the length of the XXZ chain.

4.6 Thermodynamics

Having shown how the spectra of Z and Z_t are described by (4.43), (4.44) and (4.45) we determine from it the spectrum of H and H_{WT} and proceed to study their thermodynamic behaviour. In particular we calculate the free energy and entropy of the impurity and tunnel junction.

Unlike the previous chapter we do not examine the ground state properties of the system. The reason being that for a featureless impurity like the one we are dealing with here there are no interesting questions to ask about its behavior at zero temperature, in contrast for the RL model where we could investigate zero temperature dot occupation. It would be interesting however to compute the ground state energy as a function of flux which would give us the persistent (equilibrium) current through the system. For the moment however we are interested in impurity effects but not finite size effects. As a result we will lose sensitivity to the influence of the flux Φ [128]. In the following we set Φ to zero and will address transport properties (the non-equilibrium current) at finite temperature through the Kubo formula.

Dealing directly with (4.44) and (4.45) is arduous due to their non standard form but methods have been developed to extract physical quantities in the thermodynamic limit [129, 130, 131]. These methods are either based upon taking a special value of the interaction parameter which results in drastically simplified equations or by showing that the inhomogeneous term in the T-Q Ansatz can be discounted in the thermodynamic limit to

order $1/N$. The later approach is one which we will adopt here. We have just seen that for $c \to \infty$ the eigenvalues and Bethe equations are given by (4.46) and (4.52). For large but finite c, corresponding to $U \ll 1$, the form of these equations are modified by an impurity term which is necessarily of the order $1/N$. Indeed we know that any bulk properties cannot be modified by introducing an impurity. Thus, we make the assumption that the Bethe parameters are either real, form strings of positive parity such that

$$\mathrm{Im}\{\lambda^{(j,l)}\} = \mathrm{Im}\{\nu^{(j,l)}\} = (2j+1-l)\phi/2 \tag{4.51}$$

or negative parity $\mathrm{Im}\{\lambda_j\}$ =$\mathrm{Im}\{\nu_j\} = \pi/2$ in the thermodynamic limit or come in pairs $\mathrm{Im}\{\lambda_j - \nu_j\} = \phi$. Given these assumptions the system is described by the BAE

$$\frac{\sinh^{2N}(\lambda_j - i\phi/2)}{\sinh^{2N}(\lambda_j + i\phi/2)} = \left[\frac{\cosh(\lambda_j - c - i\phi/2)}{\cosh(\lambda_j - c + i\phi/2)}\right] \prod_{k\neq j}^{N/2} \frac{\sinh^2(\lambda_j - \lambda_k - i\phi)}{\sinh^2(\lambda_j - \lambda_k + i\phi)}. \tag{4.52}$$

The continuous form of the Bethe Ansatz equations follow with the result that the distributions for the j-strings and holes, $\rho_j(x)$ and holes $\rho_j^{\mathrm{h}}(x)$ [96] satisfy,

$$Na_j(x) + \frac{1}{2}b_j(x-c) = \rho_j(x) + \rho_j^{\mathrm{h}}(x) + \sum_k^{\nu} A_{jk} * \rho_k(x) \tag{4.53}$$

$$Na_\nu(x) + \frac{1}{2}b_\nu(x-c) = -\rho_\nu(x) - \rho_\nu^{\mathrm{h}}(x) + \sum_k^{\nu} A_{\nu k} * \rho_k(x) \tag{4.54}$$

where we have used again the functions defined in (2.81).

The form of the Bethe equations is very similar to the that of the anisotropic Kondo model considered in chapter 2. Indeed if we exchange $\frac{1}{2}b_j$ for a_j we recover (2.111). The difference in the impurity terms can be understood by noticing the impurity we presently consider is not merely a particle at a fixed location but introduces a new aspect, the mixing of the left and right movers this is in contrast to the Kondo model or AKM. In addition the change in term ensures that if the non interacting limit is taken, $\phi \to 0$, the impurity term vanishes and the distributions are those of free fermions. The same limit in the AKM

would give the isotropic Kondo model instead. We also have an extra non interacting point corresponding to $\phi = \pi/2$ in which all the equations simplify considerably.

Following the standard procedure we construct the free energy, $F = E - TS$, where E is the energy and $S = \sum_j \int \left[(\rho_j + \rho_j^h) \log (\rho_j + \rho_j^h) - \rho_j \log (\rho_j) - \rho_j^h \log (\rho_j^h) \right]$ is the entropy associated to the distributions. It then minimised with respect to ρ_j and $\rho_j^{\rm h}$ which are solutions of the BAE. The result of this minimization gives the TBA equations ,

$$\begin{aligned} \log \eta_j(x) = s * \log (1 + \eta_{j+1}(x))(1 + \eta_{j-1}(x)) \\ + \delta_{j,\nu-2} s * \log (1 + \eta_\nu^{-1}(x)) - \delta_{j,1} \frac{2D}{\phi T} \arctan e^{\frac{\pi}{\phi} x} \end{aligned} \tag{4.55}$$

$$\log \eta_{\nu-1}(x) = s * \log (1 + \eta_{\nu-2}(x)) = - \log \eta_\nu(x) \tag{4.56}$$

with $\eta_j(x) = \rho_j^h(x)/\rho_j(x)$, $s(x) = \frac{1}{2\phi \cosh \pi x/\phi}$. These TBA are identical to the AKM as could have been anticipated by recalling that do not depend upon the impurity.

Having taken the thermodynamic limit and derived the TBA equations we proceed to take the scaling limit to obtain universal quantities, eliminating any dependence on D. As we shall see the the model generates an energy scale T_{KF} which will be held fixed as $D \to \infty$. Thus high and low temperature regimes will be defined with respect to T_{KF} and always small compared to D. With this in mind we introduce the universal functions [69],

$$\varphi_j(x) \quad = \quad \frac{1}{T} \log \left(\eta_j (x + \frac{\phi}{\pi} \log \phi \frac{T}{D}) \right). \tag{4.57}$$

Inserting these into (4.55) and approximating the driving term,

$$-\frac{2D}{T} \arctan \, \exp \left(\pi (x + \frac{\phi}{\pi} \log \phi \frac{T}{D}) \right) \simeq -2 e^{\frac{\pi}{\phi} x}, \tag{4.58}$$

an approximation valid since only this range of values contributes to $\eta_1(x)$, we obtain the

universal (or scaling) form of the TBA equations,

$$\varphi_j(x) = s * \log(1+e^{\varphi_{j-1}(x)})(1+e^{\varphi_{j+1}(x)})^{1+\delta_{j,\nu-2}} - \delta_{j,1} 2e^{\frac{\pi}{\phi}x}, \quad j < \nu - 1 \tag{4.59}$$

$$\varphi_{\nu-1}(x) = s * \log(1+e^{\varphi_{\nu-2}(x)}) = -\varphi_\nu(x). \tag{4.60}$$

The free energy can then be written as

$$F = F^{LL} + F^i \tag{4.61}$$

with F^{LL} being the bulk contribution to the free energy while the impurity contribution is,

$$F^i = -T \int \mathrm{d}x\, s(x + \frac{\phi}{\pi} \log \frac{T}{T_{KF}}) \log(1+e^{\varphi_{\nu-1}(x)}). \tag{4.62}$$

There are two things to note here. The first is that the dependence is on the $\nu - 1$ thermodynamic function $\varphi_{\nu-1}$ rather than φ_1 as was the case in the AKM. The second is the appearance of a scale $T_{KF} = De^{\pi c/\phi}$ which has been generated by the model. We will measure all temperatures relative to this scale and can obtain universal results by keeping T_{KF} fixed while taking $D \to \infty$. In terms of the original parameters of the Hamiltonian this is

$$T_{KF} = D\left(\frac{U}{1-U^2/4}\right)^{-\frac{\pi}{\phi}}. \tag{4.63}$$

This scale is power law in the interaction strength which matches predictions made by Renormalisation Group techniques [12]. Having identified the scale we can determine the dependence of the impurity strength on the cutoff D. The behaviour depends on the sign of the interaction strength. For repulsive interactions $\phi < 0$,

$$U(D) \sim \left(\frac{T_{KF}}{D}\right)^{\frac{|\phi|}{\pi}} \tag{4.64}$$

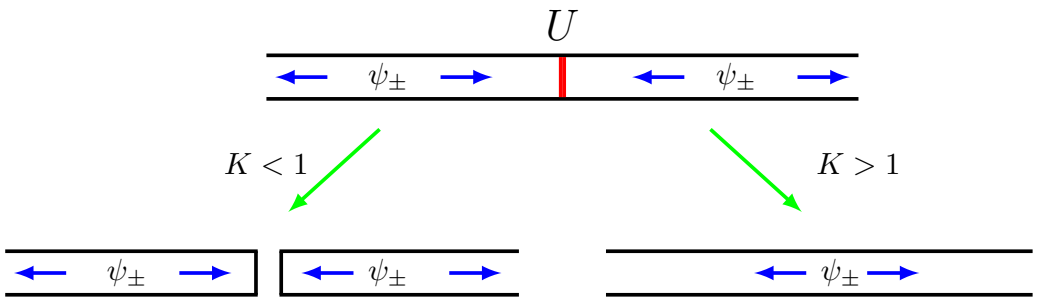

Figure 4.9: In the Kane-Fisher model the low energy behavior of the model depends on the sign of the interaction. For repulsive interactions, $K < 1$ the impurity strength grows at low energies so that the fixed point theory consists of two disconnected Luttinger liquids. In the opposite regime of attractive interactions, $K > 1$ the impurity strength weakens at low energy so that the fixed point theory describes a clean wire with non impurity.

which show $U \to 0$ as $D \to \infty$, or running the argument backwards, indicating the strengthening of the impurity at small energy increases as D is decreased. In contrast, for attractive interactions the $U(D)$ grows with the scale signifying the healing of the system at low energy, see 4.9.

Likewise, the Weak-Tunnelling Hamiltonian also generates a scale $T_{WT} = De^{\pi c_t/\phi}$. The complementary nature of these models is exposed when written in the bare parameters,

$$T_{WT} = D\left(\frac{4t}{1-4t^2}\right)^{\frac{\pi}{\phi}}. \tag{4.65}$$

The change in the sign of the exponent causes the tunnelling parameter to run oppositely to the impurity strength. The two systems thus become disjoint when the interactions are repulsive and completely joined for attractive interactions at low energies.

At this point we should replace our phase shift ϕ with the quantity K. The relation of the last chapter $\phi/\pi = 1 - 1/K$ was derived for a Luttinger liquid with hard wall boundary conditions. This result can therefore be applied to the weak tunnelling model

$$T_{WT} = D\left(\frac{4t}{1-4t^2}\right)^{\frac{K}{K-1}}. \tag{4.66}$$

while an analogous calculation for a liquid with periodic boundary conditions gives us that

$$T_{KF} = D\left(\frac{U}{1-U^2/4}\right)^{\frac{1}{1-K}}. \tag{4.67}$$

Any thermodynamic calculations are valid only when the generated scale is less than the cutoff. Accordingly we are hereafter restricted to the repulsive regime of the impurity model and the attractive regime for the Weak-Tunnelling Hamiltonian. We will only present the former but the latter is similar with the appropriate replacement of the scale.

Having taken the scaling limit we turn now to study the universal temperature dependence of the free energy. It requires the full solution of the TBA equations which can be achieved only numerically. Here we shall consider the high $T \gg T_{KF}$ and low temperature $T \ll T_{KF}$ limits and leave the study of the crossover to a later publication.

The free energy is given in terms of $\varphi_{\nu-1}$ which is coupled to all other φ_j but still we can obtain some results for high and low temperature. At $T \gg T_{KF}$ the integral in (4.62) is dominated by the behaviour at $x \to -\infty$, in this limit the driving term drops out of (4.55) and the solutions are constants. Denoting $e^{\varphi_j(-\infty)} = x_j$, we get,

$$x_j = (j+1)^2 - 1, \quad x_{\nu-1} = \nu - 1 = 1/x_\nu. \tag{4.68}$$

Similarly for low $T \ll T_{KF}$ we look for solutions at $x \to \infty$. This time we denote $e^{\varphi_j(\infty)} = y_j$ and find

$$y_j = j^2 - 1, \quad y_{\nu-1} = \nu - 2 = 1/y_\nu. \tag{4.69}$$

Using the expression for the free energy along with (4.69) and (4.68) we can calculate the difference in the impurity entropy between fixed points ,

$$S^i_{UV} - S^i_{IR} = \frac{1}{2}\log\frac{\nu}{\nu-1} \tag{4.70}$$

$$= \frac{1}{2}\log\left(\frac{1}{K}\right) \tag{4.71}$$

where we used $K = (\nu - 1)/\nu$ for our choice of ϕ. This shows the usual decrease as the system flows from the UV to the IR fixed points (a flow from weak to strong coupling regime for repulsive interactions), a decrease which in the language of the renormalisation group counts the degrees of freedom that were integrated out. The result agrees with the values calculated for the boundary terms in both the boundary Sine-Gordon model [119] as well as XXZ with parallel boundary fields [132].

We now consider the corrections to the asymptotic limits (4.68) and (4.69) which can also be calculated [132]. The corrections yield the specific heat which is found to scale as,

$$C(T \ll T_{KF}) \sim \left(\frac{T}{T_{KF}}\right)^{\frac{2}{K}-2} \tag{4.72}$$

$$C(T \gg T_{KF}) \sim \left(\frac{T_{KF}}{T}\right)^{2-2K}. \tag{4.73}$$

These indicate that both the strong and weak coupling fixed point are Non-Fermi Liquid in nature.

Using arguments from boundary conformal field theory [133] we can identify the leading irrelevant operators at both fixed points and thus determine the scaling of the conductance as given by Kubo's formula. At low temperature the conductance vanishes as $G \sim T^{\frac{2}{K}-2}$ corresponding to the effective increase of the strength of the impurity U as D is decreased noted earlier. Thus the low temperature physics is governed by strong coupling Hamiltonian where the wire is cut by the impurity and for which the Weak-Tunnelling model is the starting point. At high temperatures, in addition to the wire conductance $G_0 = Ke^2/h$, we have the impurity correction $G \sim T^{2K-2}$, its vanishing at high temperatures corresponding to the healing of the wire [12]. We expect similar results to be obtained from finite size calculations on a ring threaded by flux Φ. Performing the same analysis for the weak tunnelling model within the region $K > 1$ can be reproduced by making the replacement $K \to 1/K$ in the above formulae.

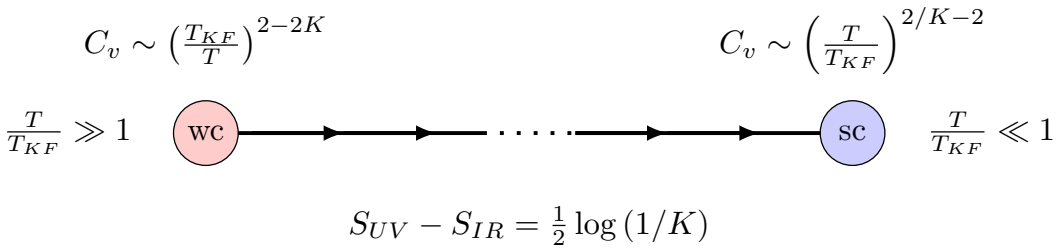

Figure 4.10: Here we summarize the results of this section. The backscattering impurity is weakly coupled at high temperature and strongly coupled at low temperature. The flow between the fixed points is characterized by the difference in impurity entropy. In the region of the fixed points the specific heat shows non fermi liquid behavior from which the dimensions of the leading relevant/irrelevant operators can be determined.

The weak tunnelling model is often used as the strong coupling description of the Kane-Fisher model[12] although the validity of this approach is not agreed upon in the literature [134, 135, 136, 137, 138]. In the above analysis we have seen that the $K < 1$ Kane-Fisher model is dual to the $K > 1$ Weak-Tunneling model. Unfortunately we cannot make any statement regarding the Weak-Tunneling model in the region $K < 1$ and its relation to the $K < 1$ Kane-Fisher model as there is no way to universally remove the cutoff.

4.7 Elementary Excitations

In the previous section we derived the impurity thermodynamics of both the Kane-Fisher impurity model and Weak-Tunnelling model with spin isotropic bulk interaction. Here we will discuss the elementary excitation of the models, which we have called *chirons* owing to their origin in the chiral degrees of freedom. The ground state of the system contains only real roots whose distribution is governed by the $j = 1$ equation of (4.53) with the $\rho_1^{\mathrm{h}}(x) = \rho_j(x) = 0$ for $j > 1$. Excitations above this ground state are obtained by adding holes in this distribution. The chiron energy, $\varepsilon = 2D \arctan e^{\frac{\pi}{|\phi|}x^{\mathrm{h}}}$, appears as the diving term in the TBA equations (4.55) with x^{h} being the position of the hole in the distribution.

Using the method of [88] which we outlined in chapter 2 we can determine their phase shift as they scatter past the impurity. To do this we note that in the absence of the impurity

the chiron energy should take on values $2\pi I^h/L$ (See Eq.(4.48)). The $1/L$ deviation of ε from this value gives the chiron- impurity phase shift. Up to an overall constant phase the impurity S-matrix is

$$\begin{aligned} S^{c,i}(\varepsilon) &= e^{i\Delta^{c,i}(\frac{|\phi|}{\pi}\log(\varepsilon/T_{KF}))}, \\ \Delta^{c,i}(x) &= \int \frac{\mathrm{d}\omega}{8\pi i\omega}\frac{\tanh(\omega/2)}{\sinh((\pi/|\phi|-1)\omega/2)}e^{i\omega x} \end{aligned} \tag{4.74}$$

This is valid for $\pi/|\phi|$ being an arbitrary rational number between 0 and 1. We see that the phase shift is non trivial at both low and high energies as both IR and UV fixed points are non trivial. This is to be compared with bare electrons which are perfectly transmitted at high energies and reflected at low energy.

Adding two holes to the ground state distribution allows us to calculate the chiron-chiron phase shift in the same manner,

$$\begin{aligned} S^{c,c}(\varepsilon_1,\varepsilon_2) &= e^{i\Delta^{c,c}(\varepsilon_1-\varepsilon_2)}, \\ \Delta^{c,c}(x) &= \int \frac{\mathrm{d}\omega}{4\pi i\omega}\frac{\sinh((\pi/|\phi|-2)\omega/2)e^{i\omega x}}{\cosh(\omega/2)\sinh((\pi/|\phi|-1)\omega/2)} \end{aligned} \tag{4.75}$$

With ε_j the energies of the two chirons. The full physical spectrum is thus built up by adding holes and strings to the ground state distribution. The interpretation of the strings is commented on below.

We now turn to discuss the relation between our approach with the bootstrap approach where the spectrum of the Hamiltonian and the various S-matrices are postulated on the basis of integrability properties. It is known that the impurity model without spin is related via bosonisation and folding procedures to the massless limit of the boundary Sine-Gordon model. Its spectrum is taken to consist of solitons, anti-solitons and their bound states known as sreathers. The dressed S-matrices, derived via the bootstrap method of [139], are non diagonal for generic interaction strength and calculating thermodynamic quantities

leads to an equation similar in structure to (4.23). For special values of the interaction however, the bulk scattering becomes diagonal and the computations simplify considerably, the right hand side becoming a mere phase. The inclusion of spin in this method is more complicated and is only achieved in certain interaction regimes [140]. In contrast the present method constitutes a bottom up approach. We have diagonalised the actual quantum Hamiltonian for all values of the interaction, our restriction to $|\phi| = \pi/\nu$ and weak bare coupling is purely for the convenience of its simplified string structure. The model has also been extensively investigated at arbitrary coupling using the Q-operator approach with the results derived therin broadly agreeing with those derived here[141, 142].

4.8 Conclusions

In this chapter we have solved exactly two related Hamiltonians, a Luttinger liquid coupled to an impurity or a tunnel junction with arbitrary boundary conditions. This was achieved via a new type of coordinate Bethe ansatz that incorporates the reflecting and transmitting properties of the impurity in conjunction with the Off Diagonal Bethe Ansatz. We found that determining the spectrum is equivalent to an analogous problem for an open XXZ chain with one boundary corresponding to the impurity and the other the associated to the type of boundary condition in the original model. The thermodynamics of both models were then studied and it was shown that a scale is naturally generated such that the impurity strength and tunnelling parameter run oppositely confirming the duality of the models. The impurity free energy for the simplest interaction regime was calculated and was seen to coincide with that obtained in [119] using the bootstrap approach. The diagonalization of the model allows us to view the system as a gas of excitations in the chiral degrees of freedom, chirons, which scatter with a pure phase off the impurity.

5

Quantum Dot in a Luttinger Liquid

So far we have studied two types of quantum impurities coupled to a Luttinger liquid. One in which a backscattering impurity is placed in the bulk of the Luttinger liquid but itself has no degrees of freedom and one in which there are impurity degrees of freedom but it is placed at the boundary of the system. In this chapter we will study two systems which incorporate both of these scenarios. They consist of a quantum dot coupled to the bulk of a Luttinger liquid realizing a backscattering bulk impurity which carries degrees of freedom. We find the exact solution of both models, constructing the eigenstates and finding the spectra using the methods of the last two chapters and study the ground state and finite temperature properties.

5.1 Introduction

Throughout this thesis we aim to highlight how remarkable the effects of coupling a quantum impurity to an interacting one dimensional lead can be. We have encountered two of the most striking phenomena in the previous chapters. The first entailed placing a quantum dot at the boundary of the system. As the dot was at the boundary it broke no symmetries of the system but it did have its own degrees of freedom which where fermionic in nature. The resulting interplay with the bulk bosonic degrees of freedom caused a strong coupling scale, T_K, to be dynamically generated and the dot to be completely hybridized with the bulk at low energies, $T, \epsilon_0 \ll T_{KF}$. This Kondo type behavior occurred even in the absence of any Kondo type coupling between the dot and the liquid. Including such a term in the form of a Coulomb interaction (the U term) between the dot and the wire we saw that the

strong coupling regime persisted even if the Kondo term was ferromagnetic .

The second type of impurity was a backscattering or Kane-Fisher (KF) type impurity placed in the bulk of the Luttinger liquid. Although carrying no degrees of freedom the impurity broke the individual number conservation of left and right movers. This also resulted in the generation of a strong coupling scale, T_{KF} below which the system would be split in two provided there were repulsive bulk interactions. We also saw that a duality existed between this model and one in which the impurity was replaced by a tunnel junction. In that system the tunnelling at the junction vanished at low energy if the bulk interactions were repulsive, however if they were attractive the tunnelling would grow at low energies and a strong coupling scale T_{WT} would be generated. The spectra of the two models were seen to be related by taking the map $K \to 1/K$.

More interesting still are scenarios in which the impurity has internal degrees of freedom and also causes backscattering. Among these, systems of quantum dots coupled to interacting leads have attracted much attention [12][143][144][111][145][113][146][147][148][149][150]. These allow for richer and more exotic phases to appear. For example, the Kane-Fisher impurity flows to strong coupling provided $K < 1$ but the dot flowed to strong coupling provided $K > 1/2$ and so one can expect interesting competition between the two effects when $1/2 < K < 1$.

Such systems are readily achievable in many experimental settings allowing for confrontation of theory with experiment [120][151]. In particular the Duke group realizes the embedded geometry, see FIG. 5.1(a) of a dot placed between two otherwise disconnected leads. To do this they use a short carbon nano tube as a quantum dot and attach it to two 2-dimensional Fermi liquid leads with tunnelling from the leads to the dot mediated via dissipative environment. It is known however that such non interacting, resistive 2-dimensional leads can be described by Luttinger liquid theory[59, 110] and by properly tuning the Fermi level on the dot using a back gate a single level can be made available thus realizing a Luttinger-resonant level model. An AFM image of the experiment is depicted in

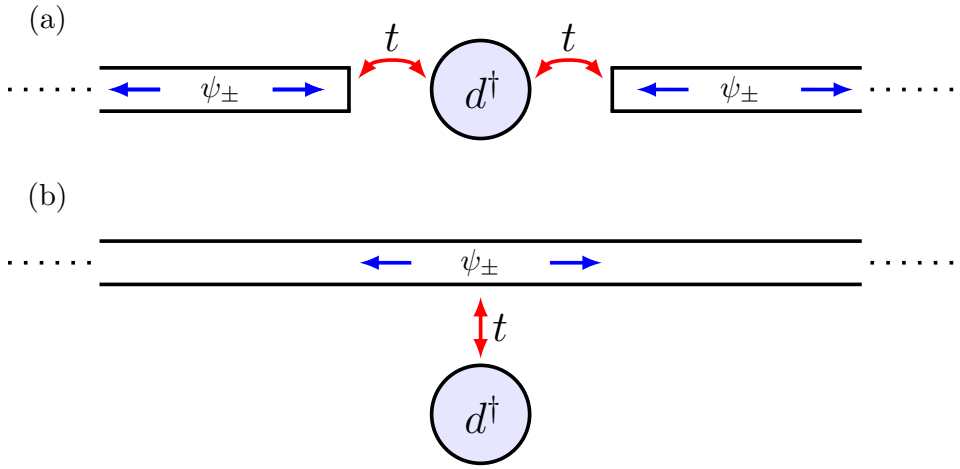

Figure 5.1: We consider two geometries of Luttinger dot system; (a) embedded and (b) side-coupled. The embedded geometry also includes a Coulomb interaction between the dot and leads. Once unfolded the side-coupled and embedded geometries are the same but with the latter containing non local interactions (5.2).

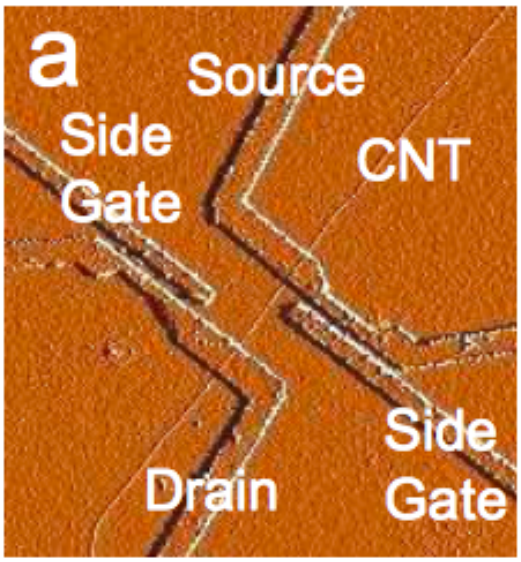

Figure 5.2: An atomic force microscope image of the setup utilized by the Duke group. A carbon nano tube is attached to a source and drain created from thin Cr films. The tunneling between the leads and dot is tuned by the side gates shown. Not shown is a back gate which tunes the Fermi level of the carbon nano tube so that it realizes a resonant level. Figures are taken from [151]

FIG. 5.2. Measurement of the conductance has revealed interesting non-Fermi liquid scaling as well as Majorana physics. Using a similar setup it may be possible to also realize the other geometry of a sidecoupled dot, see FIG. 5.1 (a). Other experimental setups also exist which may realize the Luttinger-dot system more directly, for example using on fractional quantum Hall materials as discussed in the last chapter [50, 51, 52].

In this chapter we solve exactly Luttinger liquid-quantum dot systems in both the embedded (see FIG. 5.1(a)) and side coupled (see FIG. 5.1(b)) geometries. We do this using the Bethe Ansatz approach formulated in the last chapter. We shall construct the eigenstates and determine the spectra of the models via the Bethe Ansatz equations and study both the ground state and finite temperature properties. In particular we calculate the dot occupation as a function of both temperature and dot energy.

The exact solution shows that the spectra of the two geometries are related by changing the sign of the bulk interaction, or rather $K \to 1/K$ a fact previously known through bosonization [146] and an effect which was seen in the last chapter between the KF and WT models.

In the last chapter we saw how the system consisted of decoupled charge and chiral degrees of freedom, each with their own quantum numbers and can be considered a gas of holons and chirons with the later acquiring a phase shift as they scatter past the impurity. Here we will see that the charge and chiral degrees of freedom remain coupled as the impurity can change both the charge and chirality of the bulk. At low energies we show that the dot becomes fully hybridized and acts as a backscattering impurity for the side-coupled model and as a tunnel junction for the embedded system. This creates a competition between the charge and chiral degrees of freedom when the backscattering or tunnel junction is irrelevant and leads to non Fermi liquid exponents in the dot occupation.

5.2 Models

The systems we consider consist of a quantum dot attached to a Luttinger liquid, the attachment being either in the embedded or the side-coupled geometry. For convenience we recall that the Hamiltonian of a Luttinger liquid is given by,

$$\begin{aligned} H_{\rm LL} &= -i\int \mathrm{d}x\,(\psi_+^\dagger\partial_x\psi_+ - \psi_-^\dagger\partial_x\psi_-) \\ &\quad +4g\int \mathrm{d}x\,\psi_+^\dagger(x)\psi_-^\dagger(x)\psi_-(x)\psi_+(x) \end{aligned} \tag{5.1}$$

For the side-coupled geometry we have $x \in [-L/2, L/2]$ while the embedded geometry is similar to the WT model of the last chapter and consists of two Luttinger liquids restricted to $x \in [-L/2, 0]$ and $x \in [0, L/2]$. It is convenient to bring the two systems into similar form by unfolding the embedded geometry in the standard way to give,

$$\begin{aligned} H_{\rm LL}^{\rm emb} &= -i\int dx(\psi_+^\dagger\partial_x\psi_+ - \psi_-^\dagger\partial_x\psi_-) \\ &\quad +4g\sum_{\sigma=\pm}\int dx\,\psi_\sigma^\dagger(x)\psi_\sigma^\dagger(-x)\psi_\sigma(-x)\psi_\sigma(x) \end{aligned} \tag{5.2}$$

The embedded system now consists of one branch of left-movers and one branch of right movers restricted to $x \in [-L/2, L/2]$ but unlike the side-coupled system where the left and right fermions interact locally with each other, in the embedded system after unfolding the interaction is between particles of the same chirality and is non local. We can compare this to the boundary-dot model of chapter 3 which after unfolding had only one remaining chirality. The embedded model can thus be considered a two lead generalization of that system.

As ever, the linear spectrum requires a cutoff to be imposed in order to render the energies finite imposing it on the particle momenta requires $k \geq -\mathcal{K} = -2\pi\mathcal{D}$. All physical quantities are taken to be small compared with the cutoff and at the end of the calculation we send $\mathcal{D} \to \infty$, to obtain universal results.

The quantum dot is modelled by a resonant level with energy ϵ_0 described by,

$$H_{\rm dot} = \epsilon_0 d^\dagger d, \tag{5.3}$$

coupled to Luttinger liquid via a tunnelling term,

$$H_t \;=\; \frac{t}{2}(\psi_+^\dagger(0) + \psi_-^\dagger(0))d + \text{h.c} \tag{5.4}$$

which mediates both forward and backscattering in the model, the latter changing left movers to right movers and vice versa. Furthermore in the embedded system we add a Coulomb interaction between the ends of the leads and the dot which is the same strength as the Luttinger interaction,

$$H_c = g d^\dagger d \sum_{\sigma=\pm} \psi_\sigma^\dagger(0)\psi_\sigma(0). \tag{5.5}$$

Both energy scales in the dot Hamiltonian are small compared the the cut-off, $\epsilon_0, \Gamma \ll \mathcal{D}$, where $\Gamma = t^2$ is the level width. We shall determine the spectrum and the full set of exact eigenstates of both Hamiltonians, $H^{\rm sc} = H_{LL} + H_t + H_{\rm dot}$ and $H^{\rm emb} = H_{LL}^{\rm emb} + H_t + H_{\rm dot} + H_c$, using the Bethe Ansatz approach developed in the last chapter.

5.3 Eigenstates of the models, duality and Bethe equations

To begin note that after the unfolding procedure, the two systems differ only in the two particle interaction, it is either local or non-local, meaning the single particle eigenstates are the same in both models. We construct them in what should by now be a familiar fashion: writing down the most general state which is consistent with the symmetry of the model and applying the Hamiltonian to it. Since the tunnelling to and from the dot takes place at the origin we expand the wavefunction in plane waves on either side of it, the most general

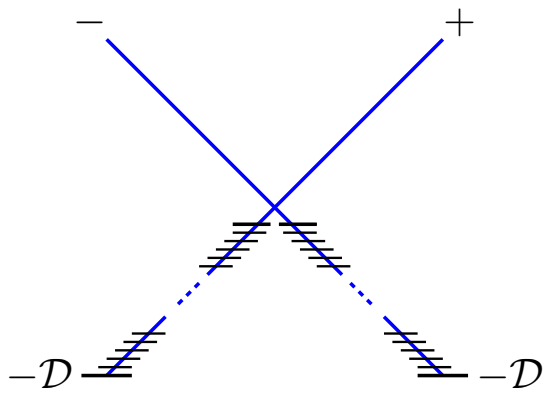

Figure 5.3: The linear derivative requires that we cutoff the bottom of the Dirac sea so that $k > -2\pi\mathcal{D}$ which we will take to infinity in the end. When the rapidity notation is used the dot energy acts as a chemical potential and in the ground state levels are filled up to $-\mathcal{K}e^{-B/2}$, with $B = B(\epsilon_0)$. In comparison to the boundary dot case there are two branches of particles corresponding to left and right movers.

form for the single particle state of energy $E = k$ being,

$$\sum_{\sigma=\pm}\int e^{\sigma ikx}\left[\theta(-x)A_{\sigma}^{[10]}+\theta(-x)A_{\sigma}^{[01]}\right]\psi_{\sigma}^{\dagger}(x)\left|0\right\rangle + Bd^{\dagger}\left|0\right\rangle, \tag{5.6}$$

The amplitudes $A_{+}^{[10]}$ and $A_{-}^{[01]}$ are those of an incoming particle and are related to the outgoing amplitudes $A_{-}^{[10]}$ and $A_{+}^{[01]}$ (see FIG. 4.4) by the bare single particle S-matrix - S, which takes an incoming particle to an outgoing one. In contrast to the KF/WT models it depends explicitly on the particle momenta due to the presence of the dimensionful tunnelling parameter t and the neceesity for the components of the S-matrix to be dimensionless. As we did for the boundary dot model it is convenient to trade in the particle

momentum k for the rapidity variable z, defined as $k - \epsilon_0 = \mathcal{D}e^{z/2}$, we have,

$$\begin{pmatrix} A_+^{[01]} \\ A_-^{[10]} \end{pmatrix} = S(z) \begin{pmatrix} A_+^{[10]} \\ A_-^{[01]} \end{pmatrix} \tag{5.7}$$

$$S(z) = \begin{pmatrix} \frac{e^{z/2}}{e^{z/2}+ie^c} & \frac{-ie^c}{e^{z/2}+ie^c} \\ \frac{-ie^c}{e^{z/2}+ie^c} & \frac{e^{z/2}}{e^{z/2}+ie^c} \end{pmatrix} \tag{5.8}$$

with $e^c = \Gamma/\mathcal{D}$. In addition the dot amplitude B is

$$B = \sum_{\sigma=\pm} \frac{1}{2} e^{(c-z)/2} \left(A_\sigma^{[10]} + A_\sigma^{[01]} \right). \tag{5.9}$$

From here periodic boundary conditions can be imposed $\psi_\pm^\dagger(-L/2) = \psi_\pm^\dagger(L/2)$ resulting in

$$e^{-i\mathcal{D}e^{z/2}L - i\epsilon_0 L} \begin{pmatrix} A_+^{[10]} \\ A_-^{[01]} \end{pmatrix} = S(z) \begin{pmatrix} A_+^{[10]} \\ A_-^{[01]} \end{pmatrix} \tag{5.10}$$

which can then be solved for the allowed values of the rapidity z.

We now proceed to the two particle case wherein the bulk interaction g enters differently in both models. We shall first consider the side-coupled model and discuss the embedded model subsequently. The construction of the two particle state follows the same logic as was used in the KF and WT models. The difference now is that the S-matrices and in particular our choice of W^{ij} will depend explicitly on the particle rapidities and the wavefuncion also contains dot terms $\propto d^\dagger |0\rangle$. For clarity of presentation we reiterate the construction here, repeating many of the same statements appropriately modified for the present purposes.

Since the two particle interaction is point-like as is the tunnelling to the dot we may divide configuration space into regions such that the interactions only occur at the boundary between two regions. Therefore away from these boundaries we write the wavefunction as a sum over plane waves. For two particles we require 8 regions which are specified not only by the ordering of the particle positions x_1, x_2 and the impurity but also according to which

position is closer to the origin. For example if x_1 is to the left of the impurity, x_2 to its right with x_2 closer to the impurity then the amplitude in this region is denoted $A^{[102B]}_{\sigma_1\sigma_2}$, $\sigma_j = \pm$ being the chirality of the particle at x_j. The region in which x_1 is closer is denoted $A^{[102A]}_{\sigma_1\sigma_2}$. The most general two particle state with energy $E = k_1 + k_2 = \sum_{j=1}^{2} \mathcal{D}e^{z_j/2} + 2\epsilon_0$ is therefore

$$\begin{aligned} |k_1, k_2\rangle &= \sum_Q \sum_{\sigma_1,\sigma_2=\pm} \int \theta(x_Q) A^Q_{\sigma_1\sigma_2} \prod_j^2 e^{i\sigma_j k_j x_j} \psi^\dagger_{\sigma_j}(x_j) \, |0\rangle \\ &+ \sum_{\sigma=\pm} \int \left[\theta(-x) B^{[10]}_\sigma + \theta(x) B^{[01]}_\sigma\right] \psi^\dagger_\sigma(x) d^\dagger \, |0\rangle \, . \end{aligned} \tag{5.11}$$

The amplitudes $A^Q_{\sigma_1\sigma_2}$ are related to each other by S-matrices which are fixed by the Hamiltonian and in turn fix $B^{[10]}_\pm$ and $B^{[01]}_\pm$. To define these S-matrices we form column vectors of the amplitudes,

$$\vec{A}_1 = \begin{pmatrix} A^{[120B]}_{++} \\ A^{[102B]}_{+-} \\ A^{[201B]}_{-+} \\ A^{[021B]}_{--} \end{pmatrix} \quad \vec{A}_2 = \begin{pmatrix} A^{[210A]}_{++} \\ A^{[102A]}_{+-} \\ A^{[201A]}_{-+} \\ A^{[012A]}_{--} \end{pmatrix} \quad \vec{A}_3 = \begin{pmatrix} A^{[201A]}_{++} \\ A^{[012A]}_{+-} \\ A^{[210A]}_{-+} \\ A^{[102A]}_{--} \end{pmatrix} \quad \vec{A}_4 = \begin{pmatrix} A^{[201B]}_{++} \\ A^{[021B]}_{+-} \\ A^{[120B]}_{-+} \\ A^{[102B]}_{--} \end{pmatrix}$$

$$\vec{A}_5 = \begin{pmatrix} A^{[021B]}_{++} \\ A^{[201B]}_{+-} \\ A^{[102B]}_{-+} \\ A^{[120B]}_{--} \end{pmatrix} \quad \vec{A}_6 = \begin{pmatrix} A^{[012A]}_{++} \\ A^{[201A]}_{+-} \\ A^{[102A]}_{-+} \\ A^{[210A]}_{--} \end{pmatrix} \quad \vec{A}_7 = \begin{pmatrix} A^{[102A]}_{++} \\ A^{[210A]}_{+-} \\ A^{[012A]}_{-+} \\ A^{[201A]}_{--} \end{pmatrix} \quad \vec{A}_8 = \begin{pmatrix} A^{[102B]}_{++} \\ A^{[120B]}_{+-} \\ A^{[021B]}_{-+} \\ A^{[201B]}_{--} \end{pmatrix} \tag{5.12}$$

The interpretation of these is exactly the same as in the previous chapter: $\vec{A}_1$ are the amplitudes where both particles are incident on the impurity but particle 2 is closer. Similarly in $\vec{A}_2$ both particles are incoming but the order in which they hit the impurity is exchanged i.e 1 is closer. In the nomenclature of the last chapter they should be related by the in-in S-matrix. The amplitudes $\vec{A}_5$ and $\vec{A}_6$ are similar but the particles being outgoing instead.

The vector $\vec{A}_8$ describes particle 2 having scattered off the impurity and is still closer to the impurity than 1 while $\vec{A}_7$ also describes particle 2 having scattered but with 1 is closer. These are related by an in-out S-matrix. The remaining two vectors $\vec{A}_3$ and $\vec{A}_4$ are similar but with particle 1 being incoming and 2 outgoing.

After applying the Hamiltonian to (5.11) we find that it is an eigenstate provided,

$$\vec{A}_8 = S^{20}(z_2)\vec{A}_1, \qquad \vec{A}_3 = S^{10}(z_1)\vec{A}_2, \tag{5.13}$$

$$\vec{A}_5 = S^{20}(z_2)\vec{A}_4, \qquad \vec{A}_6 = S^{10}(z_1)\vec{A}_7, \tag{5.14}$$

$$\vec{A}_7 = S^{12}\vec{A}_8, \qquad \vec{A}_4 = S^{12}\vec{A}_3, \tag{5.15}$$

$$\vec{A}_2 = W^{12}(z_2 - z_1)\vec{A}_1, \qquad \vec{A}_6 = W^{12}(z_2 - z_1)\vec{A}_5. \tag{5.16}$$

The S-matrices S^{20} and S^{10} which take a particle past the impurity, i.e. from incoming to outgoing are

$$S^{20}(z_2) = S(z_2) \otimes \mathbb{1}, \quad S^{10}(z_1) = \mathbb{1} \otimes S(z_1), \tag{5.17}$$

with $S(z)$ the same as in the single particle state (5.8), the S-matrix S^{12} scatters an incoming particle past an outgoing particle and is

$$S^{12} = \begin{pmatrix} 1 & 0 & 0 & 0 \\ 0 & e^{i\phi} & 0 & 0 \\ 0 & 0 & e^{i\phi} & 0 \\ 0 & 0 & 0 & 1 \end{pmatrix}. \tag{5.18}$$

where $\phi = -2\arctan(g)$ encodes the bulk interaction and $W^{12}(z_2 - z_1)$ which scatters an

incoming (outgoing) particle past another incoming (outgoing) particle is given by

$$W^{12}(z) = \begin{pmatrix} 1 & 0 & 0 & 0 \\ 0 & \frac{\sinh\frac{1}{2}(z)}{\sinh\frac{1}{2}(z-2i\phi)} & \frac{-\sinh i\phi}{\sinh\frac{1}{2}(z-2i\phi)} & 0 \\ 0 & \frac{-\sinh i\phi}{\sinh\frac{1}{2}(z-2i\phi)} & \frac{\sinh\frac{1}{2}(z)}{\sinh\frac{1}{2}(z-2i\phi)} & 0 \\ 0 & 0 & 0 & 1 \end{pmatrix}. \tag{5.19}$$

In addition the dot amplitudes are given by

$$\begin{aligned} B_{\pm}^{[10]} &= \frac{1}{2}e^{(c-z_2)/2}\sum_{\sigma=\pm}\left[A_{\sigma\pm}^{[210A]} + A_{\sigma\pm}^{[201A]}\right] \\ &\quad -\frac{1}{2}e^{(c-z_1)/2}\sum_{\sigma=\pm}\left[A_{\pm\sigma}^{[120B]} + A_{\pm\sigma}^{[102B]}\right], \end{aligned} \tag{5.20}$$

$$\begin{aligned} B_{\pm}^{[01]} &= \frac{1}{2}e^{(c-z_2)/2}\sum_{\sigma=\pm}\left[A_{\sigma\pm}^{[102A]} + A_{\sigma\pm}^{[012A]}\right] \\ &\quad -\frac{1}{2}e^{(c-z_1)/2}\sum_{\sigma=\pm}\left[A_{\pm\sigma}^{[201B]} + A_{\pm\sigma}^{[021B]}\right]. \end{aligned} \tag{5.21}$$

Inserting these expressions for the amplitudes into (5.11) we get the two particle eigenstate of the side-coupled model.

Since all amplitudes are generated from $\vec{A}_1$ by successive application of the various S-matrices, as depicted in FIG. 4.6, there are two ways to obtain each $\vec{A}_j$ both of which must be equivalent for the construction to be consistent. This consistency imposes that the S-matrices satisfy a generalised Yang Baxter equation similar to the last chapter but which is rapidity dependent

$$S^{20}(z_2)S^{12}S^{10}(z_1)W^{12}(z_2-z_1) = W^{12}(z_2-z_1)S^{10}(z_1)S^{12}S^{20}(z_2) \tag{5.22}$$

Despite the increased complexity of this relation due to the forms of W^{12} and S^{j0} this equation is still satisfied, which can be checked by substitution. Furthermore the unitarity

conditions must also hold. In addition to $S^{12}\left[S^{21}\right]^* = \mathbb{1}$, we need that

$$W^{12}(z_2 - z_1)W^{21}(z_1 - z_2) = \mathbb{1}$$

both of which are indeed satisfied.

It is important to note that while no interaction between two incoming (outgoing) particles is present in the Hamiltonian, W^{12} is necessary for (5.11) to be an eigenstate. In contrast to AKM and KF models the form of W^{12} is not a freedom afforded by the linear derivative. Recall that in those models the Hamiltonian did not fix the in-in or out-out S-matrix and one had to invoke the Yang Baxter equation to fix W^{12} and have a consistent wavefunction. In the present case W^{12} is fixed by the Hamiltonian and subsequently we checked that the consistency condition was satisfied. The lack of freedom in our choice of W^{12} stems from the additional Schrödinger equation from the "dot" part of the wavefunction i.e the part of the eigenstate $\propto d^\dagger |0\rangle$. Recall that when we looked at the boundary-dot model of chapter 3 there was also no freedom and the two particle phase shift was determined by the Hamiltonian.

We can now construct the two particle eigenstates of the sidecoupled model and then go on to impose periodic boundary conditions. Upon doing so one finds

$$e^{-ik_1 L}\vec{A}_1 = S^{12}S^{10}W^{12}\vec{A}_1 \tag{5.23}$$

$$e^{-ik_2 L}W^{12}\vec{A}_1 = S^{12}S^{20}\vec{A}_1 \tag{5.24}$$

which can be solved to determine $z_{1,2}$.

The eigenstates for higher particle number are constructed similarly and the N particle state with energy $E = \sum_{j=1}^{N} k_j = \sum_{j=1}^{N} \mathcal{D}e^{z_j/2} + N\epsilon_0$ is,

$$\begin{aligned}\left|\vec{k}\right\rangle &= \sum_{Q}\sum_{\vec{\sigma}}\int \theta(x_Q)A^{Q}_{\vec{\sigma}}\prod_{j}^{N} e^{i\sigma_j k_j x_j}\psi^{\dagger}_{\sigma_j}(x_j)\left|0\right\rangle \\ &+ \sum_{P}^{'}\sum_{\vec{\sigma}}^{'}\int \theta(x_P)B^{P}_{\vec{\sigma}}\prod_{j}^{'} e^{i\sigma_j k_j x_j}\psi^{\dagger}_{\sigma_j}(x_j)d^{\dagger}\left|0\right\rangle \end{aligned} \tag{5.25}$$

The first line here should is familiar from the previous chapter. Again $\theta(x_Q)$ are Heaviside functions which partition configuration space into $2^N N!$ regions with Q labelled by the ordering of the N particles as well as according to which particle is closest to the origin while $\vec{\sigma} = (\sigma_1, \ldots, \sigma_N)$ with $\sigma_j = \pm$. The second line is a new addition compared to the KF model, concerning as it does the occupied dot portion of the wavefunction. The primed sums indicate that one particle is removed - being on the dot - and the sums are over the remaining $N-1$ particle system. There are thus $2^{N-1}(N-1)!$ P regions. Just as in the two particle case the amplitudes are related to each other via S-matrices which act on the 2^N dimensional space

$$S^{j0} = S_j(z_j) \otimes_{k\neq j} \mathbb{1}, \tag{5.26}$$

$$S^{ij} = \begin{pmatrix} 1 & 0 & 0 & 0 \\ 0 & e^{i\phi} & 0 & 0 \\ 0 & 0 & e^{i\phi} & 0 \\ 0 & 0 & 0 & 1 \end{pmatrix}_{ij} \otimes_{k\neq i,j} \mathbb{1}, \tag{5.27}$$

$$W^{ij} = \begin{pmatrix} 1 & 0 & 0 & 0 \\ 0 & \frac{\sinh\frac{1}{2}(z_j - z_i)}{\sinh\frac{1}{2}(z_j - z_i - 2i\phi)} & \frac{-\sinh i\phi}{\sinh\frac{1}{2}(z_j - z_i - 2i\phi)} & 0 \\ 0 & \frac{-\sinh i\phi}{\sinh\frac{1}{2}(z_j - z_i - 2i\phi)} & \frac{\sinh\frac{1}{2}(z_j - z_i)}{\sinh\frac{1}{2}(z_j - z_i - 2i\phi)} & 0 \\ 0 & 0 & 0 & 1 \end{pmatrix}_{ij} \otimes_{k\neq i,j}\mathbb{1}. \tag{5.28}$$

where the subscripts denote which particle spaces the operators act upon. In order for

this wavefunction to be consistent it must satisfy the following Yang-Baxter and reflection equations,

$$S^{k0}S^{jk}S^{j0}W^{jk} = W^{jk}S^{j0}S^{jk}S^{k0} \tag{5.29}$$

$$W^{jk}W^{jl}W^{kl} = W^{kl}W^{jl}W^{jk} \tag{5.30}$$

$$W^{jk}S^{jl}S^{kl} = S^{kl}S^{jl}W^{jk}. \tag{5.31}$$

The first of these being the generalisation to N particles of (5.22) while the remaining two come from the consistency of the wavefunction away from the dot, (5.30) arises from the swapping the order of 3 particles which are either all incoming or outgoing and (5.31) is when one of the three differs form the other two. These are indeed satisfied by (5.26),(5.27) and (5.38) which is a sufficient condition for the consistency of the wave function [89]. The expressions for $B^P_{\vec{\sigma}}$ in terms $A^Q_{\vec{\sigma}}$ can also be found and are straightforward generalizations of (5.20) and (5.21). Therefore we have successfully constructed the N particle eigenstates of the side-coupled model.

The spectrum can then be determined by imposing periodic boundary conditions. As we are interested in studying properties of the dot in the thermodynamic limit the type of boundary condition imposed at $x = \pm L/2$ will not affect the result. This results in an eigenvalue problem which determines the k_j through

$$e^{-ik_jL}A_{\sigma_1\ldots\sigma_N} = (Z_j)^{\sigma'_1\ldots\sigma'_N}_{\sigma_1\ldots\sigma_N}A_{\sigma'_1\ldots\sigma'_N} \tag{5.32}$$

$$Z_j = W^{j-1j}..W^{1j}S^{1j}..S^{jN}S^{j0}W^{jN}..W^{jj+1} \tag{5.33}$$

where the matrix Z_j takes the jth particle past all others and past the impurity. By using (5.22), (5.30) and (5.31) one can show that the Z_j commute with each other $[Z_j, Z_k] = 0$ $\forall j, k$. They are therefore simultaneously diagonalisable and the spectrum of the side-coupled model is determined by the eigenvalues of the Z_j operators. In this case the Z_j are not all

the same as they were for the previous models we studied. This stems from the appearance of the dimensionful parameter t in the Hamiltonian which resulted in rapidity dependent phase shifts S^{j0} and W^{ij}. This will ultimately result in the charge and chiral degrees of freedom remaining coupled. This occurs also in the Bethe Ansatz solutions of the Anderson impurity model[35] and the Hubbard model[152] .

The manner in which we have constructed the eigenstates allows one to apply any boundary conditions to the system and we have chosen a periodic system here for convenience. As we did with the KF model however we may impose a twisted boundary condition in which case our transfer matrix is modified to

$$Z_j = W^{j-1j}..W^{1j}B_jS^{1j}..S^{jN}S^{j0}W^{jN}..W^{jj+1} \tag{5.34}$$

where

$$B_j = \begin{pmatrix} e^{i\Phi} & 0 \\ 0 & e^{-i\Phi} \end{pmatrix}. \tag{5.35}$$

with $\Phi = \int \mathcal{A}$ being the total flux threaded through the system. This can then be used to calculate the equilibrium, persistent current around the system by studying for instance $\frac{\partial E_{\rm gs}}{\partial \Phi}$. Aside from twisted boundary conditions like this one can also introduce another dot at $x = L/2$ so that the system consists of two resonant levels coupled to a Luttinger liquid at diametrically opposed parts of the periodic system. This opens up the possibitliy to study how the occupation of one level is affected by the other, the occurrence of the RKKY interaction[153, 154, 155] and the effect that the bulk interactions have on these processes.

Having obtained the eigenstates of the sidecoupled model we now do the same for the embedded dot geometry. Once the embedded system has been unfolded its eigenstates can be constructed in the same manner as we did for the side-coupled model. The single particle states are given by (5.6) however the multiparticle states are modified by the non local interaction as well as the addition of the Coulomb term, H_c. Following the same steps

as the last section one finds that the N particle state is given by

$$\begin{aligned}\left|\vec{k}\right\rangle &= \sum_{Q}\sum_{\vec{\sigma}}\int \theta(x_Q)A^{Q}_{\vec{\sigma}}\prod_{j}^{N} e^{i\sigma_j k_j x_j}\psi^{\dagger}_{\sigma_j}(x_j)\left|0\right\rangle \\ &+ \sum_{P}{}'\sum_{\vec{\sigma}}{}'\int \theta(x_P)B^{P}_{\vec{\sigma}}\prod_{j}{}' e^{i\sigma_j k_j x_j}\psi^{\dagger}_{\sigma_j}(x_j)d^{\dagger}\left|0\right\rangle \end{aligned} \tag{5.36}$$

where now the various amplitudes are related to each other by the S-matrices

$$S^{ij}_{\text{emb}} = \begin{pmatrix} e^{i\phi} & 0 & 0 & 0 \\ 0 & 1 & 0 & 0 \\ 0 & 0 & 1 & 0 \\ 0 & 0 & 0 & e^{i\phi} \end{pmatrix}_{ij} \otimes_{k\neq i,j} \mathbb{1}, \tag{5.37}$$

$$\begin{aligned} W^{ij}_{\text{emb}} = &\begin{pmatrix} 1 & 0 & 0 & 0 \\ 0 & \frac{\sinh\frac{1}{2}(z_j-z_i)}{\sinh\frac{1}{2}(z_j-z_i+2i\phi)} & \frac{\sinh i\phi}{\sinh\frac{1}{2}(z_j-z_i+2i\phi)} & 0 \\ 0 & \frac{\sinh i\phi}{\sinh\frac{1}{2}(z_j-z_i+2i\phi)} & \frac{\sinh\frac{1}{2}(z_j-z_i)}{\sinh\frac{1}{2}(z_j-z_i+2i\phi)} & 0 \\ 0 & 0 & 0 & 1 \end{pmatrix}_{ij} \\ &\otimes_{k\neq i,j}\mathbb{1}. \end{aligned} \tag{5.38}$$

and the single particle S-matrices S^{j0} the same as (5.26). The inclusion of the Coulomb term (5.5) is essential for this and in its absence the model is not integrable, despite this though the S-matrices are very similar to those of the side coupled model, indeed the in-in matrix is related to the sidecoupled version by changing the sign of the interactions, $W^{ij}_{\text{emb}} = W^{ij}|_{\phi\to-\phi}$. Similarly for the in-out matrix we have that $S^{ij}_{\text{emb}} = e^{i\phi}S^{ij}|_{\phi\to-\phi}$. Thus if it weren't for the additional phase required in the later relation the two models would exactly map to each other under $\phi \to -\phi$. To investigate this further let us impose the periodic boundary condition $\psi^{\dagger}_{\pm}(-L/2) = \psi^{\dagger}_{\pm}(L/2)$. This then results in another eigenvalue

problem,

$$e^{-ik_jL}A_{\sigma_1\ldots\sigma_N} = \left(Z_j^{\text{emb}}\right)_{\sigma_1\ldots\sigma_N}^{\sigma'_1\ldots\sigma'_N} A_{\sigma'_1\ldots\sigma'_N} \tag{5.39}$$

where Z_j^{emb} is defined similarly to Z_j in (5.33) but using W_{emb}^{ij} and S_{emb}^{ij}. The mapping can aslo be applied to the transfer matrix above so that

$$e^{-i(N-1)\phi}Z_j^{\text{emb}} = Z_j|_{\phi\to-\phi}. \tag{5.40}$$

Therefore, the spectrum of the embedded model is obtained from the side-coupled model by changing the sign of the interaction, $\phi \to -\phi$ modulo the additional phase above. An overall phase shift like this could be cancelled if one were to impose a different boundary condition on either system. For instance taking instead a twisted boundary condition $\psi_\pm^\dagger(-L/2) = e^{i\xi}\psi_\pm^\dagger(L/2)$ where $\xi = (N-1)\phi$ Mod 2π in the embedded model would give us an exact mapping between the two different geometries.

We can replace the bare phase shift ϕ by the universal Luttinger liquid parameter K using [40] [39]

$$K = \begin{cases} 1+\frac{\phi}{\pi} & \text{side-coupled} \\ \frac{1}{1-\frac{\phi}{\pi}} & \text{embedded} \end{cases} \tag{5.41}$$

meaning that in the thermodynamic limit the two models (with appropriately chosen boundary conditions) are related by taking $K \to 1/K$. A similar duality map was found to exist between the embedded and sidecoupled models using boosnization[146]. In that instance the duality was said to be between the models regardless of their respective boundary conditions. The result was derived using the same unitary transformation method that we reviewed in chapter 3, section3.8. As we saw though one must be careful when equating Hamiltonians in this fashion. By choosing the boundary conditions in each model correctly,

however one can restore the single valued nature of the correlators as in (3.80) and thereafter it is correct to say that there is an exact mapping between the two models.

As was the case for the sidecoupled model we are free to apply arbitrary boundary conditions in the embedded model and in particular we can thread the system with a flux and use it to calculate the persistent current. The calculation of the current (at $T = 0$) requires one to calculate the finite size correction to the ground state energy and so in this scenario one would need to take care with the boundary conditions in order to apply the duality mapping to the result. In any case the type of boundary condition applied to the system should not affect thermodynamic properties of the impurity in the limit $N, L \to \infty$ which is what will study hereafter and so we will disregard these intricacies. In the subsequent sections all calculations will be done for the side-coupled model with periodic boundary conditions the results of which can then be translated to the embedded model by taking $K \to 1/K$. Note that as ϕ is a phase shift and restricted to $[-\pi, \pi]$ we see that the side-coupled system may realize values of $K \in [0, 2]$ whereas the embedded system has $K \in [1/2, \infty]$ although once again we should mention that the Luttinger liquid description is only a valid low energy effective description for a much narrower range of K.

5.4 Off Diagonal Bethe Ansatz and the Luttinger limit

Our task now is to determine the eigenvalues of Z_j which we will do following the method used for the KF model. We begin by considering the monodromy matrix

$$\begin{aligned}\Xi^A(u) = \mathcal{C}K^+(u)\mathcal{R}^{A1}(u+\theta/2-z_1/2)\ldots\mathcal{R}^{AN}(u+\theta/2-z_N/2)\\ \times K^-(u)\mathcal{R}^{AN}(u-\theta/2+z_N/2)\ldots\mathcal{R}^{A1}(u-\theta/2+z_1/2)\end{aligned} \tag{5.42}$$

where $\mathcal{C} = \frac{-e^{z_j+i\phi}}{\sinh(3\theta/2)\sinh(\theta)}$ and the boundary matrices are given by

$$K^-(u) = \begin{pmatrix} 2i\cosh(\theta/2-c)\cosh u & \sinh(2u) \\ \sinh(2u) & 2i\cosh(\theta/2-c)\cosh u \end{pmatrix} \tag{5.43}$$

$$K^+(u) = \begin{pmatrix} 2\sinh(-\theta)\cosh(u-i\phi) & \sinh(2u-2i\phi) \\ \sinh(2u-2i\phi) & 2\sinh(-\theta)\cosh(u-i\phi) \end{pmatrix}. \tag{5.44}$$

with $e^c = \Gamma/\mathcal{D}$. The trace of the monodromy matrix, $t(u) = \mathrm{Tr}_A[\Xi^A(u)]$ evaluated at a particular spectral parameter will then give us each of the Z_j operators

$$Z_j = \lim_{\theta\to\infty} t(\theta/2 - z_j/2). \tag{5.45}$$

As we saw in the previous chapter this type of transfer matrix is associated with the open XXZ model and has been studied extensively, in particular using the ODBA method. Following the same procedure we find that the eigenvalues of the transfer matrix $t(\theta/2 - z_j/2)$ are

$$\begin{aligned}\Lambda(\theta/2-z_j/2) = -4i\mathcal{C}&\frac{\sinh(\theta-z_j-2i\phi)\cosh(c-z_j/2)\cosh^2(\theta/2-z_j/2)}{\sinh(\theta-i\phi-z_j)} \\ &\times\sinh(3\theta/2-z_j/2)\prod_k^N \frac{\sinh(\theta/2-z_j/2-\mu_k+i\phi)}{\sinh(\theta/2-z_j/2+\mu_k-i\phi)}.\end{aligned} \tag{5.46}$$

with the Bethe equations given by

$$\begin{aligned}&\frac{\left[i\sinh\left(-i(N+1)\phi-c-\theta/2+2\sum_{j=1}^N\mu_j\right)-1\right]\sinh(2\mu_j-i\phi)\sinh(2\mu_j-2i\phi)}{2i\cosh(\mu_j-c+\theta/2-i\phi)\cosh^2(\mu_j-i\phi)\sinh(\mu_j-\theta-i\phi)} \\ &\qquad = \prod_{l=1}^N \frac{\sinh(\mu_j+\mu_l-i\phi)\sinh(\mu_j+\mu_l-2i\phi)}{\sinh(\mu_j-z_l/2+\theta/2-i\phi)\sinh(\mu_j+z_l/2-\theta/2-i\phi)}\end{aligned} \tag{5.47}$$

In addition the Bethe parameters must also satisfy the selection rules $\mu_j \neq \mu_k$ and $\mu_j \neq \mu_k + i\phi$. Upon taking the limit, $\theta \to \infty$ (5.46) and (5.47) completely determine the spectrum of Z_j and therefore the sidecoupled Lutinger-dot model. In order to take this limit we

redefine the Bethe parameters in the following way

$$2\mu_j = \begin{cases} -\lambda_j + i\phi + \theta & \text{if} j \leq \frac{N}{2} \\ \nu_{j-N/2} + i\phi - \theta & \text{if} j > \frac{N}{2}. \end{cases} \tag{5.48}$$

Inserting these into (5.46) and (5.47) and then taking the $\theta \to \infty$ limit we have that the single particle energy is

$$e^{-i\mathcal{D}e^{z_\alpha/2}L} = -\frac{e^{z_\alpha+c}}{e^{z_\alpha/2}+ie^c} 2\cosh(z_\alpha/2+c) e^{iN\phi/2} \prod_k^{N/2} \frac{\sinh\frac{1}{2}(z_\alpha-\lambda_k+i\phi)}{\sinh\frac{1}{2}(z_\alpha-\lambda_k-i\phi)} e^{\nu_k-\lambda_k} \tag{5.49}$$

while the two sets of Bethe equations are

$$\begin{aligned} \prod_k^{N/2} \sinh(\lambda_j-\nu_k+i\phi)\sinh(\lambda_j-\nu_k) &= -e^{-\sum_\alpha z_\alpha/2+\sum_k(2\lambda_k-\nu_k)+i\phi+2c-\lambda_j} \\ &\quad \times \prod_\alpha^N \sinh\frac{1}{2}(z_\alpha-\lambda_j+i\phi) \qquad (5.50) \\ \prod_k^{N/2} \sinh(\nu_j-\lambda_k-i\phi)\sinh(\nu_j-\lambda_k) &= -\frac{e^{-\sum_\alpha z_\alpha/2+\sum_k \lambda_k+i\phi/2+c-\lambda_j}}{2\cosh(\nu_j-c-i\phi/2)} \\ &\quad \times \prod_\alpha^N \sinh\frac{1}{2}(z_\alpha-\nu_j-i\phi) \qquad (5.51) \end{aligned}$$

In addition we also have the selection rules which are now $\lambda_j \neq \lambda_k$, $\nu_j \neq \nu_k$, $\lambda_j \neq \nu_k$. Equations (5.49)-(5.51) describe exactly the sidecoupled model for all values of ϕ and c with finite N and L. Naturally these are very similar to those we encountered when analyzing the KF model and we shall take a similar approach to solving them. Indeed we can recover the Luttinger liquid spectrum, thereby validating our limiting procedure, in the same way. Leaving the details to the appendix we find that upon taking $c \to -\infty$ we get that the

energy of the system is $E = \sum_\alpha \mathcal{D} e^{z_\alpha/2} + N\epsilon_0$ where

$$e^{-i\mathcal{D}e^{z_\alpha/2}L} = e^{iM\phi - i\epsilon_0 L} \prod_k^{N/2} \frac{\sinh\left(\frac{1}{2}(z_\alpha - \lambda_k - i\phi)\right)}{\sinh\left(\frac{1}{2}(z_\alpha - \lambda_k + i\phi)\right)} \tag{5.52}$$

$$\prod_\alpha^N \frac{\sinh\left(\frac{1}{2}(\lambda_j - z_\alpha + i\phi)\right)}{\sinh\left(\frac{1}{2}(\lambda_j - z_\alpha - i\phi)\right)} = e^{i(N-2M)} \prod_{j\neq k}^{N/2} \frac{\sinh\left(\frac{1}{2}(\lambda_j - \lambda_k + 2i\phi)\right)}{\sinh\left(\frac{1}{2}(\lambda_j - \lambda_k - 2i\phi)\right)}. \tag{5.53}$$

These differ from the Bethe equations previously cited as describing the Luttinger liquid, (4.48) (4.52) which at first may seem worrying. We should recall however that the large degeneracy afforded to the system when the impurity is absent by the linear spectrum. This allows us to diagonalize the Luttinger liquid in many different bases each of which will provide a different set of Bethe equations. The expressions above actually correspond to a solution of the Lutinger liquid in the basis appropriate for sidecoupled quantum dot while those we encoutered previously were in the appropriate basis for the KF or WT models. Irrespective of the choice of basis that is made though they should all return the same eigenvalues which we can check here by inserting (5.53) into (5.52). After taking the log and summing over all particles we get

$$E = \frac{2\pi}{L}\sum_k^N n_k - \frac{2\pi}{L}\sum_j^M I_j - \frac{2M(N-M)}{L}\phi$$

which coincides with the previous result (4.48) at zero flux.

Away from the Luttinger limit we are still left with a number of complex Bethe equations to solve in order to study the our model. Rather than deal with them directly we adopt the approach of the last chapter and make the simplifying assumption that when $e^c \ll 1$ the solutions to the Bethe equations obey the string hypothesis (see FIG. 5.6). Given these

the system is described by

$$e^{-i2\mathcal{D}e^{z_\alpha/2}L} = e^{iN\phi-2i\epsilon_0 L}\left[\frac{e^{z_\alpha/2}-ie^c}{e^{z_\alpha/2}+ie^c}\right]\prod_k^{N/2}\frac{\sinh^2\left(\frac{1}{2}(z_\alpha-\lambda_k-i\phi)\right)}{\sinh^2\left(\frac{1}{2}(z_\alpha-\lambda_k+i\phi)\right)} \quad (5.54)$$

$$\prod_\alpha^N\frac{\sinh^2\left(\frac{1}{2}(\lambda_j-z_\alpha+i\phi)\right)}{\sinh^2\left(\frac{1}{2}(\lambda_j-z_\alpha-i\phi)\right)} = \left[\frac{\cosh\left(\frac{1}{2}(\lambda_j-2c+i\phi)\right)}{\cosh\left(\frac{1}{2}(\lambda_j-2c-i\phi)\right)}\right]\prod_{j\neq k}^{N/2}\frac{\sinh^2\left(\frac{1}{2}(\lambda_j-\lambda_k+2i\phi)\right)}{\sinh^2\left(\frac{1}{2}(\lambda_j-\lambda_k-2i\phi)\right)} \quad (5.55)$$

where the parameters λ_j describe the chiral degrees of freedom, z_α describe the charge degrees of freedom and the energy of the system is

$$E=\sum_\alpha \mathcal{D}e^{z_\alpha/2}+N\epsilon_0. \quad (5.56)$$

In the remainder of the chapter we use (5.54)(5.55) along with (5.56) to study the impurity properties in the thermodynamic and universal limit. We close the section by commenting that the condition $e^c \ll 1$ is quite natural to take as it states that the bare hybridization be much smaller than the bandwith $\Gamma \ll \mathcal{D}$, an assumption that is made to reduce a system to the Hamiltonian (5.1). Finally one should also check that in the non interacting limit the (2 channel) RL model is recovered. We postpone this to the next section where we recover the ground state dot occupation.

5.5 Ground state dot occupation

Having obtained the Bethe equations governing the system we can now construct the ground state. To do this we first must fill the empty Dirac sea with negative energy particles from the cutoff, $-\mathcal{D}$ up to some level determined by minimisation of the energy (and depending on ϵ_0, see FIG. 5.3). After this the thermodynamic limit $N, L \to \infty$ is taken holding the density $D = N/L$ fixed and finally we take the universal limit by removing the cutoff $\mathcal{D} \to \infty$ while holding some other scale, which has been generated by the model, fixed. We will see below that this scale is the level width Γ. Once the ground state has been found we will use it to derive exact expressions for the occupation of the dot, $n_d = \langle d^\dagger d\rangle$ as a

function of ϵ_0.

The form of the possible negative energy states entering the ground state depends upon the value of K, whether it is greater or less than 1 and so the ground state must be constructed separately in each case. Nevertheless we will find a single expression for the dot occupation valid in both regimes.

5.5.1 Attractive interactions, $K > 1$

We begin with $\phi \in [0, \pi]$ which corresponds to $K \in [1, 2]$. Here the ground state consists of so-called $z - \lambda$ 2-strings [96] wherein the rapidities form complex conjugate pairs with their real part coinciding with one of the chiral variables,

$$z_j = z^*_{N+1-j} = \lambda_j + 2\pi i + i\phi. \tag{5.57}$$

with each pair having bare energy $-2\cos(\phi/2)\mathcal{D}e^{\lambda_j}$, see FIG. 5.6. Inserting these expressions into (5.54) and (5.55) we obtain equations for the real parts of the pairs, λ_j. In the thermodynamic limit we describe them by the density $\rho_1(\lambda)$ which we split into bulk and boundary contributions $\rho_1^{\mathrm{b}}(\lambda) + \frac{1}{L}\rho_1^{\mathrm{d}}(\lambda)$. The dot occupation is then given by,

$$n_d = 2\int \rho_1^{\mathrm{d}}(\lambda). \tag{5.58}$$

The factor of 2 appears here as each λ corresponds to a pair of rapidities. These distributions, $\rho_1^{\mathrm{b}}(\lambda)$, $\frac{1}{L}\rho_1^{\mathrm{d}}(\lambda)$ are determined by the Bethe equations in their continuous form which for the bulk part is,

$$\frac{\cos\phi/2}{2\pi}\mathcal{D}e^{\lambda/2} \quad = \quad \rho_1^{\mathrm{b}}(\lambda) + \int_{-B}^{\infty} a_2(\frac{\lambda-\mu}{2})\rho_1^{\mathrm{b}}(\mu) \tag{5.59}$$

where $-B = -B(\epsilon_0)$ is the λ value of the highest filled level. When the dot energy vanishes we have that $B(0) = \infty$ and bulk distribution is easily found by Fourier transform to be

$$\rho_1^{\mathrm{b}}(\lambda) = \frac{\mathcal{D}e^{\lambda/2}}{4\pi\cos(\phi/2)} \tag{5.60}$$

with the bulk part of the ground state energy being

$$E_{\mathrm{gs}} = -\int_{-\infty}^{\infty} 2\cos(\phi/2)\mathcal{D}e^{\lambda/2}\rho_1^{\mathrm{b}}(\lambda). \tag{5.61}$$

To confirm this is indeed the ground state one can introduce excitations and check the energy is increased, the simplest type of which consists of adding holes to the distribution. Following the prodecure of chapter 2 we find that the energy of a hole turns out to be proportional to the ground state distribution i.e. a hole at $\lambda = \lambda^h$ has energy $\varepsilon^h(\lambda^h) = 4\pi\rho_1^{\mathrm{b}}(\lambda^h)$, increasing the energy. This is similar to the boundary dot model where we also employed a rapidity notation the addition factor of 2 compared to there is due to our choice of $k \sim e^{z/2}$ rather than $k \sim e^z$. The other excitations consist of breaking up a $z - \lambda$ pair and placing them above the Fermi surface such they have real rapidity. Each particle then has energy $\varepsilon^p(z) = 2\mathcal{D}e^{z/2}$ in addition to the hole introduced in the $\rho_1(\lambda)$ distribution.

When $\epsilon_0 \neq 0$ the additional term in the energy (see (5.56)) needs to be balanced by the addition of holes to the ground state with rapidities starting at $-B(\epsilon_0)$. The form of the hole energy, $\varepsilon^h(\lambda)$ gives us that [39]

$$B(\epsilon_0) = \log\left(\alpha\frac{\mathcal{D}}{\epsilon_0}\right) \tag{5.62}$$

where α is a constant. An explicit expression for α could be derived following the steps of appendix B, however to understand the behavior of the system the exact form of α is not required.

Considering now the dot part of the Bethe equations, the dot contribution to the density

satisfies,

$$f_1(\lambda - 2c) = \rho_1^{\mathrm{d}}(\lambda) + \int_{-B}^{\infty} a_2(\frac{\lambda-\mu}{2})\rho_1^{\mathrm{d}}(\mu), \tag{5.63}$$

$$\text{with} \qquad f_n(x) = \frac{1}{2\pi}\int_{-\infty}^{\infty} e^{i\omega x}\frac{\sinh(\pi - n\phi)\omega}{\sinh 2\pi\omega}. \tag{5.64}$$

The solution is obtained by the Wiener-Hopf method (see [69],[68] or [96] and references therein). Upon integrating over the result as in (5.58) we find that the exact dot occupation in the ground state is,

$$\begin{aligned} n_d &= \frac{-i}{2\sqrt{\pi}}\int_{-\infty}^{\infty} d\omega \frac{e^{-i\omega(2\log\left(\frac{\epsilon_0}{\Gamma}\right)+a)}}{\sinh(2\pi\omega)} \\ &\quad \times \frac{\Gamma(\frac{1}{2}+i(K-1))\omega)}{\Gamma(1+i\omega)\Gamma(1-i(2-K)\omega)}. \end{aligned} \tag{5.65}$$

where $\Gamma(x)$ is the Gamma function, a is the constant,

$$e^a = \frac{\phi}{\pi\alpha^2}\left[\frac{\pi-\phi}{\phi}\right]^{\frac{\pi-\phi}{\pi}} \tag{5.66}$$

and we have used (5.41) to write n_d in terms of the Luttinger K.

As there is no dependence on the cutoff we can safely take the universal limit $\mathcal{D} \to \infty$ while holding the level width Γ fixed. The width serves as both the coupling constant and as the strong coupling scale paramerizing the model, with respect to which all quantities are measured. It appears here, rather surprisingly, unrenormalized by the interactions which are present in the system and independent of the raw cut-off. This behavior is more akin to the non interacting RL model in which the bulk is a Fermi liquid than the boundary dot system of chapter 3. This is a first hint of the competition between the Kondo and KF effects which occur in this model. We will comment on this further in the next section but for now we examine the expression (5.65).

First we can check that upon inserting $K = 1$ in the above expression we recover the

non interacting result

$$n_d = \frac{1}{2} - \frac{1}{\pi} \arctan\left(\frac{\epsilon_0}{\Gamma}\right). \tag{5.67}$$

which is that of the RL model. Note that in chapter 2 we considered only a single branch of right movers and currently there are both left and right. In the non interacting limit though one can perform an odd-even transformation in the Hamiltonian, $\psi_{e,o} = (\psi_+ \pm \psi_-)/\sqrt{2}$ which decouples the odd modes and leave the one channel RL model we studied before.

The recovery of the noninteracting result is a highly nontrivial verification of our solution. To take this limit in the Bethe equations one should rescale both the rapidities and Bethe parameters $z \to \phi z$ and $\lambda \to \phi\lambda$ and then take $\phi \to 0$. This still leaves us with a set of complicated Bethe equations to solve but which nevertheless return the above result.

For other values we may evaluate (5.65) by contour integration and obtain an expansion of n_d for $\epsilon_0 < \Gamma$ or $\epsilon_0 > \Gamma$ giving

$$n_d = \begin{cases} \frac{1}{2} - \left[\sum_{n=0}^{\infty} a_n \left(\frac{\epsilon_0}{\Gamma}\right)^{2n+1} + b_n \left(\frac{\epsilon_0}{\Gamma}\right)^{(2n+1)/(K-1)}\right] \\ \sum_{n=0}^{\infty} c_n \left(\frac{\Gamma}{\epsilon_0}\right)^{n+1} \qquad\qquad \text{for} \quad \Gamma < \epsilon_0 \end{cases} \tag{5.68}$$

where a_n, b_n and c_n are constants. Furthermore the capacitance of the dot is

$$\chi = \left.\frac{\partial n_d}{\partial \epsilon_0}\right|_{\epsilon_0=0} = \frac{e^{a/2}}{\pi(K-2)\Gamma}. \tag{5.69}$$

We see that at low energy, $\epsilon_0 < \Gamma$ the system is strongly coupled with the dot becoming hybridized with the bulk. At the low energy fixed point ($\epsilon_0 = 0$) the dot is fully hybridized and has $n_d = 1/2$. The leading term in the expansion about this is ϵ_0/Γ which indicates that the leading irrelevant operator has dimension 2. We identify it as the stress energy tensor [94]. The next order term $(\epsilon_0/\Gamma)^{1/(K-1)}$ is due to the backscattering which is generated at low energies but is irrelevant for $K > 1$. At high energies, $\epsilon_0 > \Gamma$, the system becomes

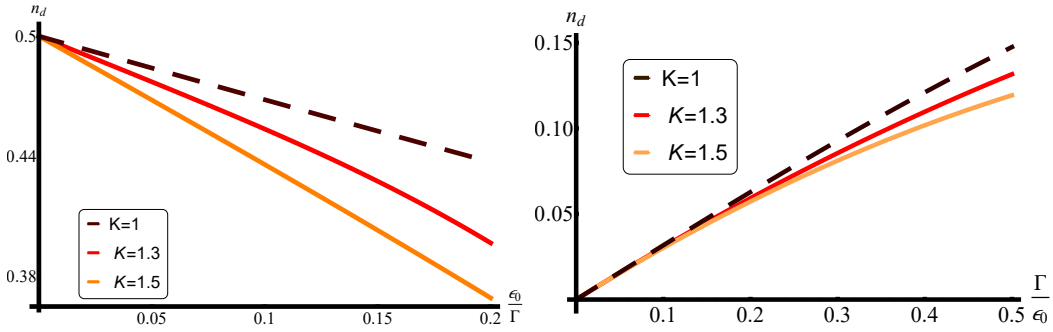

Figure 5.4: The dot occupation at small (left) and large (right) dot energy, ϵ_0/Γ, for different values of $K > 1$. The effect of attractive interactions is to suppress the dot occupation as compared to the non interacting case (dashed line). This effect becomes stronger for increasing K.

weakly coupled with the fixed point ($\epsilon_0 \to \infty$) describing a decoupled empty dot, $n_d = 0$. The expansion about this fixed point is in terms of integer powers indicating that the tunnelling operator $d^\dagger\psi(0)$ has dimension 1/2. The first few terms of the expansion are plotted in FIG. 5.4 from which we see that the dot occupation is suppressed as a function of ϵ_0 for $K > 1$ as compared to the non interacting case due to the backscattering.

5.5.2 Repulsive Interactions, $K < 1$

The ground state takes a different form in the region $\phi \in [-\pi, 0]$ which corresponds to $K \in [0, 1]$. It is constructed by taking the chiral parameters $\lambda_j \in \mathbb{R}$ to be real and the rapidities placed on the $2\pi i$ line i.e. $\mathrm{Im}(z_\alpha) = 2\pi$. Inserting these values into the Bethe equations and then passing to the continuous form we obtain a set of coupled integral equations for the distributions of the charge, $\rho_-(z)$ and chiral variables $\sigma_1(\lambda)$ which we can again split into bulk and dot contributions. The bulk contributions $\rho_-^{\mathrm{b}}(z)$ and $\sigma_1^{\mathrm{b}}(\lambda)$ are governed by the continuous Bethe equations,

$$\begin{aligned} \frac{\mathcal{D}e^{z/2}}{4\pi} &= \rho_-^{\mathrm{b}}(z) - \int_{-B'}^{\infty} a_1(z-y)\sigma_1^{\mathrm{b}}(y) \\ \int_{-B'}^{\infty} a_1(\lambda-y)\rho_-^{\mathrm{b}}(y) &= \sigma_1(\lambda) + \int_{-\infty}^{\infty} a_2(\lambda-y)\sigma_1^{\mathrm{b}}(y) \end{aligned} \tag{5.70}$$

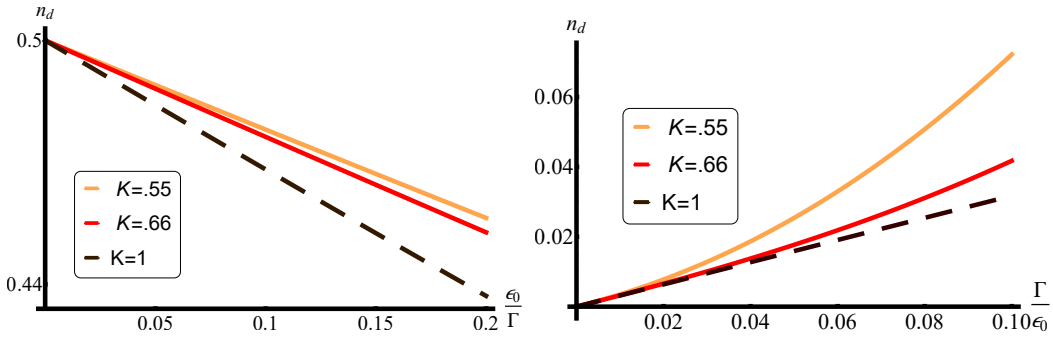

Figure 5.5: The dot occupation at small (left) and large (right) dot energy for different values of K. The effect of repulsive interactions $K < 1$ is to enhance the dot occupation as compared to the non interacting case (dashed line) with the effect increasing as K decreases.

where the rapidities are bounded by $-B'(\epsilon_0)$. When the dot energy is set to zero we have that $B'(0) = \infty$ and the bulk ground state distributions are found to be,

$$\rho_-^{\rm b}(z) = \frac{\mathcal{D}e^{z/2}}{2\pi}, \tag{5.71}$$

$$\sigma_1^{\rm b}(\lambda) = \frac{\mathcal{D}e^{z/2}}{4\pi\cos(\phi/2)}. \tag{5.72}$$

The fundamental excitations above this ground state consist of adding holes to either of these distributions. The energy of these are $\varepsilon^h(z) = 4\pi\rho_-^{\rm b}(z)$ and $\varepsilon^h(\lambda) = 4\pi\sigma_1^{\rm b}(\lambda)$ for a charge hole and chiral hole respectively. As in the previous section these are used to determine B' which gives the same relation as (5.62). The dot occupation is subsequently obtained by integrating over the dot part of the charge distribution $n_d = \int \rho_-^{\rm d}(z){\rm d}z$ which is determined by,

$$g_2(\lambda - 2c) = \rho_-^{\rm d}(\lambda) + \int_{-B'}^{\infty} g_1(\lambda - y)\rho_-^{\rm d}(y), \tag{5.73}$$

$$g_n(x) = \frac{1}{2\pi}\int_{-\infty}^{\infty} e^{i\omega x}\frac{\sinh(\pi-\phi)\omega}{2\cosh(\phi\omega)\sinh(n\pi\omega)}. \tag{5.74}$$

The solution is again determined using the Wiener-Hopf method with the result that the dot occupation for $K < 1$ is also given by (5.65). Note however that the poles at $\omega = i(K-1)(2n+1)/2$ have shifted from the upper half plane to the lower half plane. This

changes the expansions at high and low energy to be

$$n_d = \begin{cases} \frac{1}{2} - \sum_{n=0}^{\infty} a_n \left(\frac{\epsilon_0}{\Gamma}\right)^{2n+1} \\ \sum_{n=0}^{\infty} c_n \left(\frac{\Gamma}{\epsilon_0}\right)^{n+1} + b_n \left(\frac{\Gamma}{\epsilon_0}\right)^{(2n+1)/(1-K)} \end{cases} \tag{5.75}$$

with the capacitance being given by (5.69). As in the $K > 1$ region, the dot is strongly coupled at low energy and weakly coupled at high energy with the same leading terms in the expansion about these points however the term generated by the backscattering now appears in the expansion about the high energy fixed point. This stems from the fact that backscattering is relevant for $K < 1$ and leads to an enhancement of the dot occupation as compared to the $K = 1$ case, see FIG. 5.5.

The dot occupation for the embedded system is simply obtained from (5.65) by using the mapping $K \to 1/K$.

5.6 RG flow

In the previous section we derived exact expressions for the dot occupation for the side-coupled model as a function of ϵ_0 measured with respect to the strong coupling scale. This strong coupling scale is given by Γ, the level width. It does not depend on K as might have been expected for an interacting model and in fact coincides with the free model[1]. To understand why the level width is not renormalised by K we can make use of the mapping to the embedded model which can be viewed as a two lead version of the model considered in chapter 3. The strong coupling scale in the embedded model should behave similarly to the single lead case, where a dot is placed at a Luttinger liquid edge [146]. For an arbitrary

[1] In QIMs there are in fact a number of different scales present. For instance in the AKM there is T_K but also T_H which is the natural scale that emerges when studying the ground state magnetization under the applied field H. There is a certain amount of freedom in choosing these particular forms for the scale as one could also define them to include an overall constant. Often they are fixed so that a particular observable takes a natural form, e.g in the Kondo model T_H is chosen so that there is no $\log^{-2}(H/T_H)$ in the high field expansion of the magnetization. The ratio of these numbers given certain conventions like the one just stated then gives a universal number known which can be calculated with the same result using different methods. For more details see [68].

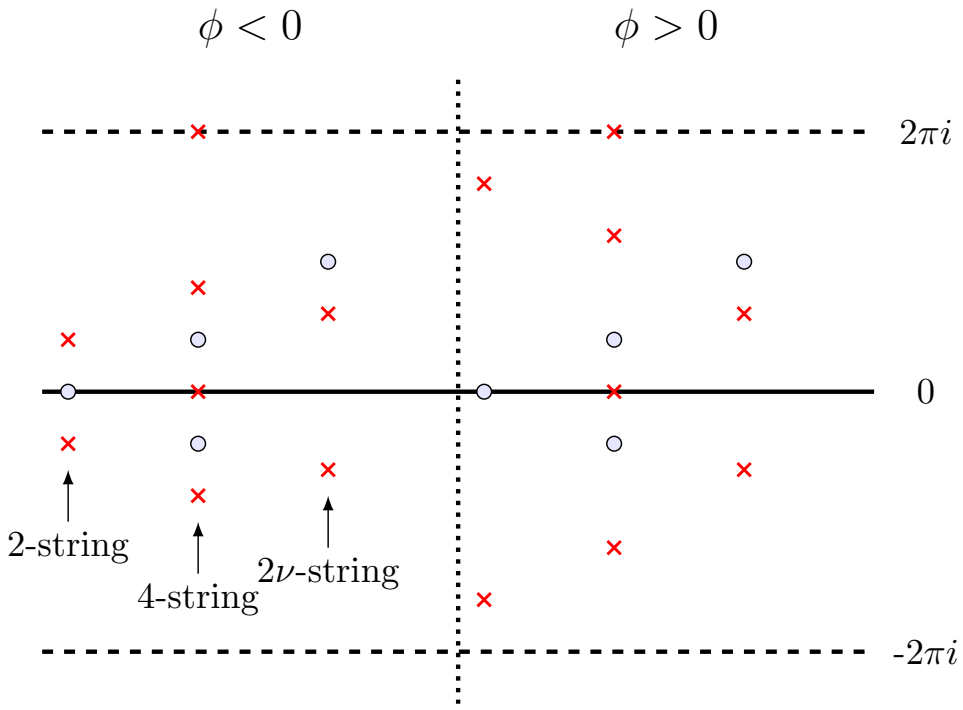

Figure 5.6: At finite temperature the rapidity and chiral variables may form $z - \lambda$ strings where n λs and $2n$ zs form a set given by (5.77). On the left we show how a 2-string, 4-string and the negative parity 2ν-string are arranged for $\phi < 0$. On the right we depict the same for $\phi > 0$. Note only the z positions are changed when going from left to right which results in a change in sign of the energy from the strings.

Coulomb interaction, U we saw that $\mathcal{D}(\Gamma/\mathcal{D})^{1/\alpha}$ where $\alpha = 1+2\left[\arctan\left(g\right) - \arctan\left(U\right)\right]/\pi$ (c.f.(3.52)). Taking $U = g$, as required by the mapping (see (5.5)), reduces this to Γ, the free value. The non-renormalization of the level width suggests that the tunnelling operator $d^\dagger\psi_\pm(0)$ should have the same dimension as the free model which is confirmed by the high energy expansions of the dot occupation. This is in stark contrast to the the fact that fermions in a Luttinger liquid (away from the edge) have dimension $(K+1/K)/4$. Thus the remarkably simple expression for the strong coupling scale and critical exponents present here stand in contrast to a quite substantial modification of the fermions in the vicinity of the dot.

We now have the following picture of the side-coupled system. For all $K \in [0,2]$ the system flows from weak coupling at high energy to strong coupling at low energy. The low energy fixed point describes a dot which is fully hybridized with the bulk and has the fixed point occupation $n_d = 1/2$. The hybridized dot then acts as a backscattering potential via co-tunnelling. The leading irrelevant operator which perturbs away from the fixed point is the stress energy tensor and results in odd integer powers of ϵ_0/Γ in the dot occupation. For $K > 1$ the backscattering is irrelevant which gives rise to odd powers of $(\epsilon_0/\Gamma)^{1/(K-1)}$ resulting in a suppression of the dot occupation at $\epsilon_0 > 0$. For $K < 1$ on the other hand it is relevant and generates no other terms in the expansion. The high energy fixed point describes a decoupled dot which has $n_d = 0$ for $\epsilon_0 \to \infty$ or $n_d = 1$ for $\epsilon_0 \to -\infty$. By reducing the energy scale we flow away from the fixed point with the tunnelling operator $d^\dagger\psi_\pm(0)$ which is the leading relevant operator and has dimension $1/2$ as in the free model. This give rise to integer powers of Γ/ϵ_0 in n_d. Additionally when $K < 1$ backscattering is relevant and causes odd powers of $(\Gamma/\epsilon_0)^{1/(1-K)}$ to appear resulting in an enhancement of the dot occupation .

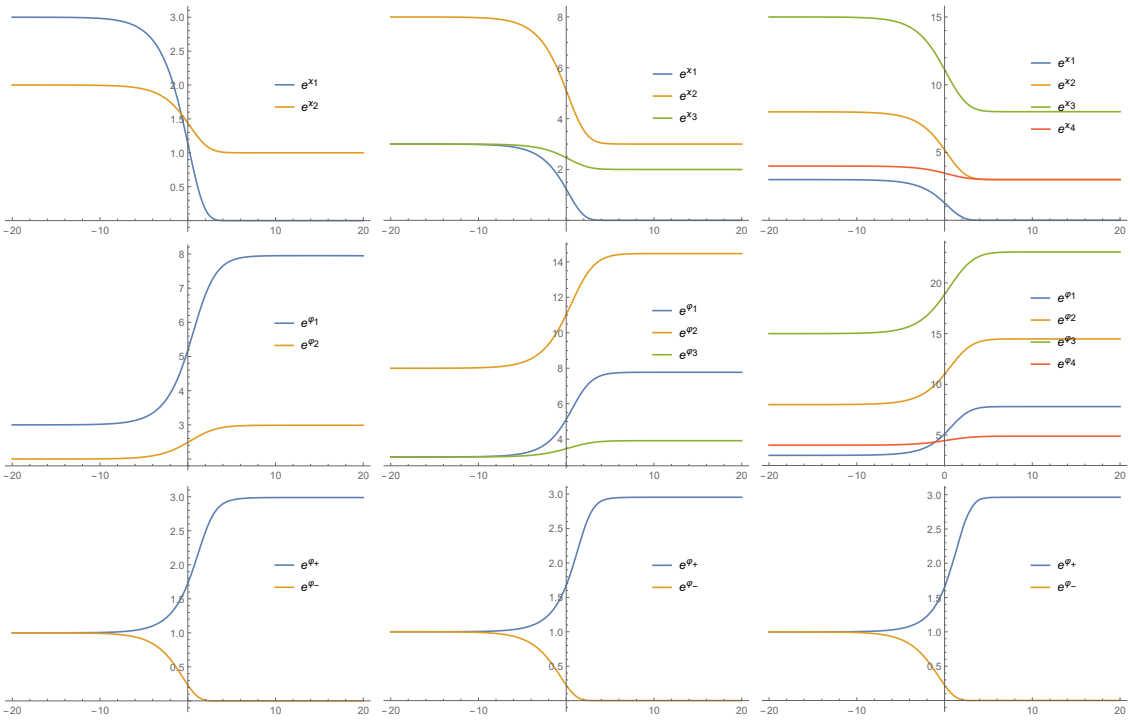

Figure 5.7: Here we plot the universal thermodynamic functions which are the solutions of the TBA (5.81)-(5.83) for several values of ν with $\epsilon_0 = 0$. In the top line with plot e_j^{χ} for $j < \nu$ and $\nu = 3, 4, 5$ from left to right respectively. In the next we plot e^{φ_j} for $j < \nu$ and $\nu = 3, 4, 5$ from left to right respectively and in the bottom line we plot $e^{\varphi_\pm}$ for the same values. These were obtained by numerically solving the TBA using an iterative procedure. In all the cases shown it is easy to confirm that the attain the asymptotic values quoted in the text (5.84), (5.86). The functions apply to both the repulsive regime where the Luttinger parameter is $K = 2/3, 4/5, 5/6$ respectively and the attractive regime where we have $K = 4/3, 6/5, 7/6$.

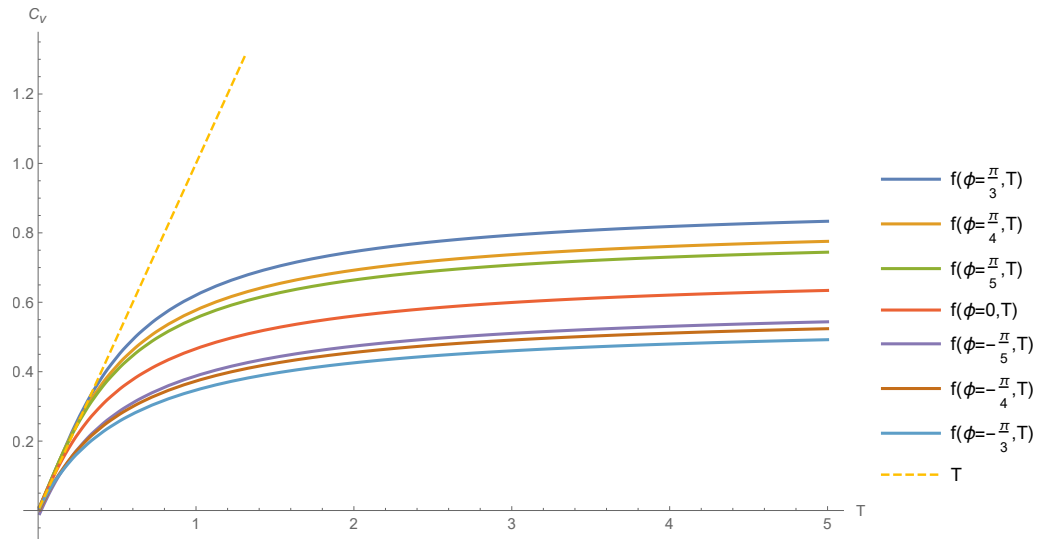

Figure 5.8: We plot here the contribution to the specific heat due to the dot as a function of T/Γ for several values of the interaction. The dashed line indicates the linear behaviour at low T. At high T the specific heat approaches a different constant according to (5.7.1)

5.7 Thermodynamics

In this section we study the finite temperature properties of the dot by calculating the free energy. As before we use the methods developed by Yang and Yang [73] and later extended by Takahashi [96] based on the string hypothesis. The form of the strings depend upon the model and the values of the parameters therein and differ somewhat from what we have encountered before. To simplify matters we take $\phi = \pm\pi/\nu$ with ν an integer so that $K = \frac{\nu\pm1}{\nu}$. With this value fixed the hypothesis states that the Bethe equations allow for the following forms of the charge and chiral variables.

The rapidities can be real or complex with $\mathrm{Im}(z) = 0, 2\pi$. These contribute bare energy $\pm\mathcal{D}e^{z/2}$ and we denote the distributions of these $\rho_\pm(z)$. The chiral variables can take on complex values so that they arrange into n-strings with $n < \nu$ such that

$$\lambda_l^{(n)} = \lambda^{(n)} + i\phi(n-1-2l), \quad l = 0, \ldots, n-1 \tag{5.76}$$

or λ can be a negative parity string and lie on the $i\pi$ line . The λ n-strings have no bare

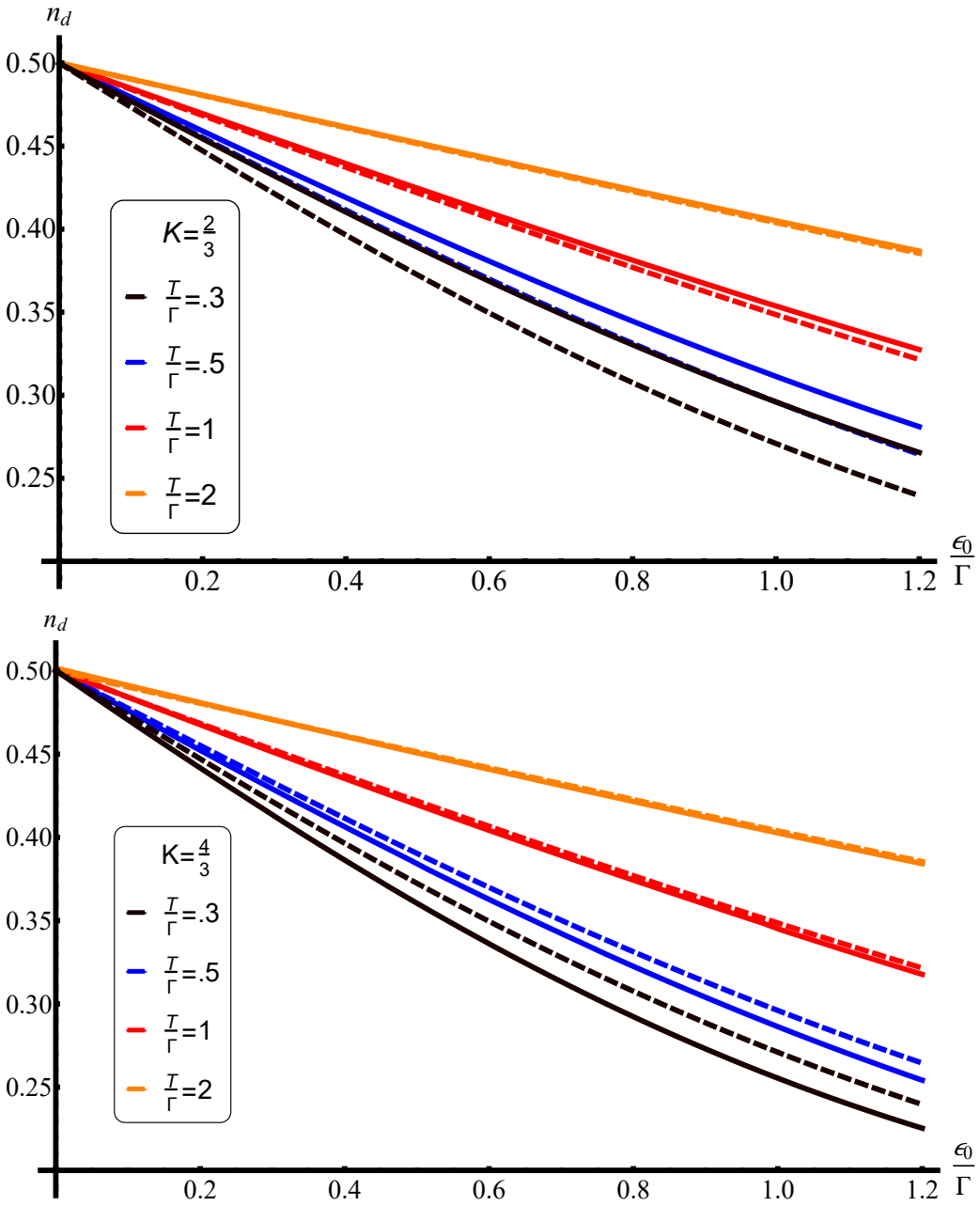

Figure 5.9: The finite temperature dot occupation is plotted as a function of ϵ_0/Γ for several values of the temperature. Above we plot the dot occupation with $K = \frac{2}{3}$ (solid lines) and $K = 1$ (dashed lines). The repulsive bulk interactions result in an enhancement of the dot occupation in comparison to the non interacting case. This is effect is most pronounced for lower temperatures. At higher temperature the interacting and non interacting curves coincide owing to the fact that the dot becomes decoupled. Below we plot the same for $K = \frac{4}{3}$ (solid lines) and plot again $K = 1$ (dashed) for comparison. The dot occupation is suppressed due to the attractive interactions wth the effect becoming more pronounced for lower T/Γ.

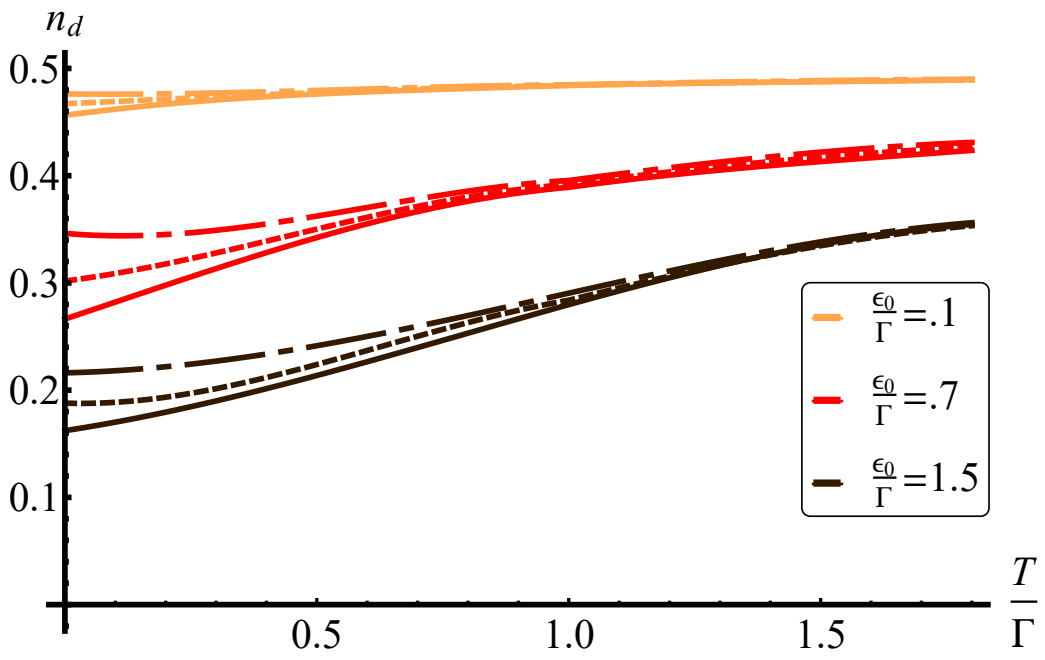

Figure 5.10: The dot occupation for fixed ϵ_o/Γ as a function of temperature. The interaction is taken to be $K = \frac{4}{3}$ (dot-dashed lines), $K = 1$ (dashed lines) and $K = \frac{2}{3}$ (solid lines). We see the enhancement and suppression of the dot occupation for repulsive and attractive interaction with the effect most pronounced as the temperature is lowered.

energy and we denote the distributions of their common real part by $\sigma_n(\lambda)$ with $n = \nu$ denoting the negative parity string. Also possible are $z - \lambda$ $2n$-strings consisting of $2n$ zs and a λ n-string taking the values

$$z_{l+1}^{(n)} = \lambda^{(n)} + i\phi(n - 2j) + i\pi + \mathrm{sgn}(\phi)i\pi \tag{5.77}$$

$$z_{l+n+1}^{(n)} = \lambda^{(n)} + i\phi(n - 2l) + i\pi - \mathrm{sgn}(\phi)i\pi \tag{5.78}$$

where $j = 0, \ldots, n$ and $l = 1, \ldots, n-1$. These contribute bare energy

$$E_n = -2\mathrm{sgn}(\phi)\cos(n\frac{\phi}{2})\mathcal{D}e^{\lambda^{(n)}/2}.$$

In addition there is also a negative parity $z - \lambda$ string

$$\lambda = \lambda^{(\nu)} + i\pi, \quad z_{1,2} = \lambda^{(\nu)} \pm i(\pi - \phi) \tag{5.79}$$

which has energy

$$2\sin(\frac{\phi}{2})\mathcal{D}e^{\lambda^{(\nu)}/2}.$$

We denote the distributions of the $z-\lambda$ $2n$-strings by $\rho_n(z)$ with $n=\nu$ indicating the negative parity string. Several string type are depicted in FIG. 5.6 for both $\phi>0$ and $\phi<0$.

Having elucidated the string structure of the model, the free energy is found in what should by now be a familiar manner. Recall the free energy is found by minimizing $F=E-TS$, where E is the energy of an arbitrary configuration of strings and S is its associated Yang-Yang entropy. We minimize it with respect to $\rho_\pm, \rho_n$ and σ_n which are solutions of the Bethe Ansatz equations. The result of this minimization gives the thermodynamic Bethe ansatz (TBA) equations which determine F. Owing to the different string structures for K greater than or less than 1 we consider each region separately.

5.7.1 $K=\frac{\nu-1}{\nu}$

We start with $\phi=-\pi/\nu$, corresponding to $K=\frac{\nu-1}{\nu}<1$, describing repulsive interactions. In this region we find the dot contribution to the free energy is

$$\begin{aligned} F_d = E_d^0 &- T\int f_0(x+2\log\left(\frac{T}{\Gamma}\right))\log\left(1+e^{\varphi_-(x)}\right) \\ &-T\int f_0 * s(x+2\log\left(\frac{T}{\Gamma}\right))\log\left(1+e^{\varkappa_1(x)}\right) \\ &-T\int s(x+2\log\left(\frac{T}{\Gamma}\right))\log\left(1+e^{\varkappa_{\nu-1}(x)}\right) \end{aligned} \tag{5.80}$$

where $E_{\rm d}^0$ is the ground state energy due to the dot, $s(x)=\mathrm{sech}(\pi x/2\phi)/4\phi$ and $*$ denotes the convolution $f*g=\int f(x-y)g(y)\mathrm{d}y$. The thermodynamic functions $\varphi_\pm, \varphi_n$ and $\varkappa_n$ are related to the distributions $\rho_\pm, \rho_n$ and σ_n respectively and are solutions of the TBA equations which in this case are

$$\varphi_+ = s * \log\left(\frac{1+e^{\varphi_1}}{1+e^{\varkappa_1}}\right), \quad \varphi_- = -2e^{x/2} + s * \log\left(\frac{1+e^{\varphi_1}}{1+e^{\varkappa_1}}\right) \tag{5.81}$$

$$\varphi_n = s * \log(1+e^{\varphi_{n-1}})(1+e^{\varphi_{n+1}})(1+e^{-\varphi_\nu})^{\delta_{n,\nu-2}} + \delta_{n,1} s * \log\left(\frac{1+e^{\varphi_+}}{1+e^{\varphi_-}}\right) \tag{5.82}$$

$$\begin{aligned}\varkappa_n &= s * \log(1+e^{\varkappa_{n-1}})(1+e^{\varkappa_{n+1}})^{1+\delta_{n,\nu-2}} \\ &\quad -\delta_{n,1}\left[\frac{e^{x/2}}{\cos(\phi/2)} - s * \log\left(\frac{1+e^{\varphi_+}}{1+e^{\varphi_-}}\right)\right]\end{aligned} \tag{5.83}$$

along with $\varphi_{\nu-1} = s*\log(1+e^{\varphi_{\nu-2}}) + \frac{\nu\epsilon_0}{T} = -\varphi_\nu + \frac{2\nu\epsilon_0}{T}$ and $\varkappa_{\nu-1} = s*\log(1+e^{\varkappa_{\nu-2}}) = -\varkappa_\nu$. Just as in the calculation of the dot occupation in the ground state the above equations are independent of the cutoff which has been removed while holding Γ fixed. These expressions give the exact dot free energy of the system in all temperature regimes. Their complicated nature precludes any analytic solution for the thermodynamic functions but are straightforwardly determined numerically through iteration of the integral equations.

Before doing this however we can examine them in the limits of low and high temperature. The functions $f_0(x)$ and $s(x)$ appearing in the free energy are sharply peaked about zero meaning that for $T \to 0, \infty$ the free energy is determined by the solutions of the TBA in the $x \to \infty, -\infty$ limits respectively. Setting $\epsilon_0 = 0$ and taking first the high temperature limit, $x \to -\infty$ we see that the driving terms in the TBA vanish and the thermodynamic functions are constants $e^{\varphi_\pm(-\infty)} = 1$,

$$e^{\varphi_j(-\infty)} = e^{\varkappa_j(-\infty)} = (j+1)^2 - 1 \tag{5.84}$$

$$e^{\varphi_{\nu-1}(-\infty)} = e^{\varkappa_{\nu-1}(-\infty)} = \nu - 1. \tag{5.85}$$

Likewise in the opposite low temperature limit $x \to \infty$ we get $e^{\varphi_-(\infty)} = 0,\ e^{\varphi_+(\infty)} = 3$,

$$e^{\varkappa_j(\infty)} = j^2 - 1,\ e^{\varkappa_{\nu-1}(\infty)} = \nu - 2 \tag{5.86}$$

$$e^{\varphi_j(\infty)} = (j+2)^2 - 1,\ e^{\varphi_{\nu-1}(\infty)} = \nu. \tag{5.87}$$

The free energy thus becomes linear in T in both the high and low temperature limit. The thermodynamic functions can be obtained by numerically integrating the TBA. In FIG.5.7 we plot $e^{\varphi_\pm}, e^{\varphi_j}, e^{\varkappa_j}$ for a number of values of ν with $\epsilon_0 = 0$. WE see that all the functions are monotonic and attain the asymototic values given in (5.84) and (5.86).

Using these we can check the RG picture we arrived at earlier using the ground state dot occupation still holds true at finite temperature. First note that the energy scale, the temperature in this case, is measured with respect to Γ which serves as both the strong coupling scale and the level width for the model. Thus the system is strongly coupled at low temperature $T \ll \Gamma$ and weakly coupled at high temperature $T \gg \Gamma$. Furthermore by inserting (5.86) (5.84) into (5.80) we obtain the g-function of the model, defined to be the difference in the UV and IR entropy of the impurity

$$g = S_{\mathrm{UV}} - S_{\mathrm{IR}} = \log 2 + \frac{1}{2}\log\left(\frac{1}{K}\right). \tag{5.88}$$

This is always positive for the range of values considered in agreement with the requirement that as we move along the RG flow by lowering the temperature, degrees of freedom are integrated out. The first term comes from the charge degrees of freedom and corresponds to the difference in entropy of a decoupled dot at high temperature compared to one fully hybridized at low temperature. The second term comes from the chiral degrees of freedom and is the same as for the Kane-Fisher model of chapter 4[119][40]. We see from this that at high temperature the dot is decoupled and as T is lowered it becomes hybridized with the dot whereupon it acts as a back scattering impurity. In the non interacting limit the $K \to 1$ this last term disappears and we recover the expected result.

We may go beyond the fixed point behaviour to get the leading order corrections and determine the specific heat. Following [69][132] we expand about the low temperature solution $\log\left(1 + \exp\left(\varphi_-\right)\right) \approx \exp\left(-2e^{x/2}\right)$ and $\log\left(1 + \exp\left(\varkappa_1\right)\right) \approx \exp\left(-e^{x/2}/\cos\left(\phi/2\right)\right)$

for $x \gg 0$. The low temperature specific heat is then found to be

$$C_v \sim \frac{T}{\Gamma} \tag{5.89}$$

which agrees with the expectation that the irrelevant operator is the stress energy tensor. In FIG. 5.8 we plot the specific heat for a number of different values of ν and see that the it is indeed linear at low temperature and then asymptotes to constant values according to

.

By numerically integrating the TBA and using them in (5.80) we can obtain the finite temperature dot occupation of the system. This is plotted in FIG. 5.9 for $K = \frac{2}{3}$ as a function of ϵ_0/Γ at different values of the temperature, T/Γ. For the same value of K we plot the dot occupation at fixed ϵ_0/Γ as a function T/Γ in the FIG. 5.10. Comparing to the dashed lines which are the non interacting values we see that the dot occupation is enhanced just as it was at zero T. This enhancement is strongest at low T and is washed out at high temperature as the system becomes weakly coupled.

5.7.2 $K = \frac{\nu+1}{\nu}$

We turn now to the case of $\phi = \pi/\nu$ or $K = \frac{\nu+1}{\nu} > 1$, attractive interactions. In this regime we will see that tunnelling to the dot is still relevant however it must compete with the backscattering that this generates which is irrelevant for $K > 1$[12]. This competition makes itself felt via changes in the free energy and TBA equations. The dot contribution to the free energy is now given by

$$\begin{aligned} F_d = E_d^0 - T \int f_0(x + 2\log\left(\frac{T}{\Gamma}\right)) \log\left(1 + e^{-\varphi_+(x)}\right) \\ -T \int f_0 * s(x + 2\log\left(\frac{T}{\Gamma}\right)) \log\left(1 + e^{\varphi_1(x)}\right) \\ -T \int s(x + 2\log\left(\frac{T}{\Gamma}\right)) \log\left(1 + e^{\varkappa_{\nu-1}(x)}\right) \end{aligned} \tag{5.90}$$

with the TBA equations being

$$\begin{aligned}
\varphi_+ &= 2e^{x/2} + s * \log\left(\frac{1+e^{\varphi_1}}{1+e^{\varkappa_1}}\right), \quad \varphi_- = s * \log\left(\frac{1+e^{\varphi_1}}{1+e^{\varkappa_1}}\right) && (5.91)\\
\varphi_n &= s * \log\left(1+e^{\varphi_{n-1}}\right)\left(1+e^{\varphi_{n+1}}\right)\left(1+e^{-\varphi_\nu}\right)^{\delta_{n,\nu-2}} \\
&\quad -\delta_{n,1}\left[s * \log\left(\frac{1+e^{-\varphi_+}}{1+e^{-\varphi_-}}\right) + \frac{e^{x/2}}{\cos\left(\phi/2\right)}\right] && (5.92)\\
\varkappa_n &= s * \log\left(1+e^{\varkappa_{n-1}}\right)\left(1+e^{\varkappa_{n+1}}\right)^{1+\delta_{n,\nu-2}} - \delta_{n,1} s * \log\left(\frac{1+e^{-\varphi_+}}{1+e^{-\varphi_-}}\right) && (5.93)
\end{aligned}$$

and $\varphi_{\nu-1} = s*\log\left(1+e^{\varphi_{\nu-2}}\right) + \frac{\nu\epsilon_0}{T} = -\varphi_\nu + \frac{2\nu\epsilon_0}{T}$ as well as $\varkappa_{\nu-1} = s*\log\left(1+e^{\varkappa_{\nu-2}}\right) = -\varkappa_\nu$. Comparing to the $K<1$ case we see that the roles of e^{ϕ_-} and $e^{-\phi_+}$ have been exchanged and that the exponential driving term now appears in the φ_j equations rather than $\varkappa_j$ ones.

We gain insight to the $K>1$ region by looking at the asymptotic solutions of the TBA. The high temperature solutions, $x \to -\infty$ remain unchanged and are given by (5.84), therefore as $T \to \infty$ the system is the same regardless of K. In the low temperature limit however the solutions are different as should be the case given the ground state is of a different form. We get that $e^{-\varphi_+(\infty)} = 0,\ e^{\varphi_-(\infty)} = 3$,

$$e^{\varphi_j(\infty)} = j^2 - 1,\ e^{\varphi_{\nu-1}(\infty)} = \nu - 2 \tag{5.94}$$

$$e^{\varkappa_j(\infty)} = (j+2)^2 - 1,\ e^{\varkappa_{\nu-1}(\infty)} = \nu \tag{5.95}$$

Using these in the g function we obtain the same form as before,

$$g = \log 2 + \frac{1}{2}\log\left(\frac{1}{K}\right). \tag{5.96}$$

Note however that although $g>0$, the second term which is due to the backscattering, is negative for $K>1$. This relative sign between the charge and chiral terms is related to the competition between the tunnelling and the backscattering. Upon taking the $K \to 1$ we recover the non interacting result. The low temperature corrections to the fixed point can

be obtained as they were in the previous section. This time however the driving terms in the TBA do not appear in the $\varkappa_1$ equation but in the φ_1 equation instead and consequently we take $\log\left(1+\ \exp\left(-\varphi_+\right)\right) \approx\ \exp\left(-2e^{x/2}\right)$ and $\log\left(1+\ \exp\left(\varphi_1\right)\right) \approx\ \exp\left(-e^{x/2}/\cos\left(\phi/2\right)\right)$ for $x \gg 0$ and find the specific heat to be

$$C_v \sim \frac{T}{\Gamma} + a\left(\frac{T}{\Gamma}\right)^{\alpha}. \tag{5.97}$$

Again the leading order term coincides with the stress tensor being the leading irrelevant operator the next order term scales as T^α where $\alpha = 2$ for $K = \frac{\nu+1}{\nu},\ \nu > 2$. It is expected however that α becomes non integer when increasing K beyond this as is the case in the ground state dot occupation.

The finite temperature dot occupation is plotted in FIG. 5.9 and FIG. 5.10. We see that the dot occupation is suppressed as compared to $K = 1$ or $K < 1$, with the effect being most pronounced at low temperature. At high T the dot becomes decoupled and the occupation approaches that of the non interacting case.

5.8 Conclusion

In this chapter we have solved two related models of quantum dots coupled to Luttinger liquids. The first consists of a dot side-coupled to the Luttinger liquid while in the second the dot is placed between two otherwise disconnected liquids. The latter also requires that a Coulomb interaction between the occupied dot and the end of the liquids is included and it is tuned to the same value as the bulk interaction. The side-coupled model however, requires no such tuning. Both models represent an amalgamation of the effects seen in the previous two chapters, exhibiting both Kondo and KF physics.

The solution shows that the two models are related by taking $K \to 1/K$ provided one takes appropriate boundary conditions. We derived the Bethe equations for both models and used them to construct the ground state and derive exact expressions for the dot

occupation in all parameter regimes. It was seen that the side-coupled system is strongly coupled at low energies so that the dot becomes fully hybridised with the bulk and acts as a backscattering potential. The effect of the backscattering is to either suppress or enhance the dot occupation depending on the sign of the interactions.

The scaling dimensions of the leading relevant and irrelevant operators about the UV and IR fixed points were found to coincide with that of the free model. The surprising result that the fixed points appear, at least to leading order to be Fermi liquid is in start contrast to the non-Fermi liquid nature of the bulk system.

We then examined the finite temperature properties of the dot by deriving the Thermodynamic Bethe equations and free energy of the system. It was seen that at low temperature dot is fully hybridised with the bulk and the interactions resulting in a suppression or enhancement of the dot occupation. The effect of the interactions is washed out at high temperature whereupon the dot decouples.

The lack of fine tuned parameters in the side-coupled model make it a good candidate for experimental realizations. Such a system may be created placing a quantum dot near a carbon nanotube, the edge of a quantum Hall sample or a topological insulator. The dot occupation can then be measured by means of a quantum point contact and compared to (5.65).

6

Summary and Outlook

The goal of this thesis was to investigate the physics of quantum impurities when coupled to a strongly correlated environment, in particular the Luttinger liquid. Furthermore we aimed to study these systems by exactly diagonalizing their Hamiltonians using the Bethe Ansatz method. After a brief introductory chapter we gave an overview of the Bethe Ansatz and its application to a number of quantum impurity models. We began by investigating the simplest of these the resonant level model and then subsequently the more complicated anisotropic Kondo model and finally the closely related interacting resonant level model. In each case we studied the ground state and excitations of the model and then calculated the free energy at arbitrary temperature. We saw that the same basic principles of the technique applied equally in the non interacting and interacting model alike modulo some additional complexity of the relevant equations in the later case.

Following this we examined our first new model which consisted of a Luttinger liquid coupled to a resonant level at the boundary. We successfully constructed all the eigenstates of the model and explored the occupation of the level at zero temperature before going onto study the finite temperature properties of the system. We saw that the strongly correlated nature of the bulk resulted in an enhancement of the density of states at the boundary which allowed for the level to become fully hybridized with the bulk at low energy and then become completely decoupled at high energy. This Kondo type of behavior occurs in the absence of any Kondo type coupling between the bulk and level. When such a term is included it was shown that Kondo screening can still take place even if the Kondo term is ferromagnetic. We compared these results to those obtained using bosonization and found

some mild discrepancies. After reviewing the methods used to obtain these and similar results we showed that the discrpancy is a result of the incorrect treatment of the bulk system in bosonization.

In the next chapter we studied a different type of impurity which causes backscattering in the Luttinger liquid. We studied the physics of this backscattering type of impurity through two related models, the Kane-Fisher model and the weak-tunnelling model. We constructed all the eigenstates of both models using a new formulation of the coordinate Bethe Ansatz which took into account all types of scattering processes that can occur in these models. The spectrum was then found by mapping the boundary condition problem to an open XXZ chain which had previously been well studied. Using this we then studied the finite temperature behavior of the system, calculating the free energy and g-function as well as determining the dimensions of the leading relevant and irrelevant operators about the IR and UV fixed points. The results were found to be in agreement with those obtained using bosonization as well as the bootstrap method. At low temperature the repulsive KF model was shown to generate a strong coupling scale, T_{KF} and flow to a strong coupling fixed point in which the system was split in two. The attractive system meanwhile was seen to exhibit non universal behavior. A duality between the KF model and WT model was discovered which mapped the KF model with Luttinger parameter K to the WT model with $1/K$ which amounts to changing the sign of the interactions. Consequently we were also able study the finite temperature properties of the attractive WT model and saw that it generated a strong coupling scale T_{WT} below which the otherwise split system would become healed.

In the penultimate chapter we studied two models which would incorporate both the Kondo-like physics of boundary dot model and the Kane-Fisher physics of the previous chapter. The two models were a resonant level sidecoupled to a Luttinger liquid and a level embedded between two liquids. In the later a Coulomb interaction was also required to maintain integrability. We found the eigenstates and spectrum of both models using the

Bethe Ansatz formulated while studying the KF model and subsequently derived expression for the ground state occupation of the level as well as the free energy. For the sidecoupled model we found that at low energy the dot becomes fully hybridized with the bulk similar to the Kondo effect in the boundary model and then acted as a backscattering impurity. When the bulk interactions were repulsive and hence backscattering was relevant we saw a resulting enhancement of the level occupation at low energy. In the opposite case we saw that although the dot remained hybridized backscattering was irrelevant and so the Kondo and KF effects were in opposition, the effect was seen in a suppression of the dot occupation at low temperature. We found that a $K \to 1/K$ duality also existed between the sidecoupled and embedded models however in contradiction to the bosonization result we showed that it required certain particular choice of boundary conditions to hold.

Many interesting and important questions remain to be answered about the models we have studied and the techniques we have used. A particularly intriguing line of inquiry regards the calculation of transport properties of the models. As mentioned inn Chapters 3 and 4, our formulation allows for one to exactly solve the systems with any boundary condition. In particular we can study the systems on a ring through which a flux is threaded by applying twisted boundary conditions. Since the gauge field associated with this flux couples to the current we can determine the ground state equilibrium current or conductance by calculating the finite size corrections to the energy in the presence of the shift. We can also adopt an approach used by Andrei[156] to study the magnetoresistance of the Kondo model. There it was shown that the magnetoresistance was related to the physical impurity S-matrix in the presence of a magnetic field a quantity that can be found exactly using Bethe Ansatz. A similar line of arguement can be applied to our models also which would allow one to calculate the non-quilibrium conductance across the impurity. Aside from transport properties, the freedom to choose any boundary condition allows one to study two-impurity systems. In the sidecoupled dot geometry for instance one can impose a rapidity dependent boundary condition at $x = \pm L/2$ so that the system consists of two resonant levels coupled

to a Luttinger liquid in a ring geometry at opposite points. By studying the finite size corrections to the energy levels caused by the impurities one can study how the occupation of each level is correlated and also study the emergence of the RKKY interaction in a strongly correlated system.

These projects both entail the study of the system beyond the approximations we have used on this thesis. Recall that in order to derive usable Bethe equations and study the systems we had to make some assumptions about the structure of the solutions in the thermodynamic limit. These simplifications were based on general grounds and properties of impurity models and were subsequently checked by comparing with other methods. In order to study the transport properties and two impurity models we would need to go beyond these approximations. A more intensive study of the Bethe equations and eigenvalues of the type we have used in this thesis is therefore required before engaging in these endeavors. While obviously necessary and useful, a study like this could produce interesting physical phenomena, for instance it is known that integrable models with open boundary conditions can support an exotic array of bound states [139, 90, 157], thus it is possible that impurity bound states like this may also exist in the models we have considered.

Lastly we recall that the real prize of being able to solve QIMs like the Kondo model was to give an exact description of the physics in the crossover regime between weak and string coupling. This was achieved both by calculating observables like the magnetization or dot occupation but also by calculating the universal Wilson number which characterizes the crossover regime and can be compared with other methods[158]. In this thesis we have achieved the former by calculated observable like the dot occupation in all regimes but not the later. It would therefore be desirable to define and calculate the equivalent of the Wilson number for these systems and compare with purely numerical methods.

References

[1] M. B. Green, J. H. Schwarz, and E. Witten, *Superstring theory. Volume 1 - Introduction*. 1987.

[2] M. B. Green, J. H. Schwarz, and E. Witten, *Superstring theory. Volume 2 - Loop amplitudes, anomalies and phenomenology*. 1987.

[3] Planck Collaboration, N. Aghanim, Y. Akrami, M. Ashdown, J. Aumont, C. Baccigalupi, M. Ballardini, A. J. Banday, R. B. Barreiro, N. Bartolo, S. Basak, R. Battye, K. Benabed, J.-P. Bernard, M. Bersanelli, P. Bielewicz, J. J. Bock, J. R. Bond, J. Borrill, F. R. Bouchet, F. Boulanger, M. Bucher, C. Burigana, R. C. Butler, E. Calabrese, J.-F. Cardoso, J. Carron, A. Challinor, H. C. Chiang, J. Chluba, L. P. L. Colombo, C. Combet, D. Contreras, B. P. Crill, F. Cuttaia, P. de Bernardis, G. de Zotti, J. Delabrouille, J.-M. Delouis, E. Di Valentino, J. M. Diego, O. Doré, M. Douspis, A. Ducout, X. Dupac, S. Dusini, G. Efstathiou, F. Elsner, T. A. Enßlin, H. K. Eriksen, Y. Fantaye, M. Farhang, J. Fergusson, R. Fernandez-Cobos, F. Finelli, F. Forastieri, M. Frailis, E. Franceschi, A. Frolov, S. Galeotta, S. Galli, K. Ganga, R. T. Génova-Santos, M. Gerbino, T. Ghosh, J. González-Nuevo, K. M. Górski, S. Gratton, A. Gruppuso, J. E. Gudmundsson, J. Hamann, W. Handley, D. Herranz, E. Hivon, Z. Huang, A. H. Jaffe, W. C. Jones, A. Karakci, E. Keihänen, R. Keskitalo, K. Kiiveri, J. Kim, T. S. Kisner, L. Knox, N. Krachmalnicoff, M. Kunz, H. Kurki-Suonio, G. Lagache, J.-M. Lamarre, A. Lasenby, M. Lattanzi, C. R. Lawrence, M. Le Jeune, P. Lemos, J. Lesgourgues, F. Levrier, A. Lewis, M. Liguori, P. B. Lilje, M. Lilley, V. Lindholm, M. López-Caniego, P. M. Lubin, Y.-Z. Ma, J. F. Macías-Pérez, G. Maggio, D. Maino, N. Mandolesi, A. Mangilli, A. Marcos-Caballero, M. Maris, P. G. Martin, M. Martinelli, E. Martínez-González, S. Matarrese, N. Mauri, J. D. McEwen, P. R. Meinhold, A. Melchiorri, A. Mennella, M. Migliaccio, M. Millea, S. Mitra, M.-A. Miville-Deschênes, D. Molinari, L. Montier, G. Morgante, A. Moss, P. Natoli, H. U. Nørgaard-Nielsen, L. Pagano, D. Paoletti, B. Partridge, G. Patanchon, H. V. Peiris, F. Perrotta, V. Pettorino, F. Piacentini, L. Polastri, G. Polenta, J.-L. Puget, J. P. Rachen, M. Reinecke, M. Remazeilles, A. Renzi, G. Rocha, C. Rosset, G. Roudier, J. A. Rubiño-Martín, B. Ruiz-Granados, L. Salvati, M. Sandri, M. Savelainen, D. Scott, E. P. S. Shellard, C. Sirignano, G. Sirri, L. D. Spencer, R. Sunyaev, A.-S. Suur-Uski, J. A. Tauber, D. Tavagnacco, M. Tenti, L. Toffolatti, M. Tomasi, T. Trombetti, L. Valenziano, J. Valiviita, B. Van Tent, L. Vibert, P. Vielva, F. Villa, N. Vittorio, B. D. Wandelt, I. K. Wehus, M. White, S. D. M. White, A. Zacchei, and A. Zonca, "Planck 2018 results. VI. Cosmological parameters," *ArXiv e-prints*, July 2018.

[4] S. Dodelson, *Modern cosmology*. 2003.

[5] E. Schrödinger, "An Undulatory Theory of the Mechanics of Atoms and Molecules," *Physical Review*, vol. 28, pp. 1049–1070, Dec. 1926.

[6] G. Mahan, *Many-Particle Physics*. Physics of Solids and Liquids, Springer, 2000.

[7] P. Coleman, *Introduction to Many-Body Physics*. Cambridge University Press, 2015.

[8] M. E. Fisher, "Renormalization group theory: Its basis and formulation in statistical physics," *Rev. Mod. Phys.*, vol. 70, pp. 653–681, Apr 1998.

[9] A. C. Hewson, *The Kondo Problem to Heavy Fermions*. Cambridge Studies in Magnetism, Cambridge University Press, 1993.

[10] T. Giamarchi, *Quantum Physics in One Dimension*. International Series of Monographs on Physics, Clarendon Press, 2003.

[11] F. Haldane, "Effective harmonic-fluid approach to low-energy properties of one-dimensional quantum fluids," *Physical Review Letters*, vol. 47, no. 25, p. 1840, 1981.

[12] C. L. Kane and M. P. A. Fisher, "Transmission through barriers and resonant tunneling in an interacting one-dimensional electron gas," *Phys. Rev. B*, vol. 46, pp. 15233–15262, Dec 1992.

[13] I. Affleck, "Quantum Impurity Problems in Condensed Matter Physics," *ArXiv e-prints*, Sept. 2008.

[14] A. Gogolin, A. Nersesyan, and A. Tsvelik, *Bosonization and Strongly Correlated Systems*. Cambridge University Press, 2004.

[15] P. W. Anderson and G. Yuval, "Exact results in the kondo problem: Equivalence to a classical one-dimensional coulomb gas," *Phys. Rev. Lett.*, vol. 23, pp. 89–92, Jul 1969.

[16] H. Bethe, "Zur theorie der metalle," *Zeitschrift für Physik*, vol. 71, pp. 205–226, Mar 1931.

[17] R. Orbach, "Linear antiferromagnetic chain with anisotropic coupling," *Phys. Rev.*, vol. 112, pp. 309–316, Oct 1958.

[18] R. J. Baxter, "One-dimensional anisotropic heisenberg chain," *Phys. Rev. Lett.*, vol. 26, pp. 834–834, Apr 1971.

[19] R. J. Baxter, *Exactly Solved Models in Statistical Mechanics*. 1982.

[20] R. J. Baxter, "Eight-vertex model in lattice statistics," *Phys. Rev. Lett.*, vol. 26, pp. 832–833, Apr 1971.

[21] H. Babujian, "Exact solution of the isotropic heisenberg chain with arbitrary spins: Thermodynamics of the model," *Nuclear Physics B*, vol. 215, no. 3, pp. 317 – 336, 1983.

[22] B. Sutherland, "Model for a multicomponent quantum system," *Phys. Rev. B*, vol. 12, pp. 3795–3805, Nov 1975.

[23] E. H. Lieb and W. Liniger, "Exact analysis of an interacting bose gas. i. the general solution and the ground state," *Phys. Rev.*, vol. 130, pp. 1605–1616, May 1963.

[24] E. H. Lieb, "Exact analysis of an interacting bose gas. ii. the excitation spectrum," *Phys. Rev.*, vol. 130, pp. 1616–1624, May 1963.

[25] M. Gaudin and J.-S. Caux, *The Bethe Wavefunction*. Mar. 2014.

[26] E. H. Lieb and F. Y. Wu, "Absence of mott transition in an exact solution of the short-range, one-band model in one dimension," *Phys. Rev. Lett.*, vol. 20, pp. 1445–1448, Jun 1968.

[27] B. Sutherland, "Model for a multicomponent quantum system," *Phys. Rev. B*, vol. 12, pp. 3795–3805, Nov 1975.

[28] C. K. Lai, "Lattice gas with nearest-neighbor interaction in one dimension with arbitrary statistics," *Journal of Mathematical Physics*, vol. 15, pp. 1675–1676, Oct. 1974.

[29] P. A. Bares and G. Blatter, "Supersymmetric t-j model in one dimension: Separation of spin and charge," *Phys. Rev. Lett.*, vol. 64, pp. 2567–2570, May 1990.

[30] H. B. Thacker, "Exact integrability in quantum field theory and statistical systems," *Rev. Mod. Phys.*, vol. 53, pp. 253–285, Apr 1981.

[31] N. Andrei and J. H. Lowenstein, "Diagonalization of the chiral-invariant gross-neveu hamiltonian," *Phys. Rev. Lett.*, vol. 43, pp. 1698–1701, Dec 1979.

[32] A. P. Bukhvostov and L. N. Lipatov, "Instanton-anti-instanton interaction in the O(3) non-linear σ model and an exactly soluble fermion theory," *Nuclear Physics B*, vol. 180, pp. 116–140, Jan. 1981.

[33] N. Andrei, "Diagonalization of the kondo hamiltonian," *Phys. Rev. Lett.*, vol. 45, pp. 379–382, Aug 1980.

[34] V. Filyov, A. Tzvelik, and P. Wiegmann, "Thermodynamics of the s-d exchange model (kondo problem)," *Physics Letters A*, vol. 81, no. 2, pp. 175 – 178, 1981.

[35] P. B. Wiegmann, "Exact solution of the s-d exchange model (kondo problem)," *Journal of Physics C: Solid State Physics*, vol. 14, no. 10, p. 1463, 1981.

[36] N. Andrei and H. Johannesson, "Heisenberg chain with impurities (an integrable model)," *Physics Letters A*, vol. 100, pp. 108–112, Jan. 1984.

[37] H. Schulz, "An exactly solvable kondo model with quadratic band energy," *Journal of Physics C Solid State Physics*, vol. 20, pp. 2375–2403, June 1987.

[38] V. Caudrelier and N. Crampé, "Exact Results for the One-Dimensional Many-Body Problem with Contact Interaction:. Including a Tunable Impurity," *Reviews in Mathematical Physics*, vol. 19, pp. 349–370, 2007.

[39] C. Rylands and N. Andrei, "Quantum dot at a luttinger liquid edge," *Phys. Rev. B*, vol. 96, p. 115424, Sep 2017.

[40] C. Rylands and N. Andrei, "Quantum impurity in a luttinger liquid: Exact solution of the kane-fisher model," *Phys. Rev. B*, vol. 94, p. 115142, Sep 2016.

[41] C. Rylands and N. Andrei, "Quantum dot in interacting environments," , vol. 97, p. 155426, Apr. 2018.

[42] J. Slyom, "The fermi gas model of one-dimensional conductors," *Advances in Physics*, vol. 28, no. 2, pp. 201–303, 1979.

[43] S. Coleman, "Quantum sine-gordon equation as the massive thirring model," *Phys. Rev. D*, vol. 11, pp. 2088–2097, Apr 1975.

[44] U. Meirav, M. A. Kastner, and S. J. Wind, "Single-electron charging and periodic conductance resonances in gaas nanostructures," *Phys. Rev. Lett.*, vol. 65, pp. 771–774, Aug 1990.

[45] R. de Picciotto, H. L Stormer, L. N Pfeiffer, K. W Baldwin, and K. West, "Four-terminal resistance of a ballistic quantum wire," vol. 411, pp. 51–4, 06 2001.

[46] L. Pfeiffer, H. Strmer, K. Baldwin, K. West, A. Goi, A. Pinczuk, R. Ashoori, M. Dignam, and W. Wegscheider, "Cleaved edge overgrowth for quantum wire fabrication," *Journal of Crystal Growth*, vol. 127, no. 1, pp. 849 – 857, 1993.

[47] I. Bloch, J. Dalibard, and W. Zwerger, "Many-body physics with ultracold gases," *Rev. Mod. Phys.*, vol. 80, pp. 885–964, Jul 2008.

[48] M. Dresselhaus, G. Dresselhaus, and R. Saito, "Physics of carbon nanotubes," *Carbon*, vol. 33, no. 7, pp. 883 – 891, 1995. Nanotubes.

[49] M. Bockrath, D. H. Cobden, J. Lu, A. G. Rinzler, R. E. Smalley, L. Balents, and P. L. McEuen, "Luttinger-liquid behaviour in carbon nanotubes," , vol. 397, pp. 598–601, Feb. 1999.

[50] A. M. Chang, "Chiral luttinger liquids at the fractional quantum hall edge," *Rev. Mod. Phys.*, vol. 75, pp. 1449–1505, Nov 2003.

[51] F. P. Milliken, C. P. Umbach, and R. A. Webb, "Indications of a Luttinger liquid in the fractional quantum Hall regime," *Solid State Communications*, vol. 97, pp. 309–313, Jan. 1996.

[52] I. J. Maasilta and V. J. Goldman, "Line shape of resonant tunneling between fractional quantum hall edges," *Phys. Rev. B*, vol. 55, pp. 4081–4084, Feb 1997.

[53] R. Citro, E. Orignac, S. De Palo, and M. L. Chiofalo, "Evidence of luttinger-liquid behavior in one-dimensional dipolar quantum gases," *Phys. Rev. A*, vol. 75, p. 051602, May 2007.

[54] A. Recati, P. O. Fedichev, W. Zwerger, J. von Delft, and P. Zoller, "Atomic quantum dots coupled to a reservoir of a superfluid bose-einstein condensate," *Phys. Rev. Lett.*, vol. 94, p. 040404, Feb 2005.

[55] L. Jiang, L. O. Baksmaty, H. Hu, Y. Chen, and H. Pu, "Single impurity in ultracold fermi superfluids," *Phys. Rev. A*, vol. 83, p. 061604, Jun 2011.

[56] B. J. Kim, H. Koh, E. Rotenberg, S.-J. Oh, H. Eisaki, N. Motoyama, S. Uchida, T. Tohyama, S. Maekawa, Z.-X. Shen, and C. Kim, "Distinct spinon and holon dispersions in photoemission spectral functions from one-dimensional $SrCuO_2$," *Nature Physics*, vol. 2, pp. 397–401, June 2006.

[57] A. Del Maestro, M. Boninsegni, and I. Affleck, "^{4}He," *Phys. Rev. Lett.*, vol. 106, p. 105303, Mar 2011.

[58] P.-F. Duc, M. Savard, M. Petrescu, B. Rosenow, A. Del Maestro, and G. Gervais, "Critical flow and dissipation in a quasi-one-dimensional superfluid," *Science Advances*, vol. 1, pp. e1400222–e1400222, May 2015.

[59] I. Safi and H. Saleur, "One-channel conductor in an ohmic environment: Mapping to a tomonaga-luttinger liquid and full counting statistics," *Phys. Rev. Lett.*, vol. 93, p. 126602, Sep 2004.

[60] H. T. Mebrahtu, I. V. Borzenets, H. Zheng, Y. V. Bomze, A. I. Smirnov, S. Florens, H. U. Baranger, and G. Finkelstein, "Observation of Majorana quantum critical behaviour in a resonant level coupled to a dissipative environment," *Nature Physics*, vol. 9, pp. 732–737, Nov. 2013.

[61] L. I. Glazman and A. I. Larkin, "New Quantum Phase in a One-Dimensional Josephson Array," *Physical Review Letters*, vol. 79, pp. 3736–3739, Nov. 1997.

[62] R. Kuzmin, R. Mencia, N. Grabon, N. Mehta, Y.-H. Lin, and V. E. Manucharyan, "Quantum electrodynamics of a superconductor-insulator phase transition," *ArXiv e-prints*, May 2018.

[63] M. Pustilnik and L. Glazman, "TOPICAL REVIEW: Kondo effect in quantum dots," *Journal of Physics Condensed Matter*, vol. 16, pp. R513–R537, Apr. 2004.

[64] D. Goldhaber-Gordon, H. Shtrikman, D. Mahalu, D. Abusch-Magder, U. Meirav, and M. A. Kastner, "Kondo effect in a single-electron transistor," , vol. 391, pp. 156–159, Jan. 1998.

[65] S. M. Cronenwett, T. H. Oosterkamp, and L. P. Kouwenhoven, "A Tunable Kondo Effect in Quantum Dots," *Science*, vol. 281, p. 540, July 1998.

[66] Z. Yao, H. W. C. Postma, L. Balents, and C. Dekker, "Carbon nanotube intramolecular junctions," , vol. 402, pp. 273–276, Nov. 1999.

[67] B. M. Garraway, "The Dicke model in quantum optics: Dicke model revisited," *Philosophical Transactions of the Royal Society of London Series A*, vol. 369, pp. 1137–1155, Mar. 2011.

[68] N. Andrei, K. Furuya, and J. H. Lowenstein, "Solution of the kondo problem," *Rev. Mod. Phys.*, vol. 55, pp. 331–402, Apr 1983.

[69] A. M. Tsvelick and P. B. Wiegmann, "Exact results in the theory of magnetic alloys," *Advances in Physics*, vol. 32, pp. 453–713, Nov. 1983.

[70] A. Georges, G. Kotliar, W. Krauth, and M. J. Rozenberg, "Dynamical mean-field theory of strongly correlated fermion systems and the limit of infinite dimensions," *Rev. Mod. Phys.*, vol. 68, pp. 13–125, Jan 1996.

[71] V. I. Rupasov and V. I. Iudson, "A rigorous theory of Dicke superradiation - Bethe wave functions in a model with discrete atoms," *Zhurnal Eksperimentalnoi i Teoreticheskoi Fiziki*, vol. 86, pp. 819–825, Mar. 1984.

[72] M. Field, C. G. Smith, M. Pepper, D. A. Ritchie, J. E. F. Frost, G. A. C. Jones, and D. G. Hasko, "Measurements of coulomb blockade with a noninvasive voltage probe," *Phys. Rev. Lett.*, vol. 70, pp. 1311–1314, Mar 1993.

[73] C. N. Yang and C. P. Yang, "Thermodynamics of a onedimensional system of bosons with repulsive deltafunction interaction," *Journal of Mathematical Physics*, vol. 10, no. 7, pp. 1115–1122, 1969.

[74] M. Dzero, J. Xia, V. Galitski, and P. Coleman, "Topological Kondo Insulators," *Annual Review of Condensed Matter Physics*, vol. 7, pp. 249–280, Mar. 2016.

[75] Y. Nishida, "Transport measurement of the orbital kondo effect with ultracold atoms," *Phys. Rev. A*, vol. 93, p. 011606, Jan 2016.

[76] Y. Nishida, "Su(3) orbital kondo effect with ultracold atoms," *Phys. Rev. Lett.*, vol. 111, p. 135301, Sep 2013.

[77] P. W. Anderson, "A poor man's derivation of scaling laws for the Kondo problem," *Journal of Physics C Solid State Physics*, vol. 3, pp. 2436–2441, Dec. 1970.

[78] K. G. Wilson, "The renormalization group: Critical phenomena and the kondo problem," *Rev. Mod. Phys.*, vol. 47, pp. 773–840, Oct 1975.

[79] P. B. Wiegmann, "Exact solution of the s-d exchange model (kondo problem)," *Journal of Physics C: Solid State Physics*, vol. 14, no. 10, p. 1463, 1981.

[80] V. Fateev and P. Wiegmann, "The exact solution of the s-d exchange model with arbitrary impurity spin s (kondo problem)," *Physics Letters A*, vol. 81, no. 2, pp. 179 – 184, 1981.

[81] K. Furuya and J. H. Lowenstein, "Bethe-ansatz approach to the kondo model with arbitrary impurity spin," *Phys. Rev. B*, vol. 25, pp. 5935–5952, May 1982.

[82] N. Andrei and C. Destri, "Solution of the multichannel kondo problem," *Phys. Rev. Lett.*, vol. 52, pp. 364–367, Jan 1984.

[83] N. Andrei and A. Jerez, "Fermi- and non-fermi-liquid behavior in the anisotropic multichannel kondo model: Bethe ansatz solution," *Phys. Rev. Lett.*, vol. 74, pp. 4507–4510, May 1995.

[84] A. M. Tsvelick and P. B. Wiegmann, "Solution of then-channel kondo problem (scaling and integrability)," *Zeitschrift für Physik B Condensed Matter*, vol. 54, pp. 201–206, Sep 1984.

[85] A. Jerez, N. Andrei, and G. Zaránd, "Solution of the multichannel coqblin-schrieffer impurity model and application to multilevel systems," *Phys. Rev. B*, vol. 58, pp. 3814–3841, Aug 1998.

[86] N. Andrei *Private communication*, 2018.

[87] S. Coleman and J. Mandula, "All possible symmetries of the s matrix," *Phys. Rev.*, vol. 159, pp. 1251–1256, Jul 1967.

[88] N. Andrei, "Integrable models in condensed matter physics," in *Series on Modern Condensed Matter Physics - Vol. 6, Lecture Notes of ICTP Summer Course* (G. M. S. Lundquist and Y. Lu, eds.), pp. 458 – 551, World Scientific, 1992, cond-mat/9408101.

[89] E. Brezin and J. Zinn-Justin, "A solvable n-body problem.," *Compt. Rend., Ser. B, 263: 671-3(Sept. 12, 1966).*, Jan 1966.

[90] Y. Wang, W.-L. Yang, J. Cao, and K. Shi, *Off-diagonal Bethe ansatz for exactly solvable models*. Berlin: Springer, 2015.

[91] V. E. Korepin, N. M. Bogoliubov, and A. G. Izergin, *Quantum Inverse Scattering Method and Correlation Functions*. Aug. 1993.

[92] C. Destri and H. J. de Vega, "Lightcone lattice approach to fermionic theories in 2D: The massive Thirring model," *Nuclear Physics B*, vol. 290, p. 168, 1987.

[93] A. G. Izergin and V. E. Korepin, "Pauli principle for one-dimensional bosons and the algebraic bethe ansatz," *Letters in Mathematical Physics*, vol. 6, pp. 283–288, Jul 1982.

[94] A. Zamolodchikov, "Tba equations for integrable perturbed su(2)k su(2)lsu(2)k+1 coset models," *Nuclear Physics B*, vol. 366, no. 1, pp. 122 – 132, 1991.

[95] N. Andrei and J. H. Lowenstein, "A direct calculation of the S-matrix of the chiral invariant gross-neveu model," *Physics Letters B*, vol. 91, pp. 401–405, Apr. 1980.

[96] M. Takahashi, *Thermodynamics of One-Dimensional Solvable Models*. Apr. 1999.

[97] C. Destri and J. Lowenstein, "Analysis of the bethe-ansatz equations of the chiral-invariant gross-neveu model," *Nuclear Physics B*, vol. 205, no. 3, pp. 369 – 385, 1982.

[98] F. H. L. Essler, V. E. Korepin, and K. Schoutens, "Fine structure of the bethe ansatz for the spin-1/2 heisenberg xxx model," *Journal of Physics A: Mathematical and General*, vol. 25, no. 15, p. 4115, 1992.

[99] K. Isler and M. B. Paranjape, "Violations of the string hypothesis in the solutions of the Bethe ansatz equations in the XXX-Heisenberg model," *Physics Letters B*, vol. 319, pp. 209–214, Dec. 1993.

[100] A. Kundu, "LETTER TO THE EDITOR: Consistent refinement of Bethe strings for spin and electron models and a new non-Bethe solution," *Journal of Physics A Mathematical General*, vol. 35, pp. L125–L132, Mar. 2002.

[101] T. Deguchi and P. Ranjan Giri, "Non self-conjugate strings, singular strings and rigged configurations in the Heisenberg model," *Journal of Statistical Mechanics: Theory and Experiment*, vol. 2, p. 02004, Feb. 2015.

[102] R. Hagemans and J.-S. Caux, "Deformed strings in the heisenberg model," *Journal of Physics A: Mathematical and Theoretical*, vol. 40, no. 49, p. 14605, 2007.

[103] B. Pozsgay, "On mathcal{O}(1) contributions to the free energy in Bethe Ansatz systems: the exact g-function," *Journal of High Energy Physics*, vol. 8, p. 90, Aug. 2010.

[104] P. Vigman and A. Finkel'Shtein, "Resonant-level model in the kondo problem," *Soviet Journal of Experimental and Theoretical Physics*, vol. 48, p. 102, 1978.

[105] V. Filyov and P. Wiegmann, "A method for solving the kondo problem," *Physics Letters A*, vol. 76, no. 3, pp. 283 – 286, 1980.

[106] G. Yuval and P. W. Anderson, "Exact results for the kondo problem: One-body theory and extension to finite temperature," *Phys. Rev. B*, vol. 1, pp. 1522–1528, Feb 1970.

[107] P. W. Anderson, G. Yuval, and D. R. Hamann, "Exact results in the kondo problem. ii. scaling theory, qualitatively correct solution, and some new results on one-dimensional classical statistical models," *Phys. Rev. B*, vol. 1, pp. 4464–4473, Jun 1970.

[108] M. Goldstein *Private communication*, 2016.

[109] V. V. Ponomarenko, "Resonant tunneling and low-energy impurity behavior in a resonant-level model," *Phys. Rev. B*, vol. 48, pp. 5265–5272, Aug 1993.

[110] K. Le Hur and M.-R. Li, "Unification of electromagnetic noise and luttinger liquid via a quantum dot," *Phys. Rev. B*, vol. 72, p. 073305, Aug 2005.

[111] A. Furusaki and K. A. Matveev, "Occupation of a resonant level coupled to a chiral luttinger liquid," *Phys. Rev. Lett.*, vol. 88, p. 226404, May 2002.

[112] E. K. Sklyanin, "Boundary conditions for integrable quantum systems," *Journal of Physics A Mathematical General*, vol. 21, pp. 2375–2389, May 1988.

[113] M. Goldstein, Y. Weiss, and R. Berkovits, "Interacting resonant level coupled to a Luttinger liquid: Universality of thermodynamic properties," *EPL (Europhysics Letters)*, vol. 86, p. 67012, June 2009.

[114] H. Bergknoff and H. B. Thacker, "Structure and solution of the massive thirring model," *Phys. Rev. D*, vol. 19, pp. 3666–3681, Jun 1979.

[115] V. E. Korepin, "Direct calculation of the s matrix in the massive thirring model," *Theoretical and Mathematical Physics*, vol. 41, pp. 953–967, Nov 1979.

[116] V. E. Korepin, "The mass spectrum and thes matrix of the massive thirring model in the repulsive case," *Communications in Mathematical Physics*, vol. 76, pp. 165–176, Jun 1980.

[117] M. Fowler and X. Zotos, "Bethe-ansatz quantum sine-gordon thermodynamics. the specific heat," *Phys. Rev. B*, vol. 25, pp. 5806–5817, May 1982.

[118] P. Fendley and H. Saleur, "Massless integrable quantum field theories and massless scattering in 1+1 dimensions," *ArXiv High Energy Physics - Theory e-prints*, Oct. 1993.

[119] P. Fendley, H. Saleur, and N. P. Warner, "Exact solution of a massless scalar field with a relevant boundary interaction," *Nuclear Physics B*, vol. 430, pp. 577–596, Nov. 1994.

[120] H. T. Mebrahtu, I. V. Borzenets, D. E. Liu, H. Zheng, Y. V. Bomze, A. I. Smirnov, H. U. Baranger, and G. Finkelstein, "Quantum phase transition in a resonant level coupled to interacting leads," *Nature*, vol. 488, no. 7409, pp. 61–64, 2012.

[121] D. Braak, J. M. Zhang, and M. Kollar, "Integrability and weak diffraction in a two-particle bosehubbard model," *Journal of Physics A: Mathematical and Theoretical*, vol. 47, no. 46, p. 465303, 2014.

[122] G. Delfino, G. Mussardo, and P. Simonetti, "Scattering theory and correlation functions in statistical models with a line of defect," *Nuclear Physics B*, vol. 432, pp. 518–550, Dec. 1994.

[123] I. V. Cherednik, "Factorizing particles on a half-line and root systems," *Theoretical and Mathematical Physics*, vol. 61, pp. 977–983, Oct. 1984.

[124] J. Cao, W.-L. Yang, K. Shi, and Y. Wang, "Off-diagonal Bethe ansatz solutions of the anisotropic spin-12 chains with arbitrary boundary fields," *Nuclear Physics B*, vol. 877, pp. 152–175, Dec. 2013.

[125] H. De Vega and A. Gonzalez Ruiz, "Boundary k-matrices for the six vertex and the n(2n-1)an-1 vertex models," *Journal of Physics A: Mathematical and General*, vol. 26, no. 12, pp. L519–L524, 1993.

[126] X. Zhang, Y.-Y. Li, J. Cao, W.-L. Yang, K. Shi, and Y. Wang, "Bethe states of the XXZ spin-1/2 chain with arbitrary boundary fields," *Nuclear Physics B*, vol. 893, pp. 70–88, Apr. 2015.

[127] Homer, *Iliad.* c.850 BC.

[128] B. S. Shastry and B. Sutherland, "Twisted boundary conditions and effective mass in heisenberg-ising and hubbard rings," *Phys. Rev. Lett.*, vol. 65, pp. 243–246, Jul 1990.

[129] Y.-Y. Li, J. Cao, W.-L. Yang, K. Shi, and Y. Wang, "Thermodynamic limit and surface energy of the XXZ spin chain with arbitrary boundary fields," *Nuclear Physics B*, vol. 884, pp. 17–27, July 2014.

[130] R. I. Nepomechie and C. Wang, "Boundary energy of the open XXX chain with a non-diagonal boundary term," *Journal of Physics A Mathematical General*, vol. 47, p. 032001, Jan. 2014.

[131] F. Wen, Z.-Y. Yang, T. Yang, K. Hao, J. Cao, and W.-L. Yang, "Surface energy of the one-dimensional supersymmetric t - J model with unparallel boundary fields," *Journal of High Energy Physics*, vol. 6, p. 76, June 2018.

[132] P. A. de Sa and A. M. Tsvelik, "Anisotropic spin-1/2 Heisenberg chain with open boundary conditions," , vol. 52, pp. 3067–3070, Aug. 1995.

[133] I. Affleck and A. W. W. Ludwig, "Exact conformal-field-theory results on the multichannel kondo effect: Single-fermion green's function, self-energy, and resistivity," *Phys. Rev. B*, vol. 48, pp. 7297–7321, Sep 1993.

[134] Y. Oreg and A. M. Finkel'Stein, "Enhancement of the Tunneling Density of States in Tomonaga-Luttinger Liquids," *Physical Review Letters*, vol. 76, pp. 4230–4233, May 1996.

[135] Y. Oreg and A. M. Finkel'stein, "Resonance in the Fermi-edge singularity of one-dimensional systems," , vol. 53, pp. 10928–10941, Apr. 1996.

[136] Y. Oreg and A. M. Finkel'Stein, "Oreg and Finkel'stein Reply:," *Physical Review Letters*, vol. 78, p. 4528, June 1997.

[137] Y. Oreg and A. M. Finkel'stein, "A single impurity in TomonagaLuttinger liquids," *Philosophical Magazine, Part B*, vol. 77, pp. 1145–1160, May 1998.

[138] M. Fabrizio and A. O. Gogolin, "Comment on "Enhancement of the Tunneling Density of States in Tomonaga-Luttinger Liquids"," *Physical Review Letters*, vol. 78, p. 4527, June 1997.

[139] S. Ghoshal and A. Zamolodchikov, "Boundary S Matrix and Boundary State in Two-Dimensional Integrable Quantum Field Theory," *International Journal of Modern Physics A*, vol. 9, pp. 3841–3885, 1994.

[140] F. Lesage, H. Saleur, and P. Simonetti, "Tunneling in quantum wires: Exact solution of the spin isotropic case," *Phys. Rev. B*, vol. 56, pp. 7598–7606, Sep 1997.

[141] V. V. Bazhanov, S. L. Lukyanov, and A. B. Zamolodchikov, "Spectral Determinants for Schrödinger Equation and Q-Operators of Conformal Field Theory," *Journal of Statistical Physics*, vol. 102, pp. 567–576, Feb. 2001.

[142] V. V. Bazhanov, S. L. Lukyanov, and A. B. Zamolodchikov, "Integrable Structure of Conformal Field Theory II. Q-operator and DDV equation," *Communications in Mathematical Physics*, vol. 190, pp. 247–278, 1997.

[143] A. Furusaki and N. Nagaosa, "Resonant tunneling in a luttinger liquid," *Phys. Rev. B*, vol. 47, pp. 3827–3831, Feb 1993.

[144] A. Komnik and A. O. Gogolin, "Resonant tunneling between luttinger liquids: A solvable case," *Phys. Rev. Lett.*, vol. 90, p. 246403, Jun 2003.

[145] A. Furusaki, "Resonant tunneling through a quantum dot weakly coupled to quantum wires or quantum hall edge states," *Phys. Rev. B*, vol. 57, pp. 7141–7148, Mar 1998.

[146] M. Goldstein and R. Berkovits, "Duality between different geometries of a resonant level in a luttinger liquid," *Phys. Rev. Lett.*, vol. 104, p. 106403, Mar 2010.

[147] M. Goldstein and R. Berkovits, "Capacitance of a resonant level coupled to luttinger liquids," *Phys. Rev. B*, vol. 82, p. 161307, Oct 2010.

[148] P. Kakashvili and H. Johannesson, "Measuring luttinger liquid correlations from charge fluctuations in a nanoscale structure," *Phys. Rev. Lett.*, vol. 91, p. 186403, Oct 2003.

[149] P. Wächter, V. Meden, and K. Schönhammer, "Charging of a quantum dot coupled to Luttinger-liquid leads," , vol. 76, p. 125316, Sept. 2007.

[150] I. V. Lerner, V. I. Yudson, and I. V. Yurkevich, "Quantum Wire Hybridized With a Single-Level Impurity," *Physical Review Letters*, vol. 100, p. 256805, June 2008.

[151] H. T. Mebrahtu, I. V. Borzenets, H. Zheng, Y. V. Bomze, A. I. Smirnov, S. Florens, H. U. Baranger, and G. Finkelstein, "Observation of Majorana quantum critical behaviour in a resonant level coupled to a dissipative environment," *Nature Physics*, vol. 9, pp. 732–737, Nov. 2013.

[152] F. H. L. Essler, H. Frahm, F. Göhmann, A. Klümper, and V. E. Korepin, *The One-Dimensional Hubbard Model*. Aug. 2010.

[153] M. A. Ruderman and C. Kittel, "Indirect Exchange Coupling of Nuclear Magnetic Moments by Conduction Electrons," *Physical Review*, vol. 96, pp. 99–102, Oct. 1954.

[154] K. Yosida, "Magnetic properties of cu-mn alloys," *Phys. Rev.*, vol. 106, pp. 893–898, Jun 1957.

[155] T. Kasuya, "A theory of metallic ferro- and antiferromagnetism on zener's model," *Progress of Theoretical Physics*, vol. 16, no. 1, pp. 45–57, 1956.

[156] N. Andrei, "Calculation of the magnetoresistance in the Kondo model," *Physics Letters A*, vol. 87, pp. 299–302, Jan. 1982.

[157] A. Y. Kitaev, "6. QUANTUM COMPUTING: Unpaired Majorana fermions in quantum wires," *Physics Uspekhi*, vol. 44, p. 131, Oct. 2001.

[158] N. Andrei and J. H. Lowenstein, "Scales and scaling in the kondo model," *Phys. Rev. Lett.*, vol. 46, pp. 356–360, Feb 1981.

[159] C. Rylands and N. Andrei, "Simplified Thermodynamics for Quantum Impurity Models," *ArXiv e-prints*, Apr. 2018.

[160] M. Bortz and A. Klümper, "Lattice path integral approach to the one-dimensional Kondo model," *Journal of Physics A Mathematical General*, vol. 37, pp. 6413–6436, June 2004.

[161] C. Destri and H. J. de Vega, "New thermodynamic bethe ansatz equations without strings," *Phys. Rev. Lett.*, vol. 69, pp. 2313–2317, Oct 1992.

[162] C. Destri and H. J. de Vega, "Unified approach to Thermodynamic Bethe Ansatz and finite size corrections for lattice models and field theories," *Nuclear Physics B*, vol. 438, pp. 413–454, Feb. 1995.

Appendices

Appendix A

Another approach to impurity thermodynamics: without strings

The importance of the transfer matrix, $t(u)$, in the solution of the Kondo problem was highlighted in chapter 2. Its eigenvalues evaluated at $u = 0$ give the Bethe momenta k_j at finite N and L. In this appendix we exploit this equivalence between the transfer matrix and the AKM Hamiltonian to derive a simplified and more general expression for the thermodynamics of the model. The method falls under the umbrella of the Quantum transfer matrix method which has been applied to spin chains and integrable QFTs. The method does not rely upon the string hypothesis and therefore does not require a restriction to say $\phi = \pi/\nu$ it can be shown however that the results in either method are equivalent. Since we predominantly use the string hypothesis in this thesis we have chosen to present this method in an appendix.

The work in this section is adapted from the preprint [159] which at the time we believed was the first time the method had been applied to QIMs. Subsequently we discovered that it also appears in earler work of Klümper [160].

Recall that in the AKM we have that all the single particle energies are the same modulo a trivial charge part

$$k_l = \frac{2\pi}{L} n_l + \frac{1}{L} \sum_j^{\mathcal{M}} p(\lambda_j, 1, 1) \tag{A.1}$$

As each energy eigenvalues is given as the sum over all single particle momenta, $E = \sum_l k_l$, we see that it splits into two parts, $E = E_c + E_s$. The first, $E_c = \sum_l 2\pi n_l/L$, is due to

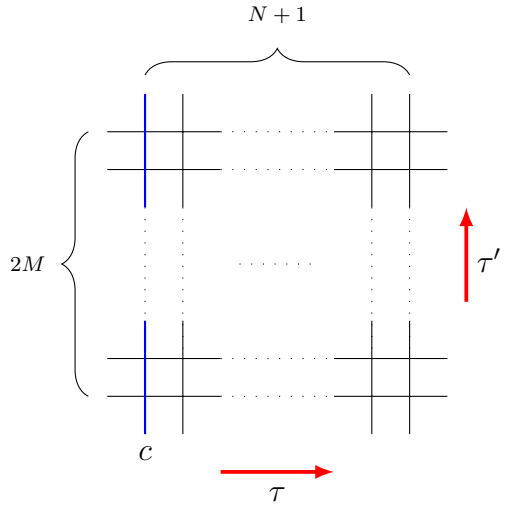

Figure A.1: The transfer matrix $\tau(u)$ defined in (**??**) is also the horizontal transfer matrix of the classical six vertex model. The partition function of (A.4) is that of a model on a square $(N+1)\times 2N'$ lattice with a inhomogeneity of c on the first vertical link and periodic boundary conditions in both directions. Alternately one can calculate the partition function using the vertical transfer matrix τ' instead.

the charge degrees of freedom and merely describes a free spinless Fermi gas. The second, $E_s = D\sum_j^{\mathcal{M}} p(\lambda_j, 1, 1)$, describes the spin degrees of freedom and is non trivial. Summing in over all single particle momenta $e^{-iEL} = e^{-i\sum_j k_j L} = e^{-iE_s L}$. This amounts to taking a power of $t(0)$ so

$$e^{-iEL}A^{[12,\ldots,N,0]} = e^{-iE_sL}A^{[12,\ldots,N,0]} = t(0)^N A^{[12,\ldots,N,0]} \tag{A.2}$$

as the trivial charge part cancels out since $e^{-iE_cL} = 1$.

Proceeding along these lines we can introduce the time variable t and write $\mathrm{Tr}\{\, e^{-iHt}\} = \mathrm{Tr}\{\, e^{-iH_st}\}\mathrm{Tr}\{\, e^{-iH_ct}\}$, where $H_{s,c}$ refer to the effective spin and charge Hamiltonians [1]. Further, as $\mathrm{Tr}\{\, e^{-iH_st}\}$ is determined only by the eigenvalues of H_s, which are in turn

[1] This can be explicitly done using bosonization

determined by the transfer matrix, we have

$$\mathrm{Tr}\{\, e^{-iH_s t}\} = \lim_{\mathrm{Univ}} \lim_{N\to\infty} \mathrm{Tr}\{\, t(0)^{2M}\} \tag{A.3}$$

with $t = \frac{2M}{N} L$ where we first take the thermodynamic limit, $N \to \infty$ holding D fixed and then take the universal limit $D \to \infty$, $M \to \infty$ such that both t, and T_K are held fixed. We thus see that the transfer matrix provides a regularization of the time evolution operator for the spin part of the AKM at finite N and L.

Carrying out a Wick rotation to imaginary time we obtain the partition function of the AKM,

$$\mathrm{Tr}\{\, e^{-\beta H}\} = \mathcal{Z}_c \lim_{\mathrm{Univ}} \lim_{N\to\infty} \mathrm{Tr}\{\, t(0)^{2M}\} \,|_{t\to -i\beta} \tag{A.4}$$

with $\mathcal{Z}_c$ being the charge part of the partition function which is easily computed through standard techniques. In what follows we are concerned only with the impurity properties which carry no charge degrees of freedom and so we will drop $\mathcal{Z}_c$ from now on with the understanding that we are considering only the spin part of the model.

The quantity $\mathrm{Tr}\{\, t(0)^{2M}\}$ is actually the partition function of the classical 6 vertex model on a $(N+1)\times 2M$ square lattice wherein $t(0)$ is the transfer matrix in the horizontal direction [19], see FIG. A.1. Due to rotational invariance we can also compute the partition function of this model using the transfer matrix in the vertical direction which is of a similar form,

$$\mathrm{Tr}\{\, t(0)^{2M}\} = \mathrm{Tr}\{\, t'(0)^N t'(c)\} \tag{A.5}$$

$$t'(u) = \mathrm{Tr}_{\bar{0}}\left[R_{1\bar{0}}(u)\ldots R_{2M\bar{0}}(u)\right]. \tag{A.6}$$

The two transfer matrices $t'(0)$ and $t'(c)$ commute and are therefore simultaneously diagonalizable. Furthermore, as the limit $N \to \infty$ of the partition function is taken first,

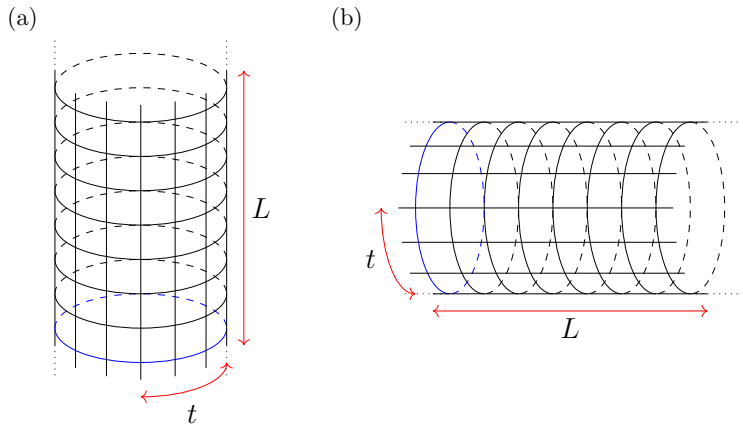

Figure A.2: The two ways of computing the partition function of (A.5). On the right, (b) we take the spatial distance $L = N/D \to \infty$ and the partition function consists of a sum over all states. On the left, (a) we view the system as being on a finite ring $t = 2M/D$ but by taking $L \to \infty$ we project onto the maximal eigenvalue only.

$\mathrm{Tr}\{\, t'(0)^N t'(c)\}$ is determined solely by the largest eigenvalue of $t'(u)$[19] see FIG. 2. The task of computing the partition function of the AKM has therefore been reduced to finding the largest eigenvalue of a six vertex model on a torus - a decidedly simpler task. The only complication being that we must compute this eigenvalue for finite M and in the end take the appropriate limits. Denoting $\Lambda = \lim_{N\to\infty} \mathrm{Tr}\{\, t'(0)^N t'(c)\}$, the largest eigenvalue, we have,

$$\Lambda = \prod_{j=1}^{M} \left[\frac{\sinh(\lambda_j + i\gamma/2)}{\sinh(\lambda_j - i\gamma/2)}\right]^N \frac{\sinh(\lambda_j + c + i\gamma/2)}{\sinh(\lambda_j + c - i\gamma/2)} \tag{A.7}$$

where the λ_j now satisfy,

$$\left[\frac{\sinh(\lambda_j - i\gamma/2)}{\sinh(\lambda_j + i\gamma/2)}\right]^{2M} = \prod_{j\neq k}^{M} \frac{\sinh(\lambda_j - \lambda_k - i\gamma)}{\sinh(\lambda_j - \lambda_k + i\gamma)}. \tag{A.8}$$

Note that now any dependence on the impurity parameter c is contained in the eigenvalue, Λ rather than the Bethe equations. This has its counterpart, in the language of conventional TBA [68, 69], where in thermodynamic limit the saddle point of the partition function is

found to depend only on the bulk and not the impurity. Taking the log of these Bethe equations (A.8) we have,

$$2Mp(\lambda_j 1,1) \quad = \quad -\pi(M-2j+1)+\sum_{k\neq j}^{M} p(\lambda_j-\lambda_k,2,1) \tag{A.9}$$

where the choice of $\mathcal{M}=M$ as well as the logarithmic branches encoded in the successive integers $(M-2j+1), j=1,...,M$ leads to maximal eigenvalue.

It is convenient to rewrite the last equation in terms of the counting function $Z(\lambda)$,

$$Z(\lambda)=2Mp(\lambda,1,1)-\sum_{k}^{M} p(\lambda-\lambda_k,2,1) \tag{A.10}$$

which has the property that, for M even, $e^{iZ(\lambda_j)}=-1$ when λ_j is a solution of (A.9) and furthermore is an analytic function in the region $|\mathrm{Im}(\lambda)|\leq \min(\gamma/2,\pi-\gamma/2)$. Using these two properties in conjunction with the Residue Theorem we are able to rewrite the sum present in (A.10) as an integral[161, 162]

$$\begin{aligned}\sum_{k}^{M} p(\lambda-\lambda_k,2,1) \quad &= \quad \oint_C \frac{\mathrm{d}\mu}{2\pi i} p'(\lambda-\mu,2,1) \\ &\qquad \times \log\left(1+e^{-iZ(\mu)}\right).\end{aligned} \tag{A.11}$$

The contour, C is taken to run from $-\infty$ to ∞ at $\mathrm{Im}(\mu)=-\eta$ and the back again at $\mathrm{Im}(\mu)=\eta$ with $0<\eta\leq\min(\gamma/2,\pi-\gamma/2)$. In this way only the poles at $\lambda=\lambda_j$ and no other non-analytic points are encircled. Inserting the integral form of the sum into (A.10) and rearranging using Fourier transforms and $2M=tD$ we find a single non linear integral equation (NLIE) which determines Z,

$$\begin{aligned}Z(\lambda)=2tD\arctan\left(e^{\pi\lambda/\gamma}\right)+2\mathrm{Im}\int_{-\infty}^{\infty} G(\lambda-\mu-i\eta) \\ \times\log\left(1+e^{iZ(\mu+i\eta)}\right)\end{aligned} \tag{A.12}$$

The function $G(x)$ present here is related to the physical two particle phase shift in the AKM and is given by[69]

$$G(x) = \int \frac{e^{i\omega x}}{4\pi} \frac{\sinh\left[(\pi/2-\gamma)\omega\right]}{\cosh\left[\gamma\omega/2\right]\sinh\left[(\pi-\gamma)\omega/2\right]}. \tag{A.13}$$

Meanwhile the driving term appearing in the (A.12) is in fact the energy of the fundamental excitation in the AKM. In the universal limit $D \to \infty$ we may replace this with $2tD\arctan\left(e^{\pi\lambda/\gamma}\right) \to 2tDe^{\pi\lambda/\gamma}$.

We now return to the eigenvalue Λ and seek to express it in terms of the counting function, Z. Taking the logarithm of (A.7) we can split Λ into a sum of bulk and impurity contributions $\log\Lambda = \log\Lambda_b + \log\Lambda_i$ with $\log\Lambda_b = -iN\sum_j^M p(\lambda_j,1,1)$ being the bulk part and $\log\Lambda_i = -i\sum_j^M p(\lambda_j - c,1,1)$ being the impurity part. Using the same trick to convert the sum to an integral we have the bulk part is,

$$\begin{aligned}\log\Lambda_b &= -itND\int_{-\infty}^{\infty} \mathrm{d}\lambda\, s(\lambda)p(\lambda,1,1) \\ &\quad +2iN\mathrm{Im}\int_{-\infty}^{\infty} s(\lambda+i\eta)\log\left(1+e^{iZ(\lambda+i\eta)}\right)\end{aligned} \tag{A.14}$$

where we have defined $s(x) = \mathrm{sech}(\pi x/\gamma)/2\gamma$. The impurity part is similarly found to be

$$\begin{aligned}\log\Lambda_i &= -it\,D\int_{-\infty}^{\infty} \mathrm{d}\lambda\, s(\lambda-c)p(\lambda,1,1) \\ &\quad +2i\mathrm{Im}\int_{-\infty}^{\infty} s(\lambda-c+i\eta)\log\left(1+e^{iZ(\lambda+i\eta)}\right)\end{aligned} \tag{A.15}$$

At this point we are in a position to perform the Wick rotation $t \to -i\beta$ and obtain the free energy of the AKM for any γ. We are mostly interested in the region $\gamma \leq \pi/2$ which contains the Toulouse point and the isotropic limit so we will restrict to this which allows

us to choose $\eta = \gamma/2$. Making the following definitions,

$$\epsilon(\lambda) = -iZ\left(\gamma\{\lambda - \log 2\beta D\}/\pi + i\gamma/2\right) \tag{A.16}$$

$$G_0(\lambda) = G(\gamma\lambda/\pi), \quad G_1(\lambda) = G_0(\lambda + i\pi - i0) \tag{A.17}$$

and then taking $D \to \infty$ holding T_k fixed we find from (A.16) the impurity part of the free energy is

$$F_i(T) = E_{i,0} - \frac{T}{2\pi}\int \operatorname{sech}\left(\lambda + \log\frac{T}{2T_k}\right)\left[\log\left(1 + e^{-\epsilon(\lambda)}\right) + \log\left(1 + e^{-\epsilon^*(\lambda)}\right)\right] \tag{A.18}$$

where $E_{i,0}$ is the dot contribution to the ground state energy and the function $\epsilon(\lambda)$ is a solution of the NLIE,

$$\begin{aligned}\epsilon(\lambda) &= e^{\lambda} - G_0 * \log\left(1 + e^{-\epsilon(\lambda)}\right) \\ &\quad + G_1 * \log\left(1 + e^{-\epsilon^*(\lambda)}\right).\end{aligned} \tag{A.19}$$

The free energy and the corresponding NLIE have a physically transparent form. The quantity $\operatorname{sech}\left(\lambda + \log\frac{T}{2T_k}\right)$ is the density of states of the dot while $\log\left(1 + e^{-\epsilon(\lambda)}\right)$ and $\log\left(1 + e^{-\epsilon^*(\lambda)}\right)$ can be interpreted as the Fermi functions of the fundamental excitation of the system and its antiparticle where we treat ϵ and ϵ^* as the quasi energies. The interactions in the system are encoded in the NLIE which couples the two excitations together via $G_0(x)$ which is the derivative of the two particle phase shift and $G_1(x)$ which is the derivative of the phase shift between a particle and its anti particle. The driving term e^{λ} is the renormalized excitation energy .

Similarly we can determine the bulk part of the free energy from (A.15),

$$F_b(T) = E_{b,0} - \frac{T^2 L}{2\pi} \int e^{\lambda} \left[\log\left(1 + e^{-\epsilon(\lambda)}\right) + \log\left(1 + e^{-\epsilon^*(\lambda)}\right) \right]. \tag{A.20}$$

Just as for the impurity free energy this takes the form of the density of states $e^{\lambda}/2\pi$ for the bulk system integrated over the Fermi functions. The similarity between the expressions for $F_b(T)$ and $F_i(T)$ at low temperatures is the basis of the Fermi-liquid description of the impurity low-temperature physics.

Appendix B

Derivation of Equation (3.45)

Here we derive the dependence of B on $\bar{\epsilon}_0$ given in (3.45). Allowing for holes the energy is given by with rapidities from $-\infty$ up to an upper bound $-B$

$$E_0/L = -\mathcal{D}\int_{-B}^{0} e^x \rho^p(x)\mathrm{d}x + \bar{\epsilon}_0 \int_{-B}^{0} \rho^p(x)\mathrm{d}x \tag{B.1}$$

The lower limit $-B$ must be determined by minimising the energy with respect to it for fixed $\bar{\epsilon}_0$ similar to our calculation of (3.9). We begin by inverting (3.35) so as to find an equation for $\rho^h(x)$,

$$\rho^0(x) = \rho(x) + \rho^h(x) + \int_{-\infty}^{-B} J(x-y)\rho^h(y)\mathrm{d}y. \tag{B.2}$$

wherein $\tilde{J} = -\tilde{a}_2/(1+\tilde{a}_2)$ and the driving term is the ground state distribution from (**??**). This is a Wiener-Hopf integral and accordingly the solution is

$$\tilde{\rho}^h(\omega) = \rho^0(-B)\frac{(G_-(\omega)G_+(i\frac{\pi}{2\Delta}))^{-1}}{\frac{\pi}{2\Delta}+i\omega}. \tag{B.3}$$

with $G_\pm(\omega)$ defined in (3.48).

Inserting (B.2) into the expression for the energy (**??**) we find that the change due to $\bar{\epsilon}_0$ is

$$\delta E/L = \bar{\epsilon}_0\left[\int \rho^0(x) - \frac{\pi}{2(\pi-\Delta)}\int_{-\infty}^{-B}\rho^h(x)\right] + 2\pi\int_{-\infty}^{-B}\rho^0(x)\rho^h(x) \tag{B.4}$$

We recognise the first two terms as counting the number of particles minus the holes and the last term as the dressed energy of adding these holes. From (B.3) one can see that $\rho^h(x) \propto e^{-\frac{\pi}{2\Delta}B}$ and so minimising the energy with respect to B we find that

$$e^{-\frac{\pi}{2\Delta}B} = \left(e^{\frac{\pi}{2\Delta}a} \frac{\pi(\pi-2\Delta)}{\tan\left(\frac{\pi^2}{2\Delta}\right)} \frac{\Gamma(1+\frac{\pi}{2\Delta})}{\Gamma(\frac{1}{2}+\frac{\pi}{2\Delta})} \right) \frac{\bar{\epsilon}_0}{\mathcal{D}}. \tag{B.5}$$

We can perform an analogous calculation in the $\Delta < \pi/3$ regime where the energy is

$$E/L \;\; = \;\; -\sum_j^{\nu-1} \mathcal{D} \frac{\sin(j\Delta)}{\sin(\Delta)} e^x \rho_j^p(x) + \bar{\epsilon}_0 \sum_j^{\nu-1} j \int \rho_j^p(x). \tag{B.6}$$

By inverting the Bethe equations using (3.40) and inserting them into (B.6) we get shift in energy due to $\bar{\epsilon}_0$

$$\delta E/L = \sum_j^{\nu-1} \int_{-\infty}^{-B} 2\pi \rho_j^0(x) \rho_j^h(x) + \bar{\epsilon}_0 \left[\sum_j^{\nu-1} \int j \rho_j^0(x) - \int_{-\infty}^{-B} \frac{\pi \bar{\epsilon}_0 \rho_{\nu-1}^h(x)}{2(\pi-(\nu-2)\Delta)} \right] \tag{B.7}$$

The first term is the contribution to the ground state energy due the added holes and the second and third count the number of particles minus holes. In order to minimize this we need not know the explicit form of the hole distributions but only that $\rho_j^h \propto e^{-\frac{\pi}{2\Delta}B}$ (c.f (B.3)). Thus we find that

$$e^{-\frac{\pi}{2\Delta}B} = \left(\frac{1}{8(\pi-(\nu-1)\Delta)} \frac{\tilde{\rho}_{\nu-2}^h(0)}{\sum_j^{\nu-1} d_j \tilde{\rho}_j^h(-i\frac{\pi}{2\Delta})} \right) \frac{\bar{\epsilon}_0}{\mathcal{D}}. \tag{B.8}$$

Appendix C

Mapping to the open XXZ model

In this appendix we derive the eigenvalues (4.40) and Bethe equations (4.41). First we will review the results of [124]. They start with the following definitions of R and K matrices,

$$R_{ij}(u) = \begin{pmatrix} \frac{\sinh u+\eta}{\sinh \eta} & 0 & 0 & 0 \\ 0 & \frac{\sinh u}{\sinh \eta} & 1 & 0 \\ 0 & 1 & \frac{\sinh u}{\sinh \eta} & 0 \\ 0 & 0 & 0 & \frac{\sinh u+\eta}{\sinh \eta} \end{pmatrix}, \tag{C.1}$$

$$K^-(u) = \begin{pmatrix} K^-_{11}(u) & K^-_{12}(u) \\ K^-_{21}(u) & K^-_{22}(u) \end{pmatrix} \tag{C.2}$$

$$K^-_{11}(u) = 2\left(\sinh\alpha_- \cosh\beta_- \cosh u + \cosh\alpha_- \sinh\beta_- \sinh u\right), \tag{C.3}$$

$$K^-_{22}(u) = 2\left(\sinh\alpha_- \cosh\beta_- \cosh u - \cosh\alpha_- \sinh\beta_- \sinh u\right), \tag{C.4}$$

$$K^-_{12}(u) = e^{\theta_-}\sinh 2u, \qquad K^-_{21}(u) = e^{-\theta_-}\sinh 2u \tag{C.5}$$

Along with these we can define a $K^+(u) = K^-(-u-\eta)$ wherein all subscripts $-$ are replaced by $+$. These then satisfy the reflection equation (RE), dual reflection equation (the RE for K^+) and Yang-Baxter (YB) equations. The parameters $\eta, \alpha_\pm, \beta_\pm\theta_\pm$ are free and but are related to the various coupling constants, and interactions strengths in the problem at hand. Given these definitions the authours define the following monodromy and transfer matrices,

$$\Theta_0(u) = K^+(u)R_{0N}(u+\theta_N)\ldots R_{01}(u+\theta_1)K^-(u)R_{0N}(u-\theta_N)\ldots R_{01}(u-\theta_1) \tag{C.6}$$

$$\tau(u) = \mathrm{Tr}_0\,\Theta(u) \tag{C.7}$$

following the Boundary inverse method we get $[\tau(u), \tau(v)] = 0$ and thus the problem is tractable. Indeed they go on to construct the eigenvalues, $\Lambda(u)$ of $\tau(u)$ via an inhomogeneous T-Q relation. For even N the result is

$$\Lambda(u) = a(u)\frac{Q_1(u-\eta)}{Q_2(u)} + d(u)\frac{Q_2(u+\eta)}{Q_1(u)} + \frac{2\bar{c}\sinh 2u \sinh(2u+2\eta)}{Q_1(u)Q_2(u)}A(u)A(-u-\eta) \quad \text{(C.8)}$$

Where the functions above are defined to be,

$$A(u) = \prod_{l=1}^{N} \frac{\sinh(u-\theta_l+\eta)\sinh(u+\theta_l+\eta)}{\sinh^2\eta} \quad \text{(C.9)}$$

$$Q_1(u) = \prod_{j=1}^{N} \frac{\sinh(u-\mu_j)}{\sinh\eta}, \qquad Q_2(u) = \prod_{j=1}^{N} \frac{\sinh(u+\mu_j+\eta)}{\sinh\eta} \quad \text{(C.10)}$$

$$a(u) = -4\frac{\sinh(2u+2\eta)}{\sinh(2u+\eta)}\sinh(u-\alpha_-) \times \cosh(u-\beta_-)\sinh(u-\alpha_+)\cosh(u-\beta_+)A(u) \quad \text{(C.11)}$$

$$d(u) = a(-u-\eta) \quad \text{(C.12)}$$

$$\bar{c} = \cosh\left[(N+1)\eta + \alpha_- + \alpha_+ + \beta_- + \beta_+ + 2\sum_{j=1}^{N}\mu_j\right] - \cosh(\theta_- - \theta_+) \quad \text{(C.13)}$$

Here the parameters μ_j are the Bethe parameters and θ_l the inhomogeneities. From this T-Q relation one obtains the Bethe equations by demanding that the function has only simple poles whose residues vanish, which gives,

$$\frac{\bar{c}\sinh(2\mu_j+\eta)\sinh(2\mu_j+2\eta)}{2\sinh(\mu_j+\alpha_-+\eta)\cosh(\mu_j+\beta_-+\eta)\sinh(\mu_j+\alpha_++\eta)\cosh(\mu_j+\beta_++\eta)} = \prod_{l=1}^{N}\frac{\sinh(\mu_j+\mu_l+\eta)\sinh(\mu_j+\mu_l+2\eta)}{\sinh(\mu_j+\theta_l+\eta)\sinh(\mu_j-\theta_l+\eta)} \quad \text{(C.14)}$$

Along with these we have so called selection rules $\mu_j \neq \mu_k$ and $\mu_j \neq -\mu_k - \eta$.

Now our problem is to diagonalise the operator

$$Z = S^{12}\ldots S^{1N}S^{1}W^{1N}\ldots W^{12}$$

in which

$$S^j = \begin{pmatrix} \alpha & \beta \\ \beta & \alpha \end{pmatrix}, \qquad W^{ij} = \begin{pmatrix} 1 & 0 & 0 & 0 \\ 0 & e^{i\phi} & 0 & 0 \\ 0 & 0 & e^{i\phi} & 0 \\ 0 & 0 & 0 & 1 \end{pmatrix}, \tag{C.15}$$

$$\alpha = \frac{1 - U^2/4}{1 + U^2/4}, \quad \beta = \frac{-iU}{1 + U^2/4}, e^{i\phi} = \frac{1 - ig}{1 + ig} \tag{C.16}$$

and $W^{ij} = P^{ij}$ is the permutation of the two spaces. In order to diagonalise this we introduce the R-matrix

$$\mathcal{R}(u) = \begin{pmatrix} 1 & 0 & 0 & 0 \\ 0 & \frac{\sinh u}{\sinh(u+\eta)} & \frac{\sinh \eta}{\sinh(u+\eta)} & 0 \\ 0 & \frac{\sinh \eta}{\sinh(u+\eta)} & \frac{\sinh u}{\sinh(u+\eta)} & 0 \\ 0 & 0 & 0 & 1 \end{pmatrix} \tag{C.17}$$

which is related to both the S-matrices present in Z,

$$\mathcal{R}_{ij}(0) = P^{ij}, \qquad \lim_{u\to\infty} \mathcal{R}_{ij}(u)|_{\eta=-i\phi} = W^{ij} \tag{C.18}$$

Thus we are lead to try diagonalise the transfer matrix, $t(u)$

$$\Xi_0(u) = \mathcal{R}_{01}(u+\theta/2)\ldots\mathcal{R}_{0N}(u+\theta/2)K^-(u)\mathcal{R}_{0N}(u-\theta/2)\ldots\mathcal{R}_0(u-\theta/2) \tag{C.19}$$

$$t(u) = \mathrm{Tr}_0\, \Xi(u) \tag{C.20}$$

Which is related to Z by

$$Z = \lim_{\theta\to\infty} t(\theta/2) \tag{C.21}$$

provided the boundary matrix is chosen so that it goes to S^0 in the limit. We can see that $\Theta(u)$ and $\Xi(u)$ are similar in structure and indeed there is a simple mapping between them.

Once we have this mapping then we can make the same replacements in (C.8)(D.13)and obtain the eigenvalues and bethe equations.

Firstly we should specify the boundary matrices. As there is no K^+ in Z we should require that either $K^+ = 1$ or that it is $\propto 1$ when $u = \theta/2$ (or B_0 for twisted boundary conditions) and after $\lim_{\theta\to\infty}$. In addition K^- should be proportional to S^0 after the same operations. Therefore we choose

$$K^-(u) = \frac{\beta}{\sinh\theta}\begin{pmatrix} 2i\cosh(c+\theta/2)\cosh u & \sinh 2u \\ \sinh 2u & 2i\cosh(c+\theta/2)\cosh u \end{pmatrix} \tag{C.22}$$

$$K^+(u) = \frac{e^{-\eta}}{\sinh 3\theta/2} \tag{C.23}$$

$$\times \begin{pmatrix} 2\left(\sinh(-\theta)\cosh(i\Phi)\cosh(u+\eta)\right. & -\sinh(2u+2\eta) \\ \left.-\cosh(\theta)\sinh(i\Phi)\sinh(u+\eta)\right) & \\ & 2\left(\sinh(-\theta)\cosh(i\Phi)\cosh(u+\eta)\right. \\ -\sinh(2u+2\eta) & \left.+\cosh(\theta)\sinh(i\Phi)\sinh(u+\eta)\right) \end{pmatrix}$$

In both cases we have taken the liberty of including an overall constant factor. One can then check that

$$\lim_{\theta\to\infty} K^-(\theta/2) = \begin{pmatrix} i\beta e^c & \beta \\ \beta & i\beta e^c \end{pmatrix}, \qquad \lim_{\theta\to\infty} K^+(\theta/2) = -\begin{pmatrix} e^{i\Phi} & 0 \\ 0 & e^{-i\Phi} \end{pmatrix} \tag{C.24}$$

Which is what we want provided $e^c = \alpha/i\beta = (1 - U^2/4)/U$. In terms of the parameters introduced previously, these are obtained by taking

$$\alpha_- = c + \theta/2 + i\pi/2, \quad \alpha_+ = -\theta, \quad \beta_- = 0, \quad \beta_+ = i\Phi, \quad \theta_\pm = 0 \tag{C.25}$$

and including an overall factor of

$$\frac{-\beta e^{-\eta}}{\sinh\theta\sinh 3\theta/2} \tag{C.26}$$

Turning our attention to the R matrices we see that they differ by an overall factor

$$\mathcal{R}(u) = \frac{\sinh \eta}{\sinh (u+\eta)} R(u) \tag{C.27}$$

We are now able to relate $\Theta(u)$ and $\Xi(u)$. Specifically we want to go from $\Theta(u)$ to $\Xi(u)$. To achieve this relabel the spaces so the orderings match, $N - m \to m + 1$ and take $\theta_k = \theta/2$ $\forall k$,

$$\Xi(u) = \frac{-\beta e^{-\eta}}{\sinh \theta \sinh 3\theta/2} \prod_{j=1}^{N} \frac{\sinh \eta}{\sinh (u - \theta/2 + \eta)} \frac{\sinh \eta}{\sinh (u + \theta/2 + \eta)} \Theta(u)|_{\theta_k = \theta/2} \tag{C.28}$$

We are interested in the eigenvalue at $u = \theta/2 = \theta_j$. At this value of the spectral parameter the second and third terms in $\Lambda(u)$ vanish so we are merely interested in

$$\Lambda(\theta/2) = -4i\beta e^{-\eta} \frac{\sinh (\theta + 2\eta) \cosh (c) \cosh (\theta/2) \cosh (\theta/2 + i\Phi)}{\sinh (\theta + \eta) \sinh \theta} \prod_{j}^{N} \frac{\sinh (\theta/2 - \mu_j - \eta)}{\sinh (\theta/2 + \mu_j + \eta)} \tag{C.29}$$

The Bethe equations are

$$\frac{\left[\cosh \left((N+1)\eta + c + i\pi/2 + i\Phi - \theta/2 + 2\sum_{j=1}^{N} \mu_j \right) - 1\right] \sinh (2\mu_j + \eta) \sinh (2\mu_j + 2\eta)}{2 \sinh (\mu_j + c + \theta/2 + \eta) \cosh (\mu_j + \eta) \cosh (\mu_j + \eta + i\Phi) \sinh (\mu_j - \theta + \eta)} = \prod_{l=1}^{N} \frac{\sinh (\mu_j + \mu_l + \eta) \sinh (\mu_j + \mu_l + 2\eta)}{\sinh (\mu_j + \theta/2 + \eta) \sinh (\mu_j - \theta/2 + \eta)} \tag{C.30}$$

Up till now we have dealt with N even however there also exists a solution for N odd. This requires the use of $N + 1$ Bethe parameters. The energy is still given by (4.40) but with the sums running up to $(N + 1)/2$. Additionally the Bethe equations are modified,

$$\frac{\left[\cosh\left((N+3)\eta + c + i\Phi - \theta/2 + 2\sum_{j=1}^{N+1}\mu_j\right) - 1\right]}{2\sinh\left(\mu_j + c + \theta/2 + \eta\right)\cosh\left(\mu_j + \eta\right)}$$
$$\times \frac{\sinh\left(2\mu_j + \eta\right)\sinh\left(2\mu_j + 2\eta\right)\sinh\left(\mu_j\right)\sinh\left(\mu_j + \eta\right)}{\cosh\left(\mu_j + i\Phi + \eta\right)\sinh\left(\mu_j - \theta + \eta\right)}$$
$$= \frac{\prod_{l=1}^{N+1}\sinh\left(\mu_j + \mu_l + \eta\right)\sinh\left(\mu_j + \mu_l + 2\eta\right)}{\sinh^N\left(\mu_j + \theta/2 + \eta\right)\sinh^N\left(\mu_j - \theta/2 + \eta\right)}$$

Appendix D

Recovering the Luttinger Liquid

In this appendix we check that upon setting the impurity strength to zero that the solution reduces to the Luttinger Liquid. First we should describe the desired result. For a Luttinger liquid we can specify the number of left and right movers as they are conserved. WLOG we can set the number of right movers to be M and the number of left movers $N-M$. For one of the right movers to traverse the system on a ring of length it must scatter past the $N-M$ left movers and so it has a total phase shift $(N-M)i\phi$. Therefore the right mover contribution to the energy is $-M(N-M)\phi/L$. Similarly a left mover has a total phase shift of $Mi\phi$ and therefore the left moving sector also contributes $-M(N-M)\phi/L$. We should hope to find that the energy reduces to

$$E = \cdots - i\frac{2M(N-M)}{L}\eta \tag{D.1}$$

Where $\eta = -i\phi$. In addition the degeneracy of this energy is $\binom{N}{M}$. Now we look to our derived Bethe equations. We will only consider N even but for N odd the same argument applies.

$$\frac{\left[\cosh\left((N+1)\eta + c - \theta/2 + 2\sum_{j=1}^{N}\mu_j\right) - 1\right]\sinh\left(2\mu_j+\eta\right)\sinh\left(2\mu_j+2\eta\right)}{2\sinh\left(\mu_j + c + \theta/2 + \eta\right)\cosh^2\left(\mu_j+\eta\right)\sinh\left(\mu_j-\theta+\eta\right)} = \prod_{l=1}^{N}\frac{\sinh\left(\mu_j+\mu_l+\eta\right)\sinh\left(\mu_j+\mu_l+2\eta\right)}{\sinh\left(\mu_j+\theta/2+\eta\right)\sinh\left(\mu_j-\theta/2+\eta\right)} \tag{D.2}$$

and that it stays the same order on both side if $\mu_j = \lambda_j + \theta/2$, $\mu_k = \nu_{k-N/2} - \theta$ for $k > N/2$. Which gave us

$$\begin{aligned} e^{2\lambda_j - 2c} \sinh^N(\lambda_j + \eta) &= e^{2\sum_k (2\lambda_k + \nu_k)} e^{3N\eta/2} \prod_{k=1}^{N/2} \sinh(\lambda_j + \nu_k + \eta) \sinh(\lambda_j + \nu_k + 2\eta) \\ e^{-\nu_j - \eta - c} \frac{\sinh^N(\nu_j + \eta)}{2\sinh(\nu_j + c + \eta)} &= \prod_{l=1}^{N/2} \sinh(\nu_j + \lambda_l + \eta) \sinh(\nu_j + \lambda_l + 2\eta) e^{2\lambda_l + \eta}. \end{aligned}$$

after taking the limit $\theta \to \infty$. Removing the impurity corresponds to $U = 0$ or taking $c \to \infty$. We see that upon doing so the left hand side vanishes and we are forced to conclude that the Bethe roots form pairs (λ_j, ν_j), of two types,

$$(\lambda_j, -\lambda_j - \eta) \quad \text{or} \quad (\lambda_j, -\lambda_j - 2\eta) \tag{D.3}$$

In terms of of the original roots we have the condition that either $\mu_{j+N/2} = -\mu_j - \eta$ or $\mu_{j+N/2} = -\mu_j - 2\eta$. However there are still $N/2$ free parameters μ_j. To constrain these we need to use this pair structure in the T-Q relation. Let's say that there are M pairs of roots such that $\mu_{j+N/2} = -\mu_j - \eta$ and that we reorder them so that these occur for $j = 1 \ldots M$. We can then sub this back into our T-Q relation for the eigenvalue $\Lambda(u)$ and take the limit $c \to \infty$. Our new T-Q relation is

$$\begin{aligned} \Lambda(u) &= \frac{-2e^{\theta/2 - u - \eta}}{\sinh\theta \sinh 3\theta/2} \frac{\sinh(2u + 2\eta)}{\sinh(2u + \eta)} \sinh(u + \theta) \cosh u \cosh(u - i\Phi) \\ &\qquad \times \prod^{M} \frac{\sinh(u - \mu_j - \eta)}{\sinh(u + \mu_j + \eta)} \frac{\sinh(u + \mu_j)}{\sinh(u - \mu_j)} \\ &+ \frac{2e^{\theta/2 + u}}{\sinh\theta \sinh 3\theta/2} \frac{\sinh 2u}{\sinh(2u + \eta)} \sinh(u + \eta - \theta) \cosh(u + \eta) \\ &\quad \times \cosh(u + i\Phi + \eta) \frac{\sinh^N(u - \theta/2) \sinh^N(u + \theta/2)}{\sinh^N(u - \theta/2 + \eta) \sinh^N(u + \theta/2 + \eta)} \\ &\quad \times \prod^{M} \frac{\sinh(u - \mu_j + \eta)}{\sinh(u + \mu_j + 2\eta)} \frac{\sinh(u + \mu_j + \eta)}{\sinh(u - \mu_j)} \end{aligned} \tag{D.4}$$

There are two things to note about this expression the first is that the $N-M$ pair of roots of the second type have cancelled out and do not contribute and also the inhomogeneous term has also vanished. As before we are only interested in taking the eigenvalues at $u = \theta/2$ and then in the limit $\theta/2 \to \infty$. With this value of the spectral parameter the second term also vanishes,

$$\begin{aligned}\Lambda(\theta/2) = \frac{2e^{-\eta}}{\sinh\theta}\frac{\sinh(\theta+2\eta)}{\sinh\theta+\eta}\cosh(\theta/2)\cosh(\theta/2-i\Phi) \\ \times\prod^{M}\frac{\sinh(\mu_j+\eta-\theta/2)}{\sinh(\mu_j-\theta/2)}\frac{\sinh(\mu_j+\theta/2)}{\sinh(\mu_j+\theta/2+\eta)}\end{aligned} \tag{D.5}$$

If we shift $\mu_j = \lambda_j + \theta/2 - \eta/2$ and take $\theta \to \infty$ get the momenta of the system

$$e^{-ikL} = e^{-M\eta - i\Phi}\prod^{M}\frac{\sinh(\lambda_j+\eta/2)}{\sinh(\lambda_j-\eta/2)} \tag{D.6}$$

from which we get that the energy is given by

$$E = \frac{2\pi}{L}\sum_{k}^{N} n_k + i\frac{N}{L}\sum^{M}\log\frac{\sinh(\lambda_j+\eta/2)}{\sinh(\lambda_j-\eta/2)} - i\frac{MN}{L}\eta + \frac{N}{L}\Phi \tag{D.7}$$

To evaluate this explicitly we need to use the Bethe equations from our new T-Q relation. As before we demand that Λ has only simple poles and that the residues vanish. The simple pole restriction gives us the selection rule $\mu_j \neq \mu_k$ and $\mu_j \neq -\mu_k - \eta$. The vanishing residues

then results in the Bethe equations

$$\begin{aligned}
0 &= \frac{-2e^{\theta/2-\mu_j-\eta}}{\sinh\theta\sinh 3\theta/2}\frac{\sinh(2\mu_j+2\eta)}{\sinh(2\mu_j+\eta)}\sinh(\mu_j+\theta)\cosh(\mu_j)\cosh(\mu_j-i\Phi) \\
&\quad\times\prod^{M}\frac{\sinh(\mu_j-\mu_k-\eta)}{\sinh(\mu_j+\mu_k+\eta)}\sinh(\mu_j+\mu_k) \\
&+ \frac{2e^{\theta/2+\mu_j}}{\sinh\theta\sinh 3\theta/2}\frac{\sinh 2\mu_j}{\sinh(2\mu_j+\eta)}\sinh(\mu_j+\eta-\theta)\cosh(\mu_j+\eta) \\
&\quad\times\cosh(\mu_j+i\Phi+\eta)\frac{\sinh^N(\mu_j-\theta/2)\sinh^N(\mu_j+\theta/2)}{\sinh^N(\mu_j-\theta/2+\eta)\sinh^N(\mu_j+\theta/2+\eta)} \qquad \text{(D.8)} \\
&\quad\times\prod^{M}\frac{\sinh(\mu_j-\mu_k+\eta)}{\sinh(\mu_j+\mu_k+2\eta)}\sinh(\mu_j+\mu_k+\eta) \qquad \text{(D.9)}
\end{aligned}$$

Performing the necessary algebra give us

$$\begin{aligned}
&e^{-2\mu_j-\eta}\frac{\sinh(2\mu_j+2\eta)\sinh(\mu_j+\theta)\cosh(\mu_j)\cosh(\mu_j-i\Phi)}{\sinh 2\mu_j\sinh(\mu_j+\eta-\theta)\cosh(\mu_j+\eta)\cosh(\mu_j+i\Phi+\eta)} \\
&\qquad\times\frac{\sinh^N(\mu_j-\theta/2+\eta)\sinh^N(\mu_j+\theta/2+\eta)}{\sinh^N(\mu_j-\theta/2)\sinh^N(\mu_j+\theta/2)} \\
&\qquad=\prod^{M}\frac{\sinh(\mu_j-\mu_k+\eta)\sinh(\mu_j+\mu_k+\eta)}{\sinh(\mu_j-\mu_k-\eta)\sinh(\mu_j+\mu_k)} \qquad \text{(D.10)}
\end{aligned}$$

We should make the same change of variables as before. Here do it in two steps for clarity. First let $\mu_j=\lambda_j+\theta/2$,

$$\begin{aligned}
&\frac{\sinh(2\lambda_j+\theta+2\eta)\sinh(\lambda_j+3\theta/2)\cosh(\lambda_j+\theta/2)\cosh(\lambda_j+\theta/2-i\Phi)}{\sinh(2\lambda_j+\theta)\sinh(\mu_j+\eta-\theta)\cosh(\lambda_j+\theta/2+\eta)\cosh(\lambda_j+\theta/2+i\Phi+\eta)} \\
&\qquad\times\frac{\sinh^N(\lambda_j+\eta)\sinh^N(\lambda_j+\theta+\eta)}{\sinh^N\lambda_j\sinh^N(\lambda_j+\theta)} \\
&\qquad=e^{-2\lambda_j-\theta-\eta}\prod^{M}\frac{\sinh(\lambda_j-\lambda_k+\eta)\sinh(\lambda_j+\lambda_k+\theta+\eta)}{\sinh(\lambda_j-\lambda_k-\eta)\sinh(\lambda_j+\lambda_k+\theta)} \qquad \text{(D.11)}
\end{aligned}$$

Now we can take the limit and shift λ_j by $-\eta/2$ and get (4.52)

$$\frac{\sinh^N(\lambda_j+\eta/2)}{\sinh^N(\lambda_j-\eta/2)}e^{N\eta-2i\Phi}=-e^{2M\eta}\prod^{M}\frac{\sinh(\lambda_j-\lambda_k+\eta)}{\sinh(\lambda_j-\lambda_k-\eta)}. \qquad \text{(D.12)}$$

Taking the log of these we obtain

$$N \log \frac{\sinh(\lambda_j + \eta/2)}{\sinh(\lambda_j - \eta/2)} = -(N - 2M)\eta + 2i\Phi + \sum_k^M \log \frac{\sinh(\lambda_j - \lambda_k + \eta)}{\sinh(\lambda_j - \lambda_k - \eta)} + 2\pi i I_j \quad \text{(D.13)}$$

where I_j is a half integer. Using this in our energy equation and the fact that we have a double sum over the antisymmetric function $\log \frac{\sinh(\lambda_j - \lambda_k + \eta)}{\sinh(\lambda_j - \lambda_k - \eta)}$ we get (4.48).